Development of Deterioration Diagnostic Methods for Secondary Batteries used in Industrial Applications by Means of Artificial Intelligence

(人工知能を用いた産業用二次電池の劣化診断法開発)

by

MSc.Eng. **Minella BEZHA**

A thesis submitted to Doshisha University, Kyoto, JAPAN
for the Degree of Doctor of Engineering

22 November 2019

ACKNOWLEDGMENTS

I would like to express my sincere gratitude to my supervisor, Prof. Dr. Eng. Naoto NAGAOKA, who gave me a great opportunity to complete my Ph.D. research at Doshisha University. An enormous gratitude to his continuous support, for his patience, motivation and immense knowledge. His dynamic versatile character, great experience inside-out Japan, through his worldwide connections and reputation, motivated me to work harder without compromising the quality of our research. I was blessed to have the possibility and great chance to travel around the world in the best International Conferences, from one continent to another one, through the economic support of my supervisor and Doshisha's University. His great mentality and approach of acting and "*thinking outside the box*", always in search of a better method, creative and novel perspective. I will always remember the relaxing time of talks, enjoyable dinners and as well the late nights spending on works and his replies by emails until early morning. His contribution was not only in the Academic and Engineering field, but as well effected my philosophy of life and thinking, through him I learned more about Japanese philosophy and their incredible culture.

I am also indebted to Prof. Dr. Eng. Yoshihiro BABA at the same laboratory, Doshisha University, for his guidance and advice throughout the study period. His technical support was highly valuable. I always enjoyed listening to his comments and suggestions, and his support for different important decisions that I had to make through my research. He's a "living lesson" of no matter how great or successful a person can be, he must be always modest and simple. An inspiration model for the new generation.

During my Ph.D. study I had the opportunity to visit different Professors and Universities in Japan or abroad. It was a great opportunity to talk with them and take into consideration their comments and guidance which directly and indirectly affected to improve the quality of my research. I would like to thank, Prof. Emeritus of Doshisha University Akihiro Ametani, President of IEEE Power Electronics Society Prof. Frede Blaabjerg at Aalborg University in Denmark, Dr. Tomy Sebastian of the IEEE Industry Applications Society Chairman, Distinguished Professor Dushan Boroyevich at Virginia Tech in the USA, Prof. Ghanim Putrus at Northumbria University, Newcastle, UK and to his Ph.D. Student Ridoy Das, Prof. Mohamed Emad Farrag at Glasgow University, Scotland, UK, Dr. Eng. Sachio Nagamitsu at Doshisha University, IEEJ I.A. Society Vice President Prof. Toshihisa Shimizu at Tokyo Metropolitan University and to Prof. Hiroshi Fujimoto at The University of Tokyo.

As well I take this chance to thank all the students in Power System Analysis Laboratory, Doshisha University, Kyoto, Japan from the period 2017-2020. For their corporation, support and help in any way, which does not include only technical aspects but also the challenges of daily life in Japan.

I am deeply thankful to the Japanese Government, Ministry of Education, Culture, Sports, Science and Technology, for believing in my potential and selecting me as the only receiver of the MEXT Scholarship for ALBANIA, through Embassy Selection and Recommendation for the period 2017-2021. This financial support during all my Ph.D. period, gave me the possibility to focus on the research and maximize the quality of my work.

The most important appreciation and gratitude go to my older brother, younger sister, father and mostly to my mother, Mrs. Bukuroshe Bezha. She is a noble model of inspiration, courage and support especially during this period of research, where her son couldn't go back home.

I would like to express my sincere appreciation to those who were not mentioned by name, but have contributed directly or indirectly for the completion of this Ph.D. research.

Finally, I would like to say that this work is dedicated to my family and to my supervisor Prof. Nagaoka.

"VERITAS LIBERABIT VOS"

Table of Contents

List of Symbols & Abbreviations

$q(0)$	:	Initial amount of charge at the starting moment	[C]
$q(t)$	:	Amount of charge at time t second during charging/discharging	[C]
$V_{\max}$	:	Maximum voltage value during charging test	[V]
$V_{\min}$	:	Minimum voltage value during discharging test	[V]
R_p	:	Resistance due to migration process in electrolyte	[Ω]
R_{ct}	:	Resistance associated with charge transfer between electrodes	[Ω]
C_{dl}	:	Capacitance due to the electric double layer	[F]
τ_{ct}	:	Time constant of charge	[s]
τ_k	:	Time constant of diffusion phenomenon	[s]
v	:	Battery voltage	[V]
i	:	Battery current	[A]
R_0	:	Series resistance	[Ω]
Z_{arc}	:	Parallel circuit composed by Resistance and Capacitance	[Ω]
R_1	:	Resistance of the first Z_{arc}	[Ω]
R_2	:	Resistance of the second Z_{arc}	[Ω]
C_1	:	Capacitance of the first Z_{arc}	[F]
C_2	:	Capacitance of the second Z_{arc}	[F]
C_0	:	Series Capacitance	[F]
E_0	:	Battery internal voltage	[V]
d	:	Duty ratio	[%]
i_{int}	:	Integral value of current	[As]
SoC	:	State of Charge	[%]
SoH	:	State of Health	[%]
R_b	:	Bulk resistance	[Ω]
R_{sl}	:	Surface layer resistance	[Ω]
R_{ct}	:	Charging-transfer resistance	[Ω]
Z_w	:	Warburg impedance	[Ω]
EV	:	Electric Vehicle	
HEV	:	Hybrid Electric Vehicle	
ALD	:	Atomic layer deposition	
IZ	:	Internal impedance	
GICs	:	Graphite intercalation compounds	
LTO	:	Lithium Titanate Oxide	
QC	:	Quick Charge	
DME	:	Dimethyl ether	
DOL	:	Dioxolane	
DMSO	:	Dimethyl sulfoxide	
DMF	:	Dimethyl formamide	
DOD	:	Depth of Discharge	
BOL	:	Beginning of life (*related with battery health*)	
EOL	:	End of life (*related with battery health*)	
OCV	:	Open Circuit Voltage	
EIS	:	Electrochemical impedance spectroscopy	
SEI	:	Solid electrolyte interphase	
LIBs	:	Lithium-ion batteries	
LUMO	:	Lowest unoccupied molecular orbital	
HOMO	:	Highest occupied molecular orbital	
DFT	:	Density functional theory	
AFM	:	Atomic force microscopy	
QC	:	Quantum chemistry	
MD	:	Molecular dynamics	

EC	:	Ethylene carbonate
PTC	:	Positive temperature coefficient
PCM	:	Protection circuit module
DMC	:	Dimethyl carbonate
DEC	:	Diethyl carbonate
EMC	:	Ethyl methyl carbonate
PC[(1)]	:	Personal computer
PC[(2)]	:	Propylene carbonate
COMPASS	:	(Condensed phase optimized molecular potentials for atomistic simulation studies)
APPLE & P	:	Atomistic polarizable potential for liquids electrolytes and polymers
CID	:	Current Interrupt Device
Ni-MH	:	Nickel Metal Hybrid
Ni-Cd	:	Nickel Cadmium
CID	:	Current Interrupt Device
LiPO	:	Lithium Ion polymer
LiFe	:	Lithium Ion phosphate
$PbSO_4$	:	Lead sulfate
AI	:	Artificial Intelligence
ANN	:	Artificial neural network
ML	:	Machine learning
OCR	:	Optical character recognition
SL	:	Supervised learning
UL	:	Unsupervised learning
SSL	:	Semi-Supervised learning
TI	:	Transductive inference
OL	:	On-line learning
RL	:	Reinforcement learning
AL	:	Active learning
SVM	:	Support vector machines
PAC	:	Probably approximately correct
VC	:	Vapnik Chervonenkis
PCA	:	Principal component analysis
QSARs	:	Quantitative structure-activity relationships
QSPRs	:	Quantitative structure-property relationships
PCBs	:	Polychlorinated biphenyls
CBP	:	Cell balancing pack
BMS	:	Battery management system
MTC	:	Multi type charger/discharger circuit
CCCV	:	Constant current constant voltage
CAD	:	Computer aid design
PV	:	Photovoltaic
LCD	:	Liquid crystal display
WT	:	Wind turbine
JC08	:	Japanese emission regulation chassis dynamometer test cycle for light vehicles (< 3500 kg GVW*), based on cold start and warm start since 2005*
ECM	:	Equivalent circuit model
BEB	:	Battery electric buses
3S4P	:	3 series connection with 4 modules connected in parallel
PE	:	Parameter estimation
FME	:	Adaptive filter-mathematical based estimation
OFR	:	Optimal frequency regions

1.   Thesis Overview

"Everything is energy and that's all there is to it. It changes the state, shape, type, composition but in the end, it is the only purest substance of the universe. Match the frequency of the reality you want and you cannot help but get that reality. It can be no other way. This is not philosophy. This is physics" - **Albert Einstein**

1.1   General

In recent years, energy and environmental issues are globally the main concern. Through the improvement and implementation of the power generation systems based on natural energy, it will be possible to solve this problem. The importance of rechargeable batteries nowadays is increasing from the portable electronic devices and solar energy industry up to the development of new Electrical Vehicles (EV) models. In addition, the necessity for larger, efficient and reliable storage systems is heightened. The rechargeable batteries are considered as the most common storage devices. EV and Hybrid Electric Vehicles (HEV) are becoming the most important technology in transportation, due to their environmental affinity and increased driving autonomy. In the running process of EVs or HEVs, the batteries experience stress from the dynamic operational environment. The charging condition is essential for designing the storage system, while the charging quality of the battery directly affects the battery lifetime and normal operation within the regulated and standardized parameters. The most used battery type is based on Li-Ion chemistry and their derivative types, due to the high energy and power density, high efficiency, higher open circuit voltage (OCV), within its class of battery, wide range of temperature for a normal operation, low maintenance, also long-term usage. However, beside its advantages it introduces as well drawbacks. It is necessary to have a protection system which helps from over charged and over discharged beyond its normal range of operation. This means that it must be connected with an integrated circuit technology, which is usually resolved by the battery management system (BMS).

Another major problem of Li-Ion batteries is the ageing process. Its ageing process depends, not only on calendar, but also on the charge/discharge cycles. Based on actual technology this type of battery withstand 500-1000 cycles for a normal and safe operation, before their capacity falls. As well the other problems, as the accurate estimation of state of charge (SoC) and state of health (SoH) are difficult to be obtained, because it is unclear which parameters affect the deterioration process. Although Li-Ion batteries have been used in real applications, still it can be considered an immature technology from most of the researchers of this field. Understanding the advantages and proposing new methods which can resolve the disadvantages or at least reducing the side effects is the main challenge.

In general, all the batteries introduce high nonlinearity in their behavior, which requires complex models to explain their characteristics. Although the conventional methods confirm and resolve specific problems but their abilities are quite limited and have lack of adaptability for new and unknown problems. In order to resolve and simplify these nonlinearity, unconventional method was used to make an efficient investigation by maximizing the usage of the genuine data obtained through practical experiments. Using practical data, it was possible to create and optimize a solid model based on the Artificial Intelligence (AI) properties, specifically expressed through Artificial Neural Network (ANN) ability. Due to the black box approach of the ANN it is possible to connect the complex physical phenomenon with a specific physical meaning expressed with a nonlinear logic between inputs and output. Using specific input data to relate with the desired output, makes possible to create a pattern connection with input and output This ability helps to estimate the desired outputs, behaviors, phenomena in real time, and at the same time it can be used as a real time diagnosis method. As well it has the ability to be optimized, improved and work in off-line processing for better results.

1.2   Organization of the Thesis

The thesis is based on 8 chapters, where it starts with explanations of the secondary batteries' chemistries, abilities, drawbacks, applicable field followed by the explanation of the AI based on ANN method. Due to the immense ability and possibility for applications of ANN not only as theoretical thinking approach but also as robust and confirmed critical problems resolving with aggressive algorithm, the ANN makes possible and open new opportunities for a real time monitoring, diagnosis and decision making. Based on these features it was possible to start the investigation of the OCV waveform characteristics of the Li-Ion battery during charging. After parallel works were made to understand the relation process and optimization of the ANN structure for each problem, respectively for the SoC and SoH estimation models.

Also, an investigation on the parameters of the equivalent circuit model (ECM), which variables are more connected with power output, capacity fade, increased of internal temperature, faster deterioration due to the fast charging/discharging, or even the optimized C ratio and the best current waveform for the charging process which helps to decrease the deterioration process. For each of the mentioned problems, a considerable amount of experiments was conducted in order to give some scientific explanations. Selecting the most interesting variables for the ANN database, it was another goal during the process of this research. This helps to increase the quality of the estimation, making the simulation and calculation time shorter, and stable. Also, an interest was shown for the generalization of each problem, from viewpoints of the ANN structure and applicability the proposed model to rechargeable batteries based on different chemistries, type of current waveform, level of load.

1.3   Objective of this study

The objective of this study is to propose new and different methods for the real time diagnosis and parameter/fault estimations for the rechargeable batteries. By combining conventional and unconventional methods, it was possible to make an efficient investigation by maximizing the usage of the genuine data obtained through practical experiment. It was possible to create and optimize a solid model based on the AI properties, specifically expressed through ANN ability. Although the conventional methods confirm and resolve specific problems, their abilities are quite limited and have lack of adaptability to new and unknown problems. The contribution is mainly focused on three problems as explained in the further chapters.

In Chapter 4, the investigation was focused on the SoC estimation model, where a basic model was introduced based on OCV estimation of the battery during charging process. This model opens the possibility to improve the model with less necessary inputs of the ANN learning process. In addition, some BMS circuits for battery pack/modules were proposed to be used during operation, which helps to maintain a higher and stable level of voltage.

In Chapter 5, a contribution was made regarding the SoH estimation, i.e., classification of deterioration. As well a scaled down simulator for the design of power storage system was proposed, which reduces the cost and removes a real size benchmark system. Another important focus of this study was based on the accurate estimation of power and energy consumption in EVs, where the total battery pack was investigated to understand the "behavior and characteristics" of the battery pack during dynamic operation. In the final step of the ANN structure for this problem, only the parameters of an arbitrary single cell from the battery pack was necessary to make an accurate power and energy consumption of EV. As well, through this study it was shown the ability to relate EV's consumption level with the battery deterioration.

In Chapter 6, a parameter estimation of equivalent circuit model (ECM) was proposed based on real time evaluation approach. By dividing into the high and low frequency regions, it was possible to relate specific parameters of ECM with specific problems and behaviors. Later a deeper investigation was introduced by dividing the frequency regions in more narrow regions and by selecting the best frequency zone for each of the

rechargeable batteries, Li-Ion, Ni-MH and Pb. The results of this study shows the ability and further possibilities for progressive improvements of the diagnostic tools as a real time approach, where it was possible to speed up the estimation time, not only with low cost but also with high-accuracy, -adaptivity, -efficiency, and with generalization ability which gives the opportunity for fast adaptation to the related industrial problems. The proposed methods are applicable to real time diagnosis applications and to offline processing. The quality and credibility of the work was continuously confirmed by the comparison with experimental results.

The author has proposed new deterioration diagnostic methods and approaches for secondary batteries, which are totally different from conventional methods. Proposal of new idea, which resolves actual problems of this field, and provision of the opportunity to investigate new problems are the main goal of the author. The proposed methods based on this study open the door to new application fields of the secondary battery from academic perspectives to industrial applications.

2. Rechargeable Batteries Li-Ion/ Pb/ Ni-MH Battery Fundamentals

2.1 Introduction

Energy is the source of life and the lifeblood of progress and modern society. From this fact it is important to make it possible a constant and reliable source of energy but at the same time an efficient storage system. During the last 50 years, human society has witnessed a critical and fast growth in mobility of devices. From the previous scenario were stationary devices were predominant, we would have to reach them in order to use, due to the necessity to be connected with power electric grid. Based on the needs for mobility systems the computer has evolved to laptop, desk phones to mobiles and so on. This drastic change has increased further the demand for portable energy sources. The needs to reduce the size, height of the storage system and with the same time increase the capacity of energy, and with higher current drain usage for power hungry applications. On the other hand, the need of friendly environment and zero pollution technology is necessary for the actual standards. The risk from the global warming, air pollution and finite fossil-fuel supplies leads to increased demands in renewable energies such as solar, wind, tidal etc. However, the renewable energy sources are intermittent, uncontrollable and not continues in time, which makes necessary for an efficient and reliable electrical energy storage (EES) [9] for a stable and consistent power delivery. There are few different EES technologies in the actual market, where rechargeable batteries are the most promising to serve high energy density applications and with their high energy efficiency [10]. Nowadays, there is a wide range of different battery chemistry, each one of them with features to be used in the best convenient way depending on the applications. However, it is important to know the past of the battery technology from the first simplest model to the most advance one of nowadays. The eldest and first evidence of the batteries have been in use for at least the past 2000 years. During a railway construction in Khujut Rabu, just outside Baghdad in modern day Iraq, unearthed a 13cm (five-inch-long) clay jar containing a copper cylinder that encased an iron rod amongst other finds form the Parthian period. In 1938, it was identified as the first model of electric cells by the German Archeologist Dr. Wilhelm Konig, back then the director of the Baghdad museum laboratory. Based on the historical data Dr. Konig concluded that their main purpose was for electroplating gold and silver jewelry for the high elite society. Figs. 2.1 shows the Baghdad battery.
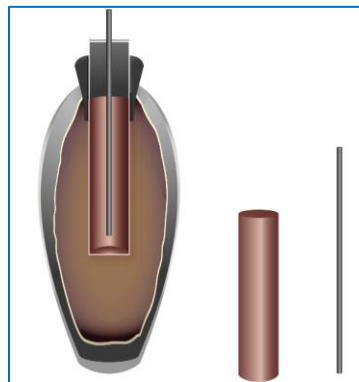
Fig.2.1. Main components of Parthian (Bagdad) battery [3]

The edge of the copper cylinder was soldered with a lead-tin alloy comparable to today's solder. The bottom of the cylinder was capped with a crimped-in copper disc and sealed with bitumen or asphalt. Another extra insulating layer of Asphalt sealed the top and also held in place an iron rod suspended into the center of the copper cylinder [3]. Two separate experiments with replicas of the cells have produced a 0.87V current in small amount which could last for 18 days. Their main chemical elements where based on an electrolyte of 5% solution of Vinegar, wine or copper-sulphate, sulphuric acid and citric acid, where were all available at that time. A very long period of struggling and with small progress was made on battery technology from that time until the mid-

1700s, where the two inventors, working in parallel but separately from each other, discovered what will become known as the "Leyden jar". This type of battery was a device used to store static electricity by lining the interior of a glass jar with a metal sheet by adding another layer of metal-sheet coating around and in the end inserting a metal rod through the top and connecting it to the inner sheet-foil. But only around mid-1700s that the term "battery" was referred to this type of device and is believed to be called by Benjamin Franklin. The next step of progress was made by the discovery of the Alessandro Volta. It was in 1800 when Volta published the results of his experiments made on so called "Voltaic Pile". This type of battery proved to be the first electrochemical storage cell [3]. The Voltaic pile is composed of two metal plates, where one is made of zinc and the other by copper in order to make the electrodes, and were separated by a piece of cloth soaked with an electrolyte made by sulfuric acid or saltwater brine. The next major evolutionary step of the modern battery came in 1859 when Gaston Plante, a French physicist, proposed the first rechargeable lead-acid storage battery known as Pb battery type. Together Camille Faure another French inventor, improved first prototype of Pb by enhancing its current performance in 1881. Based on their improved model which have been used as the basis for the modern Pb which is used nowadays in different sector of industry. Another attempt for further progress on the storage system was made by Thomas Edison which developed a nickel-based battery as a need to compete the Pb battery which was massively used in the electric cars in the early 1900s. But the real improvement and revolution of storage system will not come until the early 1970s and into the 1990s, where new chemistries were made the real implementation in the electrification which we see nowadays.

2.2 Battery types, chemistries and properties

Cells is the core element of battery. For small portable electronics, devices a single cell can satisfy their demand of energy and power requirements for a specific time, which must be evaluated to fit the acceptable value of time lasting without compromising the necessary level of safety, size and esthetic requirements. In case of large-scale applications in electric vehicles (EV) and stationary EES, it is necessary many cells to be electrically integrated into modules which are packed further in pack in order to fulfill the needs for energy. Batteries which can be used only 1 time until their full discharge are called primary batteries, which usually are used in application with low power demands in order to last for a while. Another type of battery is the rechargeable batteries, known as secondary batteries, they can be charged and discharged many times. This type is used as on-board energy storage source in all consumer electronic, power electronics, transportation domains, telecommunication. The secondary batteries dominate most of the actual industries with a wide opportunity for applications. The cell structure itself is composed of a positive electrode (cathode), a negative electrode (anode), and an electrolyte, in which the cathode and anode are physically isolated by the electrolyte. During the usage of liquid electrolyte, a porous membrane is placed as the separator between the cathode and anode to avoid their electrical contact. The separator allows the liquid electrolyte to penetrate and mechanically isolates the cathode and anode from each other. The electrolyte is in principle ionically conducting and electronically insulating, which enables the redox reaction on each of electrodes [9]. Recharge ability of a cell is based on a reversible redox reaction between the cathode and anode materials. The open circuit voltage V_0 of a cell is equal to the difference of chemical potentials between the cathode E+ and anode E- as described in (2.1)

$$U_{OCV} = E_+ - E_-$$

(2.1)

where E_+ and E_- changes depending with the value of state of charge (SoC), strictly speaking, the chemical composition of the electrode materials.

The output voltage (U) of the cell depends on the IR polarization, which is described by (2.2)

$$U = U_{OCV} - IR$$

(2.2)

where *I* express the current which pass through the cell, and *R* is the overall internal resistance of the cell, related by many factors, including electrode and quality of electrolyte materials, electrode and cell structure, temperature, deterioration progress, rated lifetime usage, cell's SoC or/with depth of discharge (DoD). During AC impedance spectroscopy, the overall resistance of a cell consists of the ohmic bulk resistance (R_b) contributed by the electronic resistance of cell's and the ionic resistance of the electrolyte composition, ohmic surface layer resistance (R_{sl}) from both electrodes. Also, the Faradic charging-transfer resistance (R_{ct}) relating to the electrochemical reactions occurring in two electrodes and changing with the SoC. Also, the Warburg impedance (Z_w) expresses the ionic diffusion on the electrolyte-electrode interface. In most general cases the R_{ct} remarkably increases near the end of charge or discharge, which hence results in a steep increase for the cell's polarization. Mostly these parameters are used to express and define the ending point of charging in many battery chargers. The energy density, generally expressed by watt-hour per unit weigh or volume, is the product of specific capacity. For a battery pack, these parameters are further affected by other components such as battery packing materials and battery electrical and thermal managements. The quality of electrolyte affects the performance of a rechargeable cell, including reversibility, coulombic efficiency, rate capability, safety, operating temperature range, and cycle life.

Energy density of a battery is the product of specific capacity and averaged output voltage. The focus is to develop a high specific capacity and high voltage cathodes. Amon high capacity cathodes, Li-rich layered as $Li[Li_{1/3}Mn_{2/3}]O_2$-$LiMO_2$ (M=Ni, Co, Mn) solid solutions, or written as Li_2MnO_3-$LiMO_2$ in the other form of descriptions, shows a high interest. In the solid solution, the electrochemically inactive Li_2MnO_3 phase stabilizes the layered $LiMO_2$ to enable a wide range of operating voltage. As explained in [9,11,12,13]. These materials typically have a 250mAh/g of specific capacity between 2 and 4.8V versus Li/Li$^+$ [14]. The most problematic matter of these materials is the high irreversible capacity (40-100 mAh/g in the first cycle), increase of voltage hysteresis (delay) also poor rate capability. As explained in [15,16], the issues start above 4.5V in the initial activation step, is due to the irreversible evolution of oxygen and resulting Li$^+$ ion loss and electrolyte solvent oxidation and electrolyte solvent oxidation. The second problem is due to the irreversible structural transition from layered to spinel lattice. Third problem is related to the nature of elevated high electronic conductivity of layered as LiMO2 and the presence of inactive Li_2MnO_3 phase. Multivalent Li$^+$ ion compounds such as polyanionic Li_2MSiO_4 (M=Mn, Fe, Co, Ni) with two Li$^+$ ion per formula unit corresponding to a 330mAh/g of theoretical capacity for M-Fe and monoclinic $Li_3V_2(PO_4)_3$ with three Li$^+$ ions per formula unit equaling to a 197 mAh/g of theoretical capacity, where in [17,18] is been investigated as the high capacity cathode material. But, the structural instability and capacity's utilization remain challenges for these multiple Li$^+$ ions materials. Comparing to the high voltage cathode material, spinel $LiNi_{0.5}Mn_{1.5}O_4$ and olivine $LiCoPO_4$ have been intensively studied. Through the Ni2+/3+ and Ni3+/4+ couples, $LiNi_{0.5}Mn_{1.5}O_4$ offers around 130 mAh/g of accessible capacity at around 4.7V comparing Li/Li+. The high operating voltage and three-dimensional fast Li+ ion diffusion make $LiNi_{0.5}Mn_{1.5}O_4$ attractive for the large size batteries to be used in the transportation vehicles and stationary EES. The most problematic matters with $LiNi_{0.5}Mn_{1.5}O_4$ are the formation of $Li_xNi_{1-x}O$ impurity phase and chemical instability in contact with the electrolyte at high operating voltages. As explained in [9] the small amount of Fe-substitution stabilizes the structure with cation-disorder in the 16d octahedral sites of the spinel lattice, which leads to remarkable improvement in both the capacity retention and rate capability. $LiCoPO_4$ has a theoretical capacity 172 mAh/g around 4.8V versus Li/Li+ of averaged operating voltage. The major issues with this material are the intrinsically low electronic and Li+ ionic conductivity of the olivine structure. Differently form $LiFePO_4$, coating of conductive carbon is not suitable for $LiCoPO_4$ because at the synthesis temperature, the highly oxidative $LiCoPO_4$ will directly oxidize carbon. Similarly, to the $LiNi_{0.5}Mn_{1.5}O_4$, very small amount of Fe-substitution significantly improves the specific capacity and cycle life [19]. It was observed from both $LiNi_{0.5}Mn_{1.5}O_4$ and $LiCoPO_4$ that the substitution process induced the self-segregation of Fe-rich phase on the surface of cathode particles, leading to the enrichment of the more stable Fe

6

cations. Due to this fact, the Fe-substitution not only stabilizes the lattice structure but also increases the chemical stability in contact with the electrolyte as explained in [20]. It will boost the capacity retention, especially at elevated temperatures for the $LiNi_{0.5}Mn_{1.5}O_4$ and $LiCoPO_4$. This fact shows the self-segregation of robust Fe cation phase may be a cost-effective strategy to overcome the chemical instability of the cathode surface in contact with the electrolyte. Another important matter is the instability of the electrolyte solvents, which is the most difficult thing, for the applications of high-voltage cathode materials, which is mainly due to the strong oxidation of the high voltage cathode materials and the high catalytic activity of the cathode particles to the electrochemical oxidation of electrolyte solvents. Few problems are related with the oxidative decomposition of electrolyte solvents on the surface of high voltage cathode particles, such as active material loss, known as dissolution, low coulombic efficiency, and uncontrollable growth of resistive surface layer. The most reliable solution to these problems is the surface coating with more robust compounds like $AlPO_4$, ZnO, Al_2O_3, and Bi_2O_3 [21]. The authors of this reference have proven that the electrolytic and thereby suppresses the formation of thick SEI layer. Development of robust cathode surfaces seems to be an attractive strategy to overcome the instability of the high-voltage cathode materials in contact with the liquid electrolyte and thereby improve the energy density, rate capability, and cycle life.   One of the main columns for the improvement of the battery performance is the high-power property. Power can describe how fast the battery can delivery energy. The ability for high power it's necessary parameter in the application for high current demand as in transportation, such as HEVs and EVs, in which fast discharge and charge are frequently required during the acceleration and braking-up of the vehicles. The amount of power delivery it can be increased by battery design and material optimization at the same time. Fig. 2.2 shows a Ragone plot of the rechargeable batteries most used nowadays in wide fields of applications.
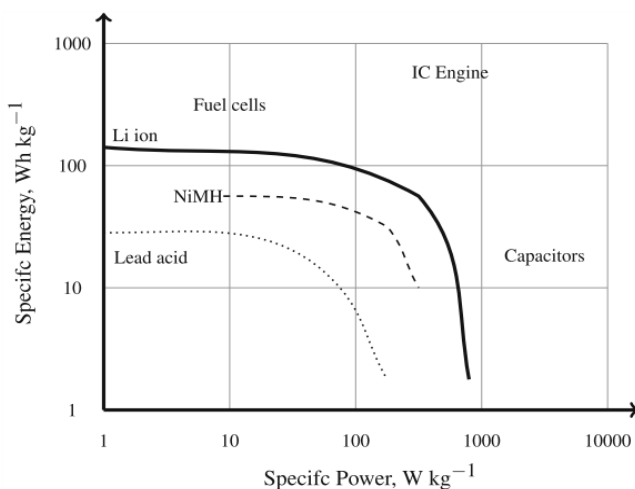
Fig. 2.2. Ragone plot.

The energy density has been increased stepwise by approximately 5Wh/kg every year, for the past several decades, and is approximately 160 Wh/kg now. However, the current energy density still does not meet the needs of vehicle electrification which is in the range of (500-700) Wh/kg [22,23]. Fig. 2.3 shows the energy density and specific energy amount of the rechargeable batteries.
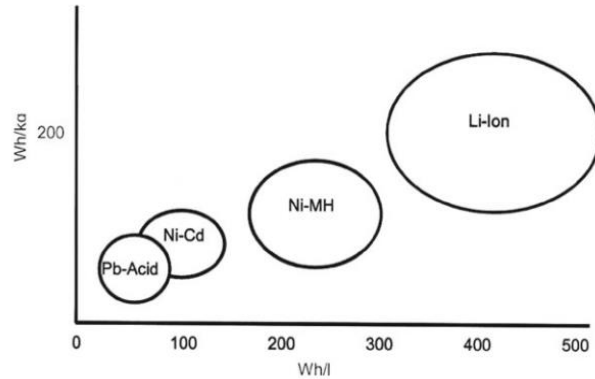
Fig. 2.3. Energy density (Wh/l) and specific energy (Wh/kg) for the major small-sealed rechargeable battery systems [1].

The most known and common method to improve the power through the battery design based on the reduced electrode thickness and increasing the content of conductive carbon in the electrode. These kinds of improvements are achieved at the cost of energy density due to the introduction of more inactive materials. From the perspective view of the cathode materials, a high power can be obtained from the reduction of particle size and the surface coating of conductive carbon. Another approach is the nanostructured materials are particularly appealing in the reduction of the particle size. There are few advantages as

a) Reducing diffusion length of the Li+ ion diffusion within the particle for high reaction rate,

b) Increasing electrode/electrolyte contact are for more effective and faster electrode reaction,

c) Accommodating volume change caused by the intercalation and deintercalation of Li+ ions for long cycle life.

Coating of conductive carbon has been widely adopted to improve the rate capability of the low electronically and ionically conductive LiFePO4. However, this technique is only limited to the low voltage cathode materials [24]. In case of high voltage cathode materials, chemist engineers explain that carbon will be chemically oxidized by the cathode materials in the coating process. Moreover, carbon may be electrochemically oxidized at high potentials that are within the charging potential range of the high voltage cathode materials [9, 25].

Carbon is the main anode material for the commercial LIBs used in portable electronics. Enriched graphite has a 372 mAh/g of theoretical capacity at an operating voltage around 0.25V comparing Li/Li$^+$ in accordance with the formation of a LiC6 graphite intercalation compound (GIC), and around 360 mAh/g can be easily accessed in practical batteries. Disordered hard carbon has higher voltage hysteresis, lower packing density, and poorer electrical conductivity, as compared with the ordered graphite. Since the intercalation of Li+ ions into graphite occurs at lower potentials than the organic solvents electrochemically reduce, organic electrolytes are thermodynamically instable with the graphite anode [26]. However, the electrolyte solvents must be first reduced before the Li$^+$ ions can be intercalated into graphite. In order to enable the operation of graphite anode, the reduction products of the electrolyte solvents anode are stably accumulated on the graphite surface to form a dense and protective film. This film is called solid electrolyte interphase (SEI), and the formation of the SEI has proven to be an important process for the manufacture in affecting the cycling performance, cycle life and safety of the LIBs.

Still today, SEI is regarded as "the most important but least understood (component) in rechargeable Li-ion batteries" which can be attributed to the complexity of the chemical and electrochemical reactions to form it and insufficient direct measurement of its physical properties. In Fig. 2.4 based on [22], it is illustrated the modelling progress in years, for the anode SEI of lithium-ion batteries.
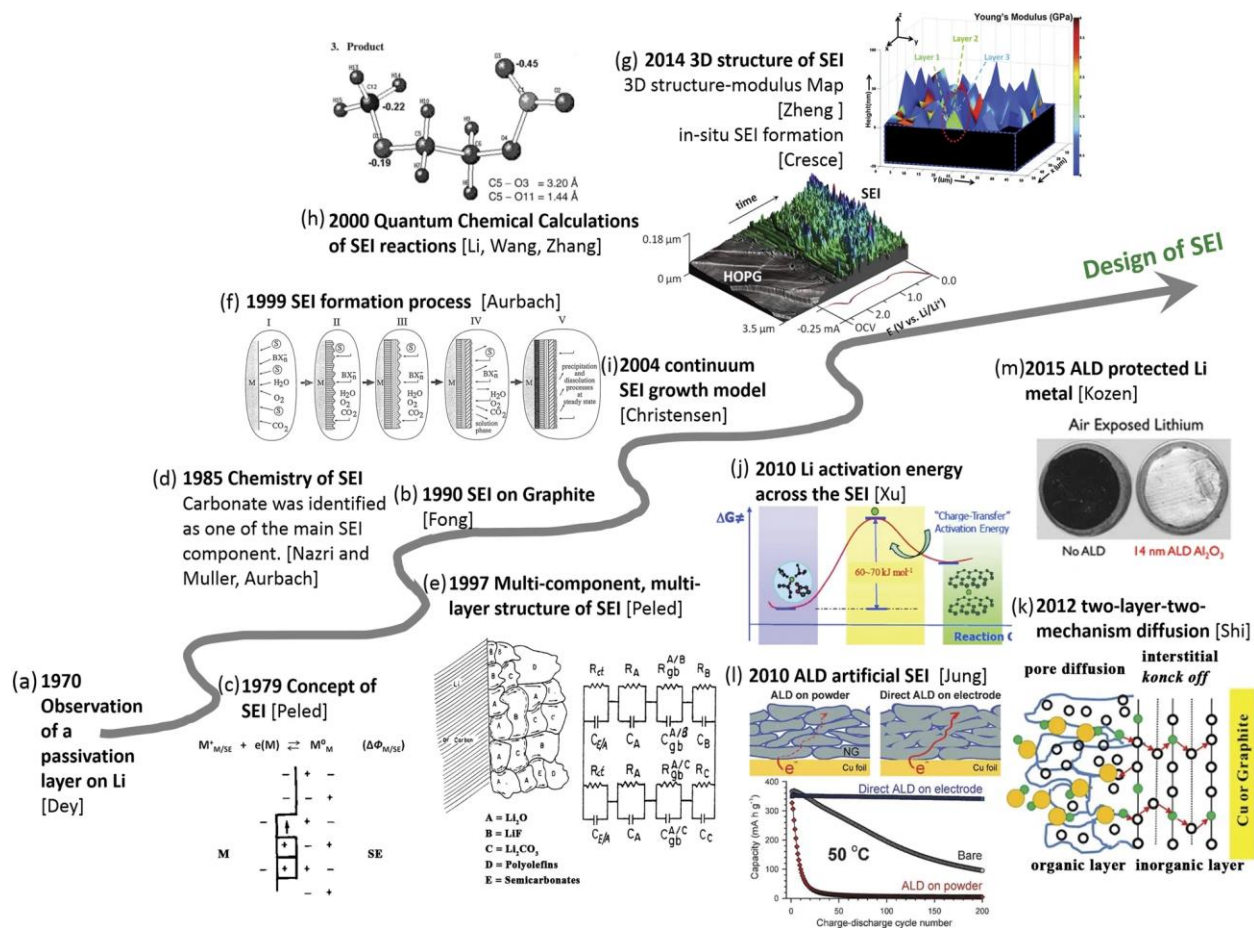
Fig.2.4. Review of the modelling progress for the anode solid electrolyte interphase (SEI) for Li-Ion batteries [22].

The progressing path of the SEI on negative electrodes, since its discovery, understanding the correct physical meaning, the designing, it is summarized through experiments and calculations within the past four decades. Where, in **a)** Early in 1970, Dey observed for the first time the passivation layer on lithium metal [29], **b)** the effective SEI layer on graphite was confirmed in 1990 [30], **c)** In 1979, Peled introduces the concept of SEI [31]. An increase of various experiments started to report the chemistry of SEI and subsequently proposed the formation mechanisms of the SEI among them as shown in **d)** Nazri and Muller [32] and Aurbach [33], which identified Li_2CO_3 as one the main components in SEI in 1985 and 1987. In **e)** Peled combined with this chemical information, introduced a pictured SEI as a mosaic structure and translated in into an equivalent circuit model (ECM) in 1997 [34]. In **f)** Aurbach illustrated the formation process of SEI starting from electrolyte reduction on electrode surface [35], **g)** shows a direct observation of the time evolution of the multi-component and multi-layer SEI formation was observed by Cresce in 2014 using in situ electrochemical AFM [36], **h)** in 2000-2001, quantum chemical calculations were employed to simulate electrolyte reduction and oxidation reaction pathways

to simulate SEI growth formation [37-39]. At **i)** in 2004, physics- based continuum models were developed to simulate SEI growth, assuming SEI is mainly Li_2CO_3 [40]. At **j)** in 2010 Xu measured the Li-ion transport energy barrier from experiment [41], **k)** based on the idea that inorganic layer of SEI is $LiCO_3$, Si calculated the Li-ion diffusion in Li_2CO_3 via a "knock-off" mechanism and, together with the porous organic layer, they proposed the two-layer/two-mechanism model [42]. In **g)** the mechanical property, namely, the Young's Modulus of SEI on a silicon anode, was measure by Zheng and they revealed modulus map along with the SEI structure map [43], **l)** the fundamental understanding of SEI lead to artificial SEI design, using atomic layer deposition, Jung, deposited nm thick Al_2O_3 coatings on an assembled graphite anode and demonstrated improved durability. In **m)** Kozen used ALD coating to protect a Li metal electrode in 2015, 45 years after Sei was observed on Li metal in the non-aqueous electrolyte [44].

To give a simple idea of the SEI failure mechanism depending on the anode materials, as illustrated in Fig. 2.5 [22].
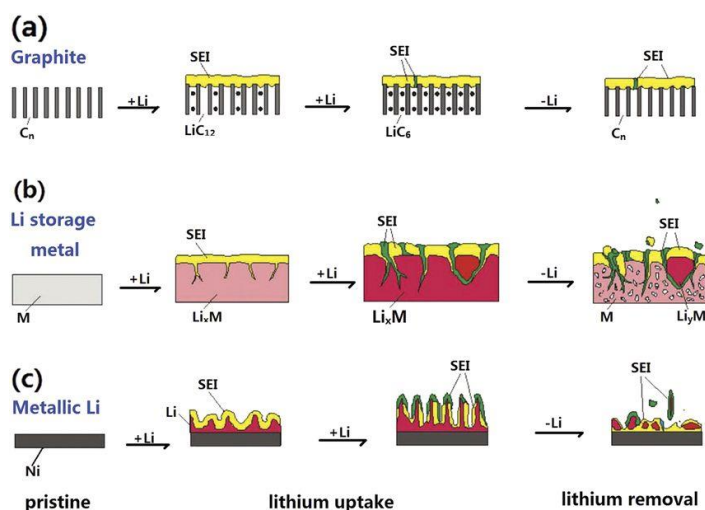
Fig. 2.5. SEI failure mechanisms for different anode materials [22].

where section **a)** shows the SEI when is relatively stable on graphite electrode but still can crack due to the volume expansion and contraction during cycling, **b)** shows more SEI mechanical failure which is expected on Li storage metals, such as Si or Sn, due to larger volume change, and **c)** shows the surface morphology change of metallic lithium which is accompanied by new SEI formation in each cycle.

Due to the fact that GICs has a low potential is favorable for increasing the battery's operating voltage, however, it meanwhile can cause other problems. The potential for the Li+ ion intercalation is so low (<0.25V versus Li/Li+) that metallic Li can be easily platted on the graphite surface during charging of LIBs, especially at high current rate and/or at cold temperature. The plated Li not only reacts with the electrolyte solvents to degrade the battery's performance, but also forms dendrites, potentially creating a safety hazard. Other drawbacks of the carbonaceous anode materials are the (10-20) % irreversible capacity in the first cycle due to the formation of SEI, low density affecting the battery's volumetric energy density, and unsuitability for fast charging due to the possibility of Li plating. Spinel $Li_4Ti_5O_{12}$ (LTO) has a 175mAh/g of theoretical capacity around 1.5V versus Li/Li+ operating voltage, it features very stable cycling stability and excellent safety. Since LTO operates at far above the reduction potentials of carbonate solvents, no SEI is formed in the first cycle [9,26,28]. Even nowadays, it is difficult for current experimental methods to characterize the SEI properties (beyond chemical composition), especially the thermodynamic and kinetic properties. Predictive modelling can

compensate for the limitations of experimental research and play an important role in understanding battery science with the length scales ranging from electrons to the full battery system as in [22,45-53]. Regarding the modeling of electrolyte reduction mechanisms, the reduction of an electrolyte on an anode surface can be viewed as the initial formation process of an SEI film, which plays an important role in the SEI composition [54,55]. It is important to explain that the electrolyte reduction mechanisms on a (bare) electrode surface might only play a role in the initial formation process of SEI. As the reduction products accumulate on the electrode surface the reduction mechanism can be different as the surface becomes more electronically insulating. This process can be considered as a part of the SEI evolution process. The simulation of this process, has not yet reached a point wherein it can be validated by experiments. EC, with high polarity and dielectric constant, is one of the most important ingredients in the electrolyte. As explained in 1995, Blint [56] calculated the binding energy of Li+ with EC and showed that it is higher than water and several other ether and carbonyl oxygen containing species. In 2000, Li and Balbuena [57], first applied QC to investigate the experimentally proposed EC reduction mechanism proposed by Aurbach [58]. It is a significant step, as the majority of Sei reaction mechanisms in the literature were deduced from experimentally observed products, and QC con confirm these mechanisms by calculating the energies of the intermediate structures along the proposed reaction pathways. Jointly, they reinforce each other to reveal the SEI formation mechanisms [22]. In 2001, Wang [59] and Zhang [60] investigated the possible reduction and oxidation pathways for EC, respectively. Following these initial QC calculations, the reduction pathways for EC have been modeled extensively [22,59,61-70]. Typically, Li-ion will be surrounded by 4-5 EC in the first solvation shell in the solution. To capture the solvent effect, Wang introduced in [59] by calculating a possible reduction processes of super-molecules of $Li^+(EC)_n$ (n=1-5) using high-level DFT method in Gaussian 98. They treated the bulk solvent as a macroscopic and continuum medium using the polarized continuum models. This detailed reaction pathways study gave many important insights. First, the solvent plays an important role. They found that isolated EC is unlikely to be reduced because of its negative adiabatic electron affinity. In fact, EC^- anion has been observed experimentally [71].

The difference between LUMO/HOMO orbitals of EC^- in gas and solution phases was shown in a later study by Yu [61]. Under the effect of a continuum solvent model, EC can be reduced via one-electron and possibly two-electron reactions in the solution. By computing the EC reduction pathways with Li^+ and increasing numbers of EC in $Li^+(EC)_n$, Wang confirmed the currently generally accepted two-step reduction pathways on the surface that $Li^+(EC)_n$ is initially reduced to an ion-pair intermediate undergoing homolytic C-O bond cleavage, giving a radical anion coordinated with Li^+ [59]. They also revealed, for the first time, all the possible products could be generated from EC decomposition, such as dilithium butylene dicarbonate (Li_2BDC), Li_2EDC, $LiO(CH_2)_2CO_2(CH_2)_2OCO_2Li$.

$Li(CH2)_2OCO_2Li$ and Li_2CO_3, some of which are just now being detected experimentally due to the difficulty in characterizing a complex system, where the formation of Li_2BDC is the most thermodynamically favored, but it has high solubility. Therefore, the compounds with low solubility in the electrolyte, such as Li_2EDC, become dominant components in SEI, as explained in [59,71]. With the development of supercomputers, *ab initio molecular dynamics* (AIMD) became feasible for larger systems [61,63,66]. With the help of AIM, Leung and Budzien tracked the initial decomposition process of liquid EC on graphite surfaces with different edge terminations. They confirmed the two EC decomposition pathways. In [59] it shows that for the first time, CO evolution, observed in experiments in [72]. The one-electron reaction pathway was further elucidated in late works [61,66] and it was confirmed by electron paramagnetic resonance spectroscopy measurement [73]. Due to the limited size in DFT- based calculations, atomistic force fields were developed and parameterized for Li-ion battery electrolyte systems to enable classical MD simulations with a longer time scale and larger system size. Classical force field, such as Condensed-phase Optimized Molecular Potentials for Atomistic Simulation Studies (COMPASS) with fixed charge, can reproduce the energetics of Li^+ interactions with organic reduction products, such as Li_2EDC and dilithium 1,2 - propylene dicarbonate (Li_2PDC) [74]. Borodin and Smith

developed a many-body polarizable force field, APPLE&P (Atomistic Polarizable Potential for Liquids, Electrolytes, and Polymers, which allows the charged ion, such as Li$^+$, to polarize the neighboring solvent molecules and anions by introducing atomic dipoles or by shifting charges in response to the electric field. They parameterized APPLE&P with QC calculations of EC and DMC complex with Li$^+$ and LiPF$_6$ [75].

Quantifying the onset voltage for EC reduction reaction is still challenging for computation at both quantum and molecular levels [67,69]. Many of the electrolyte reduction studies discussed in the mentioned references, were based on the pure EC solvent. However, the real electrolyte is usually comprised of more than one solvent and suitable additives. By taking the electrolyte mixture into account is a necessary step forwards fully comprehending the reactions at the anode/electrolyte interface [76,77]. First, every solvent and salt species will decompose at its unique voltage. Tasaki in [74] found that the order for the solvent molecule to undergo the first electron reduction is EC > PC > VC > DMC > EMC > DEC, with EC being the most likely reduced [59]. VC, on the other hand, is most likely to undergo the second electron reduction, followed by EC and PC, as VC > EC > PC. The SEI chemistry is also dictated by Li$^+$ solvation sheath, which was recently characterized by Cresce as shown in [76]. The solvent-solvent and salt-solvent local structures can dramatically change the reduction voltage and kinetics, resulting in many electrolyte concentration dependent phenomena. Another important thing is the effect of the anode surface state. The anode surface also plays an important role in determining the decomposition thermodynamics. Leung and Budzien compared EC decomposition on the basal plane of lithiated graphite (LiC6), which is terminated with =O, -OH & -H and found that C=O edges provide a larger driving force for EC reduction [63]. The observation of EC is more inclined to decompose in the presence of oxygen/hydroxyl termination is consistent with other simulation results [77]. The EC decomposition was not simulated only on graphite, but also on Li [61,78,79], Si [65,80,81], and on Sn [82] electrodes. Due to the lower potential of Li metal than graphite, the decomposition of EC on Li metal is spontaneous and much faster than that on LiC6 surfaces [61]. It was introduced in [79], where performed AIMD and showed that EC reduction pathway to form CO is energetically more favorable on the Li metal surface, different from that on graphite surface [61,66]. In [83] Camacho-Forero have shown that both DOL and DME are stable on Li metal surface during AIMD simulations, comparing with the spontaneous decomposition of EC on Li metal. They also simulated the decomposition process of lithium bis(trifluoromethanesulfonyl)imide (LiFSI) and lithium bis(fluorosulfonl)imide (LiFSI) at 1 and 4M concentrations in DME on Li metal surface and found that LiFSI shows a complete decomposition in terms of forming LiF as one of the main SEI products [78]. One of the specific applications of Li metal anode is for Li-S batteries, where the precipitation of Li2S on the anode from the shuttling of soluble polysulfide (PS) needs to be avoided. DFT and AIMD simulations have revealed that PS decomposes [57]. Regarding the buildup process of the nanometer-thick SEI layer, a kinetic Monte Carlo was used to simulate the early stage formation of SEI with regards to the lithium-ion intercalation on a graphite anode [53,105].

In addition, Ushirogata at al., [85] introduced a two-step calculation, first AIMD was performed to allow the electrolyte to decompose. Then extracted the stable SEI film components and examined their solubility in the EC solvent and their adhesion to a graphite electrode surface. They proposed a "near-shore aggregation" SEI formation mechanism, which explained in detail in Appendix, Section 8.1, Fig.A2, [85].

This "solution-mediated" mechanism instead of the "surface-mediated" mechanism would allow the formation of several tens of nanometer-thick SEI film.

Secondly, as the electrolyte is reduced, some decomposed compounds will deposit on the anode surface and gradually form the growing SEI layer [57,86].

Li-ion batteries, unlike other secondary batteries, doesn't have any redox chemical reactions, hence there is not any new chemical products. During operation, the lithium materials gets in and out of the electrodes by an intercalation reaction. Due to the open structures of the electrodes which the lithium inserts itself, and is subsequently extracted from the electrodes while the battery is discharging. During normal operation where there

are no unwanted side reactions, and hence the operation is almost completely reversible between charge and discharge. The different chemistries differ in the type of electrode used for the positive electrode to a larger extent, and in the negative electrode a graphite form is used in most of the industrial applications. In order to combine the advantages of individual compounds to result in composite cathodes. Discharge starts with all lithium in the negative electrode, graphite. Lithium that is inserted within the graphite material it's released, as it diffuses through the particle and reaches the surface of the particle. The electron, meanwhile, is conducted through the electrode which travels through the external circuit until it reaches the positive electrode. Diffusion through the electrolyte, the lithium-ion concentration in both the electrodes varies as time proceeds. In addition, there is a spatial variation of lithium concentration across the thickness of the cell. During discharging, lithium-ion concentration in both the electrodes changes as time proceeds. In addition, there is a spatial variation of lithium concentration along the thickness of the cell.

During all the chemical processes a voltage drop is occurred and the cell voltage is lower than the open-circuit voltage (OCV) during discharge. But during charging, the charge voltage must be higher than the OCV in order to account for all the transport processes [8]. But in case that the rate of discharge was too high in comparison to rate of diffusion, discharging processes will be finished earlier and lithium will not be all transferred. This effect is due to the faster and intensive reaction comparing to a low rate of diffusion within the electrode particles can result in an accumulation of lithium ion near the surface which will result on saturation. During a discharge process, different electrochemical processes are involved and occurred, such as: diffusion in the solid phase, charge transfer reaction, diffusion in the electrolyte phase, electronic conduction, diffusion in the solid phase.

In order to be more efficient in the utilization of the battery it requires to tune the rates of each process at a comparable magnitude. Based on the amount of concentration of lithium in the electrodes the rates are different, from turn maps to efficient cell configuration in terms of best thickness of the electrodes.

Given that a normal operation of a lithium-ion cell involves various processes, it can be seen that the coordination amongst these processes. Conduction in the electrolyte phase can span multiple timescales, and solid phase diffusion happens in 10-100 seconds. At the same time there are other processes slower these one, like for example, the interphase movement in electrodes that exhibit multiphase coexistence, etc. For characterization tools like the electrochemical impedance spectroscopy (EIS) the time range becomes an important variable. The basic components of the lithium-ion cell are based on the structure of the solid positive and negative electrodes sandwiching a separator and all the parts of the battery is filled with a liquid electrolyte. Still, most of the cells use the liquid electrolytes. Where the active parts, are related with those which participate in the essential physicochemical processes that convert the chemical energy to electrical or otherwise. However, the fillers or binding material are not directly considered [8]. As a matter of fact, the electrodes constituting the battery are naturally porous. This is due to the synthesis process which highly involves mixing of the active material in a solvent and then allowing the solvent to dry. Depending on the intensity of the contact and the packing density, the porous structure can have a pore size distribution in range of a micron. Due to the porous structures, the contact surface area of the active material with the electrolyte it is enhanced, which increase also the probability of the charge transfer reaction. Fig.2.6. shows a simple schematic diagram of the Li-ion battery during charging and discharging process, as the Li material moves from one side of the electrode to the other one, with different direction based on the process.
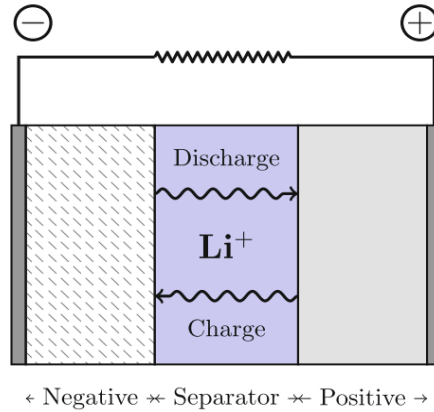
Fig.2.6. Simple schematic diagram of the Li-Ion battery

This introduces the basic framework in which the electrodes are modeled by appealing to the established porous electrode theory, as explained

The fundamental process during discharge is the transfer of Li-ion from the positive electrode to the negative electrode through the electrolyte, and opposite during charge. Each electrode section consists of the solid phase consisting of the active material, and the electrolyte, where the lithium passes through. As known, the cell is a closed system, where mass conservation is applied to the lithium in the ionized state in the electrolyte. The interaction between the solid particles of the electrode and the liquid electrolyte happen at the interface, where charge is transferred. The interaction between the solid particles of the electrode and the liquid electrolyte happen at the interface. As explained in [8], this set of 12 equations forms the fundamentals of the electrochemical model also the macro-homogeneous model. The mathematical model includes different levels of abstraction as below:

a) The solution methodology represents the porous solid phase as a collection of particles that are individually surrounded by the electrolyte phase.

b) The framework relates the electrode as a homogenous system of electrolyte and particles at every point.

c) As a consequence of the first abstraction, the diffusion of lithium in solid phase between particles is neglected. Diffusion in the solid phase is modeled, within each particle that are typically assumed to be spheres.

As confirmed the diffusion equation, which is the mass conservation equation in the solid phase, is solved in spherical coordinated to obtain the lithium surface concentration in the spheres. As the solid phase is also continuous, as matter of fact the surface concentration is the driving force for charge transfer reaction. Must be cleared that all the equations in the model are solved as a function of the thickness of the electrode, beside the diffusion in the solid phase which is solved in the spherical coordinates [8]. As explained in [2], due to this effective mapping of the output of the spherical diffusion equation into other equations that are solved in Cartesian coordinates, this model is also called as a Pseudo-2D (P2D) model.

It is important to explain the most common terms and conditions for the batteries, related with their performance and characterization.

A single cell is complete battery with two current leads and separated compartment holding electrodes, separator, and electrolyte. A module is composed of a few cells either by physical attachment or by welding in between cells. It is crucial to be connected very good with low resistance contact otherwise it will be a big problem for the thermal stability of all the pack, especially in high current charging/discharging situations. A pack is made by the electrical connections of modules. Due to the pack complexity the required safety level is higher. Also, the pack is completed as a single system for the thermal management. Fig. 2.7 shows the rhombohedral cell configuration.
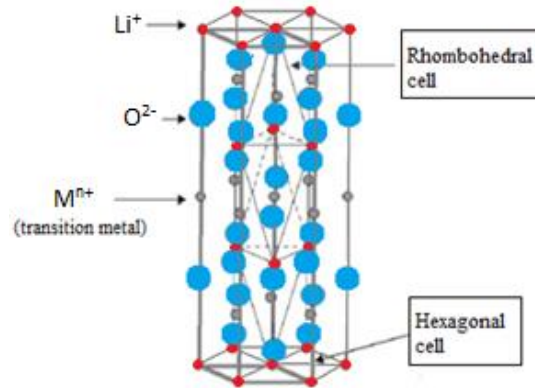
Fig.2.7. Relation between rhombohedral cell and hexagonal cell [1].

The most common forms and types of li-ion cells are enclosure as:

a) Cylindrical cells: worldwide used standard form factor for lithium-ion batteries is the small format (less than 5Ah) cylindrical cells. The two typical standard sizes are referred to 18650 which stands for 18mm diameter and 65mm in length and the second to 26650 with 26mm diameter and 65mm in length. Cylindrical cells use a single "jelly-roll" of electrodes and separator. Fig. 2.8. shows a typical 18650 cell structural composition.
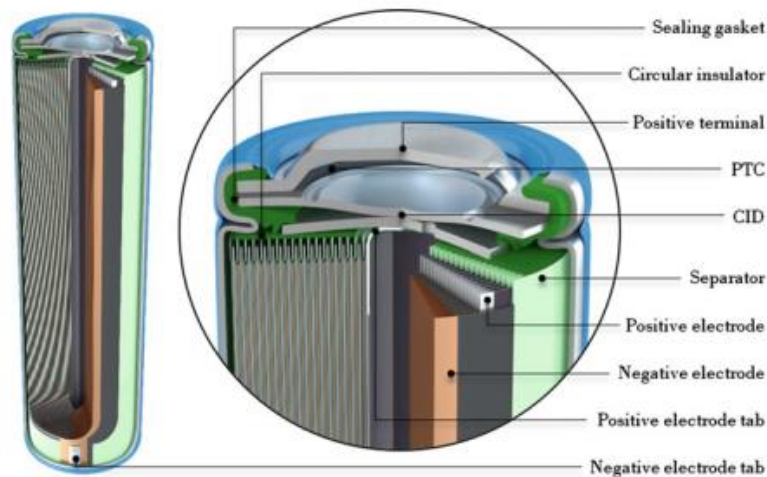
Fig.2.8. Structural composition of a common cylindrical 18650 cell [89].

b) Prismatic cells: a reliable metallic enclosure shaped in rectangular form. For a better enclosure it is sealed by a laser welding process after the assembly but before electrolyte filling [88]. Prismatic cells can be more tightly packed than cylindrical cells and at the same time are wider variety of sizes and shapes available. Vent and terminal locations may vary between manufactures. The structural composition of prismatic cell is shown in Fig.2.9.
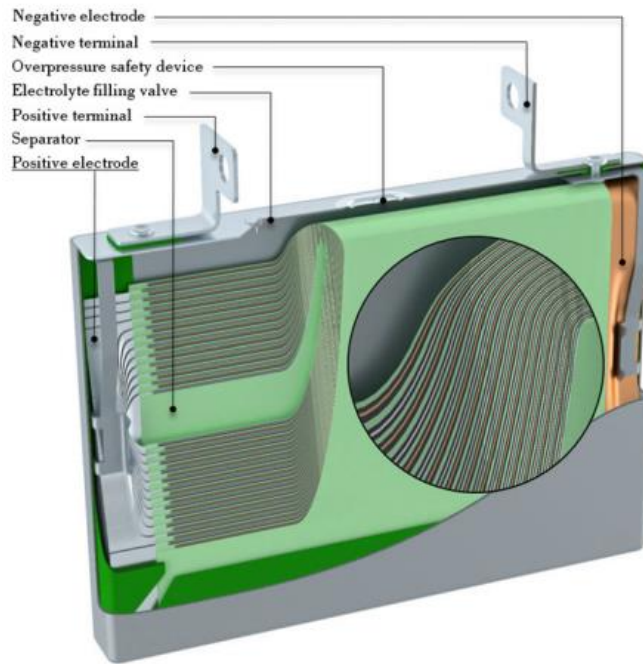
Fig. 2.9. Structural composition of a prismatic cell [89].

c) Pouch cells: are enclosed in a pouch made from two pieces of plastic film fused together around the periphery. Metallic tabs protrude from the pouch in order to be connected to the cell. Usually pouch cells are very flat in one dimension which is the direction in which the li-ions travel. The compose method of the electrode and separator may be folded, stacked or wound in pouch or prismatic cells. The structural composition of pouch cell is shown in Fig.2.10.
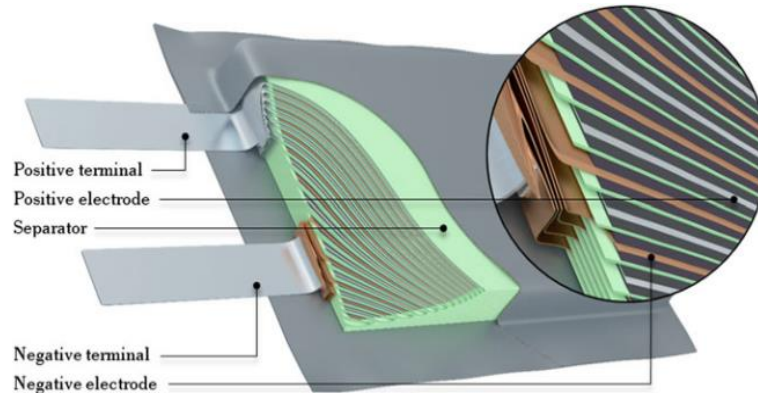
Fig. 2.10. Structural composition of a stacked pouch cell [89].

As mentioned before, the mass conservation in the solid phase of the active materials for both the electrodes is derived. The porous electrode constitutes of individual particles represented as spheres, which interact through the electrolyte.

The nickel-cadmium battery (NiCd or NiCad battery) is a type of rechargeable battery which use nickel oxide hydroxide and metallic cadmium as electrodes. As a matter of fact, the NiCd lost their dominance in the share market of applications in early 1990s when the improvement of actual and material batteries such as NiMH and Li-Ion. NiCd has a terminal voltage during discharge of around 1.2V which decreases little until nearly the end of discharge. NiCd batteries are made in a wide range of manufacturing properties such as size, capacities, from portable sealed types interchangeable with carbon-zinc dry cells, up to large scale ventilated cells used for stationary power or motive power in infrastructure applications. Figs. 2.11 and 2.12 shows the structure composition of NiCd and NiMH respectively.
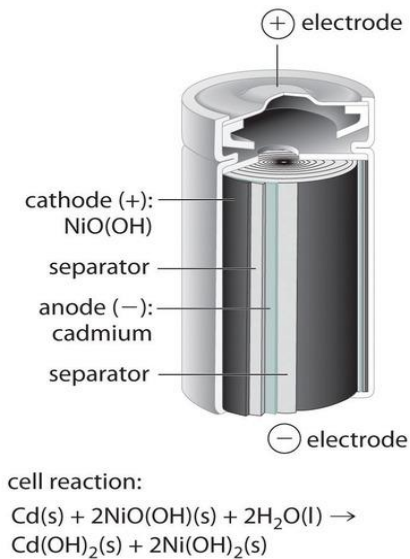
Fig. 2.11. Structural composition of NiCd cell [90]   Fig. 2.12. Structural composition of a NiMH cell [91]
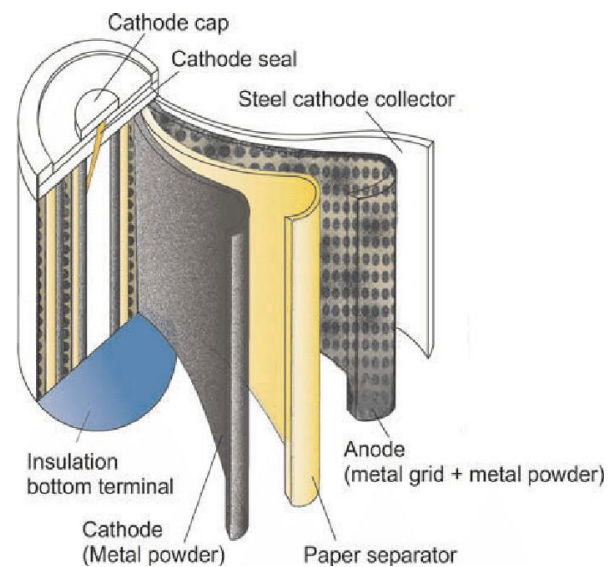
 Due to the constant improvement in chemical composition also in technological manufacturing, have increased the capacity of NiMH and decreased the cost of the battery, making them usable in a wide range of applications such as portable power tools, photography equipment, flashlights, emergency lighting, hobby R/C and portable electronic devices. Regarding the electrical properties and characteristics of the NiCd and NiMH, in general they give good values as the maximum discharge rate is approximately 1.8A, for a D size battery rate be as high as 3.5A. In case of model-aircraft, boats or even drones, it can take much larger currents even up to a hundred amps or so from specially constructed NiCd batteries, where mostly used to drive main motors. In case of 5minutes model operation for high current drain applications is easily achievable form quite small batteries, in some case even up to 10 minutes where a reasonable high power to weight configuration is achieved, comparable to internal combustion motors, though of lesser duration. In this, however, they have been largely overpassed in quality and performance by Li-Ion composition, specifically by lithium polymer (LiPO) and lithium iron phosphate (LiFe) batteries, which can provide higher energy densities.

NiCd have a nominal cell potential of 1.2V, which comparing with the alkaline and zinc-carbon primary cells are 1.5V. But the primary battery first are not rechargeable, so only 1 time use after full discharge, secondly their nominal voltage doesn't maintain in such levels but it drops very fast from 1.5V. Which comparing with the NiCd or NiMH cells terminal voltage only changes a little as it fully discharges. In general, electronic devices are designed to operate with continues DC voltage in low range 0.9V to 1V makes them appropriate to work

with primary or secondary batteries as NiCd or NiMH where the steady 1.2V is enough to allow a normal operation within its nominal values.

NiCd and NiMH offers a wide range of charging rates, depending on how the cell was manufactured. The definition of charge rate stands for the percentage of the amp-hour capacity the battery is fed as a steady current over the duration of the charge. Beside the charge speed, depending on the case and application scenario, we might need more energy to be supplied to the battery than its actual or rated capacity. Without forgetting to account the energy loss during charging, with faster charges targeting the efficiency as well.

Regarding the electrochemistry composition of NiCd is based on few parts as a nickel oxide-hydroxide positive electrode plate, a cadmium negative electrode plate, a separator and an alkaline electrolyte (potassium hydroxide). NiCd batteries in most of the cases is composed by a metal case with a sealing plate incorporated with a self-sealing as a safety valve. Where the positive and negative electrode plates, are isolated from each other by the separator, which are rolled in a spiral shape inside the case. This design is known as the jelly-roll structure and allows a NiCd to deliver an improved and higher current than a regular size alkaline cell. Usually alkaline cells have a bobbin construction where the cell casing is filled with electrolyte and contains a graphite rod, which acts as the positive electrode. As a matter of fact, a small area of the electrode is in contact with the electrolyte, which makes the internal resistance for an equivalent sized alkaline cell to higher, and so the maximum current which can be delivered is limited. Below are the chemical reactions at the cadmium electrode during discharge:

$$Cd + 2OH^- \rightarrow Cd(OH)_2 + 2e^-$$ (2.1)

Chemical reaction expressed at the nickel oxide electrode is:

$$2Ni(OH) + 2H_2O + 2e^- \rightarrow 2Ni(OH)_2 + 2OH^-$$ (2.2)

During discharge the net reaction is:

$$2NiO(OH) + Cd + 2H_2O \rightarrow 2Ni(OH)_2 + Cd(OH)_2$$ (2.3)

During charging, the reactions is the opposite of the above equations, from right to left. The alkaline electrolyte is not consumed in this reaction and therefore its specific gravity, which unlike from the Pb batteries, is not a guide to its SoC.

Regarding the NiMH battery operation, also uses positive plates with nickel oxyhydroxide (NiOOH) as the active material and aqueous potassium hydroxide electrolyte which are usually added with lithium hydroxide for increased cathode charging efficiency [92]. The NiMH batteries differ from the NiCd in that the active material in the negative plate is a hydrogen absorbing intermetallic allow, where the metal alloys fall mainly into two classes (Shukla and Martha et al. 2001), [93]:

a) the AB_5 alloys, which combine a rare earth element that forms stable hydrides (lanthanum, cerium, neodymium, praseodymium, yttrium or their mixture) with Ni, which is sometimes doped with cobalt, aluminum, or tin

b) the AB_2 alloys, which are a combination of titanium, vanadium, or zirconium (A-site) with zirconium or nickel, modified with manganese, chromium, cobalt, vanadium, or iron (B-site) based on nickel commonly blended with titanium, vanadium, and zirconium.

While AB_2 alloys yield higher energy storage densities, AB_5 alloys can hold hydrogen better, thus lowering the self-discharge rate of the battery. AB_5 alloys are also less expensive and easier to use (Hariprakash et al., 2009; Sakai et al., 1991; Shukla et al., 2001).

The equations which explains the charging/discharging process in positive and negative plates are shown as below:
Where at the positive plate

$$NiOOH + H_2O + e^- \rightarrow Ni(OH)_2 + OH^- \quad (E^\circ = 0.49V) \tag{2.4}$$
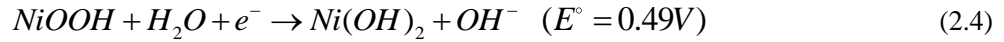
At the negative plate:

$$MH + OH^- \rightarrow M + H_2O + e^- \quad (E^\circ = -0.83V) \tag{2.5}$$
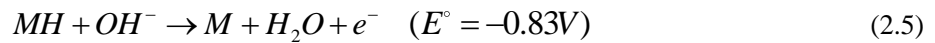
In Fig. 2. 13 is shown the schematic of NiMH battery, for the charging/discharging process.
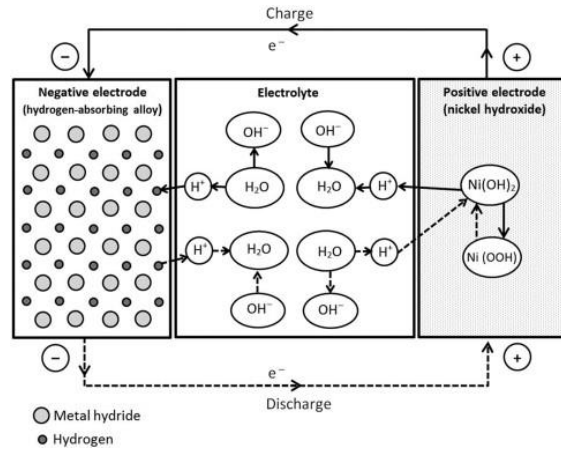
Fig. 2.13. Schematic of a normal operation for NiMH battery [93].

Regarding the overall cell reaction:

$$NiOOH + MH \rightarrow Ni(OH)_2 + M \quad (V^\circ = 1.35V) \tag{2.6}$$

It must be clear that the electrolyte quantity or concentration does not go through any net change over charge/discharge cycles. In equations (2.4) and (2.5), water generated is part of a closed loop process from a creation and absorption cycle, where during charging is consumed and during discharging is processed. This is given as an advantage from the manufactures of the NiMH over NiCd, especially combined with its sealed construction [93].

When it comes to Pb batteries, the path to the actual technology is quite long. It starts with early 1880s, when an improved Pb battery with high capacity and relatively simple technology of manufacture was created. This rapidly found various practical applications. In 1881, Gustave Trouve first use a Pb battery in his three-wheeled electric automobile, reaching a speed of 12km/h. in 1886, the first submarine propelled by Pb batteries was launched in France. A Pb battery was mounted in a small dirigible balloon which was propelled at a speed

of 4m/s. In 1899, Camille Jenatzy reached a speed record of 109km/h with his cigar-shaped electric car powered with lead-acid batteries [87]. In 1881 Camille Alphonse Faure invented an improved version that consisted of a lead grid lattice, into which a lead oxide paste is pressed, forming a plate. This design was easier for mass produce since then. Later, an improved version started to use a gel electrolyte instead of a liquid allowing the battery to be used in different positions without leaking. In Fig. 2. 14 is shown a cutaway view of Pb battery cell.

cell reaction:
$$Pb(s) + PbO_2(s) + 2HSO_4^-(aq) + 2H^+(aq) \rightarrow 2PbSO_4(s) + 2H_2O(l)$$
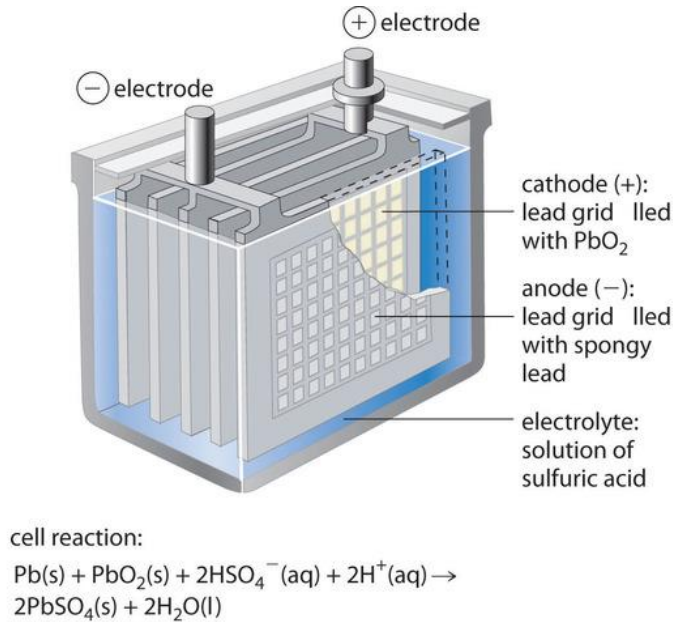
Fig. 2.14. Cutaway view of a Pb cell with its components [93].

Regarding the electrochemistry introduces interesting characteristics. In the discharged state the positive and negative become lead sulfate (PbSO4) and the electrolyte loses a considered amount of its dissolved sulfuric acid and which later primarily becomes water. The discharge process is driven by the pronounced reduction in energy when 2 H+ (hydrated protons) of the acid react with O2- ions of PbO2 in order to form the strong O-H bonds in H2O (ca- 880kJ per 18g of water.) [94]. This is a highly exergonic process which also compensates for the energetically unfavorable formation of Pb2+ ions or lead sulfate (PbSO4). Where in negative plate reaction is explained with the chemical reaction:

$$Pb + HSO_4^- \rightarrow PbSO_4 + H^+ + 2e^- \tag{2.7}$$
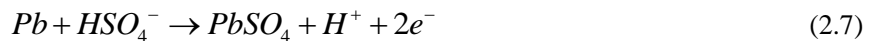
The release of two conducting electrons gives the lead electrode a negative charge. During the process where electrons accumulate, they create an electric field which attracts hydrogen ions and repels sulfate ions, which leads to a double-layer near the surface. The hydrogen ions screen the charge electrode from the solution. This will limit further reaction.

On the other hand, in the positive plate reaction is expressed by the following chemical equation:

$$PbO_2 + HSO_4^- + 3H^+ + 2e^- \rightarrow PbSO_4 + 2H_2O \tag{2.8}$$
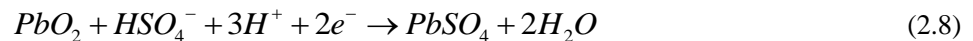
Including the advantages of the metallic conductivity of PbO2, the total reaction can be written as:
$$Pb + PbO_2 + 2H_2SO_4 \rightarrow 2PbSO_4 + 2H_2O$$

The net energy released per mol (207g) of Pb converted to PbSO4 is 400kJ, which is related to the formation of 36g of water. The sum of the molecular masses of the reactants is 641.6 g/mol, where theoretically a cell can produce two faradays of charge, from 641.6g of reactants, or 82.8Ah per kg. In case of 2V cell, this is related to 167Wh per kg of reactants, but in practice a Pb cell gives only (30-40) Wh per kg of battery, as a constrain due the fact of water mass and other constituent parts. In Tables 2.1 and 2.2 are shown the electrical properties of various batteries and their performances comparison [95,96].

Table 2.1. Electrical properties of various batteries [95,96]

System	Voltage (V)	Specific Energy (Wh kg^{-1})	Energy Density (Wh L^{-1})	Power Density (W kg^{-1})	Specific Energy of Cell* (Wh kg^{-1})	Specific Energy of Battery* (100% SOC) (Wh kg^{-1})
Sealed lead—acid (LA)	2.1	30—40	60—75	180	20—35	20—35
Nickel—cadmium (Ni—Cd)	1.2	40—60	50—150	150	40—60	40—60
Nickel-metal hydride (Ni—MH)	1.2	30—80	140—300	250—1000	50—70	40—70
Lithium-ion LiCoO$_2$	3.6	160	270	1800		
Lithium polymer	3.7	130—200	300	3000		
Lithium-ion LiFePO$_4$	3.25	80—120	170	1400		

Table 2.2. Comparison of advantages and disadvantages of each battery type [95,96]

System	Voltage (V)	Energy Cost (Wh $\$^{-1}$)	Advantages	Disadvantages
Sealed lead—acid (LA)	2.1	5—8	Cheap	Heavy
Nickel—cadmium (Ni—Cd)	1.2	2—4	Reliable, inexpensive, high discharge rate, good low temperature behaviour	Heavy, toxic material, memory effect
Nickel-metal hydride (Ni—MH)	1.2	1.4—2.8	High energy density, environment friendly	Higher internal resistance, gas formation, self-discharge
Lithium-ion LiCoO$_2$	3.6	3—5	High specific energy, low self-discharge	Expensive, requires safety electronics
Lithium-polymer	3.7	3—5	High specific energy, low self-discharge	Expensive, requires safety electronics
Lithium-ion LiFePO$_4$	3.25	0.7—1.6	Safe	Technology in development

2.3   Deterioration & Safety features

For many years, and nickel-cadmium Ni-Cd had been the only suitable battery for portable equipment from wireless communications to mobile devices such as cellphone, accessories, laptop etc. Nickel-metal-hybrid Ni-MH and Li-Ion emerged in the early 1990s, as best and reliable storage systems. Their competition was well known in the beginning, fighting nose-to-nose to gain customer's attention and acceptance. Nowadays, Li-Ion is the fastest growing and most promising battery chemistry. Li-Ion is the lightest of all metal, has the greatest electrochemical potential and provides the largest energy density for weight. Attempts are constantly made to develop rechargeable lithium batteries failed due to safety problems. Because of the inherent instability of lithium metal, especially during charging, research shifted to a non-metallic lithium battery using lithium ions. Although slightly lower in energy density than lithium metal, Li-Ion is safe, provided certain precautions are met when charging and discharging. In 1991, the Sony Corporation commercialized the firs Li-Ion battery. The energy density of Li-Ion is typically twice that of the standard Ni-Cd. There is potential for higher energy densities. The load characteristics are reasonably good and behave similarly to Ni-Cd in terms of discharge. The high cell 3.6V to 4.1V and 4.2V allows battery pack designs with only one cell. Most of today's mobile phones

run on single cell. A nickel-based pack would require three 1.2V cells connected in series. Should be mention that NiCd and NiMH cells maintain stable and steady value of 1.2V even near full discharge, but in some applications, this would be considered as a drawback, because it makes it difficult to detect when the battery charge is low. Lithium-ion is a low maintenance battery, an advantage that most other chemistries cannot claim. There is no memory and no scheduled cycling is required to prolong the battery's life. In addition, the self-discharge is less than half compared to nickel-cadmium, making lithium-ion well suited for modern fuel gauge applications. Li-Ion cells cause little harm when disposed. Despite its overall advantages, lithium-ion has its drawbacks. It is fragile and requires a protection circuit to maintain safe operation. Built into each pack, the protection circuit limits the peak voltage of each cell during charge and prevents the cell voltage from dropping too low on discharge. In addition, the cell temperature is monitored to prevent temperature extremes. The maximum charge and discharge current on most packs are is limited to between 1C and 2C. With these precautions in place, the possibility of metallic lithium plating occurring due to overcharge is virtually eliminated. Another important concern with most of rechargeable batteries, especially for high current drain applications, is the aging process. For all the manufactures remain silent about this issue. Some capacity deterioration is noticeable after one year, whether the battery is in use or not. The battery frequently fails after two or three years. It should be clear that other chemistries also have age-related degenerative effects. Especially for Ni-MH if exposed to high ambient temperatures. At the same time, Li-Ion packs are known to have served for five years in some applications. Manufactures are constantly improving Li-Ion. New and enhanced chemical combinations are introduced every six months or so. With such rapid progress, it is difficult to assess how well the revised battery will age. Storage in a cool place slows the aging process of Li-Ion. Manufactures recommend storage temperatures of $15°$ C to $35°$ C. In addition, the battery should be partially charged during storage. The manufactures recommend a 40% charge. The most economical Li-Ion battery in terms of cost-to-energy ratio is the cylindrical 18650. Regarding the lithium-polymer differentiates itself form conventional battery systems in the type of electrolyte used. This electrolyte resembles a plastic-like film that does not conduct electricity but allows ion exchange. The polymer electrolyte replaces the traditional porous separator, which is soaked with electrolyte. The dry polymer design offers simplifications with respect to fabrication, ruggedness, safety and thin-profile geometry. With a cell thickness measuring as little as one millimeter, equipment designers are left to their own imagination in terms of form, shape and size. But the dry Lithium polymer suffers from poor conductivity the internal resistance is too high and cannot deliver the current bursts needed to power modern communication devices and spin up the hard drives of mobile computing equipment. Heating the cell to $60°$ C and higher increases the conductivity, but it is not acceptable for portable applications. To compromise, some gelled electrolyte has been added. The commercial cells use a separator/electrolyte membrane prepared from the same traditional porous polyethylene or polypropylene separator filled with a polymer, which gets upon filling with the liquid electrolyte. Thus, the commercial Li-Ion polymer cells are very similar and materials to their electrolyte counter parts. No improvements in capacity gains are achieved - in fact, the capacity is slightly less than that of the standard lithium-ion battery. Lithium-ion-polymer finds its market niche in wafer-thin geometries, such as batteries for credit cards and other such applications [88]. More details are shown in Appendix, 8.1, Figs.A.7 and A.8

For example, contamination from moisture and dust must be removed and eliminated during the assembly process. As a matter of fact, humidity is factor which affect the lifetime of the battery, speeding up the deterioration process. All the steps are carefully checked and under rigorous inspection in order to increase the mechanical, electrical and thermic protection of the battery. Finally, each cell is subjected to a specific aging process in order to select out cells with micro shorts and to categorize cells by capacity which will follow the assembling procedure into battery packs. This is a process designed to identify cells with internal cell faults and micro shorts which are detected during cell fabrication.

Another type of cell fabrication, which shows some differences in the manufacturing process and safety protocols. Few changes are made during manufacturing comparing with cylindrical cells, due to the opposed the geometrical composition. Where the prismatic cells use an aluminum cell case in order to decrease its weight, and an aluminum-laminated material is used in order to decrease the thickness of the battery based on standard (4.5mm or less). For the cylindrical cell, the negative electrode, tab is welded to the bottom of the can, in case of the prismatic cell with an aluminum case, the positive tab is welded to the aluminum case. For the prismatic cell, a top cap and a tab usually are laser-welded to the cell case. If previous processes are not carried out in a dry room, the cells are dried under vacuum, overnight or for 24 hours, in order to extract any water in the cells.

Another important type of procedure for researchers is the depth profile analysis of positive and negative electrode material after charge/discharge. When depth profile is performed, it is observed that the Li is segregated in an area size of about 30nm on the surface, as shown in Fig. 2.15
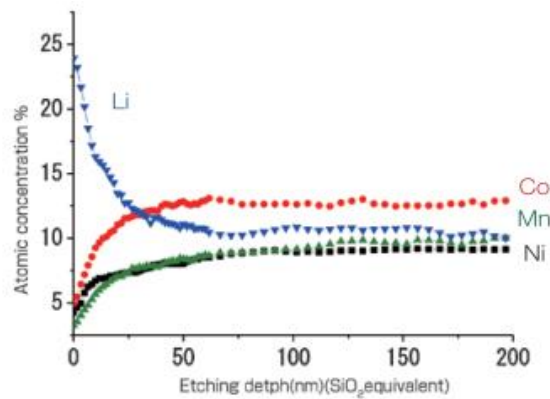
Fig. 2.15. Depth profile analysis of positive electrode material, Li [89]

A simple explanation is given in this thesis just to introduce to the readers about it, which is out of focus for this research.

Regarding the NiMH or NiCd the ability for high current drain during discharging also during charging can affect the lifetime of the battery if the temperature is not maintained within the safety zone. In case of 1C ration which stands for 1-hour charging or discharging process of the battery, we might achieve a rough 85% SoC of the cell. But also, some specialized batteries can be charged within 10 to 15 minutes at a 4C or 6C charge rate, but it is very uncommon scenario. It greatly increases the risk of the cells to get overheated and as a consequence venting due to an internal overpressure condition. Where the cell's temperature rises due to the relation with internal resistance value and the square of the charging rate. At a 4C rate, the correct amount of heat generated inside the cell can reach up to sixteen times higher than the value achieved at 1C rate. The main downside of such operation is the fast increase of internal impedance, which means a very fast deterioration of the battery, which in some scenarios might end with dangerous consequences as fire expose or explosions. In Fig 2. 16. is shown a comparison of discharge characteristics of NiCd and NiMH. The tests are taken from a NiCd and NiMH cylindrical cells at 20˚C, where the cell height =42mm, cell diameter=16.5mm, charging ratio of 1C, discharging ratio of 0.2C
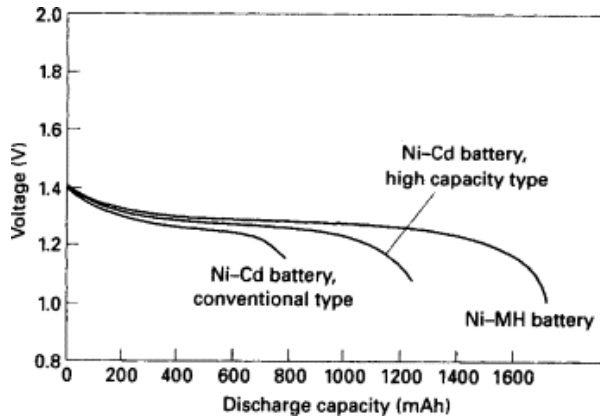
Fig. 2.16. Comparison of discharge characteristics [91]

The safe temperature range during high current operation is recommended by the manufacturer, should be in the range between -20˚C to 45˚C. During charging, the battery temperature usually is low, around the same as the ambient temperature, but as the battery nears full charge the temperature will rise to 45–50 °C. Some battery chargers which detect this temperature, increase to cut-off charging and prevent over-charging effect.

Another drawback of the NiMH and NiCd batteries is the self-discharge effect and memory effect, which makes the self-discharge where are not during charging/discharging process, approximately 10% per month at 20˚C, and up to 20 % discharge per month in case of higher temperature.

It is possible and recommended by the manufacturer, to perform a trickle charge at current levels just high enough to offset this discharge rate; in order to keep a battery fully charged. However, if the battery is going to be stored unused for a long period of time, it should be discharged down to at most 43% of capacity. It is common among researchers and manufacturers to recommend a fully discharging and even short-circuiting once it's fully discharged.

Sealed Ni–Cd cells consist of a pressure vessel that is supposed to contain any generation of oxygen and hydrogen gases until they can recombine back to water. Such generation typically occurs during rapid charge and discharge, and exceedingly at overcharge condition. It should be aware that in case the pressure exceeds the limit of the safety valve, water in the form of gas is lost. Since the vessel is designed to contain an exact amount of electrolyte this loss will rapidly affect the capacity of the cell and its ability to receive and deliver current. In order to detect and evaluate all conditions of overcharge demands, are required better and improved sophistication techniques from the charging circuit, where in case of a cheap charger an eventual damage it's normal to be occurred, even on the best quality cells.

2.4   Re-used secondary batteries and their applications

At the end of twentieth century, due to the fast increase of petroleum consumption in worldwide level, the first symptoms of a petrol crisis immediately appeared. The first to react to such a crisis, where the automobile manufacturers which decided to reduce petrol consumption by combining an electrical engine with an internal combustion engine to propel the vehicle. The hybrid electric vehicle (HEV), and depending on the level of involvement of the electric motor in the propulsion of the vehicle (battery as input source) several types of HEVs have been developed. Below are listed the types:

a) Full HEVs. In this case of automobile, the electric battery system is used mainly when the internal combustion engine works at a low efficiency and when high power is demanded. The battery is partially discharge during operation of the electric motor and recharged by the internal combustion engine. Another important process which helps with the charging process is the regenerative braking. As a

24

standard the electric systems operates at over 200V. from the actual data retrieved from the manufacturers, only by implementing this electric motor operation the fuel consumption is reduced 38% to 42% in some specific car models it can reach up to 45% fuel reduction.

b) Mild HEVs. The electric system is used mainly during the acceleration phase and for starting the vehicle. Regenerative charging of the battery when the vehicle decelerates or stops is essential for reducing the fuel consumption. The electric system in mild HEVs operates between 100V & 200V and the fuel consumption reduction in the range 14% to 19% depending on the driving mode.

c) Micro HEVs. This type uses the so-called start-stop system which turns off the engine when the car stops and the battery takes over the electric supply used for all accessories. It is confirmed that during urban driving mode, it can reduce the fuel consumption about 7%.

d) Plug HEVs. In this hybrid vehicle version, the main power supply is used to charge the battery. This system support both approaches that one of a full electric vehicles, and the conventional automobile powered by an internal combustion engine.

The full electric vehicles are driven by electric motors only, are powered only by one type of source which is the battery pack and it can be recharge from an external electric power source. For a long time, NiMH batteries where the main energy type to feed to instantaneous and high-power demand for application in full HEVs. Development to make the Li-Ion as the main suitable energy source for the HEV market in terms of cost as well, are made and introduce already as a convenient cost-performance option. Fig.2.17 shows the required energy and power for various types of HEVs.
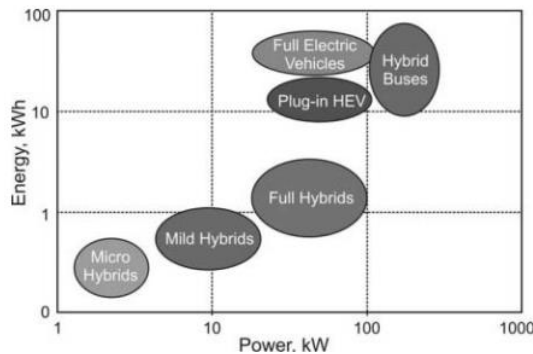
Fig. 2.17. Energy and power demands on batteries for various types of HEVs [96]

However, the Pb battery face a big problem due to the deterioration effect and mostly related with the negative plates such as:

a) The negative cannot receive high current which are generated on regenerative breaking,
b) Due to the partial SoC operation, it helps to a rapid sulfation of the negative plates.

As a matter of fact, batteries in conventional cars and micro HEVs operate at over 90% SoC with up to 5% DoD. Due to these high SoC levels, the negative plates do not suffer from sulfation. Batteries in mild HEV duties, can operate in different scenario, 70% to 90%, or 75% to 90% or even 65% to 90%. Based on these ranges, the negative plates undergo slow sulfation and it is required a special operation is needed to reverse this process. The heaviest operation is in case of full HEV batteries. Batteries in these applications operate within the (30-80) % SoC region, which facilitates rapid sulfation of the negative plates. These processes make Pb not good for the above mentioned HEV modes.

3. Artificial Neural Network (ANN) Logic

3.1 State of art

Artificial Neural Network (ANN) is the definition of the Machine Learning (ML) branch of artificial intelligence (AI) research which aims to simulate intelligent behavior by mimicking the way of biological neural networks work. It is the target of AI methods to focus on better quality of reproducing human intelligence. The focus of ANN is to imitate the same path that human does for resolving different problems [97]. It is known the "difficult age" in few decades of the ANN time path, before they reach the actual credibility and quality. Once classified as an eccentric and unpromising algorithm for the analysis of scientific data, the ANN has been improved in flash speed this last decade, into a powerful computational tool. Nowadays it can be used in all areas of science. ML in general definition is expressed as a computational method using "*experience*" to improve performance or to make accurate predictions. Where the *experience* refers to the past information available to the learner, which typically takes the form of electronic data collected, and it's made available for analysis. The nature of data could be so different, reach in diversity, complexity and behavior in form of digitized human-labeled training sets, or other types of information obtained via interaction with the environment. But how the data are retrieved, how they are analyzed, how to define the level of quality and size and amount of info. As matter of fact ML consists of designing efficient and accurate prediction algorithms. Also, some critical measures of the quality of these algorithms are their time and space complexity. But, in ML we will need additionally a notion of sample complexity to evaluate the sample size required for the algorithm. From the theoretical learning guarantees for an algorithm depend on the complexity of the concept classes considered and the size of the training sample.

The success of a learning algorithm depends on the data used, ML is inherently related to data analysis and statistics. Where the learning techniques are data-driven methods combining fundamental concepts in computer science with approach from probability, statistics, optimization. The key characteristics of an (ANN), is its ability to learn. In case that a specific mathematical model is already known and possible can describe a data, in this case ANN is unlikely to be needed, but when the logical function and rules are known only partially, or not at all, then it is possible from ANN to discover interesting relationships due to its ability to rambles in between and through the databases. NN are able to learn complex behavior and have impressive ability to adapt, even in case of a brief study they can show the ability to complete a wide genre of tasks. Where the most characteristic property of ANN's is their ability to discern patterns. However, despite the fact that this method shows interesting abilities, the main notable drawback is the "black box" solvers. The so known "rule discovery networks" which can identify and report the rules which underlie a data set, but still somehow is way from being a routine laboratory tool.

Learning algorithms have been successfully deployed in a variety of applications, as listed below:

a) Speech recognition, speech synthesis, speaker verification,

b) Computer vision tasks, e.g., image recognition, face detection,

c) Optical character recognition (OCR),

d) Natural language processing, part of speech tagging,

e) Computational biology applications, e.g., protein function, medicine testing structure or structured prediction,

f) Text or document classification, e.g., spam detection,

g) Fraud detection (credit card, telephone) and network intrusion,

h) Unassisted vehicle control (robots, navigation),

i) Games, e.g., chess, backgammon,

j) Medical diagnosis,

k) Classification, systems optimization, generalization, detection of faults and assisted-decision making approach,

l) Recommendation systems, search engines, information extraction systems.

Should be clear that the mentioned point above are not the only possible field of application. This list is by no means comprehensive, and learning algorithms are applied to new applications every day.

Classification: Assign a category to each item. For example, document classification may assign items with categories such as politics, business, sports, or weather while image classification may assign items with categories such as landscape, por- trait, or animal. The number of categories in such tasks is often relatively small, but can be large in some difficult tasks and even unbounded as in OCR, text classification, or speech recognition.

Regression: Predict a real value for each item. Examples of regression include prediction of stock values or variations of economic variables. In this problem, the penalty for an incorrect prediction depends on the magnitude of the difference between the true and predicted values, in contrast with the classification problem, where there is typically no notion of closeness between various categories.

Ranking: Order items according to some criterion. Web search, e.g., returning web pages relevant to a search query, is the canonical ranking example. Many other similar ranking problems arise in the context of the design of information extraction or natural language processing systems.

Clustering: Partition items into homogeneous regions. Clustering is often performed to analyze very large data sets. For example, in the context of social network analysis, clustering algorithms attempt to identify "communities" within large groups of people.

Dimensionality reduction or manifold learning: Transform an initial representation of items into a lower-dimensional representation of these items while preserving some properties of the initial representation. A common example involves preprocessing digital images in computer vision tasks.

3.2 Neuron Model and Network Architectures

The general composition of neural networks (NN) is based on simple elements which operates in parallel. Which, as was mentioned previously these elements are inspired by biological nervous systems. The network function is explicitly determined largely from the level and quality of this connections between elements. The NN itself must be trained in order to perform a specific function or task through the process of adjusting the values of the connections, called as "weights" between elements. Naturally the NN are in constant process of changes, adaptation, adjusted or trained so that specific input can be correctly connected with the output based on the "black box" approach or logic.
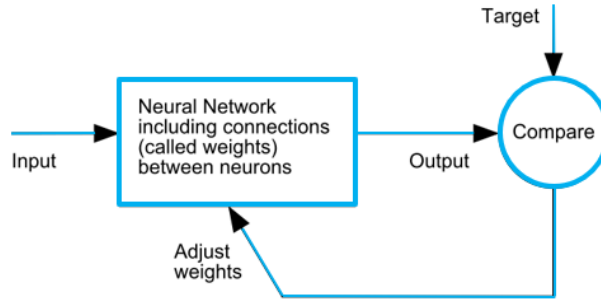
Fig. 3.1. Simple diagram of ANN model based on supervised learning

Batch training of the NN progress from the changes of weight and bias values based on an entire set of input vectors. A continues process of trainings changes the value of weights and biases or known as the coefficients, as a need of presentation for each specific input vector. The continues or aggressive training is referred with the name adaptive or on-line training model. The main goal and ability of NN is the training process which makes it useful to resolve problems which are difficult for conventional computers or human beings.

The neuron model and the structure of the NN describe how a network transforms its relation between input and output. This configuration can be viewed as a computation. This relation can be names as a computation. Based on the model and structure of each NN it possible to express its quality and limitations on what this specific NN can compute. It is necessary to explain the basic components which create the Neuron Model. A neuron with a single scalar input with or without is shown in Fig.3.2.
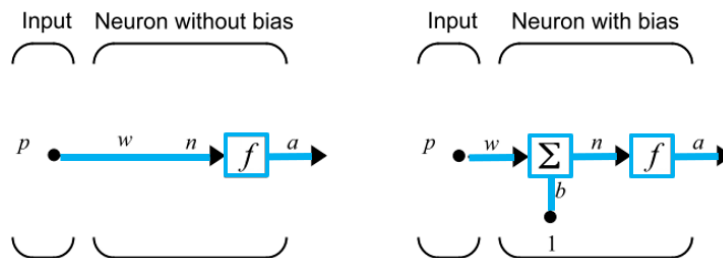
Fig. 3.2. Simple Neuron model

The scalar input p is transmitted through a connection which increase its strength by the scalar weight w, to form another scalar output wp. In this case the weighted input wp is the only argument of the transfer function f, which gives the scalar output a. The neuron on the right has a scalar bias, b, which is generally is conceptualize as simply being included to product wp as described by the summing junction or by shifting the function f to the left side by a value b. It should be clear that bias is almost like a weight, but it has a constant input of 1. The transfer function net input n, again a scalar, is the sum of the weighted input wp and the bias b, where this sum is the argument of the transfer function f. Specifically w and b are variable scalar parameter which can be adjusted in order to make the NN to work better. Also based on the goal or job, the weight and bias parameters are adjusted to meet the best performance and expectations. It should be clear that the bias b is variable parameters of the neuron. It not known as input, but the constant 1 which relates the bias as an input and it should be recognized as such, in case the linear dependence of input vectors is considered in the model.

28

| a) Hard-limit | b) Linear (pureline) | c) Log-sigmoid |
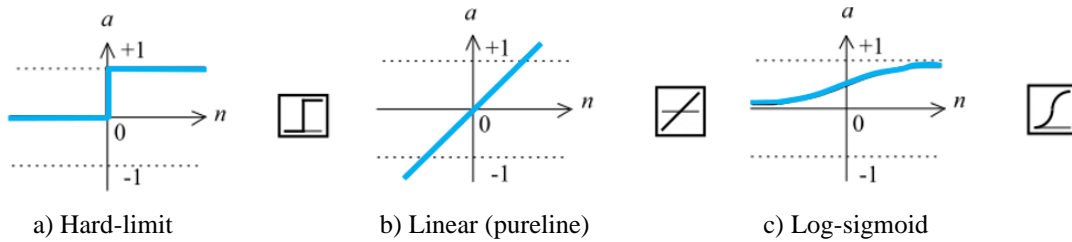
Fig. 3.3. Main Transfer Functions

The hard-limit transfer function shows the limits of the output for the neuron, for two values 0 or 1, in our case as shown above in Fig.3.3a. Usually this function is useful to create NN which focused in classification decisions. Also, in Fig.3.3b is shown the linear transfer function, which is helpful in linearization and simplification problems, when the reduce of the mathematical order is required. Regarding the Log-Sigmoid transfer function is generally used in backpropagation NN, due to the fact that this function is differentiable.
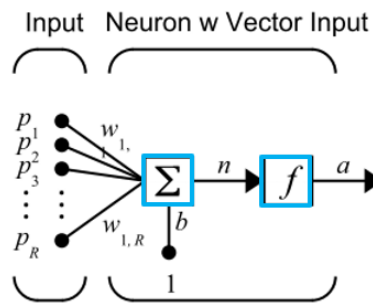
Fig. 3.4. Main Transfer Functions

A neuron with a single R-element input vector is shown below. Where the individual element inputs are expressed as p_1, p_2,...., p_R and are multiplied by weights $w_{1,1}$, $w_{1,2}$, ... $w_{1,R}$. The parameter R represents the number of elements in input vector. The weighted values are inserted to the summing junction. This product of sum is expressed by Wp, as a result of the matrix W and the vector p. The neuron has a bias b, which is summed with the weighted inputs to form the net input n. The n which express the sum, is the argument of the transfer function f, expressed as below:

$$n = w_{1,1}p_1 + w_{1,2}p_2 + ... + w_{1,R}p_R + b \qquad (3.1)$$
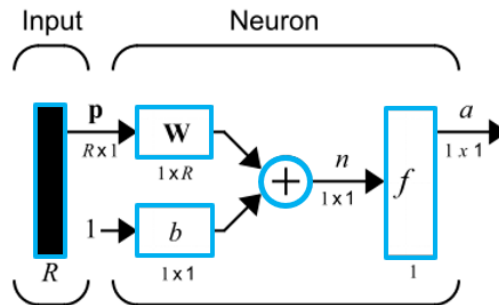
Fig. 3.5. Single Neuron Structure

In this case the input vector p is expressed by the vertical bar (black). The dimensions of p are expressed by the Rx1. The input of the function f is n, and the sum of the bias b and the product Wp. As well this figure shows the

composition of a *layer* for the NN, where it includes the combination of the weights, the multiplication and summing function, transfer function and bias *b*. Always the size of the matrices will be shown every time a specific abbreviated network notation is used. By combining two or more neurons together in order to create a layer, and it is possible to make NN which contains one or more layers at the same time. A one-layer network composed by *R* input elements and *S* neurons, and each element of the input vector *p* is connected to each neuron input through the weight matrix *W*. The *i*th neuron has a summer that gathers its weighted inputs and bias to form its own scalar output $n(i)$. Different $n(i)$ are collected and they introduce the *S*-element network with input vector composed by *n*. Finally, the output of this neuron layer forms the column vector *a*.

In Fig. 3.6 is shown a single layer of neurons structure. In the left side is the theoretical one and the right side a real one made by the author. Where *R* represents the number of elements in input vector, and *S* the number of neurons in layer. Should be clear that the number of inputs for each layer can be different from the number of neurons.

As well it is possible to create a single layer of neurons based on different transfer functions, where the two networks will be connected in parallel for a normal operation.

a) Theoretical Structure   b) Proposed NN structure by the author
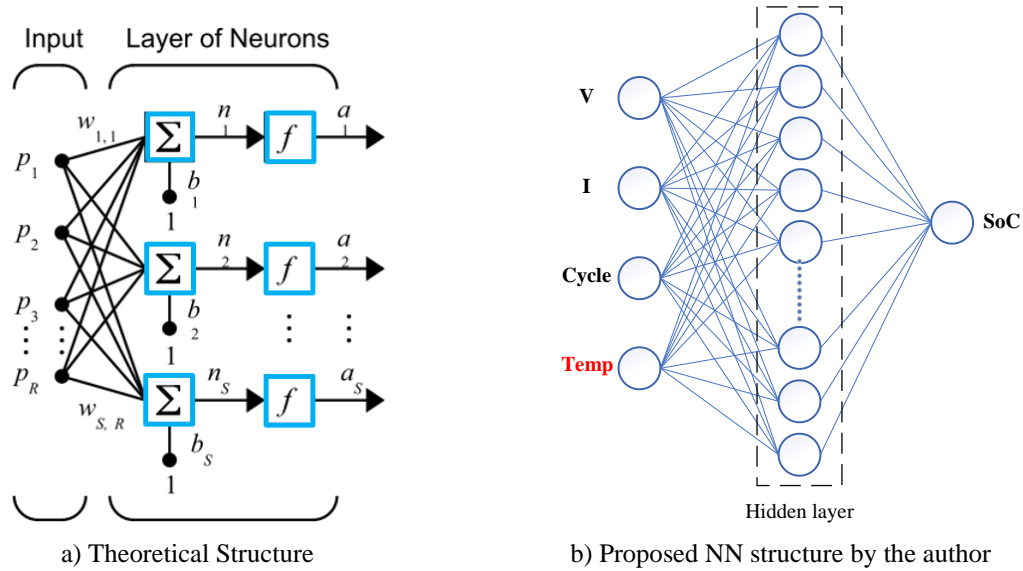
Fig. 3.6. A Single-Layer of Neurons Structure

The weight matrix *W* is composed as below and it's used as input vector for the network

$$W = \begin{bmatrix} w_{1,1} & w_{1,2} & \cdots & w_{1,R} \\ w_{2,1} & w_{2,2} & \cdots & w_{2,R} \\ & & & \\ w_{S,1} & w_{S,2} & & w_{S,R} \end{bmatrix} \qquad (3.1)$$

$$a^1 = f^1(IW_{1,1}p + b_1) \qquad a^2 = f^2(LW_{2,1}a^1 + b^2) \qquad a^3 = f^3(LW_{3,2}a^2 + b^3)$$

$$a^3 = f^3(LW_{3,2}f^2(LW_{2,1}f^1(IW_{1,1}p + b_1) + b_2) + b_3)$$
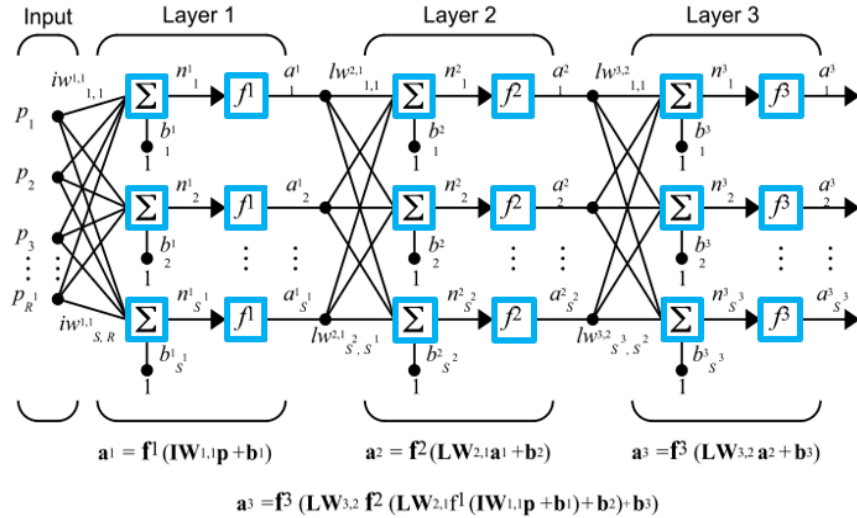
Fig. 3.7. A three layers of Neurons structure

$$a^1 = f^1(IW_{1,1}p + b_1) \qquad a^2 = f^2(LW_{2,1}a^1 + b^2) \qquad a^3 = f^3(LW_{3,2}a^2 + b^3)$$

$$a^3 = f^3(LW_{3,2}f^2(LW_{2,1}f^1(IW_{1,1}p + b_1) + b_2) + b_3) = y$$
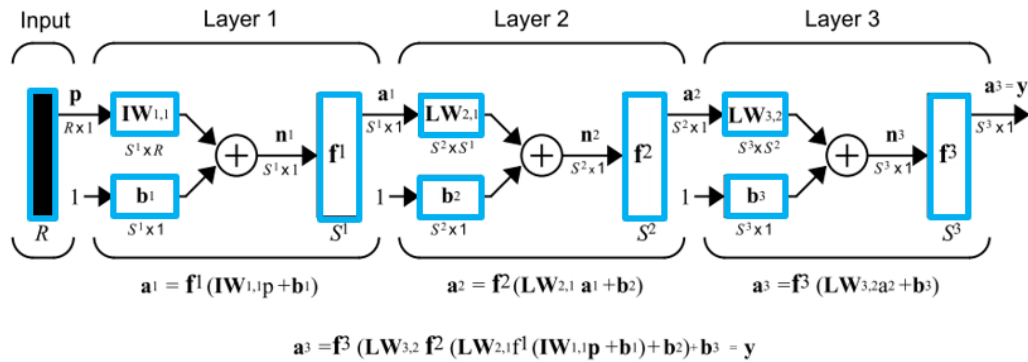
Fig. 3.8. A three layers of Neurons based on abbreviated model

Rosenblatt created few variations of the perceptron. One of the simplest models was based on a single-layer network whose weights and biases could be trained to produce a correct target vector when presented with the related input vector [99]. This training technique is named the perceptron learning rule. Perceptrons in most cases are suitable for simple problems in pattern classification. They're recognized for abilities as being fast, reliable and in addition they can be used for more complex networks based on the understanding level of the perceptron. A perceptron neuron, which uses the hard-limit transfer function *hardlim,* is expressed as below:

$$a = \mathbf{hardlim}(\mathbf{W}p + b)$$
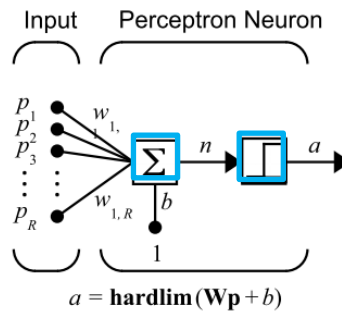
Fig. 3.9. A three layers of Neurons based on abbreviated model [98]

Where R is equal with the number of elements in input vector. Specifically, each external input is evaluated with an appropriate weight w_{ij}, and the total sum of the inputs is sent to the hard-limit transfer function. Also, it has an input of 1 sent to this sum through the bias, which as mentioned before from the hard-limit transfer function, where returns a 0 or a 1, as shown in Fig. 3.3a. The perceptron neuron produces a 1 if the net input into the transfer function is equal to or greater than 0; otherwise it gives a 0 logic. Due to the hard-limit transfer function which gives to the perceptron the ability to classify input vectors grouping and dividing the input "pool" into two regions. Specifically, outputs will be evaluated with the value of 0 in case that the net input n is less than 0, otherwise it will be evaluated with 1 if the net input n is 0 or greater. The input "pool" or space of a two-input based on hard limit function of the neuron is shown as in Fig. 3.10.
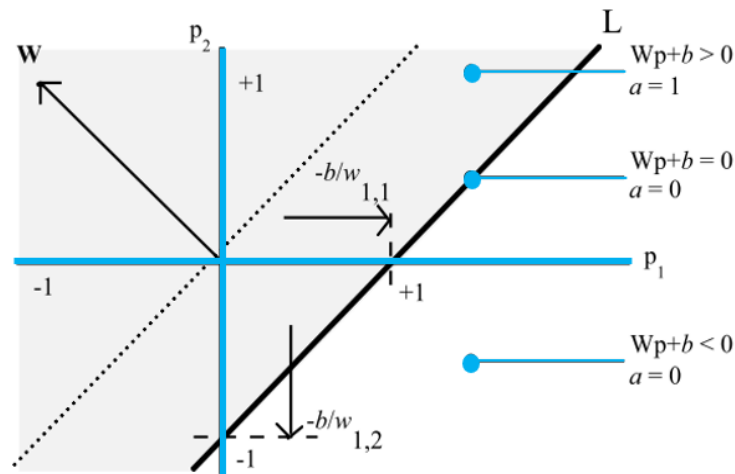
Fig. 3.10. Two classifications regions based on hard limit neuron

The two classification regions are formed based on the rule "*decision boundary*" line L at $Wp+b=0$, where $w_{1,1}=-1$, $w_{1,2}=+1$ and $b=+1$. Input vectors below and to the right of the line L deduce the neuron to output 0, and the opposite for the input vectors above and to the left of the line L will results the hard limit neuron to output 1.

In general, hard-limit neurons without a bias will have a classification patterns going through the origin [98]. By adding the bias, allows to the neuron to solve problems where the two sets of input vectors are not located from different sides of the origin. The bias allows the decision boundary to be shifted away from the origin. A simple example was done by the author, based on MATLAB R2019a, in order to give a practical approach to this model. Where in the left side of Fig.3.11 is shown the Neural Network Design, for the decision boundaries, where after the first training the weight are evaluated and the boundary should be moved forward on the right up corner, which correctly can divide white and black circles. On the right side it shown the boundary, which correctly divide the two different circles (based on the color criteria for this specific case), also the values of the weights and bias are now changed from the previous moment as shown in the left side.
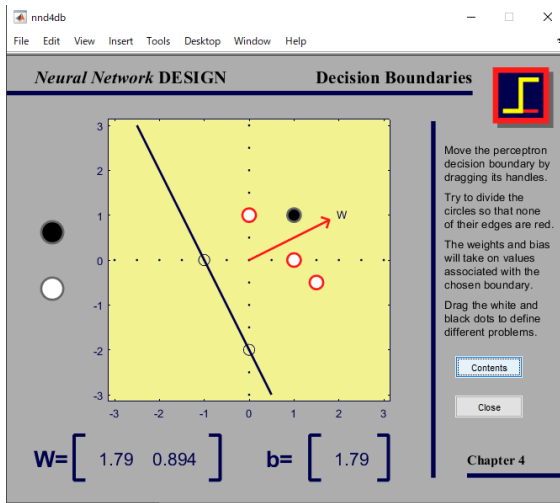
a) Before optimizing the boundary   b) after optimizing the boundary
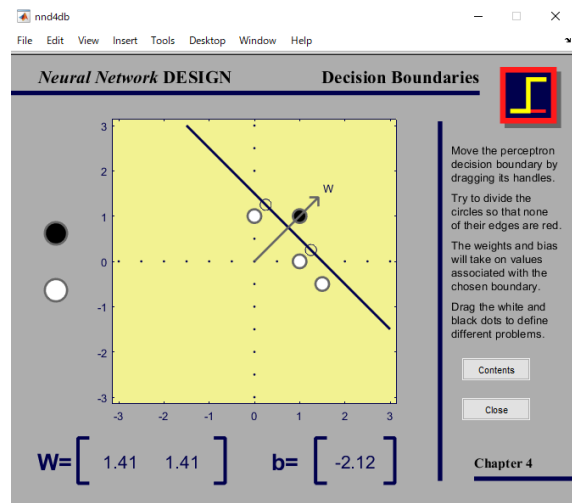
Fig. 3.11. NN model for the decision boundaries net

Fig. 3.12 shows an example of Perceptron Classification model through Neural Network Design, computed as well in MATLAB R2019a. This is a simple model where the author wanted to give example for 3D pattern classification which is based on three criteria as texture, shape and weight of the fruit. This classification can be used by the farmer or delivery company before they are sent to the supermarket or grocery shop, which helps not only to reduce the time of classification of products by as well to make another classification inside the same group. This can be used as quality classification.
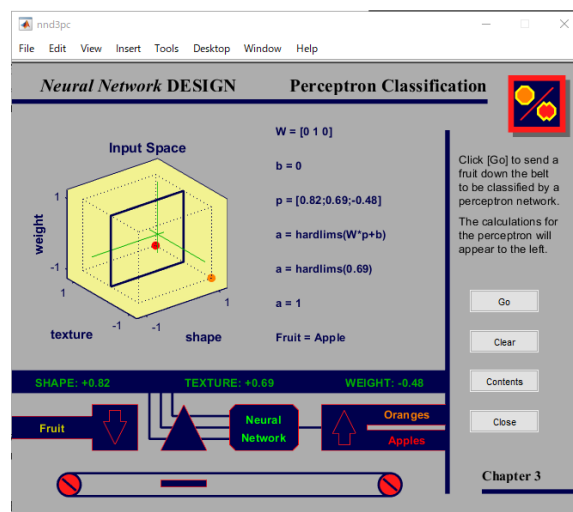
Fig. 3.12. NN model based on the perceptron classification net

3.3 Machine learning Algorithm

There are different definitions and terminology regarding the evaluation of ML algorithms in practice. Spam, fault and error detection is the main problem of learning to an automatically classification for our goal or to resolve our problem.

Examples: Items or non-continuous, instantaneous data used for learning or evaluation. These examples will be used for our learning process and finally for the testing.

Features: The set of attributes, which often represented as a vector, it is associated to specific or bunch of examples. In the case of email messages, some relevant features may include the length of the message, the name of the sender, various characteristics of the header and the same time the presence of specific keywords.

Labels: Values or categories assigned to examples. In classification problems, examples are assigned for specific categories, for instance, third input data or noisy information. Usually these items are as real-valued labels.

Training sample: Examples used to train a learning algorithm, these training examples regarded for each specific problem which we would like to relate it with. The training sample varies for different learning scenarios, which will help in the final step for a better generalization of the problem.

Validation sample: It is quite important the existence of such samples, which directly are used to tune the parameters of a learning algorithm, especially when working with labeled data.

Testing samples: Examples used to evaluate the performance of a learning algorithm. The test sample is separated from the training and validation data and is not made available in the learning stage. In this stage the test sample consists of a collection information or examples which the learning algorithm must predict labels based on features. These predictions are then compared with the labels of the test sample to evaluate the performance or accuracy of the algorithm.

Error or Loss function: It is a function which measures the difference, or loss, between a predicted label and a true label. Relating the set of all labels as ϕ and the set of possible predictions as ϕ', a loss function M is a mapping $M: \phi \times \phi' \rightarrow R_+$. Where in most of cases, $\phi=\phi'$ and the loss function is bounded, but these conditions are not always hold. Natural examples of such loss function includes the zero-one (or misclassification) loss defined over $\{-1,+1\} \times \{-1,+1\}$ by $M(\phi, \phi') = 1_{\phi=\phi'}$ and the squared loss defined over $L \times L$ by $M(\phi, \phi') = (\phi, \phi')^2$, where $L \subseteq R$, which is typically a bounded interval.

Hypothesis set: A set of functions mapping features (feature vectors) to the set of labels ϕ. In case of fault detection scenario, these may be a set of functions mapping the problem to $\phi=\{fault, non-fault\}$. More generally, hypothesis may be functions mapping features to a different set ϕ'. Of course, there can be some linear functions which do the mapping of the problem feature vectors to a real number interpreted as scores ($\phi'=R$), with higher score values more indicative of "fault" than lower ones.

In practical cases, the amount of labeled data available is often too small to set aside a validation sample since that would leave an insufficient amount of training data. As opposite way, an adaptive method known as *n-fold cross validation* is generally used to extract the labeled data for model selection and for training as well [98]. Let θ denote the vector of free parameters of the algorithm. For a fixed value of θ, the method consists of first randomly partitioning a given sample S of m labeled examples into n subsamples, or folds. The ith fold is thus a labeled sample $((x_{i1}, y_{i1}), ..., (x_{imi}, y_{imi}))$ of size m_i. Then, for any $i \in [1, n]$, the learning algorithm is trained on all but the ith fold to generate a hypothesis h_i, and the performance of h_i is tested on the ith fold. The

parameter value θ is evaluated based on the average error of the hypotheses h_i, which is called the cross-validation error.

This quantity is denoted by $R_{CV}(\theta)$ and defined by

$$Rcv(\theta) = \frac{1}{n}\sum_{i=1}^{n}\frac{1}{m_i}\sum_{j=1}^{m_i}L(h_i(xi_j), y_{ij}) \tag{3.2}$$

In general machine learning applications, n is typically set from 5 to 10, n-fold cross validation is used as follows in model selection. The full labeled data is first split into a training and a test sample. The training sample of size m is then used to compute the n-fold cross-validation error for a small number of possible values of θ. Where θ is next set to the value θ_0 for which cross validation error is smallest and the algorithm is trained with the parameter setting θ_0 over the full training sample of size m. Its performance is evaluated on the test sample as already described in the previous section. The special case of n-fold cross validation where $n=m$ is called *leave-one-out cross-validation,* due to the fact that each iteration exactly one instance is left out of the training sample. As shown in [100], the average leave-one-out error is an approximately "unbiased" estimate of the average error of an algorithm and can be used to derive simple guarantees for some algorithms. Which in general, the leave-one-out error introduce a highly cost to compute, since it requires training n times on samples of size m-1, but in case of some specific algorithms it admits a very efficient computation. Often n-fold cross validation is also used for performance evaluation. In this case, for a fixed parameter setting θ, the full labeled sample is divided into n random folds with no distinction between training and test samples. The performance reported is the n-fold cross-validation on the full sample as well as the standard deviation of the errors measured on each fold.

The main scenarios to describe ML are few and different, in terms of difference in the types of training data available to the learner, methodology and the order by which training data is received and the test data used to evaluate the learning algorithm. These scenarios are listed as below

Supervised learning (SL): The so called "learner" receives a set of labeled examples as training data and makes predictions for all unseen points. This is the most common scenario associated with classification, regression, and ranking problems. The SL focuses on the task of learning function that correlate an input to an output based on example input-output pairs [101].

Unsupervised learning (UL): Is a term used for Hebbian learning, which is one of learning methods without teachers, and also is known as self-organization [102, 103]. The main application of UL is in the field of density estimation in statistics or probabilistic features. The learner receives unlabeled training data, and makes predictions for all unseen points. Since in general no labeled example is available in this specific field, it can be difficult to quantitatively evaluate the performance of a learner. Clustering and dimensionality reduction are example of UL problems.

Semi-Supervised learning (SSL): In this case the learner receives a training sample consisting of both labeled and unlabeled data, making predictions for all unseen points. SSL is a common in the case where unlabeled data is easily accessible but labels are costly to obtain. The wide range and diversity of problems introduced in applications, including classification, regression or ranking tasks, which are grouped as part of SSL. The possibility that the distribution of unlabeled data accessible to the learner, which helps to obtain a better performance than in the SL case.

Transductive inference (TI): For this setting the learner receives a labeled training sample and a set of unlabeled test points at the same time, similar as in the SSL case. However, the goal of the TI is to predict labels only for these particular test points. TI seems to be an easier task and matches the opportunity to be used in a wide application. But as in the SSL, the assumption under which a better performance can be achieved in this setting.

On-line learning (OL): In this case, comparing form the other models, the OL includes few rounds of training and testing phases which are intermixed. In each specific round, the learner receives an unlabeled training point, making predictions, receiving correct label, and incurs loss. The main target and goal of the OL case is to minimize the cumulative loss over all rounds. Differently from the previous settings, during OL it is not possible to accept distributional assumption.

Reinforcement learning (RL): The training and testing phases are also intermixed in RL. This method is different from the previous approach. The RL is based on an agent which learns how to behave in an environment by performing actions and seeing the results, for each action it received a reward. The RL requires clever exploration tools. Randomly selecting actions without reference to an estimated probability distribution shows poor performance. [100]. In order to collect information, the learner actively interacts with the environment and in some cases affects the environment, and receives immediately a reward for each specific action. The main goal of the learner in case of RL is to maximize his reward over a course of actions and iterations with the environment. But still, no long-term reward feedback is provided by the environment, and the learner is faced with the exploration versus exploitation [100]. The learner must choose between exploring unknown actions to gain more information versus exploiting the information already collected. Advanced algorithm utilizes dynamic programming techniques as explained in [104-106].

Active learning (AL): The learner adaptively or interactively collects training examples of data, which are typically by querying an oracle to request labels for new points. The objective in AL is to achieve a performance which is comparable based on the standards of SL case. But with fewer labeled examples. AL is often used in applications where labels are expensive to obtain.

Regarding the fundamental and mathematically algorithms, which discusses the depth of theoretical foundations and the same time their practical applications. The specified topics includes a wide and rich approaches which are suitable for different type of problems. Main models of algorithms are listed as below:

a) Support vector machines (SVM), margin theory model,

b) Probably approximately correct, (PAC) learning framework, learning guarantees for finite hypothesis sets,

c) Vapnik-Chervonenkis (VC) dimension [Hypothesis space H defined over instance space x is the size of the largest finite subset of x shattered by H. If arbitrarily large finite sets of x can be shattered by H, then VC(H)], Rademacher complexity,

d) Kernel methods, rational Kernels, positive definite symmetric kernels, representor theorem,

e) Boosting, analyzing of empirical error, generalization error, margin bounds,

f) OL, mistake bounds, the weighted majority algorithm, the exponential weighted average algorithm, the Winnow and Perceptron algorithms,

g) Ranking algorithm, ranking with SVMs, Rank Boost, bipartite ranking,

h) The multi-class SVMs, multi-class classification, multi-class boosting, one-versus-all, one versus-one, error correction methods,

i) Kernel ridge regression, support vector regression, linear regression,

j) Applications to classification and regression, Stability-based analysis,

k) Principal component analysis (PCA), kernel PCA, Johnson-Lindenstrauss Lemma, Dimensionality reduction, applications to classification and regression,

l) Learning automata and languages,

m) RL, Markov decision processes, planning and learning problems,

3.4   Applications

As already explained ANNs have an inherent ability to model nonlinear systems. Since there are many scientific nonlinear and complex relationships, it is considerable and valuable advantage for the ANN's users. In [97] it is explained and shown the QSARs (quantitative structure-activity relationships) and QSPRs (quantitative structure-property relationships) have been used to quantitatively link molecular properties, such as dipole moment or shape, to a biological and other types of activity, but there is little theoretical justification for the view that linear models are the most effective. It has been proven to be a productive field for the nonlinear abilities of networks. As already proposed a new QSAR model for use in environmental applications [107], in which residuals from a linear regression equation on the water/octanol partition coefficients are modeled using ANN which takes molecular descriptors as input. Cartwright [108] used self-organizing maps to investigate the relationship between structure and biodegradability in PCBs (polychlorinated biphenyls), which are important environmental pollutants. After this, Zitko in [109] with a similar aim. A comparison between experimental and predicted biodegradability, an error within the range of 25% was achieved in most of the cases. This concluded the fact that the results of the biodegradability of disubstituted PCBs was more likely to be more challenging than that of other types of PCB.

In self-organizing maps, an injudicious choice of map size can seriously reduce the effectiveness of the algorithm. As already a considerable number of methods exist already [97], in which the algorithm locates its own optimum size. For the "growing grid" method, rows or columns are added as the calculation proceeds [110], and for the "incremental grid growing" new nodes are generated at the boundaries of the map [111], where this latter procedure can direct to disjoint networks in which the network fragments into several separate grids. In the "growing neural gas algorithm" [112]. It is known in the earliest applications of growing networks structure, Walker, Cross, and Harrison [113], where used for visualization of biomedical data that linked patient age and ten between positive and negative posterior probabilities for breast cancer cases. From their work they showed a convincing division between positive and negative posterior probabilities for breast cancer cases. For growing cell structure (GCS) method was first introduced with a primitive model as triangular network: where during training it is possible to remove or add nodes [114]. Sammon's mapping has been applied to the assessment of similar data sets, Wu and Yen in [115] compared this technique to GCS and showed a good separation of data

derived from the chemical abstracts from research papers related with polymer cements. Fonseca's group [116] investigated the use of self-organizing maps in the identification of crude oils, with next work from Cartwright [117]. In Cartwright research, neural networks were used to identify degraded oil spills. Fonseca's group used GC-MS data to assess a data set containing 188 samples; where the trained structure of the network was capable to identify roughly two thirds of samples available within the test set. Zhang and coauthors [118] investigated a problem common to many spectroscopic techniques, that of overlapping spectral features. A wide range of methods exists to tackle such problems, including neural networks. But any type of procedure that relies on learning must be applied with care. It is known that the quantity of data specifying each spectrum gives rise to the possibility of overfitting in trained methods [119]. Zhang's group investigated three types of networks in the quantification of overlapped peaks in micellar electro-kinetic capillary chromatography [97]. They assessed spectra first simplified by a PCA pre-analysis and were applied the method to mixtures of vitamin B1 and diazolium, whose UV absorption spectra are very similar. This is a similar earlier investigation into the use of ANN's in chromatography [97,1120,121,122].

A number of groups investigated the applicability of ANNs to the study of fuels and prediction of their properties. Most fuels are mixtures of many components in varying proportions, respectively to a wide range of properties. In [123] applied ANNs to the prediction of the cetane number of different components in diesel fuels. Many experiments are made to predict the octane number of fuels using networks [124] have been built upon by various researchers including Basu [125], which used ANNs to analyze data from NMR, LC, and GCMS experiments. Several reviews provide an overview of the application of neural networks to the life sciences and medicine. Pylosysis has used ANN in order to identify bacterial strains of industrial importance [126]. But a fast increase of usage in the analysis if food and drink or online monitoring of its quality. As example is the study in [127], where the authors combined multiple regression analysis with ANNs to determine the relation between phenolic composition and antioxidant activity, a specific topic which was studied in [128, 129].

Considering the well-known ability to handle non-linearity as confirmed in different fields, it was a great opportunity for the authors of this thesis to focus and try to utilize these characteristics in order to progress in the investigation of rechargeable battery's behavior. Trying to learn and to explain the physical meaning behind any results or unknown behaviors, investigating the deterioration of the Li-Ion, Ni-MH and Pb in order to define an accurate online State of Health (SoH). This approach to attempt an online investigation and estimation of the battery deterioration, can directly help to decrease the overall amount of cost related with the maintenance. By introducing an accurate and reliable online SoH of the battery cell/pack it possible for a continues operation, which doesn't stop the normal operation due to a diagnosis process. An online State of Charge (SoC) of the battery was investigated in order to compete with actual methods and technology, where this method could help to increase the credibility of the proposed method. But it necessary to understand and explain the characteristics of the internal impedance (IZ). Many researchers by using conventional methods have shown their results of the estimated parameters of the equivalent circuit model. But all of them cannot explain the high level of non-linearity, cannot avoid problems related from the conventional mathematical models which accumulates error due to the elevated order of the ECM, initial SoC value, etc. The author of this research have decided that for the elevated non-linearity is necessary to utilize acceptable non-linear approach, as ANN.

4.   State of Charge (SoC) Estimation and Evaluation
4.1   State of art

State of charge (SoC) is a key indicator of the battery capacity. Nowadays this is an interesting and open research as well an important engineering problem. As a matter of fact, a problem is remained unsolved due to lack of understanding of the fundamentals physics, due to weak mathematical framework, or due to technology limitation at that time. However, in case of SoC estimation it remains unsolved due to an additional and completely different reason that makes this an exciting area of research. The SoC parameter is not a measurable quantity unlike other variable like temperature or concentration. Also estimated SoC as a quantity is not clearly defined either. The most used method as a state of art, it is computed by Coulomb counting. This pertains to measuring the current at every time step, and. And integrating over time. This quantity is the net capacity the cell has lost during the particular operation and by subtracting the form the total capacity, the available capacity or SoC is estimated. In order to know the total capacity of the tank, which in our case example is the battery capacity, it can be measured by outflow of the electron over a period of time. But this method has some drawbacks. To start list, firstly is the matter of initial capacity which can be known if the cell is fully charged or discharged. But in case that the battery cell is taken and used through random situation, the initial capacity may not be known accurately. In addition, the error is accumulated as time passes during time, as matter of fact because this method is based on integration of the function during time. Additionally, many conditions like temperature affect the maximum cell capacity, also humidity, and quality of the chemical material which compose the battery. These variables also directly affect the lifetime of the battery. In case that the battery cell goes into non-isothermal operation, the maximum capacity keeps shifting from the correct value making this method problematic. Without forgetting the fact that current sensors can be inaccurate, and operational issues as sensitivity of measurement errors make this estimation method unreliable. On the other hand, an alternative method is to compute from the cell voltage itself. Another method is the Open Circuit Voltage (OCV) of an electrode, which is a unique function of SoC. Electrochemically speaking, the OCV of an electrode is a function of the Lithium concentration in the electrode. So, the task of computing SoC is resulted to a reverse engineering from the information of cell voltage with the known OCV-SoC relationship. The OCV is defined as the cell voltage at equilibrium. However, while is being used on board, the system is far from equilibrium. So, in the end a mathematical model that gives out the OCV from measured voltage and current signals becomes necessary to develop. In order to obtain OCV from the cell voltage, effect of all transport processes have to be removed. This process includes some method of model inversion and comes with the usual complications..

4.2   Conventional methods

Development of reliable and efficient energy storage system is one of aggressive challenges for the industrial applications particularly in smart grids and automobile applications as electric vehicles (EVs). Lithium-Ion Batteries (LIBs) are the most used type of batteries due to their high energy and power density, high efficiency, high open-circuit voltage (OCV), wide range of temperature operating and long-term usage [130]. The importance of rechargeable batteries nowadays is increasing in the portable electronic devices, solar energy industries and in the development of electric vehicles (EVs). The upcoming Electric Vehicle (EV) and Hybrid Electric Vehicle (HEV) are becoming the most important technology in transportation, because of their environmental affinity and increasing driving autonomy. The battery performance directly influences their total performances and efficiency of the Battery Management System (BMS) with power controller for this kind of vehicles. The improvement of the energy storage system as well as interest to further advance of the battery technology is one of the main purposes of the researchers of this field. The rechargeable batteries have a crucial role in the storage system, especially in the mobile equipment, because the period of its usage and the flexibility of its function are determined by the battery [131-133]. One of the main challenges is the SoC, which expresses the amount of energy available in the battery. Many models have been developed for the estimation of the SoC, and some have good points and bad points. The typical methods to estimate the SOC can be summarized in two

main philosophies the direct and indirect methods. However, in this research they will be divided in 6 main groups related with their experimental approach including inside the direct and indirect methods.

a) Current counting method

The second approach is based on measuring the energy such as coulomb counting (CC), uses the current reading of the battery over the operation period in order to calculate the SOC level. This is often known as current integration. However, the SOC must be calibrated due to its error accumulation over time. Current counting is easy to use, low cost and low computational complexity to estimate the SoC of the battery [130].

$$SoC(k) = SoC_{(0)} + \frac{1}{C_n} \int_0^k (\eta \cdot I(t) - S_d)\,dt \tag{4.1}$$

where $SoC_{(0)}$ is the initial SoC, $I(t)$ is the current at time t, Cn is the nominal capacity of the battery, η is the coulombic efficiency, and S_d is the self-discharging rate. However, this method introduces few main drawbacks as the unknown initial SoC, self-discharge rate and current-sensor errors which serves as error sources for this method.

b) OCV method

OCV method uses the non-linear relationship between the battery electromotive force in the open circuit state and SoC to estimate the SoC [135]. Despite the fact that the relationship is stable, it is not the same for different batteries. It is closely related with capacity and chemical composition of the electrode material of the battery. Massive experiments should be conducted at different cycle of usage [136], in order to obtain correct values of the most important parameters. These variables can be the open circuit voltage (OCV), charging current, internal resistance or AC internal impedance [137-139]. Kalman filter (KF), which is based on the time series approach, mainly based on the step process estimation and the linear quadratic estimation (LQE). KF is an algorithm that uses a series of measurements observed over time. Although the data contain statistical noise and other inaccuracies, the method stably and accurately estimates unknown variables comparing with those by methods based on a single measurement, because KF estimates taking into account a joint probability distribution over the variables for each timeframe. Also, extended Kalman filter (EKF) is used in estimation theory, like the nonlinear version of the KF which linearizes an estimate of the current mean and covariance. In the case of well-defined transition models, EKF has been used as a standard in the theory of nonlinear state estimation.

c) Internal impedance method (IZ)

Internal impedance describes the electric characteristic of the battery and depends on current, SoC, SoH, temperature, etc. Although the impedance has been measured by a sinusoidal alternating current (AC) method, the method is difficult to apply to the online electrical impedance spectroscopy (EIS). The relation between the SoC and internal impedance is non-stable, and the measurement is accompanied with high cost. In addition, the value of internal impedance changes slowly which introduce difficulties to observe the SoC [140-142].

d) Electrical circuit model (ECM)

The main objective of this method is to explain the chemical compositions and reactions through an electrical and a mathematical approach. It is important to define the correct and best ECM for each type of battery or problem that need to be resolved. Although the accuracy of the estimation will be improved by increasing the complexity of the circuit with parallel RC blocks, it comes with higher cost and time consuming as well. Even

if the number of blocks is reasonably determined from a viewpoint of numerical calculation, the synthesized model cannot explain all the electrochemical processes of the battery. The trade-off relation between accuracy and computational complexity should be kept in mind. Although each ECM could explain the behavior of the battery according to the response of the elements, its accuracy depends on the model's agreement. The accuracy of the complex model may be high, but the nonlinearity of the model parameter makes difficult to build it [143-1446].

e)   Electrochemical method

Electrochemical method theoretically gives the most accurate SoC estimation. However, this method can be effectively used for off-line design and performance analysis for LIBs. The equations used for this method describe the physicochemical phenomena like diffusion, electrochemical kinetics occurring inside the battery etc. This model is typically and computationally challenging owing to a system with relation of time-varying partial differential equations. The methods based on Electrochemical Impedance Spectroscopy (EIS), which have found many applications for accurate analysis in the diagnosis of the Li-Ion battery. The chemical reaction has a strong effect in the impedance characteristics. The main drawback is lacking of generality, which lead to wrong SoC estimation in certain battery types (chemistries).

f)   Pressure method

This method can be applied to certain Li-Ion and Ni-MH batteries. The internal pressure increases rapidly when the battery is charged. Usually it is employed in an extra protection system as a pressure switch indicating full-charging.

However, there are other methods which are closely related with the indirect method. These methods propose an approach which relate the measured battery signals (voltage, current, temperature, cycle usage etc.) with the battery SOC battery model or chemistry composition. This method is based on a high accurate and reliable model in order to obtain the characteristics of the real-life battery and predict its behavior under a wide variety of conditions. The indirect methods are composed as well by other main groups called: model-based methodologies, adaptive filter-based methodologies, adaptive artificial intelligence-based (AI). The battery SoC estimation and real time diagnosis is a complex nonlinear system. Although the SoC estimation is essential technology, its accuracy and reliability should be improved still until now. The SoC can be expressed through different methods and parameters, but the simplest definition is the ratio between the actual capacity and the reference capacity, which is expressed as the maximum value related on some specific conditions specified from the manufactures, i.e., voltage, current, temperature, deterioration. The types of methods to estimate a reliable model for the SoC estimation used in the literature are numerous. The estimation of SoC and level of deterioration are closely related with the internal characteristics of battery, which could not be directly measured during operation by the conventional methods. However, a time series estimation by an appropriate algorithm with a measurement of the indirect parameters of the battery enables the SoC and deterioration estimation. The charging process of EV is very important, because its quality affects the battery state of health (SoH), which means more mileage and quality of the battery pack system [144,147]. The charging process can be also done during driving, i.e., by regenerative brake. If it is not controlled in appropriate matter, it easily damages the battery. Any motor controller is required for achieving a closed loop management in order to charge the batteries at a constant current. Table 4.1 shows the advantages and drawbacks of each method in EV applications for a reliable and trusty SoC estimation.

Table 4.1 Conclusions of the SOC estimation models

Model	Positives	Negatives	Recommended for EV
OCV	Simple, low cost	Not practical in dynamic systems, requires low current and long- time of rest	NO
CC	Simple, low cost	Error accumulation, not possible to specify the initial SOC value	YES
KF (Kalman Filter)	High accuracy, including also error and noisy signal	For every battery type need a high accuracy model, not general, high computational requirement	YES
ANN	High accuracy, strong, versatile usage in specific or general problem.	Requires big amount of data, high computational system during training in case of online training algorithm, with offline estimation & evaluation process is used [148].	YES

4.3   Proposed method based on ANN

Nowadays many different types of batteries based on lithium-ion are in production and commercial. It is of great importance to understand the differences between them, because each of these batteries is used for different applications based on their needs. The spider chart for LIBs with various anode and cathode materials is shown in Fig.4.1. One of the important variables to mention is the C-rate which explains the current value required for the battery to its rated capacity within the specified time. With the help of this chart it is possible to understand the advantages and drawbacks for each LIB type. The heat generation, charging/discharging ability, rated power and energy, thermal stability and deterioration level can be used for the further study of the real time SoC & SoH estimation of the battery cell/pack. As well these data can be used for a generalization of the problem.
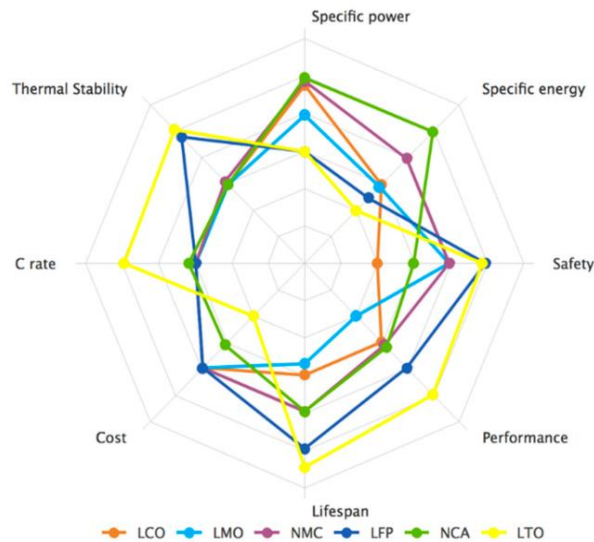
Fig. 4.1. Spider chart for LIBs with different chemistry materials [149].

For actual and future technologies of energy storage systems, the need for an online diagnosis (during operation) without the removal of the battery is very crucial in order to increase the efficiency and lifetime of the battery, to reduce the cost of conventional diagnosis system, and to reduce the non-operational time due to the maintenance schedule.

The SoC can be defined by different methods and variables, but the most used definition is the ratio between the actual capacity and the reference capacity, which is the maximum actual value based on some specific conditions. These conditions refer to the constant current rate and ambient temperature, as well other conditions as cycles of usage (level of deterioration), chemical composition etc. Because battery is an energy storage device based on chemical composition, so many difficulties are introduced for a direct SoC measuring method. Each method introduced in the previous chapter shows difficulties and drawbacks in the process of the estimation of SoC. The result obtained from a discharging test of the battery until the end of discharge process based on the criteria is mentioned in the datasheet of the manufacturer. Fig.4.2 shows a full charging and discharging process which concludes one cycle of test. The results are obtained by Constant-Current-Constant-Voltage (CCCV) charging and CC discharging with 1C (2.25A) and with lower and upper voltages are 2.7V and 4.2V, respectively. This characteristic can be obtained without the removal of the battery, and involves important information for the SoH or SoC estimation. Two variables, voltage and current are used in this research paper as the parts of the input data for the proposed artificial neural network (ANN) structure.
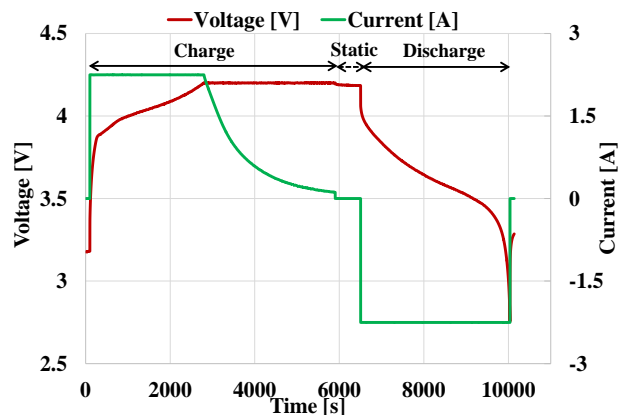
Fig. 4.2. Charge and Discharge waveform
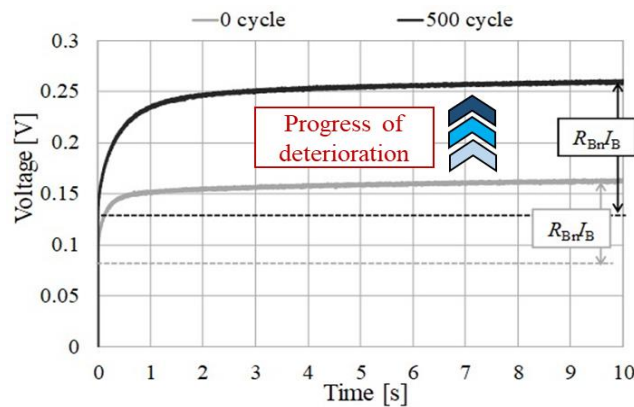
Fig. 4.3. Voltage difference during the deterioration.

Fig.4.3 shows the voltage deviations of a same battery but in different level of deterioration (a new battery with 0 cycle from a full deteriorated of 500 cycles). It is clear in Fig.4.3 that the effect of deterioration really affects the voltage level, terminal voltage, due to the degradation of the chemical composition which affect the internal impedance of the battery.

Regarding this chapter, few papers and research topics already investigated by the author will be introduced in this part of the thesis. An adaptive online learning algorithm based on an ANN is used based on adaptive learning algorithm, after confirming this method another more advanced method is introduced which tries to reduce the amount of input data required, reducing the estimation time and increasing the accuracy of the model. As already explained in chapter 3, the ANN has self-learning skills and adaptability to demonstrate a complex non-linear model as explained in [150, 151]. It accurately estimates the SoC without knowing the internal structure of the battery and the initial SoC.

Usually, the ANN method uses the LIB terminal voltage, discharge or charge current, and ambient temperature as the input and SoC as the output. The novel in this paper is the modified input time-delayed neural network model that takes into accounts both deterioration and temperature effects. This study investigates further on the reduction of input data for low power computational hardware in order to reduce the cost from a viewpoint of industrial applications. An online training and offline update weights, which enables offline decision-making for the SoC estimation, is introduced to reduce the needs not only for high computing power but also for large memory storage of the whole system. Fig.4.4 shows Cole-Cole plots of a battery during charging until the SoC reaches to 100%. These characteristics involve very important information which shows the increase of the internal impedance during charging, which clearly explains the physical meaning of the electrochemical process.
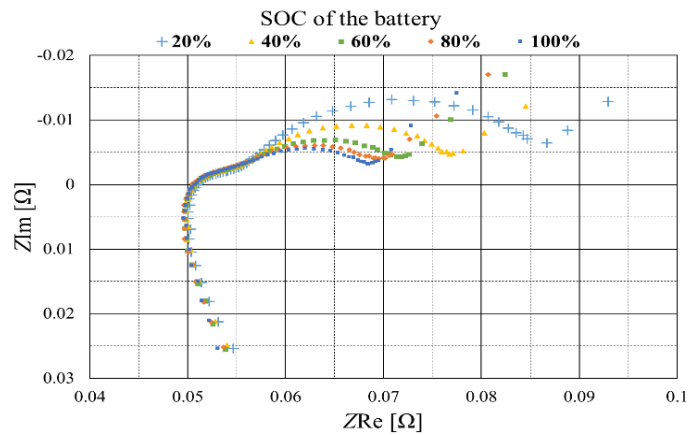
Fig. 4.4. Cole-Cole plot related with SoC%

Figs. 4.5 and 4.6 show the characteristics of voltage and current during charging and discharging in CCCV mode. These data are genuine and all obtained through real experiments. The author would like to emphasize the effect of ratio in the SoC process. These data are used in the database of the proposed ANN during the training process. Some experiments are initiated even from different level of upper voltage, not only from 4.2V but also from 4V or 3.8V, in order to imitate a real scenario of usage of the battery during moment when the battery is not full charged/discharged. This helps to increase the quality of the estimation and improve the generalization of the ANN.
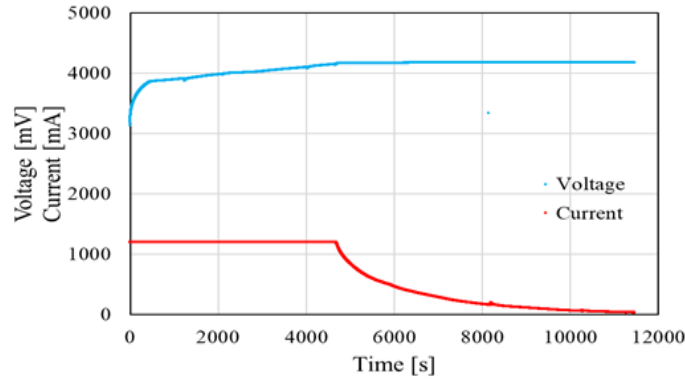
Fig. 4.5. Characteristics of Li-ion during CCCV charging

As shown in Fig.4.6, in this experiment there have been used different type of charging and discharging ratio. It was necessary to investigate such parameter, in order to evaluate the effect of ratio in SoC time, battery temperature, speed up process of deterioration due to increase of current. All this information was included inside the training process of the ANN. It is true the fact that, more accurate data and larger diversity of experiments directly increase the accuracy of the estimation, but at the same time it increases the complexity of the structure. It requires a better and optimized model in order to capture any possible non-linearity amongst the inputs or between inputs and output.
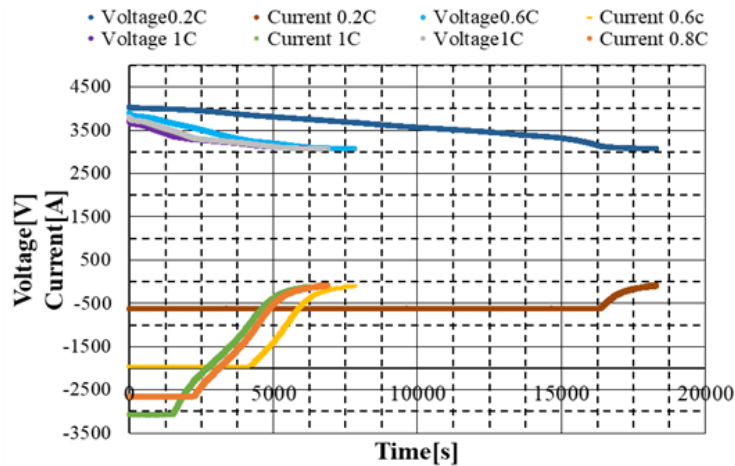
Fig. 4.6. Comparison of discharging characteristics between different current ratio during CCCV mode

As already explained in the previous chapter regarding ANN method, it based on three processes, learning, validation and test. The proposed NN is processed in MATLAB R2019a. In the training process, the selection of the most appropriate NN configuration is crucial. The typical structure of the ANN is composed of an input layer, a hidden layer and an output layer. In the proposed structure, the number of input types is 4, voltage (V), current (I), cycles and temperature (Temp). Regarding the voltage and current, it is very easy to obtain these data during operation with actual sensors without the stoppage of the operation. Most of actual low-cost devices give this information without any extra cost, and this helps for the online diagnosis system. It should be clear that on this investigation 4 data have been proposed to be used for the ANN structure. The author have made also few different experiments using even structures with only 3-input besides the 4-input structure, making possible combinations of these data. In Fig.4.7 are shown the proposed ANN structures.

45

| a) V, I, Temp. | b) V, I, Cycle, | c) V, Cycle, Temp | d) I, Cycle, Temp |
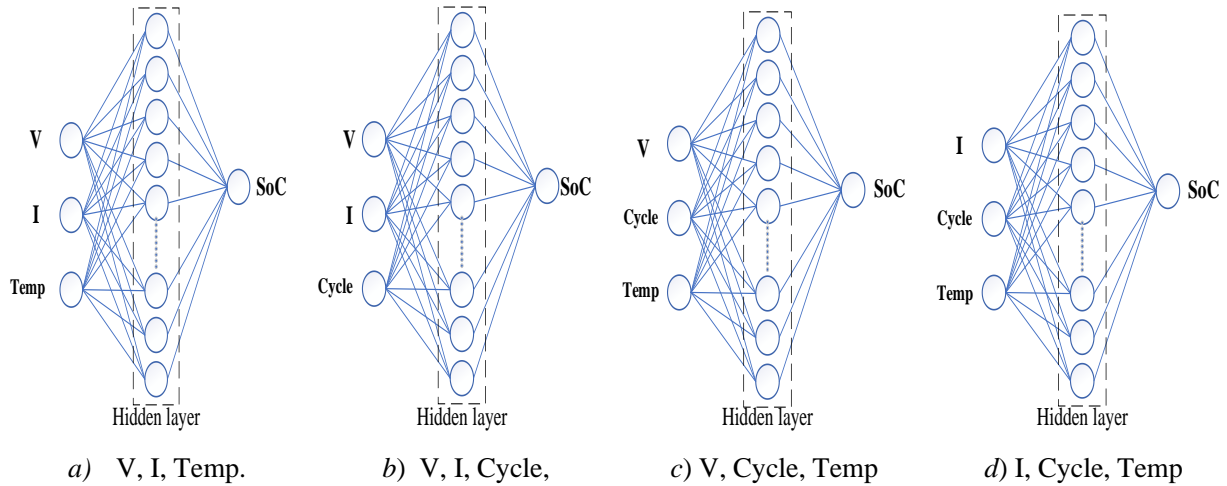
Fig. 4.7. Proposed ANN structure based on 3 inputs combinations from 4 parameters

The attempt to confirm the quality of the estimation based on 3 inputs was made as a possible opportunity to reduce the cost of the device in term of processing power.

The Regarding the cycles information, the author have used two types of the counting cycle data, one structure during every 50 cycle of deterioration, and the other is every 100. The first type means that only 11 data cells are required for from 0 cycle battery to a full deteriorated battery of 500-cycle. The later structure (every 100-cycle) needs only 6 data cells. Even if the number of data is reduced to almost half, the increase of the error is only 2.3% in the worst case. Which means that this value is inside the acceptable value of error for low cost device including the feature of mobility of the proposed circuit MTC. But in case where the user wants to have high accuracy, like researchers, then the second type of 11 data cells during every 50 cycles can be usable for them. This cycle counting is very easy to be achieved, and is realized in low cost. This method is applicable to any industrial systems without difficulties. The dynamic temperature, i.e., battery surface temperature can be entered as the fourth and final input. The signal can be used as a precaution to protect the system. However, a temperature sensor has to be installed on the battery cell. Ambient temperature can be used as the fourth data because the sensitivity against the data is low. In this paper, 25 and 35 degree Celsius are used for the ANN. To reduce the cost further, the fourth data can be optional. However, the estimation error slightly increases. Fig.4.8 shows the temperature information of the ambient, cell body and transistor which are obtained through the sensors.
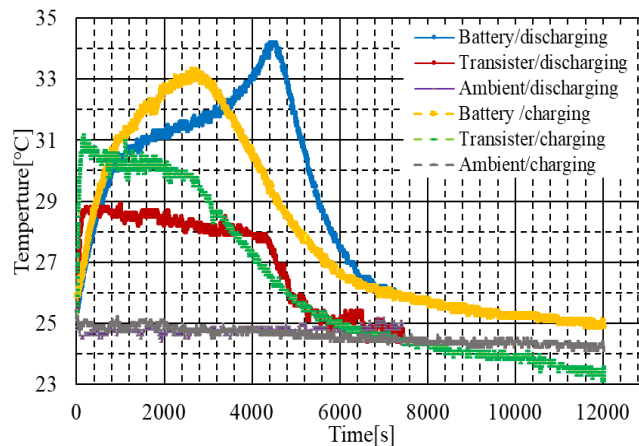
Fig. 4.8. Temperature characteristics during charging and discharging with 3A

Both experiments during charging and discharging are introduce in order to include the dynamic behaviour during different operations. Regarding the transistor temperature this information is not used as the input for the proposed ANN structure, but is just introduced as a possible extra information for the industrial applications. The surface temperature of the battery is the most important information regarding the temperature comparing to the ambient which is more stable characteristics as shown in Fig.4.8. The transistor temperature is the related with the power transistor of the MTC device which control the charging/discharging ratio. This info is important to shows the range of current operation for normal operation within the nominal values. As well it is used as an evaluation system regarding the safety and reliability of the application. To simplify it helps to stop the charging or discharging process if the temperature is increased above the normal value.

Fig. 4.9 shows the proposed ANN structure. During the training process, these data are obtained using 10 new batteries, and deteriorated from 0 cycle to 500 cycles. For the voltage and current input, 350 data are used for each of them. For the cycle input (3rd input), 6 or 11 data cells are used based on the selected mode also for the temperature around 400 data cells were used in the training process in case of a variable temperature system, except the case of static temperature. The fourth input, respectively the temperature is shown in red in different color, in order to emphasize the fact that this data was optional for use. Which means that through the experiments it was observed the amount of effect in the SoC estimation in terms of accuracy and calculation time. So, it possible to give to the user a higher grade of freedom to choose or neglect this effect, as a good optional way to reduce the necessary amount of data.
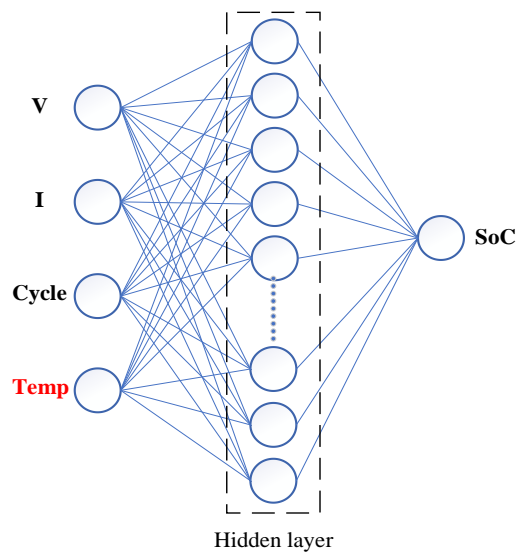
Fig. 4.9. Temperature characteristics during charging and discharging with 3A

The ANN with double or single hidden layers, are tested in this paper. The best structure is with 11 and 22 neurons with a single hidden layer, and with 26 and 31 neurons with two hidden layers. The initial learning rate which is referred as a configurable step size hyperparameter, in the beginning of the training process was set to 0.11 and in the end after the optimization the learning rate was set to 0.021. It is a well-known approach and recommended from expert of this field to start with a little bit higher learning rate in the beginning and later to reduce this coefficient. By doing so it can optimize the learning process without forcing it to increase error in later phases and have consequences as overfitting or linearizing some parameters which should not be corrected or simplified.

The best estimation model was achieved by this model with average error of 1.85% in 86% of the estimated cases, 2.35% average error for 11% of the cases and for 3% of the estimated cases were evaluated with maximum error of

2.9% in the worst case. Fig.4.10 shows the measured and estimated OCV-SoC characteristics.
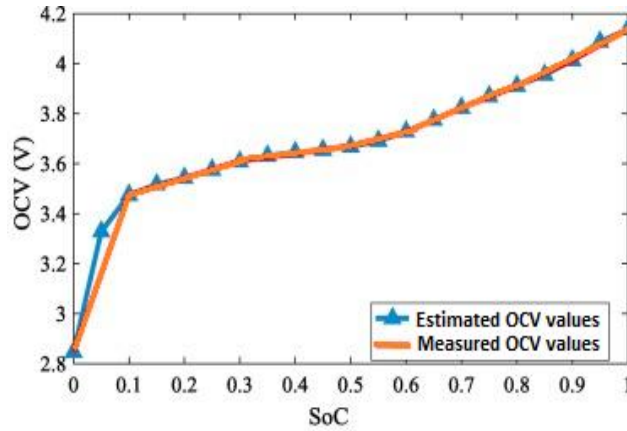
Fig. 4.10. Comparison between the estimated and measured OCV

Despite the good results achieved from this specific approaches and ANN model, the author tried to improve this model. To propose a better model in all meanings, which includes the fact of reducing the amount of required data to, faster estimation, better generalization of the method, including the temperature info without increasing the total cost of the device, increasing the total capacity of the pack, and increasing the voltage by composing more complex one that a single or double series cells. To make this possible it was necessary to investigate on a better ANN structure and also including the BMS as a crucial part in order to maintain a balanced voltage of all the cells at an equal value of voltage.

4.4   Cell balancing pack effect, BMS

As already explained in the previous chapter ANN's does not rely on the mathematical equation or equivalent circuit model to explain the relation between the input variables and output product for resolving the problem. It is because the ANN characteristics are based on the black box approach, which does not require any knowledge about the system's internal dynamics. It is appropriate to resolve the problem with nonlinear mathematical tools. For example, higher-order cumulants usually are used to infer new properties regarding the data of non-Gaussian processes [152, 153]. In multiple-signal processing, it's common to define the combinational relationship among the cumulants of h stochastic signals, $\{x_i\}$, $i \in [1, h]$, and their moments of order r, $r<h$, expressed by Leonov-Shiryaev formula [154-156];

$$Cum(x_1,...x_h) = \sum (-1)^{r-1} + (r-1)! \cdot E\{\prod_{i \in s_1} xi\} \cdot E\{\prod_{i \in s_2} xj\} \cdot .....E\{\prod_{i \in s_k} xk\}, \qquad (4.2)$$

where the addition operator is extended over all the partitions, as one the form $(s_1, s_2, ..., s_r)$, r=1, 2, ..., h; and $(1 \leq i \leq r \leq h)$; being s_i a set belonging to a partition of order r, of the set of integers 1, ..., h. Let $\{x(t)\}$ be an hth-order stationary random real-valued process. The hth-order cumulant is defined as the joint hth-order cumulant of the random variables $x(t)$, $x(t+\tau_1)$, ..., $x(t+\tau_{r-1})$. In other words, the complexity will increase the error and the necessity to use high-end industrial systems, which include the stochastic relation inside the calculation method. This study will investigate further on the optimization and simplification of the ANN structure by reducing the necessary input cells for accelerating the calculation, training and estimation without sacrificing the accuracy. After that, the accuracy of this model will be investigated in order to adapt to this environment of data without any equivalent circuit model. Fig.4.11 shows the steps of the proposed method, where the data are obtained through practical test and used for the training of the ANN and database creation, and later testing the stability and quality of the ANN. During estimation the results are compared at the same time with practical test based

on unsupervised learning process (UL). If the accuracy is low, then ANN will continue to train and updating its weights until the error is reduced and the structure is to finally optimized.
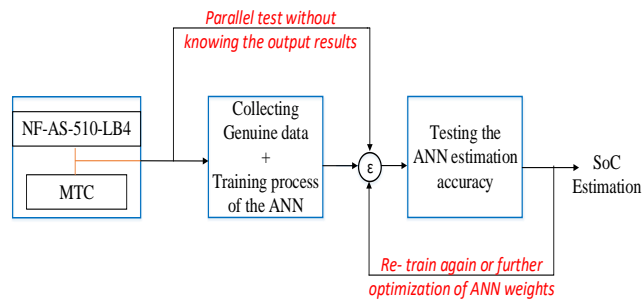
Fig. 4.11. Block diagram of the proposed methods

The focus of this paper will be based on the improved model which is confirmed by the author from their previous work, precisely [138,139,150,155]. It is important and valuable to progress from that previous work because it has shown a great potential for improvement due the accurate and robust characteristics from the proposed NN model. This paper investigates further in few directions as reducing the number of input data, reducing the estimation time, improving accuracy and the generalization characteristics. But, at the same time maintaining the simplified properties for low power computational hardware, has been kept in mind. As already explained in [150], terminal voltage, discharge/charge current, and ambient temperature are used as the input, and the SoC as the output of the modified input time-delayed NN model. It takes into accounts both deterioration and temperature effects. Comparing to the previous study, the experimental data are obtained from two different devices; one is an industrial device NF-AS-510-LB4 battery test-system as shown in Fig.4.12.
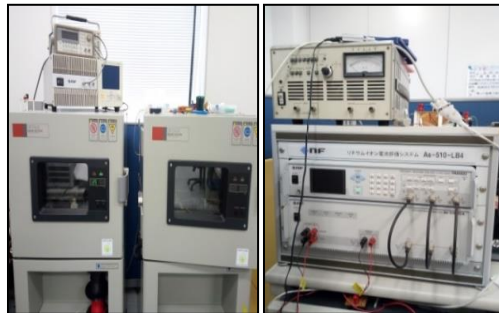
Fig. 4.12. Li-Ion battery test NF-AS-510-LB4.

The NF-AS-510-LB4 will help the study by providing important data with high accuracy, as cole-cole plot, SoC and SoH evaluation, also, will help to do the training of the ANN for the case of static temperature test structure. This means that the chamber of this device can maintain a very good static temperature in order to relate the temperature effect on the SoC, beside other inputs. The second device will be multi-type charger/discharger circuit (MTC), as shown in Fig.4.13 which is created by the author and already confirmed in many practical projects [138,147,155,156].
.
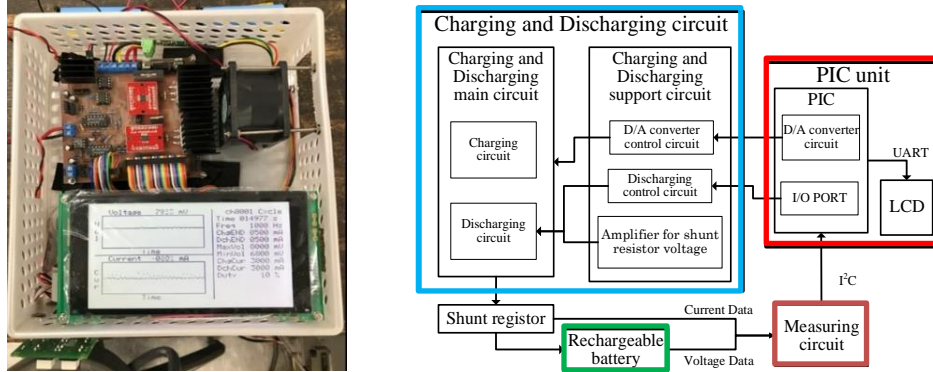
Fig. 4.13. Multi type chemistry charger/discharger device [12]

All the data related with SoC value are genuine, which means they are retrieved through practical experiments and test done through practical devices, respectively MTC and NF-AS-510-LB4. MTC shows good flexibility in terms of type of battery, level of voltage, current waveform, mobile and low cost, incorporating the dynamic temperature test structure of the ANN.

At the same time during the charging/discharging, a data logger GL820 measures the temperature of the battery surface, ambient temperature and other electronic components important for the stability of the MTC system in real time, which is very important in industrial applications or in EVs [158,159]. Another innovative of this study comparing to previous one is the usage of high-power type battery for 1 cell experiments and for battery pack system. Table 4.2 shows the technical specification of MTC, and in Fig. 4.14 is shown the temperature measurement device, midi Logger GL820. During this experiment, this device will measure the temperature of the battery cell, the transistor of MTC during charging/discharging and the ambient temperature.

Fig. 4.14. midi LOGGER GL820

Table 4.2 Specifications of The MTC Charger/Discharger Device

No.	Item	Min.	Typ.	Max.
1	Supply voltage [ACV]	100	–	240
2	Operating voltage [V]	–	12	–
3	Operating current [A]	–	–	2
4	Nominal Battery voltage operation [V]	2	–	12
5	Battery current [A]	-3	–	3
6	Frequency range [Hz]	0.01	–	1000
7	External DAC [V]	0	–	2
8	Temperature range [°C]	0	–	50
9	Size [mm]	208W×282D×72H		
10	Protection type for PCB	Emergency stop switch		
11	Cooling method	Forced-air cooler		

Table 4.3 shows the specifications of the tested Li-ion battery.

Table 4.3 Primary Specifications of Li-Ion cell

Model		ICR18650BF
Dimensions (mm)	Diameter	18.3±0.2
	Height	64.95+0.15/-0.30
Weight *2(g)		46
Charge (CCCV)	Max. voltage (V)	4.2
	Max. current (A)	2.25
Discharge (CC)	End voltage (V)	2.75
	Max. current (A)	6
Nominal voltage (V)		3.7
Minimum capacity (mAh)		3250
Type		High-Capacity type

The battery pack system behavior and characteristics is crucial to be investigate for power system applications, as EVs or PV systems. Because the SoC on a battery pack its quite different comparing to that on a single cell where the ECM and deterioration is easier to be explained [160-163]. Another different thing is the effect of deterioration on the battery pack, where the cells can have different SoH, which means that the SoC level will be different and the total SoC of the pack can be unstable. For the case of battery pack, a BMS is connected. Fig. 4.15 shows the BMS and battery pack composition. The total battery pack capacity is 13Ah, maximum voltage of 12.6V and minimum voltage 8.1V. The proposed BMS includes few functions which will protect from over/under voltage, short circuit and overcurrent situations.
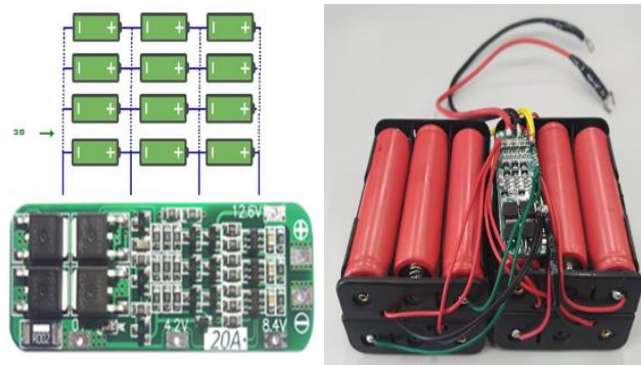
a) BMS diagram of the circuit   b) Battery pack composition

Fig. 4.15. Charging/Discharging for 18650 Li-Ion cells with 3series and 4 parallel battery pack

A 3-series system is used because it is an acceptable value of 12.6 V to explain the behavior of scaled down storage system. In addition, we might encounter batteries with different SoH, which requires to confirm the generality of this method. Regarding the parallel connection up to 4 packs, it is important to increase the capacity in order to have a longer test period during charging/discharging. This helps to test the stability of the system,

obtaining more data for the learning stage of the ANN and also a better simulation to imitate the EV's scaled down storage.

Table 4.4 Features of the proposed BMS 3SxP circuit

Features	*Value*
Type of battery	Li-Ion, Li-MnO
Single cell overcharge protest voltage [V]	4.28-4.6
Overcharge protect delay [sec]	0.5-1.5
Single cell over discharge protect [V]	2.72-2.88
Single cell over discharge protect recover voltage [V]	2.9-3.1
Overcharge protect current [A]	60
Over discharge protect delay [A]	60
Temperature protection	Yes
Disconnect protect	Yes
Shortage protect	Yes
Shortage delay [μs]	100-600
Charging Current [A]	20
Discharging Current [A]	20
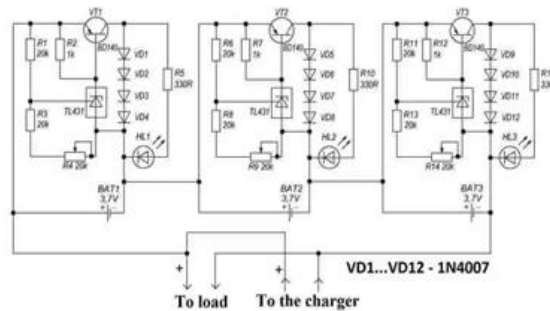
Fig. 4.16. Simple diagram of the BMS

In Fig.4.17 is shown the proposed single cell BMS circuit.

Fig. 4.17. Single cell connected with a Custom BMS

Figs. 4.18 - 4.22 show the experimental results obtained from the tests. In Figs. 4.18 and 4.19 are shown the voltage and current information obtained during charging and discharging.
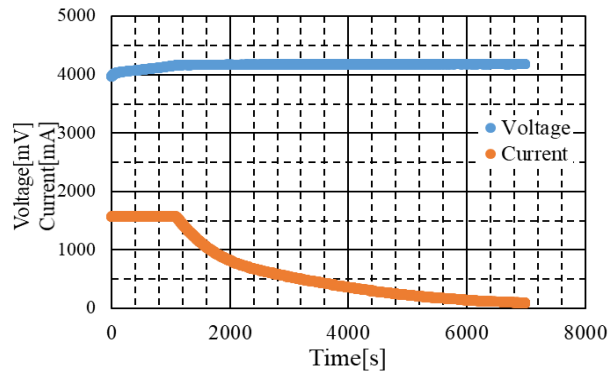
Fig. 4.18. CCCV Charging characteristics, 0.5C ratio, Re=20mΩ (81.5 - 100)% SoC, 52 Cycles
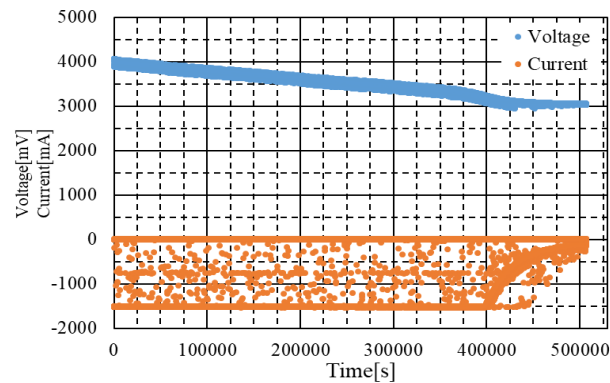
Fig. 4.19. Pulse Discharging characteristics, 0.5C ratio, Re=20mΩ, Duty cycle 50%, 53 Cycles

The two modes, CCCV and pulse waveform are used in order to increase the database and generality of the ANN. The operation by pulse current waveform shows lower deterioration, also the temperature is lower. However, it takes more time to do the charging/discharging depending on the current value and duty cycle.

In this section, the current ratio of the tests was in the range from 0.1C, 0.2C, 0.4C, 0.5C, 0.6C, 0.8C, 0.94C and 1C. The external resistance was selected arbitrary with the value of R_e=20mΩ, but it can be changed depending on the user's needs.
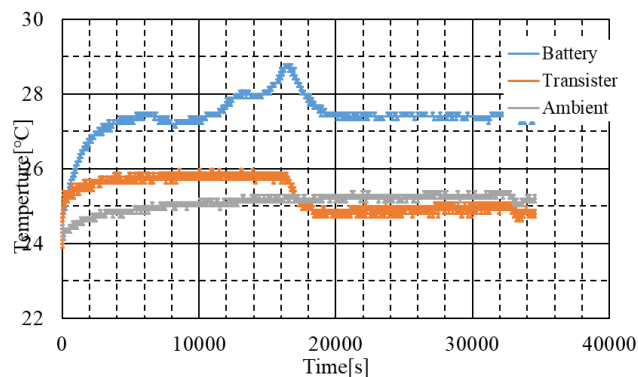
Fig. 4.20. Pulse Discharging characteristics, 3A- 0.94C ratio, Re=20mΩ, Duty cycle 70%, 149 Cycles
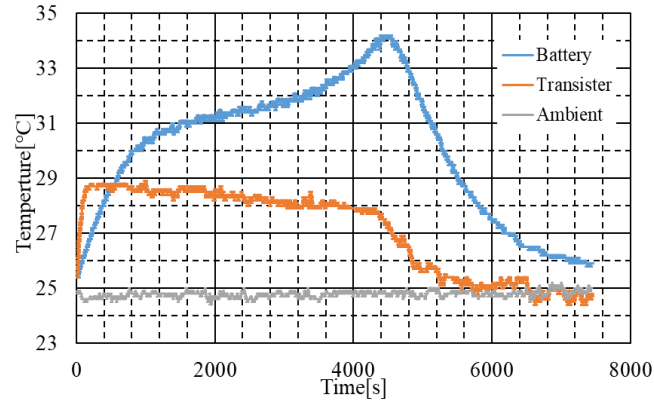
Fig. 4.21. CCCV Discharging characteristics, 3A- 0.94C ratio, Re=20mΩ, 132 Cycles
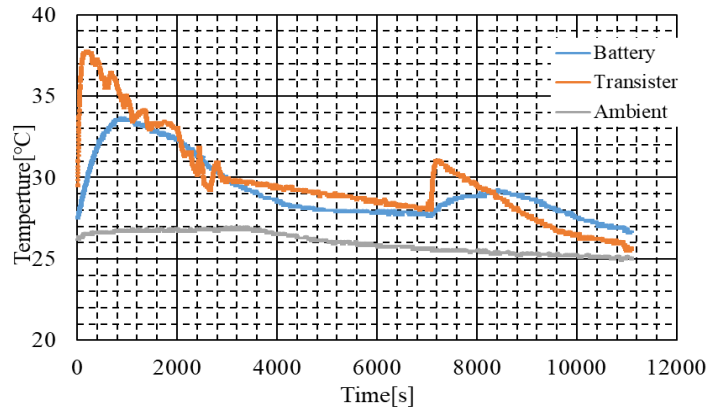
Fig. 4.22. Pulse Discharging characteristics, 3A- 0.94C ratio, Re=20mΩ, Duty cycle 80%, 352 Cycles

The dynamic temperature, i.e., battery surface temperature can be entered as the fourth and final input. The signal can be used as a precaution to protect the system. Ambient temperature can be used as the fourth data because the sensitivity against the data is low. In this paper, the tests are done from 25 to 35 degree Celsius which are used for the ANN. To reduce the cost further, the fourth data can be optional.

Both experiments during charging and discharging are introduced in order to include the dynamic behaviour during different operations. Regarding the temperature of the transistor within the MTC, this information is not used as a mandatory input for the proposed ANN structure, but it's just introduced as a possible extra information for the industrial applications. During the training process, the selection of the most appropriate NN composition is very important, and each of the ML techniques have their typical structure and properties depending on the specific problem, as explained in [164-168]. But, in this paper SL and UL methods will be the main focus for the optimized ANN model. The typical structure of the ANN is composed of an input layer, a hidden layer and an output layer. The proposed NN is processed in MATLAB R2019a. In this study, 4 structures as shown in Fig. 4.23 are proposed to investigate the SoC estimation.

| a) MISO 4 Inputs
1 hidden layer | b) MISO 4 Inputs
hidden layer | c) MISO 3 Inputs
1 hidden layer | d) MISO 3 Inputs
2 hidden layer |
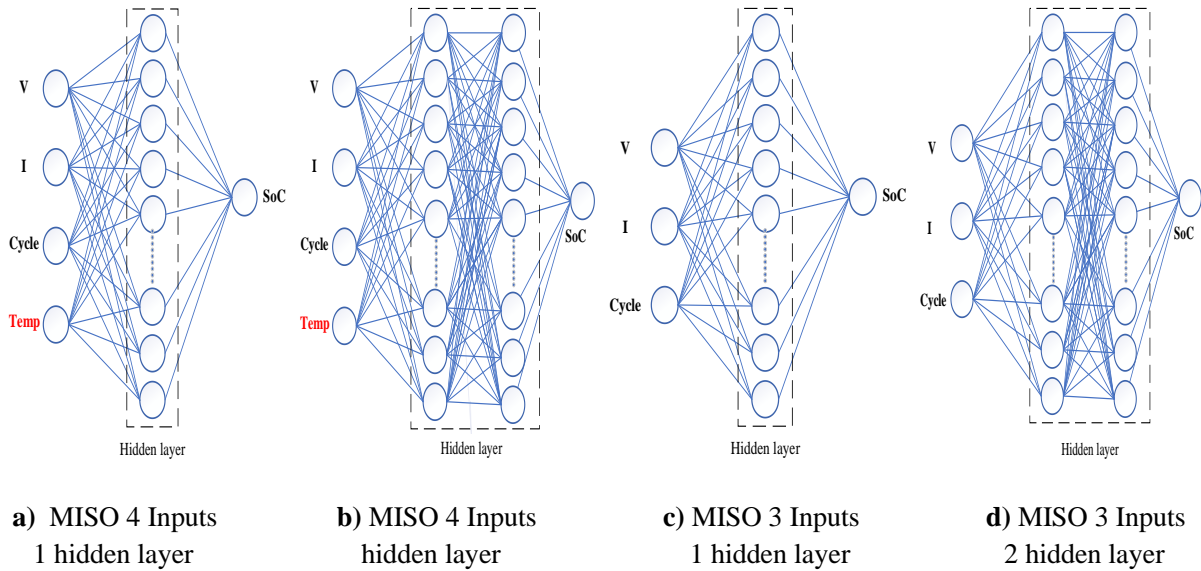
Fig. 4.23. ANN structure for the proposed model, where **a)** & **b)** with dynamic temperature structure, **c)** & **d)** with static temperature structure

The type of inputs is the same as in [155], but the number of required cells is drastically reduced. As well the number of neurons in the final structure is simplified and the ANNs are stable during all the test despite the complexity of the total process. Should be mentioned that the final data of SoC are obtained through the practical experiments and test done from the two devices respectively, NF-AS-510-LB4 and MTC, as explained in chapter 3. In the proposed structures, the number of input types is 4, voltage, current, cycles and temperature. Table 4.5 shows the results of the new method.

Table 4.5 Advantages & Comparisons of The Proposed Method

	Previous method	*The new method*	
Estimation time [s]	Single cell / 2 cells	Single cell	Pack
	23.9 - 32.4	15 - 22	22 - 29
Peak error [%]	2.9	2.1	
Average error [%]	1.9	1.4	
Capacity of the system [mAh]	6500	13,000 / 26,000	
Number of cells V/ I/ C/ Temp	400/350/11/100	100/100/11/ (100 or 50)	

The two types of method for counting cycles are tested to develop the low-cost approach; one is every 50-cycle of deterioration, and the other is 100. The former means that only 11 data cells are required for from 0 cycle battery to a full deteriorated battery of 500-cycle. The later structure (every 100-cycle) needs only 6 data cells. During the training process, the data are obtained using 10 new batteries, and deteriorated from 0 cycle to 500 cycles. For the voltage and current input, 100 data cells are used for each of them, when in the previous were used 400 cells for the voltage input and 350 cells for the current input. Regarding the temperature input, around 100 data cells were used in the training process in case of a variable temperature system which is 1/4 comparing

with the previous stud, except the case of static temperature. Fig.4.24 shows the performance and error rate of the ANN.
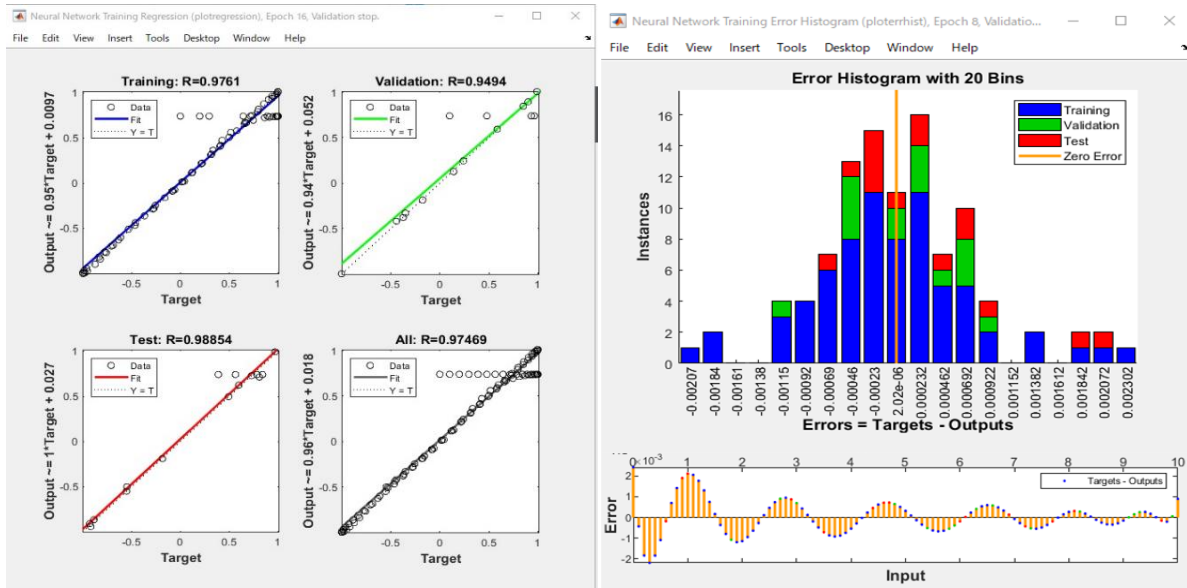
Fig. 4.24. ANN performance specs for the MISO 4 inputs 1-layer structure

4.5   Large scale & industrial applications

In this part, a scaled simulator for designing the power storage system is developed using the feature of the arbitrary current charging/discharging. The system enables to simulate a storage system for any power plant with a load such as a wind power generation, and a photovoltaic power generation. In addition, the system can model a battery charger with a pulse current method for prolonging the battery life for the electric vehicle. The characteristics of the storage system can be investigated using a real battery such as lithium ion, nickel hydride and lead acid batteries for comparative experiments. The system simulates the storage systems taking into consideration the battery chemical reaction that is difficult to include in conventional numerical simulations. In addition, the battery characteristics are easily tested by the proposed simulator. As a result, the practical simulation of future power-storage systems is realized. The low-cost and small-sized simulator can be used for designing not only power storage systems but also into consumer apparatuses.

In recent years, energy and environmental issues are universally concerned. It is expected that power generation systems using natural energy will be spread in the future to solve the problems. In addition, a large number of storage systems will be introduced for stabilizing the power generation. Although the characteristics of rechargeable batteries have to be fully understood for efficient operation and effective development of the system, it is generally difficult to examine the characteristics using actual storage systems. Even if a test is scaled down by using a cell removed from the storage system, a large-current charging/discharging circuit is still required. The cost reduction of this method is unnoticeable. Recently, computer-aided design (CAD) is widely used to improve the efficiency of the storage system. For the numerical simulation in the CAD, battery characteristics should be included. Some kind of battery model, as well as the storage system is indispensable in the numerical analysis. However, this simulation cannot strictly consider the electrochemical reaction of the battery, because no numerical model included the reaction process is proposed. As a result, the storage system cannot be accurately analyzed.

A battery charger/discharger with an arbitrary current waveform has developed first by the author [156]. In this paper, the system is applied to a storage-system simulator. Since the developed simulator can charge and discharge any types of rechargeable batteries, the system can simulate the charging and discharging characteristic

using single cell constituting the battery pack installed in the storage system. In this paper, storage systems combined with an actual photovoltaic (PV) and with a wind power generation are simulated using the scale-downed current according to the rated current of the battery for the simulation. The simulation can be performed regardless of the capacity of the power plant by the proposed method. The characteristics of the real battery in the battery pack are taken into account. The proposed system enables more practical design and development of future storage systems considering the electrochemical reaction.

4.5.1 Scaled simulator

a) Configuration

Since rechargeable batteries have the risk of ignition and explosion due to over-charge or -discharge, a protection system such as a battery management system (BMS) is essential to monitor and control the battery current and voltage for safety charging and discharging. Fig. 4.25 shows a block diagram of the proposed system. It is composed of three blocks: a charging and discharging circuit, the microprocessor board named "PIC unit" to control the battery charging/discharging, and a measuring circuit to obtain the battery voltage and current data. The main circuit is configured with a charging and a discharging circuit. Each operation is regulated by a same charging management integrated circuit (IC) as a BMS. Because the discharging circuit is also controlled by the charging management IC, the support circuit consisting of three blocks to assist the discharging circuit, and to protect the main circuit from over voltage and current. The appearance of the system is shown in Fig. 4.26 The operation of the system is controlled by a Programmable Interface Controller (PIC) equipped on a microprocessor board MA350 manufactured by Micro Application Laboratory Corp. Because various rechargeable batteries are widely used, the simulator has to manage a wide voltage range. Optimal design of the storage system brings out the full potential of each battery. To examine the characteristic, the simulator has to respond to any typical secondary batteries, such as a Li-ion, nickel metal hydride (Ni-MH), and lead acid (Pb) batteries. Therefore, the specification of the battery voltage ranges covers from 2 to 12V, 12.6V nominal value. If the voltage of the battery pack is within the range, the number of series batteries is unlimited.
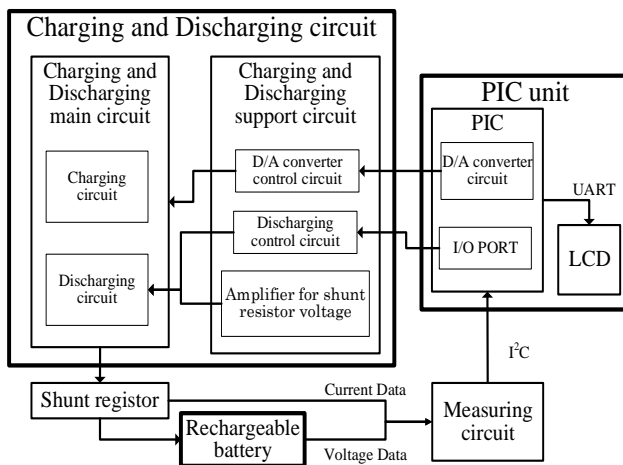
Fig. 4.25. Block diagram of charging/discharging system.
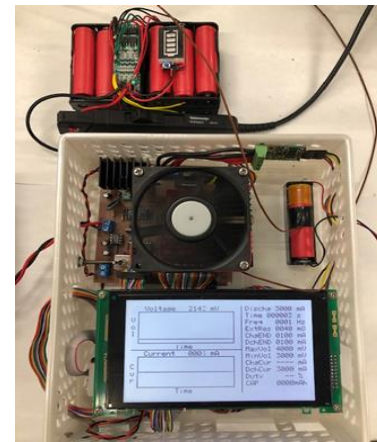
Fig. 4.26. Improved MTC Charging/Discharging device for 18650 Li-Ion cells with BMS circuit

Although the charging and discharging current of the present system is limited to 3 A, the maximum current can be easily expanded by replacing some devices, such as a current control transistor. The developed simulator is based on the current control method. However, the system can control the battery according to the battery power, by calculating the current from measured battery terminal voltage.

b) Performance

After the power source is turned on, the user inputs information such as the upper and lower voltage limits of the test battery for safe operation. Then, test conditions such as frequency and the current value are also entered. The test conditions of the system are set by the controller with a rotary encoder, and the conditions are always displayed on the Liquid Crystal Display (LCD) during the test. The charging and discharging circuit are controlled by a feedback system based on the voltage and current data always transferred from the measuring circuit. These measured data are saved to an SD card and also displayed graphically.

Figs. 4.27 and 4.28 shows the system performances when a lithium-ion battery cell is charged and discharged by the system. The battery current can be controlled by the built-in microcomputer or an external oscillator. Fig. 4.27 shows an example of the internal oscillator. The target current waveform is sinusoidal with an amplitude of 3 A and a frequency of 1 Hz. The difference of 120 mA between the target and measured currents indicates that the accuracy of the developed simulator is sufficient. From the measured voltage and current, the battery characteristic can be obtained. For example, the capacitive characteristic of the internal impedance is obtained from the phase difference, and the impedance of 130 mΩ is obtained from the voltage fluctuation amplitude of 400 mV and the current amplitude of 3 A. To investigate the validity of the characteristic in a high-frequency region, the arbitrary waveform having the current amplitude of 1 A and the frequency of 1 kHz is entered as the external signal input. From Fig. 4.28, a delay of 130 μs is observed at the switching from the charging to the discharging. The time is required for controlling the operation of the charging management IC by the microprocessor.
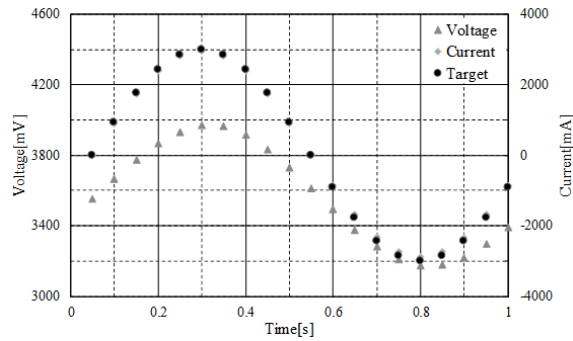
Fig. 4.27. Voltage response of a Li-ion battery to a sinusoidal current.
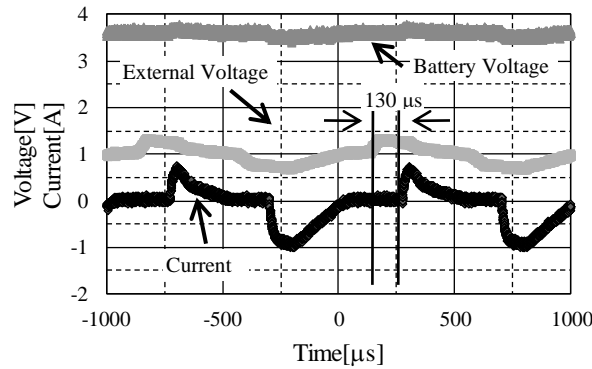
Fig. 4.28. Voltage response of a Li-ion battery to an arbitrary current of 1 kHz frequency

Fig. 4.29 shows an example of the characteristic of a Pb battery pack by a Constant Current Constant Voltage (CCCV) charging. The developed system can charge and discharge the battery by not only this simple current waveform but also the other waveforms such as a pulse waveform. Recently, pulse waveform charging has been considered to extend battery life in EVs [156, 157, 169, 170]. Fig. 4.30 illustrates voltage responses of three type of batteries by a pulse current discharging. The figure easily clarifies each battery characteristic as transient responses. For instance, the voltage fluctuations give that the resistance of the Ni-MH battery connected in series is higher than that of the Li-ion battery cell and the Pb battery pack. The high resistance limits the maximum charging/discharging current of the battery in the storage system.
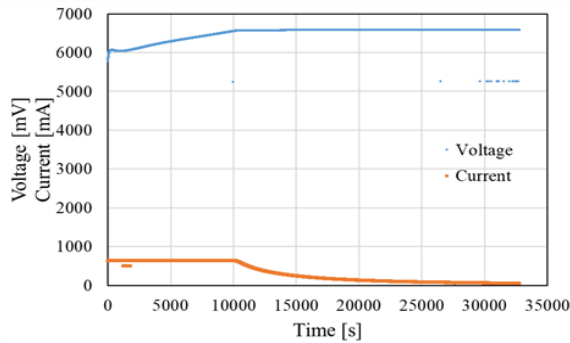
Fig. 4.29. Voltage response of Pb battery by CCCV charging waveform
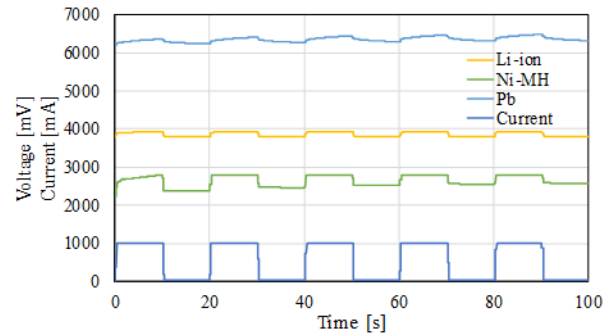
Fig. 4.30. Voltage response of different batteries an arbitrary current of 1 kHz frequency

4.5.2 Scaled Simulation Using Actual Power Generation Waveform

With the progress of battery technology for storage and the rapid spread of power generation using natural energy, it is expected that the stability of power system will be improved by using storage system [171,172]. In this paper, a storage system for stabilizing the power fluctuation of an independent power system, i.e., without any interconnected power grid is studied by scaled generated and load powers. Thus, the difference between the generated and load powers becomes the input or output power of the storage system. When the generated power is greater than the load power, the battery is charged. The battery simulating the storage system is charged or discharged by the developed simulator according to the scaled generated and load powers. For a safe and stable operation of the battery, the proposed system automatically moves to Constant Voltage (CV) mode when the battery voltage reaches to its maximum (charging) or its minimum (discharging). In the mode, the charging or discharging current is decreased, and the operation is ended when the current reaches the minimum value. In the case of an independent power system, when the generated power is lower than the load power, the load has to be rejected. If the load power is lower, generation power has to be suppressed by a Power Conditioner System (PCS) of the PV generator or the blade controller of the wind generator. The developed simulator has the ability to simulate the situations.

a) Photovoltaic generator's storage system

PV power generation converting solar energy directly into electricity has attracted attention due to its renewability and sustainability. Although the PV generation is excellent as a daytime power supply at a high-power demand, it cannot generate at night. Furthermore, its generation energy depends on the weather, topography, etc., and its power is reduced by shading by clouds. To cover the instability of the PV generation, rechargeable batteries are juxtaposed for smoothing the power and for storing the generated power in the

daytime. In this section, the operational characteristics of an independent PV power station of 2 kW capacity are simulated. The voltage and current in the simulation are sampled at every second. Fig. 4.31 shows an example of the generated power in winter of 2016. Large fluctuations in the generated power are observed due to cloudy weather conditions. A storage system of 5 kWh capacity realized by 18650 type Li-ion batteries is assumed as a storage facility in this simulation. The rated voltage and the capacity of the Li-ion battery cell are 3.7 V and 2250 mAh, respectively, i.e., its storage capacity is about 8 Wh. The charged or discharged power for the test using the simulation is reduced to 1/625. The waveform from 9:30 to 10:30 (one hour) in Fig. 4.31 is used for the simulator's test. The maximum generated power is 1.8 kW and the duration less than 400 W is at least 10 minutes in the period. Fig. 4.32 shows the voltage and current characteristic of the battery cell starting from an initial SOC of 50 % with the scaled current waveform assuming a constant load of 1 kW. The test is carried out using the measured data sampled at every 1 s.
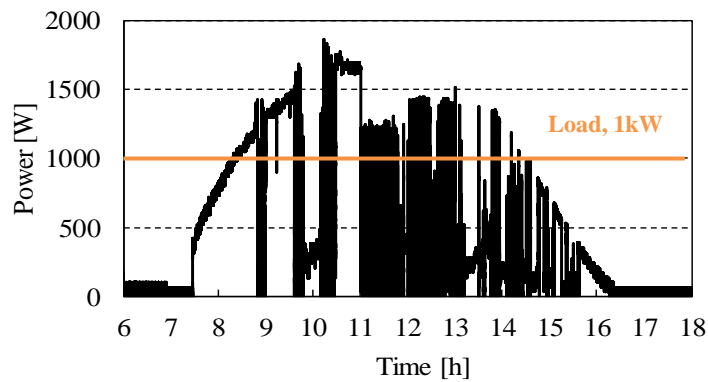
Fig. 4.31. Generated power by a solar panel array in February 2016.

When the generated power is larger than the load power of 1 kW, the battery is charged and its voltage rises. On the other hand, when the generated power is smaller, the deficient power is supplied from the battery to the load. Due to the discharging, the battery voltage decreases.
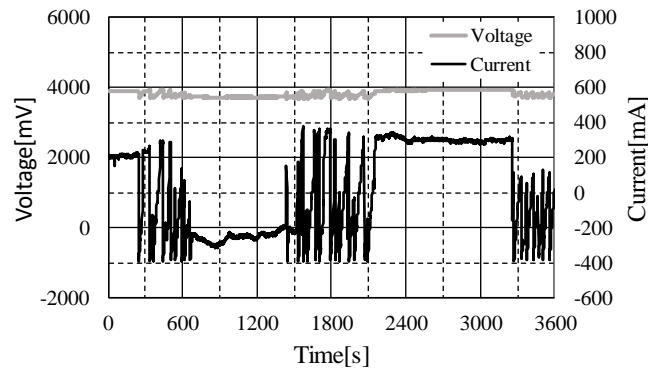
Fig. 4.32. Voltage and current waveform of Li-ion battery charged and discharged by a scaled power with a constant load

b)   Wind power generator's storage system

Wind power is another common renewable energy source. Unlike PV generation, the wind power plant can generate the power at night. Because the output fluctuates according to the wind speed, the system is usually connected with a grid, i.e., the wind generation requires a coordination with conventional large-scale generations such as thermal or hydroelectric power plant. To use the wind generation as an independent power source, it is necessary to install any secondary battery for stationary storage and smoothing the power. The developed system can simulate the storage system which has any capacity. In this section, an independent 20 kW wind power plant is simulated based on a measured wind power obtained in winter as an example. In this paper, the operational characteristics under two power patterns are simulated for 4 hours. One of the examples, has the period where the generated power is smaller than the average power of 6.5 kW is more than one hour, as shown in Fig.4.33. In this case, a constant load power of 8 kW is assumed, and it is higher than the average generated power. In the other case as shown in Fig. 4.34, the generated power is greater than the power of the load at the beginning, and the generated power gradually declines to 2 kW at the end of the observation time
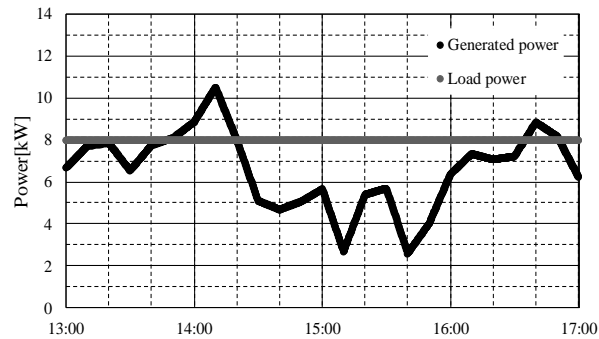
Fig. 4.33. Estimated generation power of a wind power plant and its constant load.
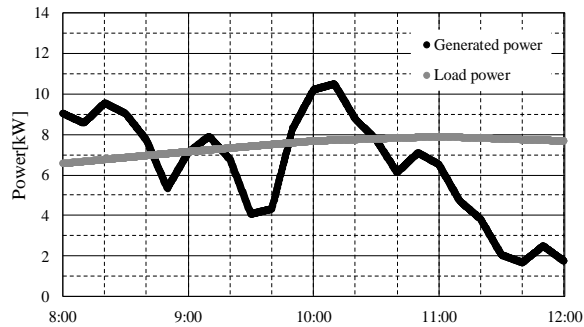
Fig. 4.34. Estimated generation power of a wind power plant and its variable load

The variable load with the maximum load power of 8 kW is assumed based on the daily load curve reported as the standard power system model by the Institute of Electrical Engineers of Japan [173].
In the simulation in this section, a storage facility having a 22 kWh capacity is assumed. The scaled power ratio of the developed simulator to the wind generator is 1/2750. Figs. 4.35 and 4.36 show the battery currents and voltages obtained by the proposed test system, with a sampling frequency of 100 mHz using the assumed powers. Additionally, the initial SOC of the batteries is assumed to be 50 % or 100 %. The current increases or decreases according to the difference between the generated and load powers in the period when the voltage of the test battery is between the lower and the upper limit voltages.
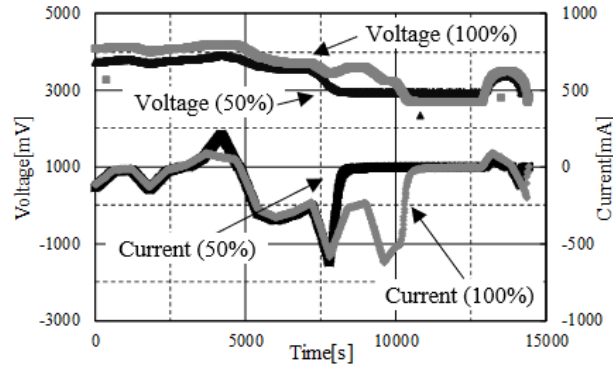
Fig. 4.35. Voltage and current waveforms of Li-ion simulated by a scaled power of a wind generation assuming a constant load
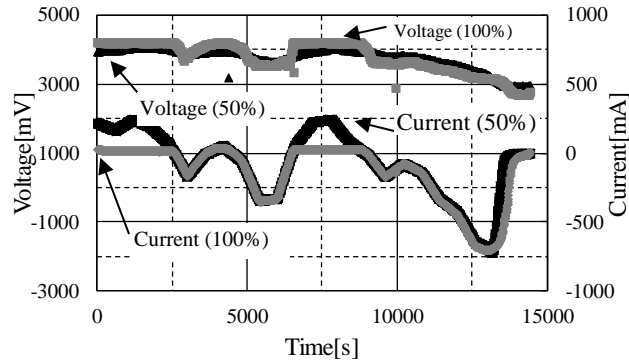
Fig. 4.36. Voltage and current waveforms of Li-ion simulated by a scaled power of a wind generation assuming a variable load.

Moreover, before the voltage reaches the upper limit or lower limit voltage, the developed simulator decreases the battery current. If the SOC reaches to 100 % or 0 %, the battery is disconnected to protect for over-charge or over-discharge. The developed system in this study can simulate the operational characteristic of the storage system regardless of the battery type. As a result, the operating condition of the storage system can be reproduced according to the given power generation and load power. In addition, the simulation is carried out using an actual battery cell installed in the storage system in the wind power generation. Due to the usage of the actual battery, the deterioration characteristics of the battery are automatically taken into consideration. In addition, it is possible to know how the battery will be deteriorated by the assumed operation.

c)   Electric Vehicle's storage system

Although engine-driven automobiles using fossil fuels have been mainly used, electric vehicles (EVs) currently have attracted attention due to depletion of oil resources and environmental pollution. The EV consists of a storage system, a controller, and an electric motor. Its regenerative energy can be effectively used, and noise and running costs can be reduced compared with the conventional automobile. Nevertheless, the EV has a shorter mileage than that of conventional vehicles, further improvements, such as the efficient operation of the storage system, are desired. In order to solve these issues, the developed simulator is useful for testing the characteristics using a cell in the EV battery pack with actual driven data [174]. In this section, the charging and discharging

characteristic is simulated using a practical current EV equipped with a 24-kWh battery pack. Fig. 4.37 shows a cell current during an EV driving, and the positive value indicates battery is charged by the regenerative energy. At t=24400 and 25400 s, a large discharge current pulses due to sudden acceleration are observed.

In the simulation, a scaled model is synthesized under an assumption that the capacity ratio is 30, which is determined from the configuration of the battery pack. Fig. 4.38 shows the simulated result. This simulation gives important information to engineers for developing efficient battery operating methods and SOC estimation methods.
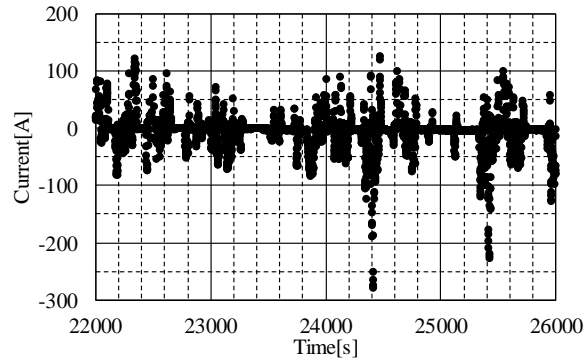
Fig. 4.37. Charging current of a battery pack while EV is driven.
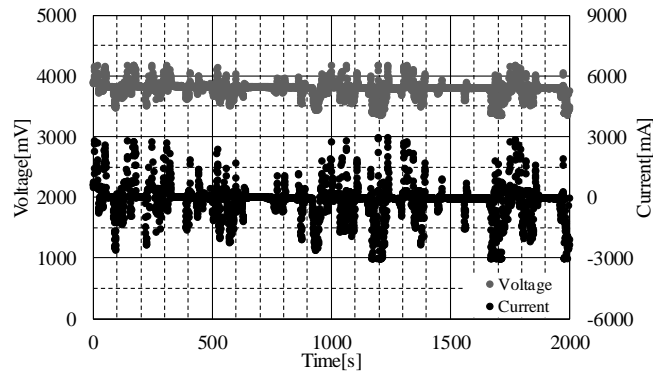
Fig. 4.38. Scaled simulation per Li-ion cell by EV driven current.

The large current for the sudden acceleration cannot be modelled, because the charge and discharge current is limited to 3 A according to the current specification of the simulator. The limitation will be removed by enhancement of the output part of the simulator.

4.6   Conclusions

In engineering field, it is important to improve the technology, the technique and finding new ideas or approaches, but the most important thing is how to use such information and where to apply these new techniques. The correct and fast SoC is topic which introduces high interest for all the industry sector. Should be highlighted the fact that a possible online monitoring and diagnosis of the battery without the need to stop the

normal operation it is possible through this research, which was possible to achieve through unconventional methods respectively with AI by ANN technique.

On the first part of ANN investigation was introduces a SoC estimation method with elevated accuracy and in a short time of calculation. The proposed method was based on adaptive ANN model which asymptotically achieves optimal error rates for realizing stochastic rules. The data used for this study are all genuine data obtained through practical experiments which introduce a correct physical meaning and relation with all the variables. Li-Ion batteries with different level of deterioration are used in order to obtain and understand the differences from the obtained data. After the final optimization of the proposed structure, the accuracy of the model was obtained with the maximum error of 2.9% in the worst case. The estimation can be concluded in the range from 23.9 to 32.4 seconds.

This model is mostly focus on the online learning approach, in order to make an optimized generalization for further application in different fields as portable devices or even as a stationary one for the renewable energy applications

An advance SoC estimation method for the Li-Ion and rechargeable batteries is proposed in the second part of this chapter. The proposed method is based on adaptive ANN model which asymptotically achieves optimal error rates for realizing stochastic rules. Through this method, an improved SoC estimation was achieved with a higher accuracy, less estimation time, and a high generality. In addition, the number of input cells is drastically reduced up to 1/4. The estimation can be concluded in the range from 15 to 29 seconds by 34% faster than that of the previous method on single cell or battery pack, and maintained stable during all the tests. This study reduced the difficulty due to nonlinear characteristics without the need of initial conditions. These results can help researcher in the investigation of an accurate & low-cost approach for the SoC estimation, which helps for further application in different fields from EVs to the renewable energy applications [175,176].

Finally, in this chapter a scaled hardware simulator of the energy storage system is developed. It uses a single or few cells in order to simulate a practical battery pack to consider the real battery characteristic. The developed simulator can charge and discharge any rechargeable battery, such as Li-Ion, Ni-MH, or Pb battery. Although the developed simulator has a high generality, it is inexpensive and portable. The scaling ratio of the simulator is determined by the ratio of the current or power of the battery pack specimen to the specification of the simulator. If the power is given, the current is calculated using measured battery voltage by an embedded computer on the simulator. According to the scaled current, the battery specimen is charged and discharged by the simulator. As a result, it is a simulation of the storage system using a real battery. The capacity of the target storage system is taken into account by the scaling factor. Because the battery in the storage system is frequently charged and discharged, its deterioration characteristic has to be known at the design stage of the storage system. The characteristic can be obtained using a practical operational condition which is realized by a current control circuit installed in the simulator.

Storage systems for stabilizing the output power of solar and wind power generation are simulated as examples. The capacities are 2 kW and 20 kW, respectively. In addition, an EV with a battery capacity of 24 kWh is tested. The storage capacity is easily changed based on the scaling factor by assuming or predicting the power generation and load power from various parameters such as the intensity of solar radiation and wind speed, etc. In addition, this system can indicate the difference of the storage characteristic due to the type of secondary battery. Since the developed simulator uses actual batteries, the simulated result automatically includes the effect of electrochemical reactions which cannot be explained by the numerical simulations.

The application fields of the developed simulator are not restricted, because the developed simulator has a capability of arbitrary current control, i.e., waveform, amplitude, duty cycle. From the above, the developed simulator in this paper can contribute to the efficient operation and optimum design of the storage system by providing useful information to the system design. In addition, the developed simulator can contribute to the investigation of prolonging the battery life and SOC estimation, since the simulator uses a practical battery.

The main contribution of the author regarding the problems in this chapter are based on these publications:

1) **Published Journals**

   a) M. Bezha and N. Nagaoka, "*Improved ANN for Estimation of Power Consumption of EV for Real Time Battery Diagnosis*", IEEJ Journal of Industry Applications IA 2019/03(E) Special Issue on Motion Control and its Related Technologies, Vol.8, No.3, pp.532-538.

2) **International Conference Papers**

   a) M. Bezha and N. Nagaoka, "*An Adaptive Model of SOC Estimation for Li-Ion Battery by using ANN for Real-Time Diagnosis*" IEEJ 2019 Annual meeting, Sapporo, Hokkaido, Japan, 12-14 March (2019).

   b) M. Bezha and N. Nagaoka, ""*Online learning ANN model for SoC estimation of the Lithium-Ion battery in case of small amount of data for practical applications*", IEEE 10th International Conference on Power Electronics – ECCE Asia (ICPE 2019-ECCE Asia), Busan, Korea, 27-30 May (2019).

   c) Ryo Gondo, M. Bezha, Makoto Ishii, Takahiro Shoda, Tomoyuki Suzuki, N. Nagaoka, "*Development of Scaled Simulator for Designing Power Storage System*", IEEE 54th International Universities Power Engineering Conference, UPEC 2019, Bucharest, Romania, 3rd-6th September (2019).

   d) K. Yamamoto, M. Bezha, Y. Baba, N. Nagaoka,"*Investigation of voltage and current measurement of Li-ion battery with a BMS*",13th ISET/ISS & 6th ISLH Conference, Chonburi, Thailand, 29-30 November (2019).

   e) M. Bezha and N. Nagaoka, "*Advanced SoC Estimation of Li-Ion Batteries Accelerated through ANN with Adaptive Algorithm*", 11th IEEE PES Asia-Pacific Power and Energy Engineering Conference- IEEE APPEEC 2019, Macau, China, 1st-4th December (2019).

5.   State of Health (SoH) Estimation and Evaluation

5.1   State of art and Conventional methods

Proper usage of the batteries affects how long the battery in PV/EV systems will last. It is necessary to achieve the correct estimation of State of Health (SoH) which directly can affect the total cost of the system and its efficiency. As a matter of fact, the battery cost in EV applications is (35-50) % of the total cost of the cars. Their classification of deterioration and when the battery pack is not any more efficient then we should know which will be the next application of usage. This introduces a big challenge. The electrification of transportation is one of the main priorities for human society, in order to reduce the CO_2 emissions. Based on the indicators acquired from The World Bank, around 21% of total fuel combustion is used in transportation, which directly inflicts on the CO_2 emissions value. The re-used battery market it's very big, especially in developed countries which have embraced the zero-emission vehicles based on full battery electric system. China as one of the biggest manufacturers and users of the EV, or Battery Electric Buses (BEB) where 99% of worldwide users have been deployed in China, it means that this market needs to prepare his self to manage the re-used batteries. This fact has pushed the researchers and companies to investigate further for the improvement of battery technology. This need has enhanced the actual level of manufacturing. Depending on the application field each battery type has different performances and attributes; thermal stability, C rate, cost, safety, power, energy, lifespan, mechanical stress support. But due to these variables, the performance quality of the battery will deteriorate as a matter of time [177-180]. By doing an observation to the charging or discharging characteristics of the EV's battery, it is possible to evaluate the overall dynamic characteristics which are the main noticeable factor which helps on the deterioration of the storage system beside the natural lifespan. On the other hand, the storage system applied on PV farms, small off-grid system, power grid or any other type of stationary storage system (3S) have different characteristics of its charging/discharging plan. In EVs, the needs of the high capacity drain, fast charging ratio of small factory packed batteries can increase the effect of deterioration and make it even not usable anymore for EV applications. The increase of internal resistance parameters can limit the output current which effects the power drain level. But for stationary storage system, the increase of the internal resistance is not such a big problem as in EV's because they can afford a little more the limitation and reduction of current by connecting more batteries in parallel. The space ratio is more flexible in 3S, but still important to be consider. The capacity fade plays a bigger role and importance in the 3S based on the change of the C_n values in the equivalent circuit model (ECM).

a)   *Estimating the level of deterioration*

The deterioration effect of the battery storage systems is one of the main concerns, which cannot be resolved, even if we use the battery within the nominal operational values. From this point of view, the correct estimation of SoH becomes a must diagnosis. Many researchers have introduced a different type of diagnostical models. This paper will not focus only on the accurate SoH estimation with low computational requirement resources, no need for costly devices. But it will introduce the correct moment for switching the used battery from high current drain applications to medium to a low current of usage as systems focused on capacity ratio. China is one of the biggest markets around the world for electric vehicles, especially in BEB. From 425,000 BEBs worldwide at the end of last year, around 421,000 were in China. This value of BEBs is 17.3% of China's total bus fleet and is expected to rise to more than 600,000 by 2025, according to BNEF. The BEB market will guide and decide the future of EVs and their technology, as one of the most important parts of public transportation. After a specific deterioration of the batteries, which limits the performance of the EVs they are sent into the recycling factories, where the cost is high. Another way is by sending it into a second-hand market where is sold out for a cheap price. This chapter proposes a diagnostical process, classification process and re-use of the battery in another application field. Finally, when the performance of the re-used battery is below the minimum requirement, they can be sent to recycling factories. If re-use of the batteries in a small/medium-scale off-grid

system as a stationary storage system is realized, the cost of PV-system storage can be reduced by using all the extra power juice which is left from the batteries.

b) *Classification process of the re-used batteries*

The proposed idea is based on the switching the re-used batteries from EV into HEV and finally to 3S systems, after a diagnostical test and analyses, by Artificial Neural Network (ANN) technique as a viable alternative method. The ANN approach will estimate the SoH and the switching time of the battery system from one application to another one with the target for maximum usage of on the ANN logic. This test and diagnosis are already confirmed in [139, 174]. This approach gives the opportunity for an online monitoring and real-time diagnosis which can satisfy the required accuracy level of the users. Fig.5.1.a shows the typical optimal battery lifetime usage of Li-Ion.
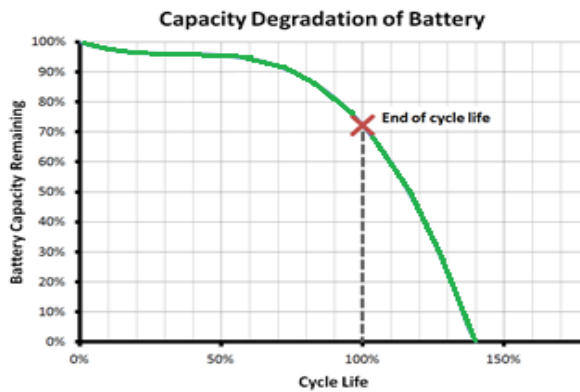
Fig. 5.1.a Characteristics of an optimal battery lifetime usage.

With the help of the ANN approach, it helps to understand the correct time of switching the system of usage based on the online learning model which can be obtained from the BMS data of the EV owner. The idea of this study is shown in Fig. 5.1.b with two steps of deterioration until it goes for the recycling process.

Fig. 5.1.b Diagram logic of the proposed idea.

After being used for e-mobility for high power drains like EVs it can be shifted to HEVs. This is the first level of deterioration and switching option. Based on the values during monitoring, after a second diagnosis and confirmation it will be shifted from e-mobility to a stationary application.

c) *Experimental approach and tests*

The two most important electrical entities, which describe the performance of Li-Ion batteries, for the high current drain as e-mobility or in 3S applications, are capacity and the power capability. From a conventional method as DC pulse technique, based on the current injection method but enhanced with the fast estimation and elevated generalization ability of ANN. This method will allow making an accurate estimation of capacity & power decrease of the batteries. In this section, Li-Ion batteries are used for the experimental tests in order to

retrieve genuine data, and the simulations and estimations are carried out using MATLAB R2019a. Single-cell battery and battery pack approach are used in this study in order to simulate a real scenario of a battery storage system. As well The BMS model for the battery pack is included to enable a good voltage balancing during charging/discharging. This approach helps to increase the lifetime of the new/used battery and extracting as much as possible energy from the pack. Fig. 5.2. shows the configuration of the cells.
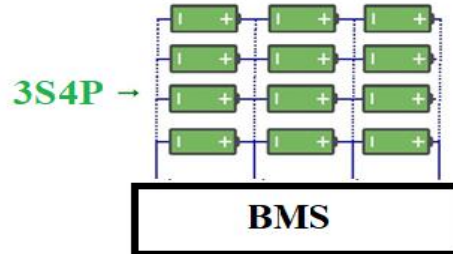
Fig. 5.2. Charging/Discharging 3S circuit for 18650 Li-Ion cell battery with 4 parallel pack model

Regarding the inputs of the ANN structure entities like the voltage, current, temperature and number of cycles are included. To make a good generalization, massive experiments should be conducted at different temperatures and cycles of usage as in [135, 138]. Finally, the estimated values will be compared with measure one in order to verify the accuracy of the proposed model. In order to simulate and accurate behavior of the dynamic discharge characteristics of EV`s battery pack, the scale down BSS.

5.2   Proposed Methodology

a) Experimental concept

The experimental data will be obtained based on the 3S4P pack connected with a BMS system, with features like over/under voltage and current protection during charging/ discharging of the pack. In order to imitate a real EVs battery pack discharge during operation, the scale down system will be discharged by two different types of loads. One will be a programmable load which will do the CCCV protocol and the other load type will be a manual controlled by a 12V DC brushless motor type, with 2 gear speed for high current drill usage.

Table 5.1 Specification of the 12 V DC Brushless Motor.

Features	Value
Torque [Nm]	1st gear 7.0 / 2nd gear 12.0
Speed [min^{-1}]	1st gear 0~1170/ / 2nd gear 0~330
Max. Battery Voltage [V]	12.6
OEM Battery Chemistry	Ni-Cd
OEM Battery capacity [Ah]	3
Proposed Battery Chemistry	Li-Ion
Proposed Battery Capacity [Ah]	13
Cell Battery type	18650, high-capacity type

These tests will be based on 2 different stress test, one test will finish in 20s with frequency sampling of 500Hz and the second test will be concluded in 100s with frequency sampling of 100Hz. For each of these 2-stress test the number of samples are maintained equal in order to maintain the same input data structure of the ANN model, which will be explained in the next chapter. The total samples are 10,000, where for the 20s stress test is every 2ms, and for the 100s stress test is every 10ms. The Voltage and Current samples can be obtained from the 12.6 V pack system or even from each single cylindrical cell. More than 10 different patterns of loads are concluded

for each of these 2-stress test, in order to increase the generalization of the model. The pattern is totally random imitating a daily driving behavior of the driver. Slowly increase or decrease of the speed, suddenly stop of the motor, or even suddenly speed up of the DC motor at highest speed settings. Due to the fact that the DC motor have 2 gears these can used as power saving mode or performance mode test. Fig.5.3 shows the full stress test for 20s.
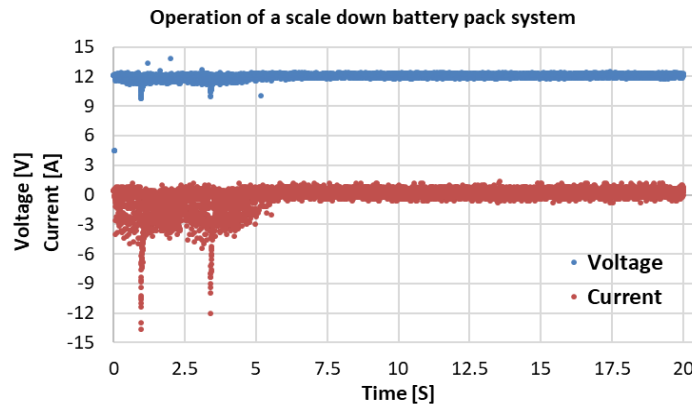
Fig. 5.3. Discharging of the 3S4P pack during 20seconds stress test

Figs. 5.4 and 5.5 show the V, I waveform during the starting moment of the motor, at the highest gear speed, reaching a max speed of 19%.
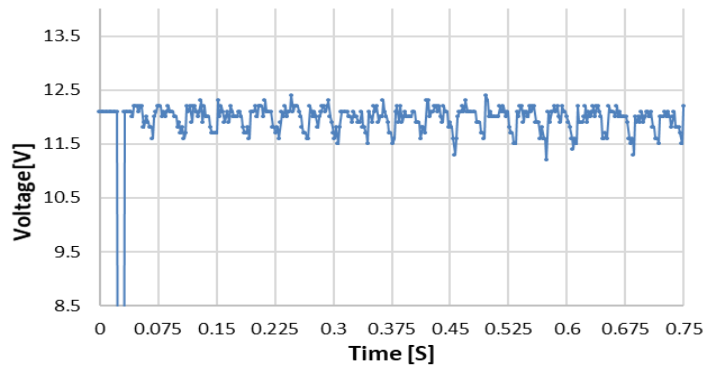
Fig. 5.4. Voltage waveform at the start of discharging pack for the 20seconds stress test
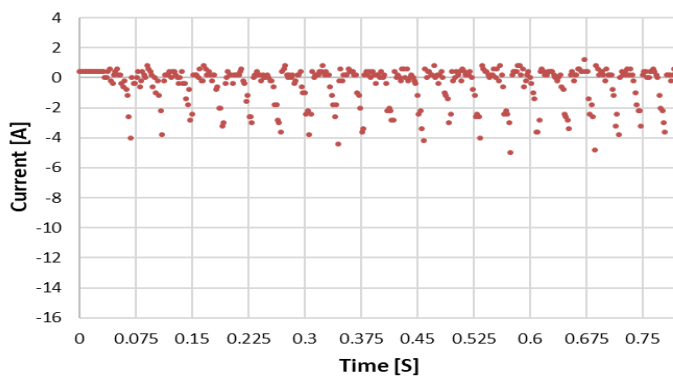
Fig. 5.5. Current waveform at the start of discharging pack for the 20s stress test

69

In Figs. 5.6 and 5.7 are shown the V and I waveform during the first high peak increase at the maximum speed level. This increment of the speed is immediately and as is shown in the figures the voltage has a drop of around 3V and with a drain of current of 13A for 0.2s. And After that, the speed immediately decreases around 60%. And later the second-high peak is happening for almost the same period of time.
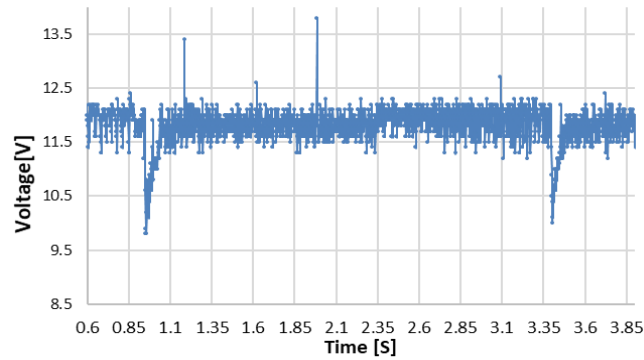
Fig. 5.6. Voltage waveform at the first peak speed for the 20s stress test
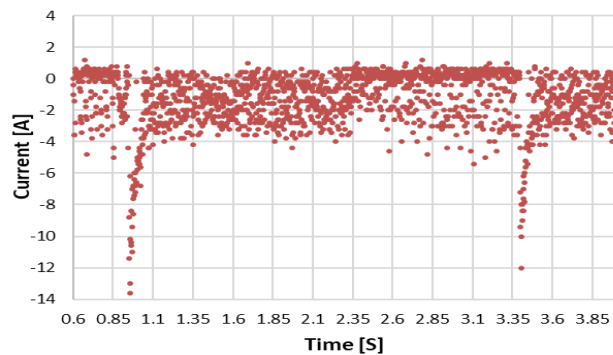
Fig. 5.7. Current waveform at the first peak speed for the 20s stress test

In Fig. 5.8 is shown the 100s stress test. It is easy so observe the difference of the test in terms of speed, level of V and I drop. The 100s stress test is important, because it can show the stability of the battery pack for a longer period and for more aggressive behavior.
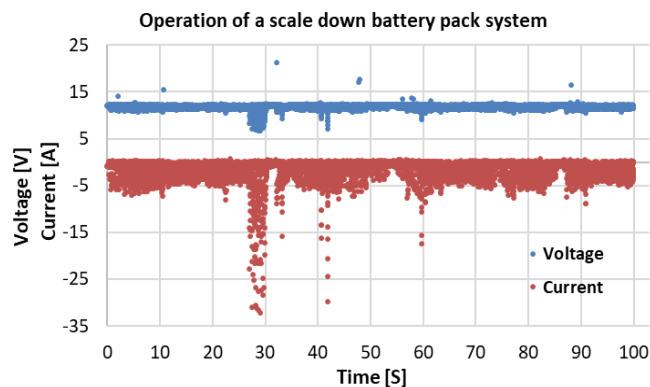
Fig. 5.8. Discharging of the 3S4P pack during 100seconds stress test with 3 different high peak speed test moments

5.2.1 ANN model

As always, this approach is based on three processes, learning, validation and test. The proposed NN is processed in MATLAB R2019a. This NN structure will be based on cascade system and the output of the first will be used as the input of the second one. For the V and I input 10,000 samples will be used, and the third input it can be an optional variable. This input shows the number of cycles or as known the lifetime period of a battery.
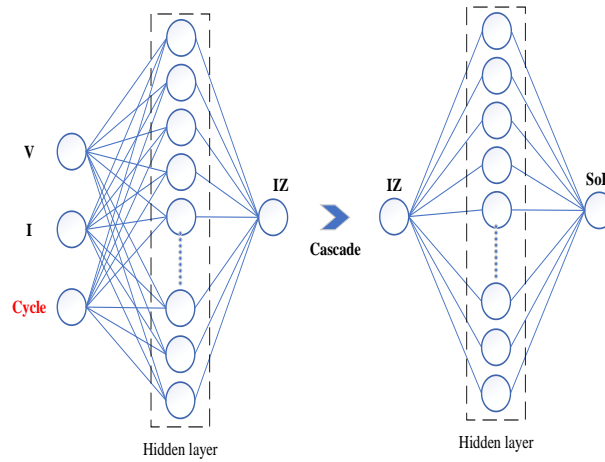
Fig. 5.9. Proposed ANN cascade structure with 1 hidden layer
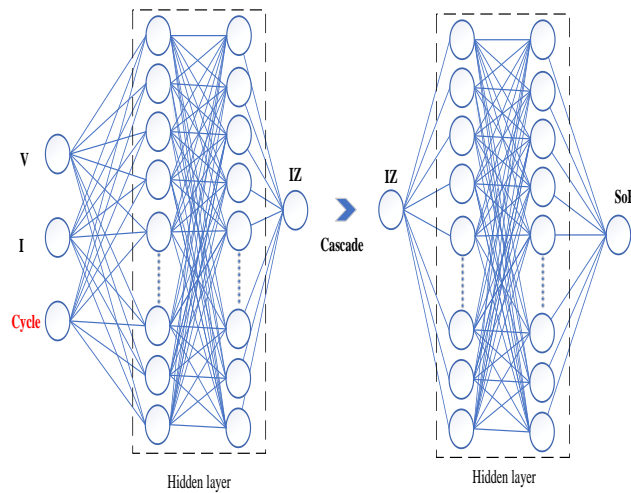
Fig. 5.10. Proposed ANN cascade structure with 2 hidden layers

In this study a cascade NN structure is used and the internal impedance (IZ) is expressed through the ECM's parameters of the second order, as shown in Fig.5.11. There is different type of ECM proposed by other researchers [140,141,143,180]. The number of the IZ parameters are 6. In this study the author decided to choose a second order model in order to include the DC characteristics as well the AC transients. Of course, it is known that a higher order is better to explain the battery characteristics and the SoH or SoC estimation can be more accurate, but the complexity of the model it's increased which will affect the calculation time and increase the

cost of the device in terms of computational power. In Chapter 6 it will be explained more in detail regarding the ECM.

After finishing the stress test with the 12 cells another test will be held by the NF-AS-510-LB4 battery test-system, in order to obtain the correct values of the circuit parameters.
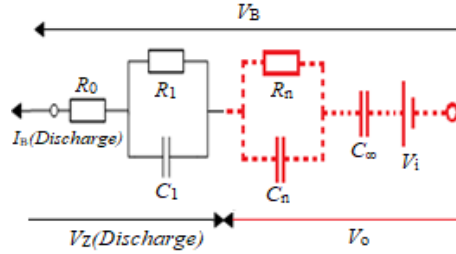
Fig. 5.11. Proposed ECM of the second order

Below are shown the results of the estimated parameters through ANN algorithm and compared with the measured values, for each of the battery cells. Where the Measured values are obtained from the NF-AS-510-LB4, during different scenarios, which includes charging or discharging process, different ratio and different SoH or SoC settings. In order to clarify "*the different SoH or SoC value*", it means that for the training of the ANN and

Table 5.2. Parameters of Cell 1

Parameters	Measured	Estimated
R_0 (mΩ)	47.9	48.18
R_1 (mΩ)	2.4	2.61
R_n (mΩ)	57.5	58.25
C_1 (kF)	0.65	0.59
C_n (kF)	1.9	1.61
C_∞ (MF)	3.6	4.1

Table 5.3. Parameters of Cell 2

Parameters	Measured	Estimated
R_0 (mΩ)	50.2	52.3
R_1 (mΩ)	2.42	2.23
R_n (mΩ)	59.1	58.95
C_1 (kF)	0.75	0.65
C_n (kF)	2.1	2.39
C_∞ (MF)	3.94	4.1

Table 5.4. Parameters of Cell 3

Parameters	Measured	Estimated
R_0 (mΩ)	56.8	57.09
R_1 (mΩ)	2.46	2.12
R_n (mΩ)	58.1	57.11
C_1 (kF)	0.82	0.93
C_n (kF)	1.9	1.65
C_∞ (MF)	3.65	3.52

Table 5.5. Parameters of Cell 4

Parameters	Measured	Estimated
R_0 (mΩ)	49.2	51.95
R_1 (mΩ)	2.38	1.94
R_n (mΩ)	58.9	60.03
C_1 (kF)	0.85	1.02
C_n (kF)	1.94	2.27
C_∞ (MF)	3.62	3.54

Table 5.6. Parameters of Cell 5

Parameters	Measured	Estimated
R_0 (mΩ)	51.3	49.7
R_1 (mΩ)	2.43	2.22
R_n (mΩ)	60.7	61.17
C_1 (kF)	0.74	0.82
C_n (kF)	1.95	2.15
C_∞ (MF)	3.85	4.03

Table 5.7. Parameters of Cell 6

Parameters	Measured	Estimated
R_0 (mΩ)	49.3	50.2
R_1 (mΩ)	2.35	2.43
R_n (mΩ)	58.1	59.6
C_1 (kF)	0.8	0.78
C_n (kF)	1.95	1.89
C_∞ (MF)	3.7	3.66

Table 5.8. Parameters of Cell 7

Parameters	Measured	Estimated
R_0 (mΩ)	50.2	49.65
R_1 (mΩ)	2.31	2.46
R_n (mΩ)	58.8	57.5
C_1 (kF)	0.73	0.72
C_n (kF)	1..88	1.81
C_∞ (MF)	3.85	3.9

Table 5.9. Parameters of Cell 8

Parameters	Measured	Estimated
R_0 (mΩ)	49.8	46.65
R_1 (mΩ)	2.33	2.46
R_n (mΩ)	58.2	58.5
C_1 (kF)	0.75	0.74
C_n (kF)	1.88	1.81
C_∞ (MF)	3.61	3.69

Table 5.10. Parameters of Cell 9

Parameters	Measured	Estimated
R_0 (mΩ)	49.3	47.65
R_1 (mΩ)	2.3	2.48
R_n (mΩ)	58.5	57.35
C_1 (kF)	0.7	0.721
C_n (kF)	1.9	1.85
C_∞ (MF)	3.61	3.69

Table 5.11. Parameters of Cell 10

Parameters	Measured	Estimated
R_0 (mΩ)	49.5	49.7
R_1 (mΩ)	2.41	2.46
R_n (mΩ)	59.2	58.35
C_1 (kF)	0.72	0.721
C_n (kF)	1.95	1.81
C_∞ (MF)	3.57	3.68

Table 5.12. Parameters of Cell 11

Parameters	Measured	Estimated
R_0 (mΩ)	51.5	53.01
R_1 (mΩ)	2.35	2.18
R_n (mΩ)	59.2	61.9
C_1 (kF)	0.78	0.84
C_n (kF)	1.87	1.74
C_∞ (MF)	3.82	4.01

Table 5.13. Parameters of Cell 12

Parameters	Measured	Estimated
R_0 (mΩ)	51.3	50.8
R_1 (mΩ)	2.1	2.2
R_n (mΩ)	59.3	60.6
C_1 (kF)	0.85	0.87
C_n (kF)	1.9	1.95
C_∞ (MF)	3.65	3.72

5.2.2 Proposed methodology in EVs applications (power, energy, SoH estimation)

In this sub section, an ANN model, which estimates the power consumption of an EV during the deterioration process of power storage, is described. This network provides important information for real-time battery diagnosis, such as state of charge of a Li-Ion battery for an EV or HEV. The data are retrieved from a scaled experiment, based on the JC08 test cycle. The network is presented as a practical alternative to analytical and empirical methods. It can predict the power consumption by an optimal solution and categorize the deterioration of the power storage with high estimation precision and within short time.

The attention to develop and update the energy storage system is one of the important purposes of the researchers of EV as well as power system. The rechargeable batteries are considered as the most common storage devices. In the running process of EV or Hybrid Electric Vehicle (HEV), the batteries experience stress from the dynamic operational environment. The charging condition is essential for designing the storage system, while the charging quality of the battery directly affects the battery life and continual mileage. If the charging process is not controlled, it will damage the battery. The cooperative control for motor and battery is indispensable. One of ways to develop models of EV or HEV for individual components like the storage unit is through rigorous analytical procedure. Due to its typically time-consuming and the simplifying assumptions required to make the analysis tractable, it impairs the value of such models. An alternative way is to employ conventional empirical methods, which are variations of the classical regression theme. These models are unwieldy and are usually only suitable for low-end nonlinearities. Solving the difficulties of non-linear models, it introduces to us, new challenges, which must be concluded with a good performance and accuracy.

One of the representative energy-storage types is Li-Ion batteries. This type of battery is one of the most promising power sources for the energy storage system of the EVs, due to the advantages of high energy density, environmental protection, long cycle life [180, 182]. As other batteries, issues like aging and fault occur in Li-Ion batteries as time goes, and they are circularly used.

The simplified models cannot represent the behavior of the battery exactly, also the models are not universal because they may lead to wrong estimation in certain battery types. Few models have been improved with hybrid modelling design [143]. The real time estimating diagnosis is a complex nonlinear system. Even now the accuracy and reliability of the SOC estimation remains to be improved. SOC or fault prediction are depending by the internal characteristics of battery which could not be measured. The conventional method of the computers is based on the algorithmic approach i.e. the computer follows a specific path and type of instructions in order to solve a problem. The application of the ANN in the estimation of the SOC under the variable of the voltage charge, it provides a tool to deal with the above difficulties. Should mention that ANN does not rely on the explicitly expressed relationship between input variables and the SOC. Because of their characteristics based on the black box approach which do not require any knowledge about the system's internal dynamics [148,185,186,187]. The relationship between the input variables and the SOC is formed through training. For the learning process there are many ML methods, this approach is called indirect method. These indirect methods can be categorized as below:

a) *Parameter estimation (PE)*
b) *Adaptive filter-mathematical based estimation (FME)*
c) *Adaptive AI (AAI)*
d) *Hybrid model estimation (HE)*

When an analytical model is unknown, too complex or incomplete, a typical alternative is to try to forecast by building a model that takes into account only previous outcomes, with neglecting any exterior influence. A

75

time series $\{x(t)\}$ can be defined as a function x of an independent variable t, stemming from a process for which a mathematical description is unknown. A time series is a sequence of vectors, $x(t)$, $t = 0, 1,….,n$, where t represents elapsed time. In practice, for any given physical system, the variable x will be sampled to give a series of discrete data points, equally spaced in time. It must be clear that not always the model with the highest resolution has the best predictive power, so that superior results can be obtained by using only every nth point in the series. Different models have been compared in the literatures in search for the best trade-offs between performance and maintenance cost. Observers have been improved with hybrid modelling design [143]. One of the most important differences between an observer and machine learning techniques is that machine learning uses data regression methods, so they can be easily trained using real world data, since they are data-driven models. Learning machines are trained using known inputs and outputs. After this, the trained ML is used to provide estimated output for unknown inputs.

5.3   EV specification
5.3.1 Methodology and Experimental Results
In this section, the study is based on the data taken from the EV model. These data are scaled down to be adapted for the practical experiment conducted in the laboratory. Table 5.14 shows the official data from the EV model

Table 5.14. Specifications of the EV model.

Occupant capacity	5
Cruising range	228 km - (JC08)
Motor	80 kW
Electricity consumption	0.114 kWh/km
Battery	Li-Ion 24 kWh
Acceleration 0-60mph	11.6 seconds

Should be mentioned that the battery is modular in format and consists of 48 series connected modules, each module with 4 parallel cells, in total of 192 cells. Table 5.15 shows, the specification of JC08 mode.

Table 5.15. Specifications of JC08 mode

Average speed	24.4 km/h
Maximum speed	81.6 km/h
Time	1204 seconds
Mileage	8.172 km
Load ration	29.7%

The JC08 driving schedule is schematically shown in Fig. 1. In the transitional period emissions were determined using weighted averages from different cycles, like the previous 10-15 mode. This test mode had been fully phased-in by October 2011 as below:

➢   25% of JC08 cold start + 75% JC08 hot start

The experimental data are conducted for the same period of time as the JC08 model, which is 1204 seconds.
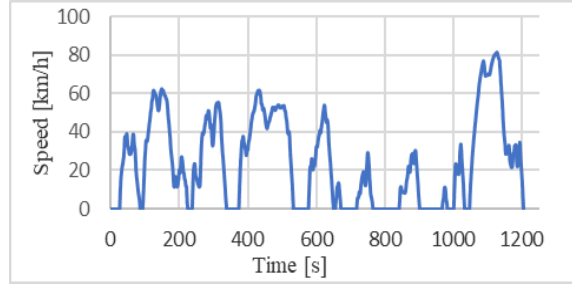
Fig. 5.12. JCO8 mode speed pattern.

As was mentioned before, the data are retrieved based on the JC08 mode cycle. Same thing is for Fig. 5.13, where the power consumption of the experimented model is simulated the.
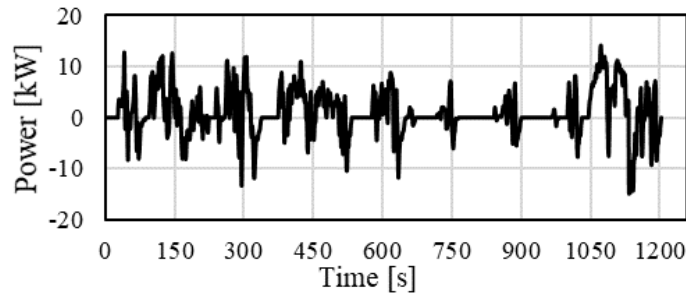
Fig. 5.13. JCO8 mode speed pattern.

In order to make it applicable for laboratory experiment, the average power consumption of the system is 3-times less comparing to the real specifications of the EV model. It means that the retrieved data will be multiplied by 3, in order to be adapted for the real EV model. The average power consumption of the proposed model conducted experimentally is 1.03 kW, which comparing with the EV model is approximately from 2.6 to 3 kW.

The proposed model is based on the modified BPNN algorithms by updating and adjusting the weights values. The value of the weights is calculated in the training phase by minimizing the loss function, their values determine how the neural network will reply to a specific time series inputs, which is important in the training phase for the accuracy of the ANN. One of the most used technique for the training of the ANN is the back-propagation of error [141]. In this experiment, the collected data are different and rich in term of technical environmental processing as the speed of the car, air resistance, rolling resistance, accelerating resistance, running resistance, power consumption, voltage characteristics etc. In the beginning the proposed model was trained with 10 neurons in the hidden layer and then increased up to max 30 neurons for the best value of training. This model started with a low number of neurons in order to prove the accuracy and to verify the best value of neurons.

Table 5.16 shows the specification of the Li-Ion battery used for this paper. Total rated capacity is 2.2kWh.

Table 5.16. Specifications of the Lithium-Ion battery.

Nominal capacity	1.2 kWh 24Ah type
Number of batteries module	2
Rated capacity per battery	1.1kWh 22Ah
Nominal output voltage	51.2 V
Charging voltage	56.7 V ± 0.8V
Maximum Charge current	24.0 A
Charging time	2.5 hours

Figs. 5.14 and 5.15 show the schematic diagram of DC distribution test system used for the scaled-down experiment and a typical EV system.
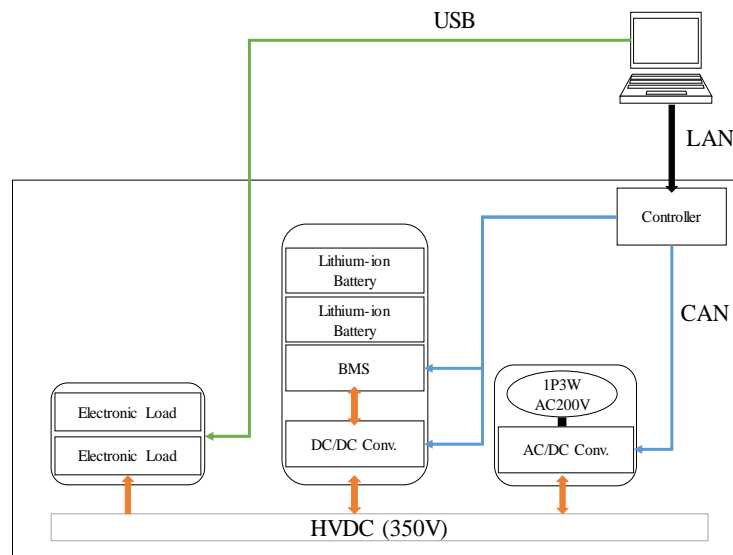
Fig. 5.14. Schematic diagram of DC-distribution system.
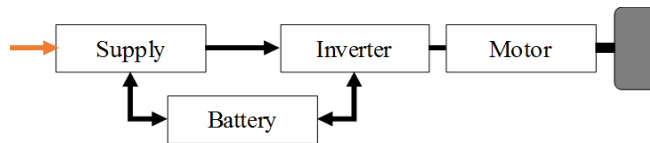
Fig. 5.15. Schematic diagram of EV system.

A dynamic characteristic of the EV is implemented into the control program of the distribution test system in order to simulate a JC08 test mode characteristics. By this proposed model, the experimental data shown in Fig. 5 can be obtained. Should be mentioned that in this study the characteristics of the inverter are neglected.
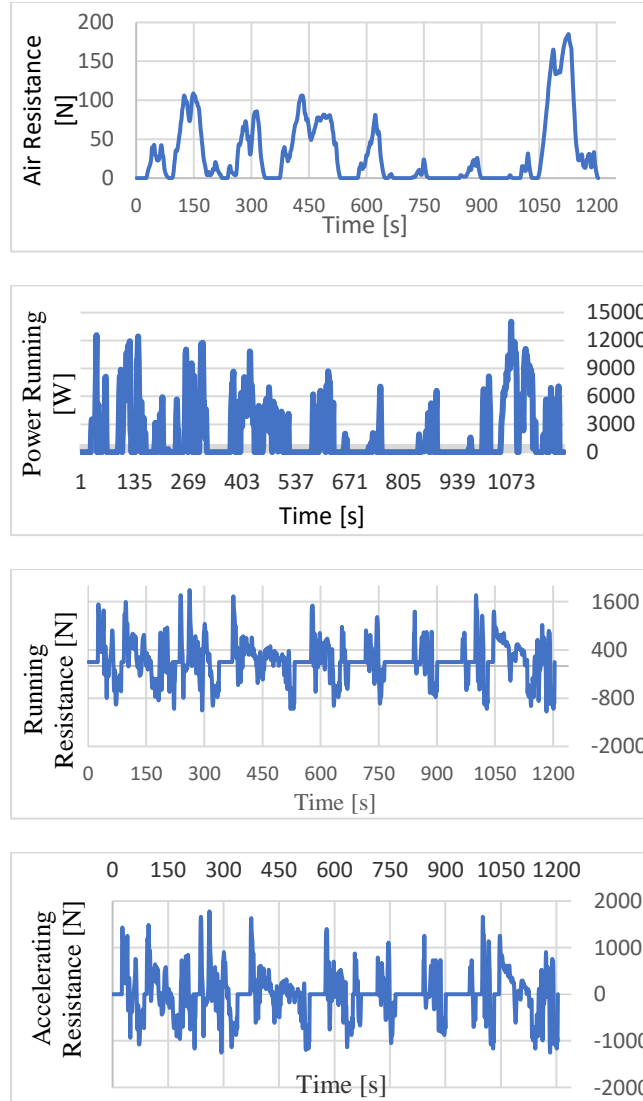
Fig. 5.16. Plots of the experimental data retrieved.

The data from the charging process of Li-Ion battery, were achieved using these devices As-510-LB4 (NF Co.) as shown in the previous chapter. It's important to clarify that these data are not obtained by an actual run of the car on the road. But they are generated based on the original data from an original successful commercial EV model. The generated data shown in Fig.5.16 where used in the beginning in order to train the ANN model. The accuracy was very good but due to the high computation time and hardware it was necessary to reduce the number of data in order to make more applicable for small embedded circuits. In the final structure of this study these data are neglected, due to the small differences of accuracy from the model with these data. The outputs are compared with the desired target values and an error is produced. Then the weights are adapted to minimize the error. The relation of output:

$$Q_i^{(l)} = fs[I_i^{(l)}] \tag{5.1}$$

$$I_i^{(l)} = \sum W_{ij}^{(l)} Q_j^{(l-1)} \tag{5.2}$$

Equation (5.1) can be transformed into:

$$fs(I) = 1/[1 + \exp(-I)] \tag{5.3}$$

The initial values of weights are assumed to be random, and the weight between the ith neuron of the $(k-1)^{th}$ layer and the ith neuron of the kth layer is defined as $W_{ij,k}$. The adapted equation of the weight is given by the following:

$$W_{ij},k(t_n) = W_{ij},k(t_{n-1}) - \frac{\alpha E(t_n)}{W_{ij},k(t_{n-1})} \Delta W_{ij},k(t_{n-1}) \tag{5.4}$$

where $0<\alpha<1$, and $E=1/2 \ \Sigma(y_i - b_i)^2$. $I=1…n$, y_i is i^{th} actual output, b_i is i^{th} simulation output. But for different problem it's not always good to increase the number of layers or neurons, because the system can go unstable and will get high error and poor optimization. In this section the MATLAB and LabVIEW software have been used. Each type of battery has a specific equation model for charging or discharging process. For the Li-Ion battery, the open-circuited voltage E_o is calculated with a nonlinear equation based on the actual SOC of the battery as follows [143,188]:

$$V_b = E_0 - R \cdot i \tag{5.5}$$

During discharge:

$$E_O = E_k - K \frac{Q}{Q - \int i \cdot t} i_t - K \frac{Q}{Q - \int i \cdot t} i^* + Ae^{(-B \cdot i \cdot t)} \tag{5.6}$$

During charge:

$$E_o = E_k - K \frac{Q}{Q - \int i \cdot t} i_t - K \frac{Q}{\int i \cdot t - 0.1Q} i^* + Ae^{(-B \cdot i \cdot t)} \tag{5.7}$$

where E_o is the open circuit voltage, E_k is the battery constant voltage, K is the polarization constant, Q is the battery capacity, i_t is the actual battery charge, i^* is the low frequency current dynamics, A is the exponential zone amplitude, B is the exponential zone time constant inverse $(Ah)^{-1}$, V_b is the battery voltage, and i is the battery current. Equations 5.5-5.8 should be used in case of non-ML methods which makes this approach difficult due to his high nonlinearity. In our case these equations will be used for the Simulink model.

All the collected data must be normalized for a standardized value. This process helps to create patterns to correlate the input vector with corresponding output vector. This range of the data will be from 0 to 1. Equation (5.8) explain the formulated normalization:

$$A_i = \frac{b_i - \min(b_i)}{\max(b_i) - \min(b_i)} \tag{5.8}$$

where i^{th} is the corresponding element of the input vector, b_i the original value of the input, A_i is the normalized value between 0 and 1, $min(b_i)$ and $max(b_i)$ are the minimum and the maximum value for each specific vector data. The range value of the voltage characteristic is from 3.1907V to 4.199V, based on a new battery sample. Fig.5.17 shows the voltage input, which was obtained through the data from the charging process of the ICR18650PD Li-Ion battery.
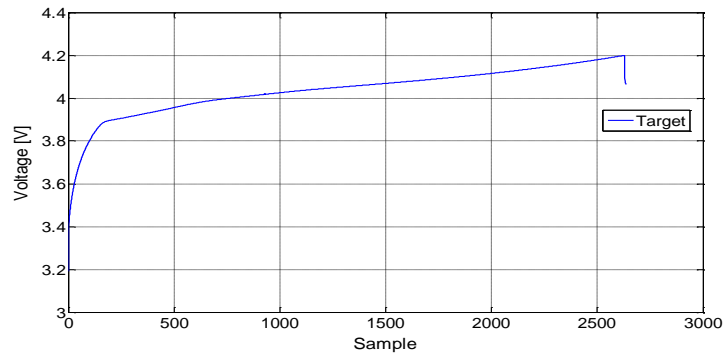
Fig. 5.17. Voltage data from the charging process [ICR18650PD]

Based on this waveform an investigation was made by the author, which was focused on the estimation of voltage characteristics of Li-ion battery during charging mode. It was possible to check the waveform in some specific zones and related any possible abnormally or difference of slope from CC to CV mode. As matter of fact due the deterioration the of battery the electrolytic material starts to lose their conductive ability and decrease the efficiency and the consequences are the increase of internal impedance, capacity fade and less current drain ability. However, the shape itself doesn't change so much. But, with the ability of ANN to understand small and unrelated parameters dynamic effect, it is possible to relate this voltage waveform with SoC estimation and in some specific cases it is even possible to do a SoH classification of the cell. The methodology of this research is explained as follow:

The charging mode is built, by 2635 samples, when every sample is taken every 2 seconds. So, all the process is 1.47 hour long. The range value of the voltage characteristic is from 3.1907 V to 4.199 V. The characteristic is shown in Fig.5.17.

These data, will be used for the training and as a target later for the simulation of the network. For different type of battery there are specific equations for charging or discharging equations model.

The battery block implements a generic dynamic model parameterized to represent most popular rechargeable batteries. This model will be based on equation (5.7), which explains the charging model of the Li-Ion battery. Fig.5.18 shows the battery equivalent circuit of the block models for the MATLAB software emulation. In the beginning, the network was started with 15 neurons in the hidden layer and the input layer was composing by a vector with 2635 elements.
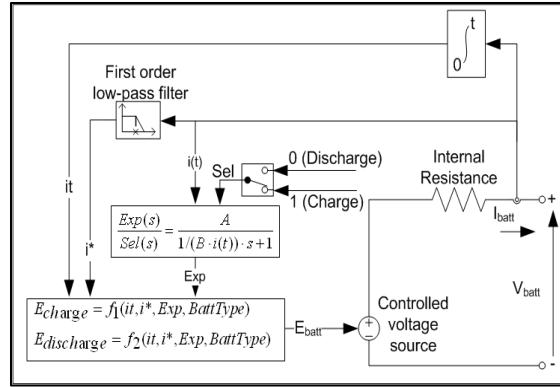
Fig. 5.18. Block diagram of the battery equivalent circuit

For this study a configuration of ECM is based on 2nd order model. Of course, there different models for low to high orders. Each of them express specific behaviors and characteristics. Fig.5.19 shows the equivalent circuit which can express the electrical composition of the Li-Ion cell. By this circuit it is possible to define parameters related with the capacity fade and the SOC through the analysis and calculation of the internal impedance [144]. The proposed ANN structure is shown in Fig.5.20.
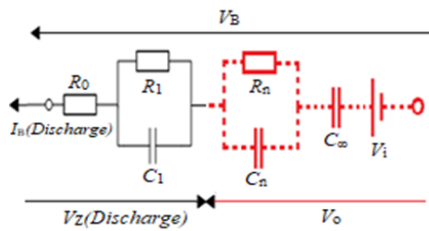
Fig. 5.19. ECM composition of 2nd order
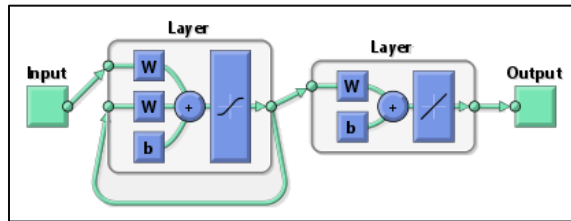
Fig. 5.20. The GDPBNN with adaptive learning rate model

Through GDPBNN structure with adaptive learning rate, it was possible to start some simulation to evaluate the performance of this model. Fig.5.21 shows the achieved simulated data after few trainings of the network, but the accuracy is not good yet even if the waveform of the predicted data is similar but with a value far from the desired target. Fig. 5.22 shows the results of the optimized NN model after few trainings.
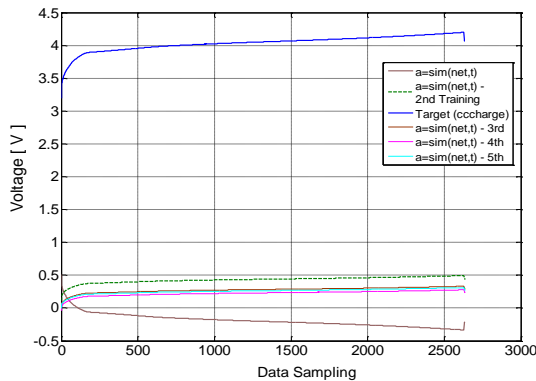
Fig. 5.21. Plot of Target and Simulated data
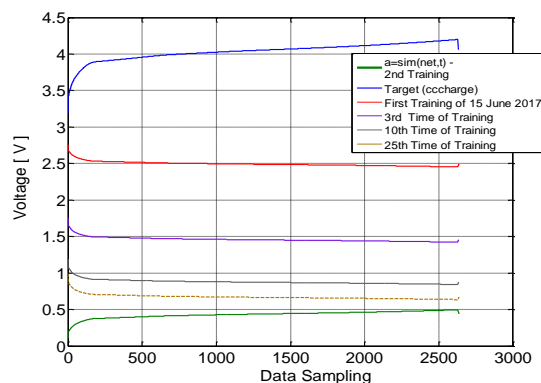
Fig. 5.22. Changed model of NN with simulated data

The simulated plots are starting to get near the target value but the still the response is not good. However, it's necessary, to tune and calibrate the learning rate process and to optimize the error of the output value in order to change the value of the bias and weight for the adaptive network. After obtained this characteristic, was realized that the system needs to reset the minimum and maximum value, so after doing this thing a new type of model was created and simulated. For this problem it is necessary to change the simulated model and keep in mind the times series estimation model. For a complete mathematical model describing a studied phenomenon when is known and not so difficult, forecasting it could be an easy task. However, when an analytical model is unknown, too complex or incomplete, a typical alternative is to try to forecast by building a model that takes into account only previous outcomes of the phenomenon while ignoring any exterior influence. More formally, a time series $\{x(t)\}$ can be defined as a function x of an independent variable t, stemming from a process for which a mathematical description is unknown. A time series is a sequence of vectors, $x(t)$, $t = 0, 1,...n$, where t represents elapsed time. For simplicity we will consider here only sequences of scalars, although the techniques considered generalize readily to vector series. x can be a value which varies continuously with t, such as voltage. In practice, for any given physical system, the variable x will be sampled to give a series of discrete data points, equally spaced in time. The rate at which samples are taken dictates the maximum resolution of the model: but, it is not always the situation when the model with the highest resolution has the best predictive power, so that superior results may be obtained by using only every n-th point in the series.

One of the main goals for the neural networks stand to the estimation of future developments of the time series from values of x up to the current time. Formally this can be stated as: find the function $f: R^N \rightarrow R$ such as to obtain an estimate of x at time $t+d$, from the N steps back from time t, so that:

$$x(t+d) = f(x(t), x(t-1), ..., x(t-N+1)) \tag{5.9}$$

$$x(t+d) = f(y(t)) \tag{5.10}$$

where $y(t)$ is the N vector of lagged x values. Normally d will be one, so that f will estimate the next value of x.
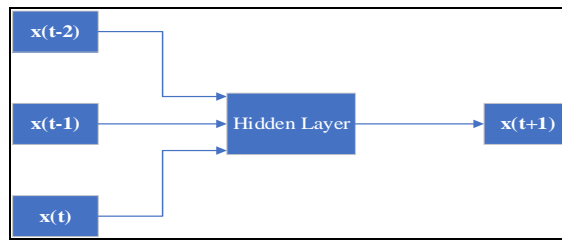
Fig. 5.23. Diagram of the time series processing function

Through the reformulated model of adaptive BFPNN Times Series Estimation, it was possible to improve the learning ability. After few trainings and defining the values of bias and weights it was possible to obtain the results as shown below. Fig.5.24, shows the new simulated data which have been obtained after changed the number of neurons in the hidden layer and changed the value of bias and weights. The updated NN model is with 35 neurons. Now the model is modified with changes in the learning rate, number of epochs and parameter goal. (*net.trainParam.lr=0.3; net.trainParam.epochs=1500; net.trainParam.goal=10^{-12}.*)

Fig.5.24 shows the state of the trained network after the 1st and 9th time. The difference in the simulated result are optimized fast and with good accuracy as shown in the Fig.5.25 and 5.26.

83
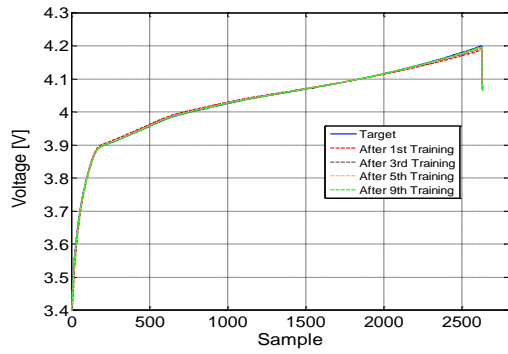
Fig. 5.24. Plots of Target and Simulated data   **Fig.** 5.25. Starting zone of the charging plot
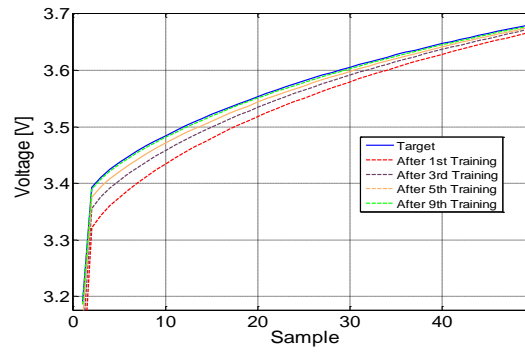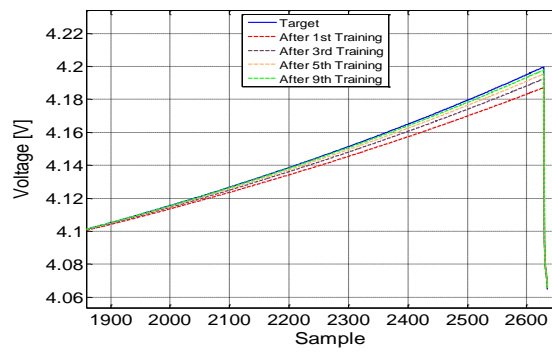
Fig. 5.26. Ending zone of charging plot
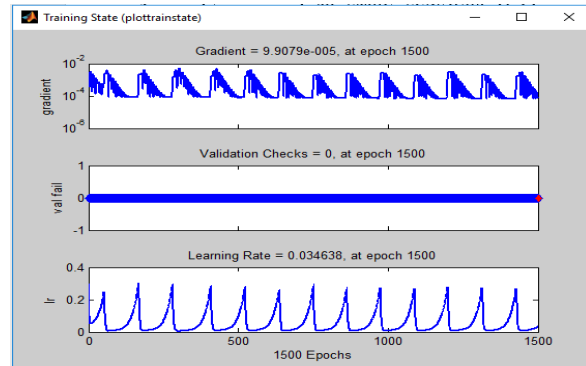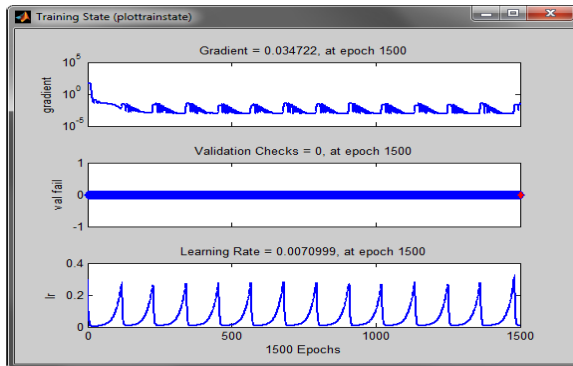
Fig. 5.27. Training state after the 1st training (left) and plot after the 9th training
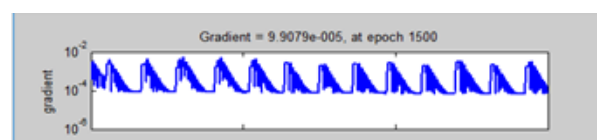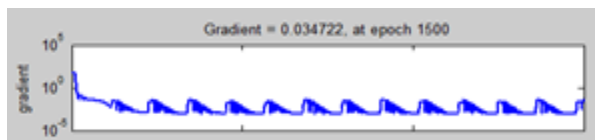
Fig. 5.28. Training state after the 1st training (left) and plot after the 9th training

Figs.5.27 and 5.28 shows the differences of the gradient between the 1st training and the 9th training. In the second picture, the gradient which is in the range of 9.9079 e-5, which mean the accuracy is getting very high.

Table 5.17. Comparison between target value and the estimation

	Min Voltage V]	Max Voltage [V]
Target	**3.1907**	**4.1999**
After 1st Training	3.0603	4.1873
After 3rd Training	3.1519	4.1915
After 5th Training	3.1588	4.1956
After 7thTraining	3.1770	4.1972
After 9thTraining	3.1864	4.198

Table 5.17 shows the comparison of the estimated values of the voltage for each estimation after the ith training of the NN. The minimum and maximum values are shown in order to make clear the differences and to observe the stability of the model.
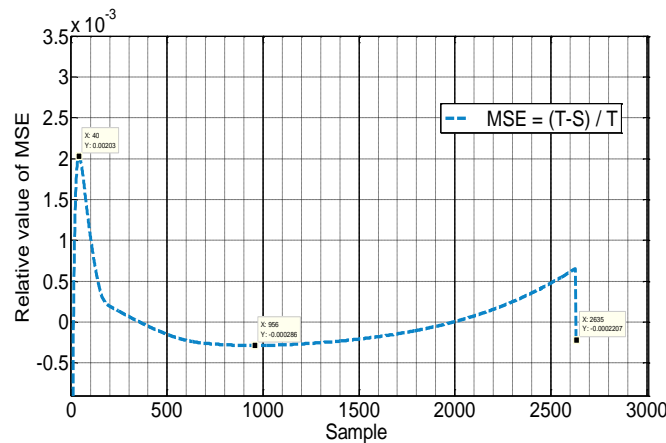
Fig. 5.29. Relative error of the estimated output

Fig.5.29. shows the relative error calculated for every samples estimated. This plot can be divided in 3 zones, first one regarding to the first peak obtained in the 40th epochs, which the error is increasing because of the learning process and the dynamic changes. The second zone of this plot is the less dynamic characteristic, which continue around the 2000th epochs, when the third zone start to increase the error. By relating the plot of the relative error with the charging plot, these peaks error accumulation or increases comes because of the fact of the CCCV charging process, by the composition of two processes, when first stand for constant current (CC) and the second for the constant voltage (CV). After confirming the ability of this approach, it was possible to use it further for the battery pack of the EV's.

The obtained characteristics are adapted to the number of data cells equal to the process of JC08 mode and the scaled model. The first experiment was based on a new battery with 0 cycle usage. In order to make this model more applicable, the required data, and computational power have been reduced in this paper. As shown in Fig. 5.30, only the speed and battery voltage, i.e., without the current information, gives the estimated power consumption. Because the battery current has close relations between the speed and its slope, the ANN understands the relations.
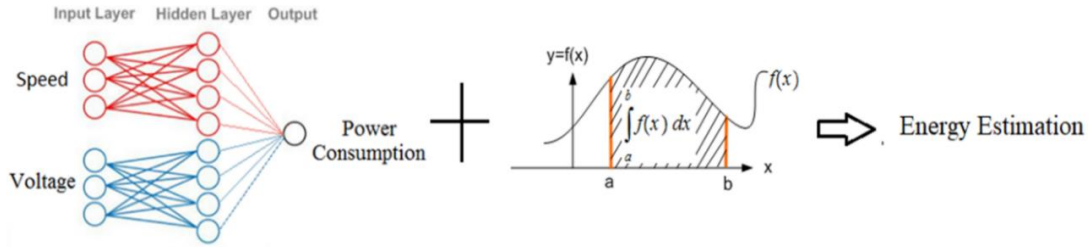
Fig. 5.30. NN structure model for the Power and Energy Consumption
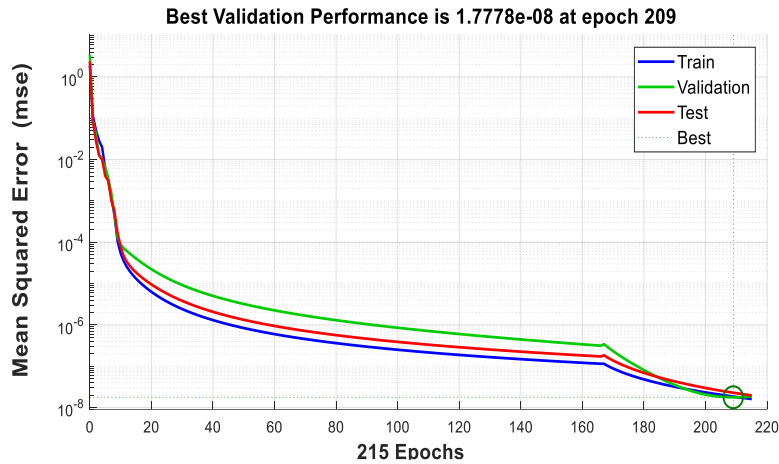
Fig. 5.31. NN structure model (left) and performance (right)

5.3.2 Testing

As mentioned before, the data used as input data for this simulation are few, but in order to reduce the quantity of calculated data and time of processing, only 2 main input data are used for the training process, as speed of the car and voltage of the battery, which can be obtained easily through the sensors. The output will be the power consumption. If the other extra data such as the air resistance, running resistance, and/or acceleration resistance are used, the accuracy of the estimation is increased. Also, it is important to mention that in this study the temperature of the battery and the humidity of the room have been neglected. The experimental data are retrieved in 20 minutes and 4 seconds based on the JC08 test mode. The quantity of the data used as main input for this model is 2x3x1204 samples, which stands 2[input]x 3[vectors]x 1204[sec] in total makes 7224 samples. Each of these samples was obtained every 1 seconds. This simulation has been carried out by the PC: EPSON ENDEAVOR Model MR4700E with the specs, as shown in Table 5.18

Table 5.18. Specifications of the PC used for this study.

CPU	i7 6700 3.40 GHz / L3 Cache 8MB
RAM	8GB DDR4 / 2133 MHz
HDD	1 TB

86

As shown in Table 5.18 all the computational power is concluded under a medium performance desktop PC. It was necessary to use such specs in order to increase the training processes of the ANN. However, it doesn't mean that for the estimation process of the problem it is necessary to use i7 CPU. It can be carried out even by limited processing power the small single-board computers i.e., Arduino, FPGA, Raspberry Pi, etc.

Fig.5.32 shows the simulated plot of the estimated power from the Li-Ion cell of 0 cycle after few learning stages. Its accuracy is satisfactory for the prediction of the battery power consumption based on the actual EV model and the use of LabVIEW as a comparison and adaptation of the scaled-down model. As shown in Fig.5.32, the estimation process is solid during all the simulation, with a good response in term of stability and continuity. The characteristics for the Power consumption of EV's is very dynamic with fast changes and high peaks. The test is long and gives the opportunity to observe the natural behaviors which can be assimilated inside the ANN logic.
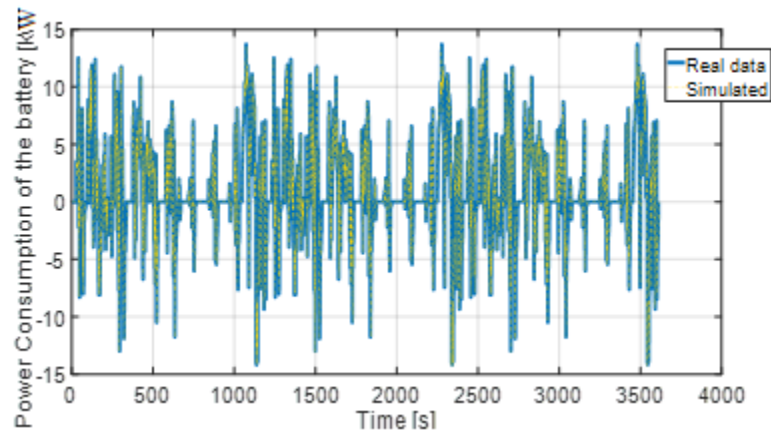
Fig. 5.32. Comparison of the experimental data with the simulated data

Figs. 5.33 & 5.34 show the estimation for different cycles.
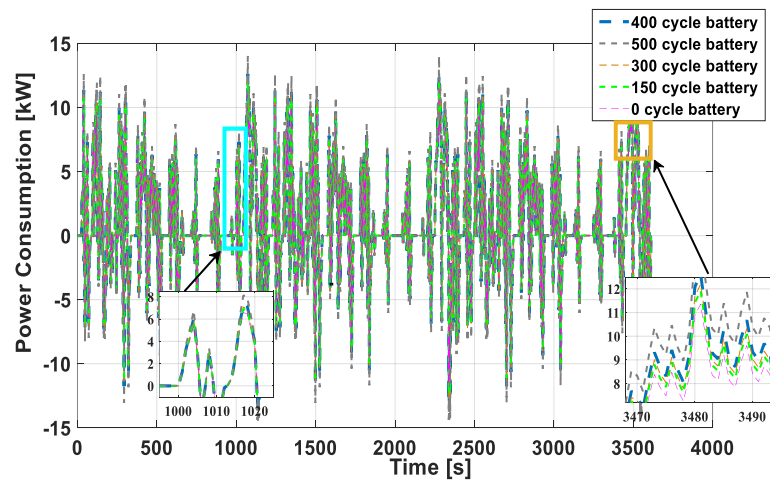
Fig. 5.33. Estimated value from different cycles.
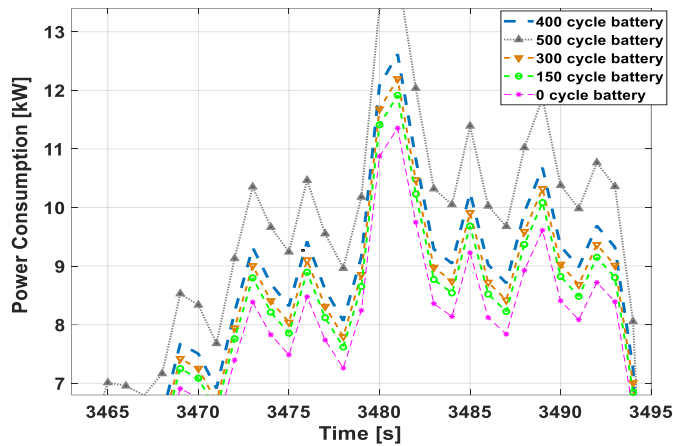
Fig. 5.34. Zoomed zone during current peaks

More the battery is deteriorated, more power and energy the EV will need in order to finish the test for the same conditions, so it means the power output of the battery will be reduced. By integrating the power vector, it is possible to obtain the energy characteristic, which helps to understand better the effect of the battery deterioration in the mileage autonomy of the EV. Fig.5.35 shows the plots of this deterioration. Through time it's possible to calculate how much is the distance covered by the car, also to understand the differences of the mileage of the EV during deterioration. In the region of the highest current peak, the maximum difference from a new battery of 0 cycle to 300 cycles is 13% and from the new battery of 0 cycle to 500 cycles is 19%. When the Li-Ion cell get deteriorated at the maximum value of 500 cycles the difference is increased in a nonlinear proportion. Also, the nonlinearity of the characteristic is included in the estimation model as it's showed during all the energy accumulation period.
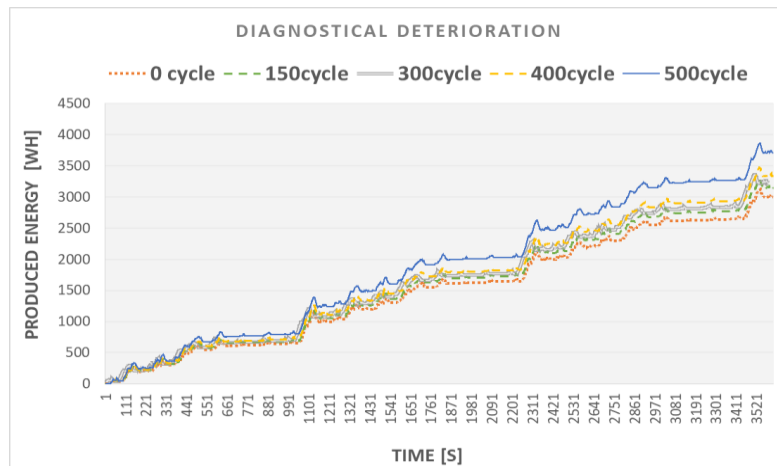
Fig. 5.35. Estimated value from different cycles.

This non-proportional change of consumption due to the deterioration effect is really important to be absorbed by the ANN model. This can remove the linearize models, which can give an accuracy which is indeed in doubt most of the times. In order to increase the accuracy of this model it is necessary to create a correct and genuine database. This model cannot be used only to estimate the power or energy consumption, but it can be used as a classification model for the level of deterioration of the battery pack, modules or even in the scale of single cells diagnosis.

5.4 Applications & Conclusions

In this chapter, an improved ANN model was proposed for the estimation of the power consumption of EV. The power consumption was accurately estimated with high accuracy, low computational power and within short time. The aim of this study is to simplify the difficulty of the real time diagnosis for the estimation of the battery supply by the rechargeable batteries and to excavate further for possibilities in the implementation of industrial applications. The proposed NN was processed in MATLAB and LabVIEW software. The first input data retrieved experimentally are overwritten by the data taken from the sensor in real-time from the dynamic process of EV. The estimated output was based on the single cell Li-Ion high-capacity type ICR18650PD, tested in ambient temperature of 25°C. The final version of the NN model structure was based only on speed and voltage input, so it requires only 2 data sample every second after training. All the calculation was processed in PC-Desktop with medium specs, which makes it more practical for further implementation in small circuit. In the second part of the improvement, the further NN model was based on the same battery type model but with 20 batteries with different deterioration level. The results obtained from experimental samples, demonstrate a good and stable generalization of the model. It was possible to estimate the power and energy of the EV from batteries with different cycles which makes possible to classify and categorize the deterioration of the rechargeable batteries. This information helps to indicate the maximum mileage of the EV, as well helps for the real time diagnosis of the SOH, providing foundations for further industrial applications. The future work will be based on the SOC online estimation which is important in application as charging station of EV or in other diagnosis fields.

During the investigation of voltage waveform, the predicted method was developed by an GD-BFPNN model, based on simulation code which was processed in MATLAB, from the voltage characteristic of charging model of the Li-Ion battery. In the first part of this study, the experimental data was used from a typical BP network and by modifying the settings was achieved a prediction with not a good accuracy. But with the adaptive GD-BFPNN model the system was capable to predict and learn fast. The accuracy was very high and calculated very fast less than, 1 minute. By making possible to predict the charging voltage of a rechargeable battery as Li-Ion, it can simplify the nonlinear and difficulty relation of some input variables in the fault detection diagnosis and real time prediction, for the industrial applications.

The future work is to achieve a good result from the charging process of battery and to adapt the network to learn also from the discharging process in order to achieve a better understanding of the SOC and real time estimating diagnosis of battery.

The main contribution of the author regarding the problems in this chapter are based on these publications:

1) **Published Journals**

   a) M. Bezha and N. Nagaoka, "*Improved ANN for Estimation of Power Consumption of EV for Real Time Battery Diagnosis*", IEEJ Journal of Industry Applications IA 2019/03(E) Special Issue on Motion Control and its Related Technologies, Vol.8, No.3, pp.532-538.

2) **International Conference Papers**

   a) M. Bezha and N. Nagaoka, "*Diagnostical system for the Rechargeable batteries in future application*", 6th T.I.M.E Doctoral School on Vulnerability, Risk and Resilience of Complex Systems and Critical Infrastructures, Centrale Supélec, Université Paris -Saclay, Paris, France, 23-27 October (2017).

b) M. Bezha, N. Nagaoka, "*An ANN for Estimation of Power Consumption of EV/HEV for Real Time Battery Diagnosis*", SAMCON IEEJ International Workshop on Sensing, Actuation, Motion Control and Optimization, Tokyo Denki University, Tokyo, Japan, 6-8 March (2018).

c) M. Bezha, N. Nagaoka, "*Predicting Voltage Characteristic of Charging Model for Li-Ion Battery with ANN for Real Time Diagnosis*", IEEJ & IEEE IPEC2018 International Power Electronics Conference, Niigata, Japan, 20-24 May (2018).

d) M. Bezha, R. Gondo, N. Nagaoka, "*A Dual ANN Model for Estimation of Internal Impedance of rechargeable cell battery*", IEEE 53rd International Universities Power Engineering Conference, 4th-7th September (2018), Glasgow, Scotland, with co-author Ryo Gondo and Prof. Naoto Nagaoka.

e) Ryo Gondo, M. Bezha, Makoto Ishii, Takahiro Shoda, Tomoyuki Suzuki, N. Nagaoka, "*Development of Scaled Simulator for Designing Power Storage System*", IEEE 54th International Universities Power Engineering Conference, UPEC 2019, Bucharest, Romania, 3rd-6th September (2019)

f) M. Bezha, N. Nagaoka, "*A fast diagnosis for classification of re-used Li-Ion batteries for PV and EV systems by the ANN model*", IEEE 8th Global Conference on Consumer Electronics-GCCE 2019, Osaka, Japan, 15-18 October (2019)

g) K. Yamamoto, M. Bezha, Y. Baba, N. Nagaoka, "*Investigation of voltage and current measurement of Li-ion battery with a BMS*" 13th ISET/ISS & 6th ISLH Conference, Chonburi, Thailand, 29-30 November (2019),

6.   Equivalent Circuit Model & Mathematical Modelling

This chapter will explain the electrical circuit compositions of the batteries with the proposed models. Their complexity, pros and cons of each of them of the internal impedance and their parameters will discussed. In addition, the proposed procedure of the parameter estimation will be explained which includes the physical meaning of the values. Another important matter is the mathematical modelling for the used methods; it will be explained in order to simplify the chemistry difficulty, which is a quite complex. Also, a solving method for the high nonlinearity of the battery parameters will be one of the main focus in this chapter, and finally the application field and approaches will be explained briefly in the end of this chapter.

6.1   Introduction

Due to the exponential increase of the rechargeable batteries market, especially high demand for Li-Ion batteries, it requests the fundamental understanding and mathematical modelling explanation, and the simplification of the high order equations. By achieving these, it is possible to incorporate these models inside the battery management system or in the embedded circuits. Many researchers from different majors and fields contribute from their respective background in the battery field for an improvement of the storage system. Features like; increase of capacity, current ration, stable voltage, better internal impedance, longer lifetime, better thermal and mechanical stability, lighter, wider range of voltage and shapes for industrial applications. However, without understanding the fundamentals, or even investigating further in the simplification of the complex models, it is impossible to advance in the battery field. The electrochemical burdens and their complexities introduce a big barrier for the further improvements. Even a pivotal contribution can hence be made by explaining the fundamentals in a coherent manner. Due to this offering possibly would enable scientist and researchers from multiple domains appreciate the bedrock principles and continue further investigation. Battery is mostly an electrochemical system, and any level of understanding cannot shift this premise. The common approach to run from the electrochemical models to algorithms used for the real-time estimation or diagnosis systems on a microchip it is physics based. This chapter will explain the electrochemical modeling which is derived from thermodynamics and a physics-based model order, also the mathematical model order and high nonlinearity reduction approach. As an important example of the electrochemical complexity, is the charging/discharging process which introduces difficulties for the normal operation. This chapter focuses on the battery modelling parameters, the most appropriate order of ECM's, methodology, and classification of the deterioration.

The technology of portable energy storage is rapidly improving due to the need for high-energy capacity and fast charging capabilities. This is further compounded by the desire for smart and autonomous devices. In all battery systems from the small portable devices to large-scale storage systems, improvements in the battery manufacturing technology is the main goal for high technology battery companies and electric vehicle manufacturers. For mobile computer manufacturers, the operating time is still the weak point while the chips and operating systems are becoming more efficient in terms of saving power. The dynamic characteristic of the battery, i.e., the operational characteristics of the battery driven equipment, is closely related to the State of Charge (SoC) and the maximum chargeable/dischargeable current. This is because the maximum battery current is limited by the terminal voltage, which depends on the SoC and the internal impedance of the battery. As explained and confirmed in [140, 141], the internal impedance can be expressed by a resistor, which expresses the voltage drop in a high frequency region, and some RC parallel circuits, which expresses the transient characteristics of the battery. On the other hand, the battery health is a key factor in improving and advancing new technologies. An accurate lifetime estimation and diagnosis of deterioration become an important task in order to increase the battery capacity. The internal impedance is known as an index of the battery deterioration. It is necessary to develop a diagnostic system, which can operate without removing the battery so as to maintain the normal operation of the processes. The aging of the rechargeable batteries is a concern, especially when they

are used for applications that could potentially have long-life usage. The battery can efficiently operate only inside its safety zone when a practical and accurate diagnosis system is installed [190]. An estimation method for the internal impedance, which is one of the key parameters determining the battery deterioration, has been proposed based on the circuit theory with different approaches to estimate the internal impedance directly or to relate factors that contribute to the battery deterioration, as explained in [139, 140, 141, 144, 145, and 190]. The computational time and memory requirements of the on-board diagnostic system are points that need to be improved. This research introduces an improved parameter estimation method based on Artificial Neural Network (ANN) logic. The battery terminal voltage and the load current waveform are used for the estimation of the parameters. By dividing the frequency characteristic into two regions, an accurate evaluation of the maximum current and the capacity fade of the battery can be estimated. The deterioration level and discharging rate was increased for a better generalization algorithm.

During charging or discharging processes, the Li-Ion undergoes diffusion inside the solid porous electrodes. The porous electrode region is abstracted to be composed of individual particles, which are assumed to be spheres of finite radius, that interact with the electrolyte that surrounds each particle.

The most simplistic representation of the mass conservation in the solid phase is provided by the Fick's law of diffusion in the spherical coordinates. This logic is given by:

$$\frac{\partial c_{si}}{\partial t} = \frac{1}{r^2} \frac{\partial}{\partial r} \left(D_{si} r^2 \frac{\partial c_{si}}{\partial r} \right) \tag{6.1}$$

where c_{si} is the concentration of lithium in the solid particles, when $i=p$, n providing an index for either the positive or negative electrode. The spherical symmetry results in the boundary condition at the center of the sphere.

$$\left. \frac{\partial c_{si}}{\partial r} \right|_{r=0} = 0 \tag{6.2}$$

It should be mentioned that the concentrations of the solid and the electrolyte phases are connected by the condition at the surface of the particles. At the surface, the flux of lithium is given by the pore wall flux given by the charge transfer reaction.

$$-D_s \left. \frac{\partial c_s}{\partial r} \right|_{r=R_{pi}} = j_i \tag{6.3}$$

It is necessary a fundamental explanation and description of mass and charge flux in the solution phase it is necessary to derive the mass and charge balance equations in the electrolyte region. The framework is derived in this subsection. Based on the concentrated solution theory and from [8], the flux is defined as

$$N_i = \psi_i c_i \nabla \mu_i \tag{6.4}$$

where ψ_i is the mobility of ion i, which is given by the Einstein relation as below:

$$\psi_i = \frac{D_i}{k_B T} \tag{6.5}$$

where D_i is the mass diffusivity, k_B the Boltzmann constant, and T is the absolute temperature. Related to the mass flux, a current flux can be defined as well

$$J_i = z_i e N_i \tag{6.6}$$

But for other systems as the electrochemical one, μ_i is constructed including the contribution from the activity a_i, charge on the ion z_i and the electronic charge e, as well as the potential ϕ, as shown below.

$$\mu_i = k_B T \ln(a_i) + z_i e \phi \tag{6.7}$$

The activity parameter is related to concentration c_i through the activity coefficient γ_i via the relation $a_i = c_i \gamma_i$, from this

$$\mu_i = k_B T [\ln(c_i) + \ln(y_i)] + z_i e \phi \tag{6.8}$$

and

$$\nabla \mu_i = k_B T \nabla [\ln(c_i) + k_B T \nabla \ln(y_i)] + z_i e \phi \tag{6.9}$$

$$\nabla \mu_i = k_B T \frac{\nabla c_i}{c_i} \left[1 + \frac{\nabla \ln(\gamma_i)}{\nabla \ln(c_i)} \right] + z_i e \nabla \phi = k_B T \frac{\nabla c_i}{c_i} \left[1 + \frac{\partial \ln(\gamma_i)}{\partial \ln(c_i)} \right] + z_i e \nabla \phi \tag{6.10}$$

Derived from the above equations, the flux can be expressed as follow:

$$N_i = -\psi_i c_i \nabla \mu_i = -\frac{D_i}{k_B T} c_i \left(k_B T \frac{\nabla c_i}{c_i} \left[1 + \frac{\partial \ln(\gamma_i)}{\partial \ln(c_i)} \right] + z_i e \nabla \phi \right) \tag{6.11}$$

The above equation can be further simplified.

$$N_i = -D_i \left[1 + \frac{\partial \ln(\gamma_i)}{\partial \ln(c_i)} \right] \nabla c_i - \frac{D_i}{k_B T} c_i z_i e \nabla \phi = D_i \nabla c_i - \frac{z_i e}{k_B T} D_i c_i \nabla \phi \tag{6.12}$$

Where the electric conductivity σ_i is expressed as:

$$\sigma_i = (z_i e)^2 \psi_i c_i = (z_i e)^2 c_i \frac{D_i}{k_B T} \tag{6.13}$$

From the above equation, the flux is derived

$$N_i = -D_i \nabla c_i - \frac{z_i e}{k_B T} D_i c_i \nabla \phi \qquad (6.14)$$

The conductivity of the electrolyte is defined as the sum of conductivities of the ions $\sigma = \Sigma_i \sigma_i$. Electro neutrality is invoked to identify that $c_i = c_+ = c_- = c$. The current density is

$$i_e = -e \nabla c \sum_i z_i D_i - \sigma \nabla \phi \qquad (6.15)$$

$$= -\nabla c \sum_i z_i e D_i \left[1 + \frac{\partial \ln(\gamma_i)}{\partial \ln(c_i)} \right] - \sigma \nabla \phi \qquad (6.16)$$

$$= -\nabla \ln(c) \frac{k_B T}{e} \sum_i \frac{\sigma_i}{z_i} \left[1 + \frac{\partial \ln(\gamma_i)}{\partial \ln(c_i)} \right] - \sigma \nabla \phi \qquad (6.17)$$

Where the final relation is expressed as the total current density in the electrolyte derived from the conductivity matter. Also, this expression is same in terms of diffusivities

$$i_e = -e \nabla c \sum_i z_i D_i - \frac{e^2 c}{k_B T} \nabla \phi \sum_i z_i^2 D_i \qquad (6.18)$$

Another important physical explanation is required to explain the mass conservation in the electrolyte in liquid phase.

$$i_e = -e \nabla c \sum_i z_i Di - \frac{e^2 c}{k_B T} \nabla \phi \sum_i z_i^2 D_i \qquad (6.19)$$

and the electrolyte potential is expressed as

$$\nabla \phi = \frac{i_e + e \nabla c \sum_i z_i Di}{-\dfrac{e^2 c}{k_B T} \sum_i z_i^2 D_i} \qquad (6.20)$$

In order to eliminate the electrolyte potential from the equation for the mass flux.

$$N_i = -Di \nabla c_i + \frac{\dfrac{z_i e}{k_B T} D_i c}{\dfrac{e^2 c}{k_B T} \sum_i z_i^2 D_i} \left(i_e + e \nabla c \sum_i z_i Di \right) \qquad (6.21)$$

In case of a porous electrode, the conservation equation is used for the fractional volume occupied by the electrolyte. As the concentration is defined in terms of the pure electrolyte, the conservation is expressed as below:

$$\varepsilon \frac{\partial ci}{\partial t} = -\nabla N_i + R_i \tag{6.22}$$

The corresponding equation for the mass flux is given by

$$N_i = -\varepsilon \psi_i c_i \nabla \mu_i \tag{6.23}$$

By some modifications, it results in

$$N_i = -\varepsilon D_i \nabla c + \frac{\dfrac{z_i e}{k_B T} D_i c}{\dfrac{e^2 c}{k_B T} \Sigma_i z_i^2 D_i} \left(i_e + e\varepsilon \nabla c \sum_i z_i D_i \right) \tag{6.24}$$

Also, the mass flux had the corresponding divergence given by

$$\nabla N_i = -\nabla \left(\varepsilon D_i \nabla c \right) + \nabla \left(\frac{z_i D_i}{e \Sigma_i z_i^2 D_i} i_e \right) + \nabla \left(\frac{\varepsilon \nabla c z_i D_i \Sigma_i z_i D_i}{\Sigma_i z_i^2 D_i} \right) \tag{6.25}$$

By a further simplification for univalent ion

$$\nabla N_i = -\nabla \left[\varepsilon \nabla c \left(D_i - \frac{z_i D_i \Sigma_i z_i Di}{\Sigma_i D_i} \right) \right] + \nabla \left(\frac{z_i t_i}{e} i_e \right) \tag{6.26}$$

The equation which includes the Li⁺ ions is

$$\nabla N_+ = -\nabla \left[\varepsilon \nabla c \left(t_- D+ + t_+ D- \right) \right] + \nabla \left(\frac{t_+}{e} i_e \right) \tag{6.27}$$

Where the total chemical diffusivity is expressed $\left(t_- D+ + t_+ D- \right) = D$, and t_-, t_+ are the transference numbers of the ions.

$$\nabla N_+ = -\nabla \left(\varepsilon D \nabla c \right) + \nabla \left(\frac{t_+}{e} i_e \right) \tag{6.28}$$

Further substitutions in the mass conservation equation

$$\varepsilon \frac{\partial c}{\partial t} = \nabla\left(\varepsilon D \nabla c\right) - \nabla\left(\frac{t_+}{e} i_e\right) - R_+ \tag{6.29}$$

Expressed in molar units

$$\varepsilon \frac{\partial c_e}{\partial t} = \nabla\left(\varepsilon D_e \nabla c_e\right) - \nabla\left(\frac{t_+}{F} i_e\right) - R_+ \tag{6.30}$$

In order to avoid proliferation of variables i_e is considered to be in molar units, A/m^2. This rate of consumption is expressed through the Faradays law as below

$$R_+ = a_{p,n} j_{p,n} = \nabla \frac{i_e}{F} \tag{6.31}$$

The mass flux of lithium due to this reaction is defined in terms of the surface areas of the particles of the active material. In order to include this quantity into the conservation equation that is defined for a unit volume of the electrode, it is multiplied by the specific surface area per unit volume of the electrode expressed by $a_{p,n}$. Conventionally p and n are used for the positive and negative electrode regions. The mass conservation equation is expressed by:

$$\varepsilon \frac{\partial c_e}{\partial t} = \nabla\left(\varepsilon D_e \nabla c_e\right) + \left(1 - t_+\right) a_{p,n} j_{p,n} - \frac{i_e}{F} \nabla t_+ \tag{6.32}$$
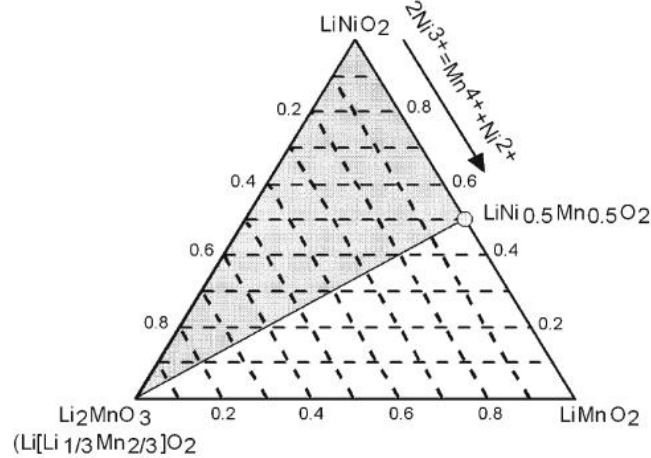
Fig. 6.1. Region of Li$_2$MnO$_3$-LiNi$_x$Mn$_{1-x}$O$_2$ solid solution painted in pseudo-ternary phase diagram [1].

6.2 Parameter estimation of internal impedance

Rechargeable batteries are crucial for the technological advancement when it comes to autonomous systems and devices. Different types of ECM have been proposed by the researchers, which helps us to understand and explain the chemical composition or electrochemical reaction of the rechargeable batteries. These circuits have different degrees of complexity and nonlinearity, which can express different behaviors. The response is different because it is highly dependent on the type of the rechargeable battery.

6.2.1 Battery Equivalent Circuits

At a selection of ECM, the following characteristics of the model must be taken into consideration. Firstly, the model can explain the battery behavior including the DC and transient characteristics, or not. Secondly, there must be trade-offs between performance and cost in some points, such as accuracy, complexity of the model, experimental and computational time, in order to provide a cost-efficient system in the end. In general, these models can be divided into three main groups:

1) Electrochemical models,

2) Mathematical models,

3) Electric equivalent circuit models.

Despite the fact that the electrochemical model can accurately explain the operational characteristics of the battery, these models unfortunately have high complexity. This introduces new problems such as the degradation of Li-Ion is often caused by harmful side-reactions inside the battery, where lithium plating is a typical example that consumes cyclable lithium. Usually side-reactions depends on the overpotential. In case when the overpotential can be estimated, then some algorithms can be developed to minimize the side-reactions inside the cell, which results in improved battery reliability. To estimate the electrochemical states, an accurate and computational efficient electrochemical model is required however it requires a long computational time for the calculations [191-193].

Mathematical models are based on the derived equations from the data retrieved through experiments. The high grade of the equations and nonlinear behavior of the battery makes these models unable to fully explain and estimate the variables and the phenomenon, which happens during operation [193-195]. Electric equivalent circuit models are very suitable for the purpose of real-time estimation due to their simplified mathematical and numerical approach. Many types of the equivalent circuit have been proposed and each are suitable for a specific purpose, such as studying the DC or transient characteristics as explained in [139,144].

Several examples of the equivalent circuit of a battery are shown in Fig. 6.2a–c, based on their scale of complexity. Fig. 6.2a illustrates the simplest model that is composed of a resistor and an internal voltage source. Although the model can explain and shows satisfactory accuracy in calculating the DC characteristic, it cannot express the operational characteristic during the dynamic process, i.e., the transient behavior of the battery. Fig. 6.2b shows a more complex equivalent circuit of the battery. The impedance of the model that consists of a series resistor R_{B0} with an RC parallel circuit (R_{B1} and C_{B1}) can be written by the first order rational function. Fig. 6.2c illustrates a more sophisticated model that is expressed by a high-order rational function.

(a)   (b)
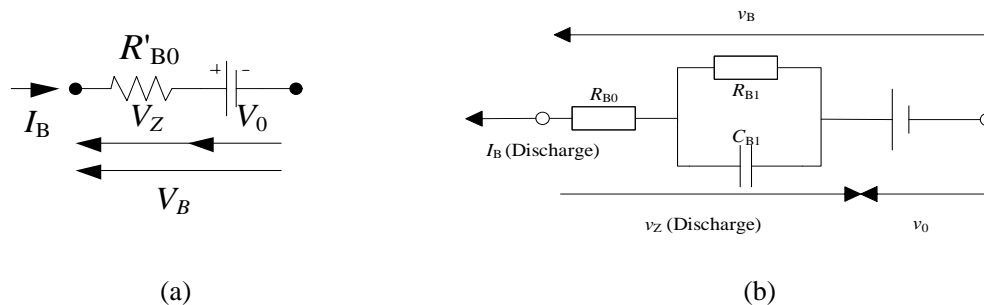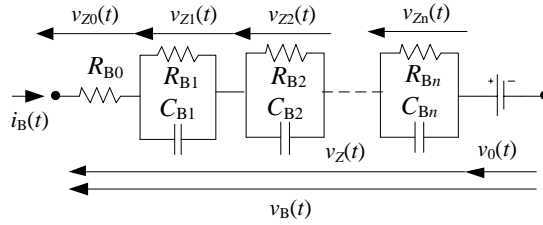
(c)

Fig. 6.2. (a) Simplest conventional model. (b) First order model. (c) High order model.

Although the accuracy of the model increases with an increase in the number of RC circuits, the estimation of the parameters becomes difficult. The internal voltage in each model V_0 expresses an open-circuit voltage (OCV) of the battery. In general, the OCV is determined by its SoC and it shows only small changes in its value due to the deterioration effect.

a) Conventional Modelling

Different methods and approaches, which estimate the deterioration of the batteries, have been proposed. Despite the fact that the frequency characteristics of the internal impedance can be accurately measured based on the AC superimposition method, still it requires a removal of the battery, even for dynamic systems like EV, HEV, PHEV [196]. This method cannot be used during operation as an online process. The frequency characteristics can be obtained from the battery voltage and current waveforms, i.e., transient responses with discrete Laplace Transform (DLT)) [142, 181, 197]. Although this method is applicable for diagnosis during operation, still requires a long computational time in order to obtain the characteristics at a wide frequency range. Different proposed methods are based on a logarithmic segmented Laplace Transformation as already confirmed and explained in [193], as well explained in exponential & logarithmic Fourier transformation applications in [198, 199]. This method makes possible to study the wideband characteristics. This algorithm simplifies and reduces the complexity, and also a low-cost diagnostic system can be realized. However, it needs to secure the numerical stability.

.

b) Proposed Model

The ECM applied in this thesis are shown in Figs. 6.3 and 6.4. It is provided by a modification of the electric equivalent circuit shown in Fig. 2c. This ECM consists of the second order circuit with the capacitor C_∞ connected in series. The invers of the capacitance corresponds to the slope of the voltage shown in Fig. 6.5 The need to insert this capacitor is also clarified to explain the dynamic characteristic from the experimental results. The series capacitor expresses the characteristic of the battery in a low frequency region. For example, it explains the changing speed. In addition, the capacity fade can be detected by the capacitance C_∞. Based on different problems and the required accuracy or level of complexity a 2nd order or 3rd order model shown in Figs. 6.3 and 6.4 is acceptable for elevated quality of estimation. Different investigations are made by the author based on these two models. In further pages it be shown the possible usage and results. Fig. 6.6 shows an example of a capacity fade of a Ni-MH battery cell.

98
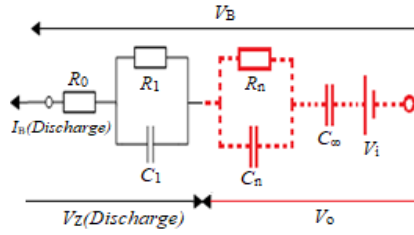
Fig. 6.3. Proposed equivalent model of 2nd order.
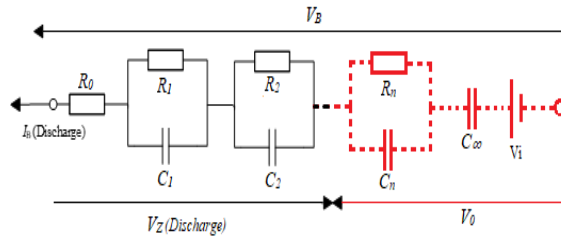
Fig. 6.4. Proposed equivalent model 3rd order
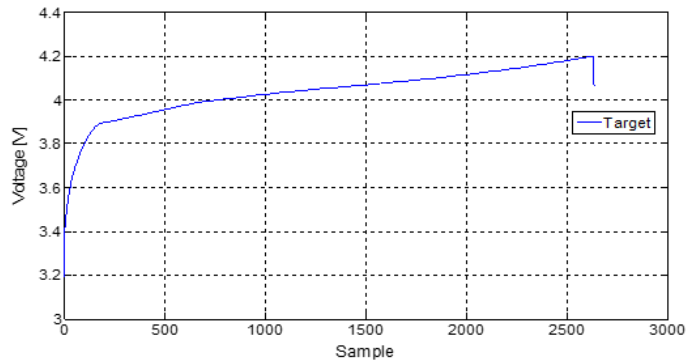
Fig. 6.5. Voltage characteristics of a Li-Ion battery during a constant current charging
(ICR18650PD, 1 sample/s).
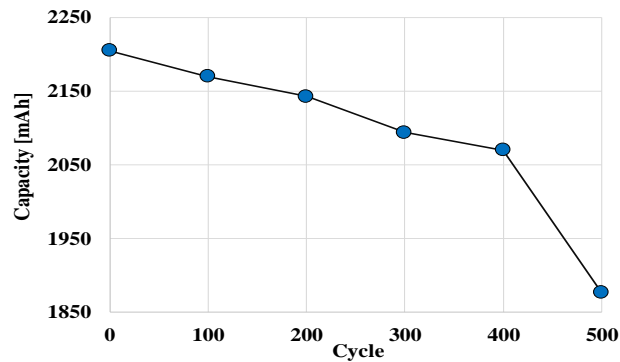
Fig. 6.6. Capacity fade vs. number of charging/discharging cycles.

The composition of the proposed diagnosis method is based on two steps. First, the hardware is developed to obtain the experimental data, which will be used for the training model of ANN. In the second step, this ANN is used in order to estimate the desired characteristics.

The circuit is based on that described in [156], which can charge and discharge Pb, Ni-MH or Li-Ion battery by an arbitrary current waveform. In addition, the measured voltage and current waveforms are saved to an SD-card.

c)   Diagnostic Approach by the Proposed Circuit

From the comparisons of the characteristics and estimated values between the different types of batteries, the credibility and accuracy of the proposed method can be confirmed. The Li-Ion battery shows many advantages compared to the other types of batteries. Figs. 6.7 and 6.8 shows the characteristics of the Li-Ion cell battery.

Table 6.1 shows the main specifications for the Li-Ion battery used in this study, cylindrical single cell 18650.

Table 6.1. Primary Specifications of Li-Ion cell.

Model	ICR18650PD
Diameter [1]	18.3 s ± 0.2
Height [1]	64.95 + 0.15/−0.30
Weight [2] (g)	46
Max. voltage [3] (V)	4.2
Max. current [3] (A)	2.25
End voltage [4] (V)	2.75
Max. current [4] (A)	6
Nominal voltage (V)	3.7
Minimum capacity (mAh)	2250
Type	High-Capacity type

[1] Dimensions of fresh cell without tube, [2] Approximate values. [3] Charge (CCCV), [4] Discharge (CC).
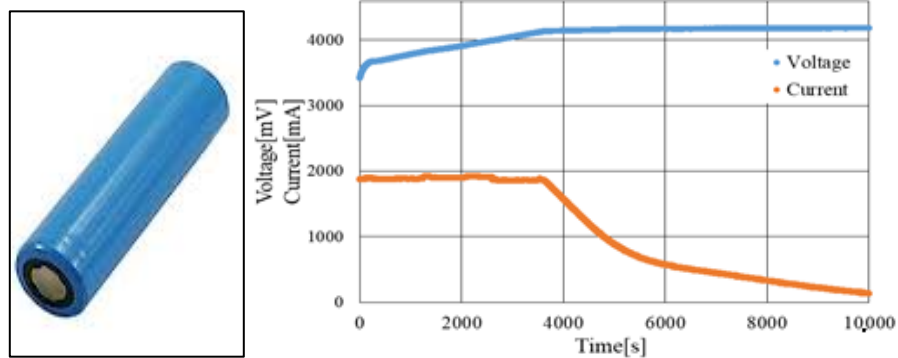
Fig. 6.7. Charging characteristic of ICR18650PD Li-Ion cell during CCCV mode.
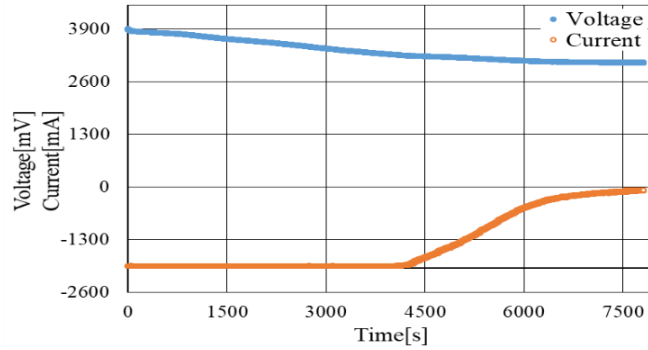
Fig. 6.8. Discharging characteristic of ICR18650PD Li-Ion cell during CCCV mode.

The experiments conducted in this study were made at 25°C as a constant ambient temperature, during the practical test in room size, not inside the chamber of a typical of industrial devices, where the temperature is highly monitored and maintained constant with error of ±0,25°C. Instead of that the device was tested in a normal laboratory room where the temperature can change with different rate than that of a closed chamber. It must be clear that this method is not based on temperature-compensated model like [200, 201], due to constant temperature at 25°C, also some data are obtained from experiments conducted at 30°C, which are inserted in the ANN database. The Ni-MH battery chemistry is a hybrid of the proven positive electrode of the sealed Ni-Cd battery with the energy storage features of metal alloys based on development for advanced hydrogen energy-storage concepts. Its discharge voltage profile is relatively flat, and it has a lifetime of several hundreds of cycles regarding the recharge capability. When it comes to high rate discharges it's very efficient and capable of delivering such power without causing instability for the operation. Ni-MH retains 50-80% self-discharge rate within 12 months. It's lighter than Lithium batteries as well can be recycles for a better environmental-friendly effect. Table 6.2 shows the specification for the Ni-MH used in this study.

Table 6.2. Primary Specifications of Ni-MH Panasonic-BSG cell.

Model	HHR-380A
Diameter	17
Height	67
Weight (g)	53.52
Nominal voltage (V)	1.2
Discharge Rate (mA)	740
Standard Charge Current (mA)	370
Rated capacity (mAh)	3700
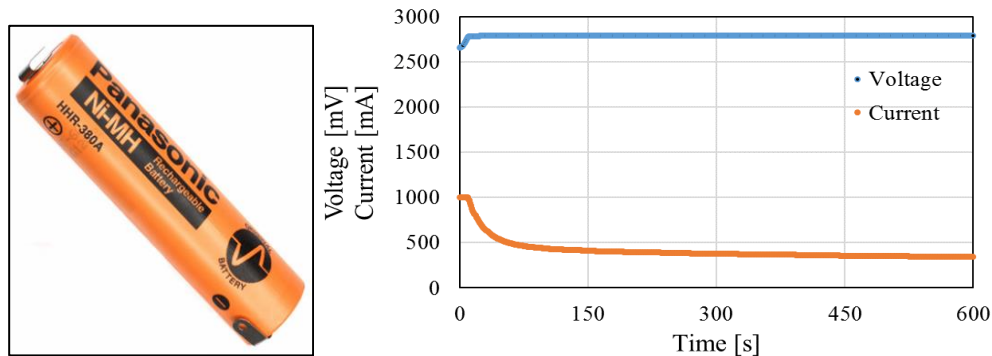
Fig. 6.9. Charging characteristic of HHR-380A Ni-MH 2 cell in series during CCCV mode.

101
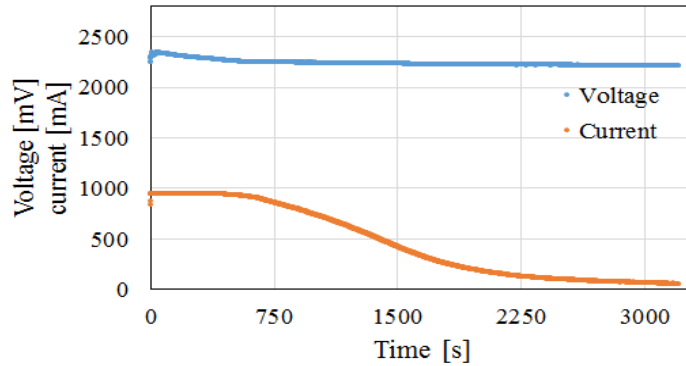
Fig. 6.10. Discharging characteristic of Ni-MH 2 cell in series during CCCV mode.

Figs. 6.9 and 6.10 shows the characteristics of a Ni-MH battery obtained by the CCCV charging and discharging, respectively. In the experiments, two Ni-MH batteries are connected in series, because the voltage across the cell is lower than the voltage specification of the developed charging/discharging circuit. The rated capacity of each battery is 3.7Ah and is charged/discharged by a current rate of 0.2C, 0.5C, 1C.

Lead-acid battery known as Pb battery is the most common rechargeable battery. Despite having a very low energy-to-weight ratio and a low energy-to-volume ratio, its ability to supply high surge currents means that the cell has a relatively large power-to-weight ratio. This battery has few advantages and drawbacks. Despite the drawbacks, still Pb batteries are very used in low budget projects or in initial low-cost situation investment. The chemical composition of Pb batteries is well known to be very complex compared with other commercial battery technologies. With the new Japanese Pb batteries technology by Hitachi Ltd. (Tokyo, Japan), producing with Pure Lead, Punching Carbon technology (PPC), which have improved the capacity, discharging rate, lifetime and environmental applicability. But in this study a common Pb battery was used, without the cutting-edge technique of PPC, Table 6.3 shows the specifications of a deep-cycle type Pb battery used in the experiment. Figs. 6.11 and 6.12 show the Pb characteristics during charging/discharging.

Table 6.3. Primary Specifications of the valve-regulated lead-acid battery.

Model of Product	NP3-6
20-h Rated Capacity	3.0 Ah
Nominal Voltage	6 V
Maximum Charging Current	$0.25C_{20}$ (= 0.75 A)
Maximum Discharging Current	$3C_{20}$ (= 9 A)
Temperature Range	−15 to 40 °C
Cutoff Discharging Current	5.25 V (under $0.2C_{20}$)
	5.10 V ($0.2C_{20}$ to $0.5C_{20}$)
	4.65 V ($0.5C_{20}$ to $1.0C_{20}$)
	3.90 V (over $1.0C_{20}$)
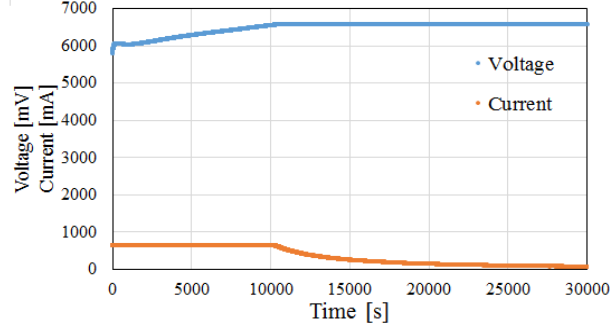
Fig. 6.11. Characteristic of NP3-6 Pb battery during CCCV charging mode.
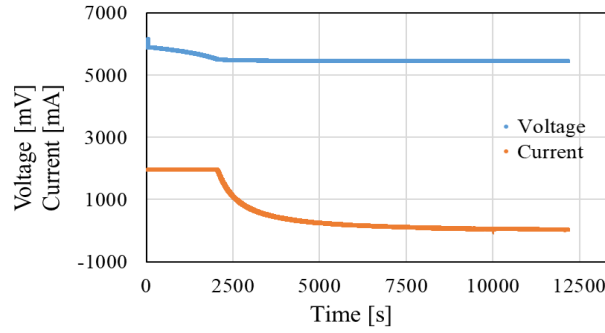
Fig. 6.12. Characteristic of Pb battery during CCCV discharging mode.

As already mentioned in the previous section, the proposed method divides the estimation region into two frequency regions. The regions can be specified in a time domain that uses the ANN as its input signal. The conditions are:

$$\Delta t_1 \leq \frac{1}{2 f_{\max}}, T_2 \geq \frac{1}{f_{\min}} \tag{6.33}$$

(where Δt_1 represents the time step of the first (high) frequency region, T_2 is the maximum observation time of the second (low) region, $f_{\max}$ is the maximum observation frequency and $f_{\min}$ is the minimum frequency resolution. The sampling method is based on the results from Equation (6.33). The number of the samples for each region is composed based on the following equation:

$$N_k = \frac{1}{N_{reg}} 2^{\left(2 \log_{10} \frac{f_{\max}}{f_{\min}} + \varepsilon \right)}, \quad \varepsilon \geq 2 \tag{6.34}$$

where N_k is the number of samples of the k-th section, N_{reg} (=2) is the number of regions and ε is the overlap coefficient. During the high frequency region, the sampling time was constant with the same Δt. Furthermore, in the low frequency region, the sampling time was constant in order to maintain the same characteristics.

A main focus for this study involves finding the optimal frequency regions (OFR) in order to explain and estimate the deterioration of the batteries based on the values of the ECM parameters. From one battery type to another one, the best OFR will be different. Li-Ion is a high-performance energy battery with very low memory effect and long last cycle performance. In contrast, Ni-MH is affected by the memory effect and will approximately lose up to 35% of their stored energy in 3 months (up to 40% for Ni-Cd battery). Compared with the lead acid battery, it self-discharges the same amount in one year.

Figs. 6.13 and 6.14 explains the relation between the equivalent circuit and the electrochemical meaning of the internal impedance using the Cole–Cole plot. The parameters R_0, R_1 and C_1 are obtained through the high frequency sampling mode. The other parameters obtained through the low frequency sampling mode explain the transient characteristic of the kinetically controlled region, which is closely related to the SOH.
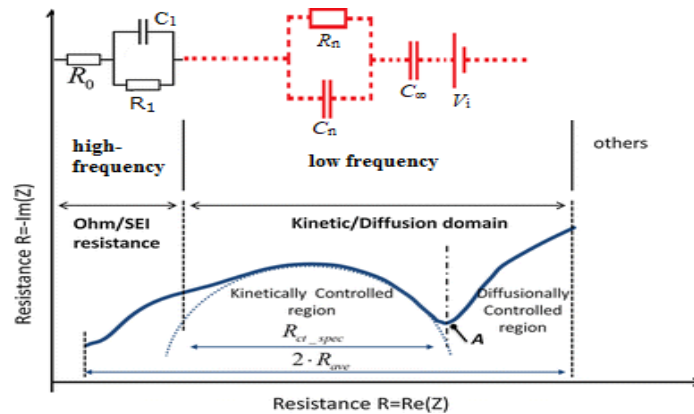
Fig. 6.13. Relation of variables of 2nd order in the frequency response.
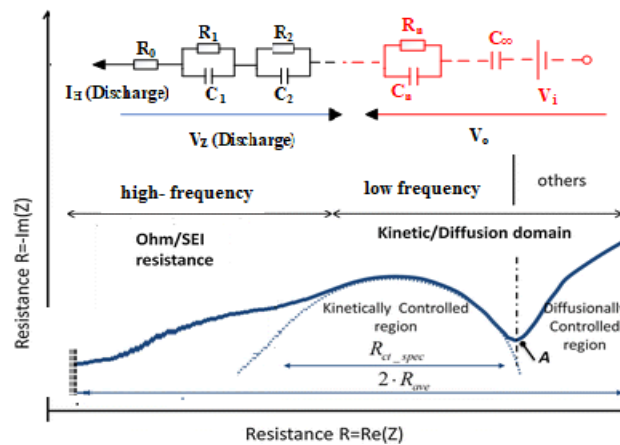
Fig. 6.14. Relation of variables of the 3rd order in the frequency response.

As shown in Figs. 6.13 and 6.14 the ECM is more complex in the last one, although the frequency response might seem similar, in the case of higher order it is shifted a little more in the right, making the high frequency zone response wider in appearance.

In Fig. 6.15 is shown the typical frequency borders. Point A is positioned with the frequency of 1 MHz and is related to electronic conductivity, Point B at 1 kHz is obtained through the SEI film and Point C at 10 Hz is related to the charge transfer at the electrode/electrolyte interface. Point D at 10 mHz expresses the diffusion in the electrode and electrolyte phase. The lowest frequency region Point E occurs at 1 mHz, which has a state of charge that changes during the impedance measurement.
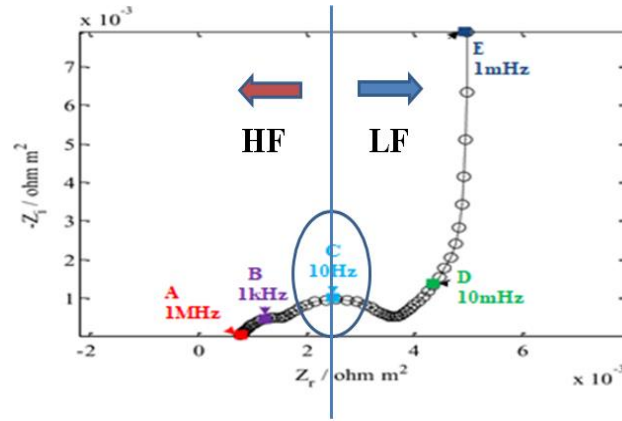
Fig. 6.15. Cole–Cole plot impedance characteristics through the frequency spectroscopy.

Table 6.4 shows the regions with a specific frequency range, where the minimum frequency value of the low frequency region is 10mHz and it increase with 1,2 and 3 decades, maintaining same minimum frequency for each case. Same for the high frequency region, where the minimum value is 10Hz and it increase up to 10kHz. Table 6.5 shows the proposed combinations for a further accurate investigation in order to be used for the proposed estimation method. The author of this present study is aware that the combinations are infinitive but this study wants to maintain a possible and actual scenario for measurements and simultaneously simplify the dividing range.

Table 6.4. Frequency of regions.

Low Freq.	High Freq.
10 mHz–100 mHz	10 Hz–100 Hz
10 mHz–1 Hz	10 Hz–1 kHz
10 mHz–10 Hz	10 Hz–10 kHz

Table 6.5. Proposed combinations.

Cases	Low Freq.	High Freq.
Case 1	10 mHz–100 mHz	10 Hz–100 Hz
Case 2	10 mHz–100 mHz	10 Hz–1 kHz
Case 3	10 mHz–100 mHz	10 Hz–10 kHz
Case 4	10 mHz–1 Hz	10 Hz–100 Hz
Case 5	10 mHz–1 Hz	10 Hz–1 kHz
Case 6	10 mHz–1 Hz	10 Hz–10 kHz
Case 7	10 mHz–10 Hz	10 Hz–100 Hz
Case 8	10 mHz–10 Hz	10 Hz–1 kHz
Case 9	10 mHz–10 Hz	10 Hz–10 kHz

In each case, depending on the battery type, we will show and will try to explain which case is more appropriate to use in order to reduce the point of frequency for an optimal calculation time/accuracy rate. In [144], the low and high frequency regions were wide in order to explain the physical meaning of each variable for the proposed ECM. However, the most efficient region will be investigated in this study.

6.3 Methodology and Models

6.3.1 Designing the optimal structure

The proposed ANN method is processed in MATLAB R2018b, and the hardware specifications of the PC used in this study are shown in Table 6.6. The author believes that it is necessary to show the computational power which was used to perform this process.

Table 6.6. Hardware Specifications.

CPU	i7 6700 3.40 GHz / L3 Cache 8MB
RAM	8GB DDR4 / 2133 MHz
HDD	1 TB

During the training process that is the first step, the selection of the most appropriate NN configuration is crucial. The typical structure of the ANN is composed of an input layer, a hidden layer and an output layer. The input signals are multiplied by the weights before being calculated through the mathematical function, which expresses the activation of the neuron. The next necessary step of the process is to compute the output of the neuron. A higher weight of the artificial neuron expresses a strong relation with the input. It expresses that the specific input is more significant. The neuron is inhibited by the negative weight. Depending on the weights, the state of the neuron will be changed. The output is optimized by adjusting the weights of an artificial neuron according to the specific inputs, i.e., by learning with a "teacher." This is the main role of the ANN in the training phase for finding an algorithm in order to obtain the desired output from the NN automatically. The relation between the input and output is shown in Equation (6.34):

$$a = \sum_{i=1}^{R} W_{ij} p_i + b_i$$

$$(6.34)$$

where W_{ij} is the weight, p is the input and a is the output. As explained in [141, 148, 149, 186, 198] the weight between the i-th neuron of the $(k-1)$-th layer and the i-th neuron of the k-th layer is defined as $W_{ij, k}$. in order to define the most appropriate adapted values.

$$W_{ij}, k(t_n) = W_{ij}, k(t_{n-1}) - \frac{\alpha E(t_n)}{W_{ij}, k(t_{n-1})} \Delta W_{ij}, k(t_{n-1})$$

$$(6.35)$$

where $0 < \alpha < 1$ and $E = 1/2 \sum (y_i - b_i)^2$, $i = 1 \ldots n$, y_i is i-th actual output and b_i is i-th simulation output.

In addition to this, the time series prediction approach is applied for the Linear Prediction Error Methods (L-PEM), which can be applied to different arbitrary model parameterizations. One of the positive things of this method is that it can be applied to a wide region of model parameterizations. Based on the previous samples as in the case of $x(t - \Delta t)$, $x(t - 2\Delta t)$, …., $x(t - k\Delta t)$, the value of $x(t)$ needs to be predicted. The required value can be expressed as a function of the previous k samples:

$$\bar{X}(t|t-\Delta t,\cdots,t-k\Delta t)=\Phi(x(t-\Delta t),\cdots,x(t-k\Delta t)) \tag{6.36}$$

$$\bar{X}(t|t-\Delta t,\cdots,t-k\Delta t)=\sum_{i=1}^{k}\theta_i x(t-i\Delta t) \tag{6.37}$$

In Equation (6.36), the left side of the equation expresses the one-step-ahead prediction of the output and Φ is an arbitrary function of the past-observed data. If the function Φ is linear, the prediction is called a linear PEM, which is expressed in Equation (6.37). In the case that the last data set is composed of linear combinations of the k previous ones, the objective is to find Θ_i, which is a vector coefficient. The optimum weight Θ_i is obtained as a solution of (6.38) and it can be found by minimizing the distance between the predicted outputs $\bar{x}$ from the measured results $x(t)$. With the help of Equation (6.38), it is possible to obtain the optimum weight Θ_i. With more data, it can be easier to see a convergence.

$$\frac{d}{d\theta_k}\sum_{i=1}^{k}\left\|\bar{X}(t-i\Delta t)-x(t-i\Delta t)\right\|^2=0 \tag{6.38}$$

In this study, the improved dual ANN structure is proposed in order to obtain the parameters, which are related to one of the specific frequency regions. As in the previous study, theoretically the parameters of the equivalent circuit will be obtained from a pair of the battery voltage and current waveforms during its operation. The internal voltage is expressed as a function of the SOC. The series resistor R_0 and the parallel R_1C_1 circuit in Figs. 6.3 and 6.4 explains the voltage drop in a high frequency region and the other R_nC_n circuit with the series capacitor C_∞ expresses this in the low frequency region. The transient characteristic of the battery can be expressed by the circuit.

During an investigation based on this explanation, the author has used a 3rd order model as shown previously in Figs. 6.4 and 6.14. On this study an investigation of ANN structure based on the parameters of ECM were divided in two main groups, one group related with high frequency region (HF) and the other group related with low frequency region (LF). The parameters if IZ obtained from each of these two regions were divided into two groups, real components and imaginary component. Two change the words, the ANN structure was based on 4 main inputs Z^{HF}_{Re} and Z^{HF}_{Im} are the input obtained in the high-frequency sampling mode, and Z^{LF}_{Re} and Z^{LF}_{Im} are the input obtained in the low-frequency sampling mode.
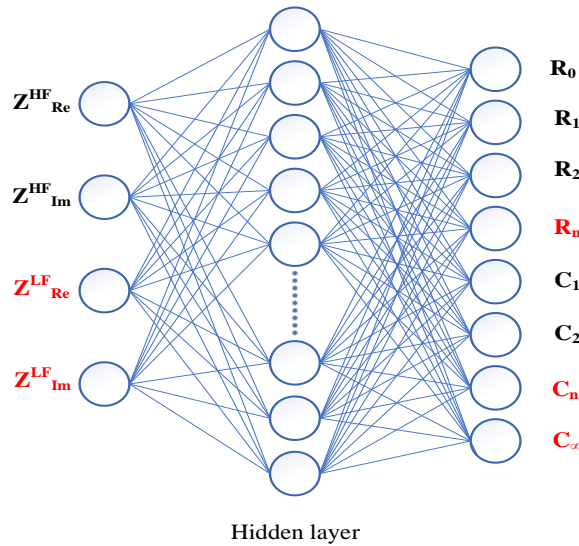
Fig. 6.16. ANN structure for the proposed model

The number of frequency points used is 200, which for the proposed ANN. It means the number of the input cells is 400, 200 cells are for real components and the other 200 for the imaginary components of the internal impedance. Fig. 6.16 shows the structure of the NN model.

For the training process were used 6 different Li-Ion cell battery with same specifications as shown in Table I, but with slightly differences in deterioration level. Also, in this study were used different settings al the ANN algorithm in order to tune the most appropriate estimation.

Tables 6.7 and 6.8 show the estimated parameters with those of the conventional model calculated by NF As-510-LBA based on AC superposition method. With this device, the calculation time including the impedance measurement is 30-40 minutes depending by the number frequency points and other settings. The estimation time of the proposed model was very fast after the optimization of the NN model by the training process. The best case was obtained within 30 seconds. Also, the response was solid during all the estimation process for all the 6 different cases used in the experiment.

Two cases were investigated;

case 1: 1 hidden layer with 11 neurons, and case 2: 1 hidden layer with 20 neurons.

Must be said that NN structure with 2 hidden neurons were investigated and their results were very satisfactory, however the focus of this investigation was the simplification of the model than the elevated accuracy.

Table 6.7. Estimated ECM parameters Case 1

PARAMETERS	Estimated	Measured
$R_0 (m\Omega)$	47.65	46.9
$R_1 (m\Omega)$	22.265	22.35
$R_2 (m\Omega)$	31.12	31.05
$R_n (m\Omega)$	57.2	56.87
$C_1 (KF)$	0.86	0.91
$C_2 (KF)$	1.14	1.19
$C_N (KF)$	1.95	1.914
$C_\infty (MF)$	3.57	3.52

Table 6.8. Estimated ECM parameters Case2

PARAMETERS	Estimated	Measured
$R_0 (m\Omega)$	45.15	44.85
$R_1 (m\Omega)$	21.145	21.21
$R_2 (m\Omega)$	28.12	27.95
$R_n (m\Omega)$	55.8	56.1
$C_1 (KF)$	0.86	0.91
$C_2 (KF)$	1.19	1.21
$C_N (KF)$	1.87	1.85
$C_\infty (MF)$	3.38	3.42

Table 6.9. Training Performance Comparison from Different Functions and Discharging Ratio

Training Function	Discharging Current					
	0.25C		0.3C		0.5C	
	step	time(s)	step	time(s)	step	time(s)
traingdm	390	38	298	33	225	20
trainbfg	16	4	17	5	14	4
trainlm	8	3	9	3	8	3

The data used during the training for the proposed ANN were 400 cells, respectively 200 cells for each component, real and imaginary component of the internal impedance. Error was less than 3% in the worst scenario for the 1-hidden layer structure (Table 6.7). Another important thing to be mentioned is the necessity

of the initial value in the conventional methods, due to the high non-linearity of the ECM. However, the initial value is not required in the proposed method.

Now turning back for the study based on 2nd order model, as shown in Fig. 6.17. In the ANN structure, the inputs U and I are the data are genuine one obtained from the devices as illustrated in Fig. A1-A2 [137] explained in Appendix. In each frequency region, the desired outputs, i.e., the circuit parameters are estimated. This is similar with the structure confirmed and explained above, i.e., a single ANN structure.

(a)   (b)
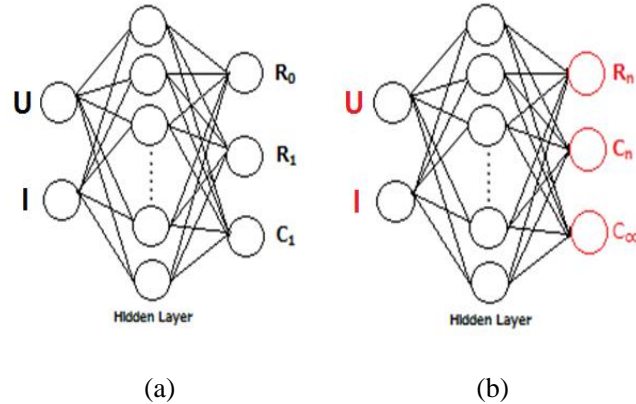
Fig. 6.17. ANN structure for the proposed model: (**a**) structure used for high frequency region and (**b**) structure used for low frequency region.

Table 6.10 shows the results of the previous study for the wide frequency range. This was the most accurate case, especially based on the Li-Ion battery estimation.

Table 6.10. Estimated Circuit Parameters.

Parameters	Measured	Estimated
R_0 (mΩ)	48.3	46.65
R_1 (mΩ)	2.3	2.46
R_n (mΩ)	58.2	56.35
C_1 (kF)	0.7	0.721
C_n (kF)	1.88	1.81
C_∞ (MF)	3.58	3.69

The estimated cases are shown as below. In these estimations, the data obtained from some deteriorated batteries are included in order to emulate a real situation for estimating SoH. In simple words, it means that a generalized estimation model of the battery deterioration. Tables 6.11 - 6.19 shows the results and comparison for each of 9 cases shown in Table 6.5.

.

Table 6.11. Results of Case 1.

Parameters	Measured	Estimated
R_0 (mΩ)	47.9	55.18
R_1 (mΩ)	2.4	2.81
R_n (mΩ)	57.5	67.85
C_1 (kF)	0.65	0.54
C_n (kF)	1.9	1.61
C_∞ (MF)	3.5	4.1

Table 6.12. Results of Case 2.

Parameters	Measured	Estimated
R_0 (mΩ)	50.2	55.3
R_1 (mΩ)	2.42	2.13
R_n (mΩ)	59.1	51.95
C_1 (kF)	0.75	0.65
C_n (kF)	2.1	2.39
C_∞ (MF)	3.74	4.13

Table 6.13. Results of Case 3.

Parameters	Measured	Estimated
R_0 (mΩ)	50.8	57.09
R_1 (mΩ)	2.46	2.12
R_n (mΩ)	58.1	52.11
C_1(kF)	0.82	0.93
C_n (kF)	1.9	1.65
C_∞ (MF)	3.65	3.22

Table 6.14. Results of Case 4.

Parameters	Measured	Estimated
R_0 (mΩ)	49.2	57.95
R_1 (mΩ)	2.38	1.94
R_n (mΩ)	58.9	70.03
C_1 (kF)	0.85	1.02
C_n (kF)	1.94	2.27
C_∞ (MF)	3.62	3.04

Table 6.15. Results of Case 5.

Parameters	Measured	Estimated
R_0 (mΩ)	51.3	47.7
R_1 (mΩ)	2.43	2.22
R_n (mΩ)	59.7	64.17
C_1 (kF)	0.74	0.82
C_n (kF)	1.95	2.15
C_∞ (MF)	3.7	4.03

Table 6.16. Results of Case 6.

Parameters	Measured	Estimated
R_0 (mΩ)	50.5	53.01
R_1 (mΩ)	2.35	2.18
R_n (mΩ)	59.2	63.94
C_1(kF)	0.78	0.84
C_n (kF)	1.87	1.735
C_∞ (MF)	3.72	4.01

Table 6.17. Results of Case 7.

Parameters	Measured	Estimated
R_0 (mΩ)	48.9	50
R_1 (mΩ)	2.32	2.45
R_n (mΩ)	58.9	60.7
C_1 (kF)	0.81	0.75
C_n (kF)	1.92	1.81
C_∞ (MF)	3.61	3.69

Table 6.18. Results of Case 8.

Parameters	Measured	Estimated
R_0 (mΩ)	49.3	50.2
R_1 (mΩ)	2.35	2.43
R_n (mΩ)	59.3	60.6
C_1 (kF)	0.85	0.87
C_n (kF)	1.95	1.89
C_∞ (MF)	3.65	3.72

Table 6.19. Results of Case 9.

Parameters	Measured	Estimated
R_0 (mΩ)	48.3	46.65
R_1 (mΩ)	2.3	2.46
R_n (mΩ)	58.2	56.35
C_1 (kF)	0.7	0.721
C_n (kF)	1.88	1.81
C_∞ (MF)	3.58	3.69

Based on the estimated values for 9 cases, Fig. 6.18 shows the absolute error values for each case. For each case of frequency regions, two columns are used to explain the minimum and maximum errors. In order to have a better generalization, the model has to also be aware of the different levels of deterioration. For each of the cases, the numbers are different because all the measure was made at different cycles of usage.

It is clear that even in Fig. 6.19, the cases 7–9 achieve the lowest error. For R_0, R_n, C_∞, the cases 7 and 8 have almost the same accuracy, which means that if you want to estimate the SOH, we recommend to use the transient characteristics in case 7 in order to have less frequency points compared to the cases 8 or 9. However, if the researchers want to focus in the R_1, C_1 and C_2, the case 8 is better compared to the case 7 or 9. Based on the same technique on the Li-Ion, the estimation was achieved for the Pb and Ni-MH batteries.
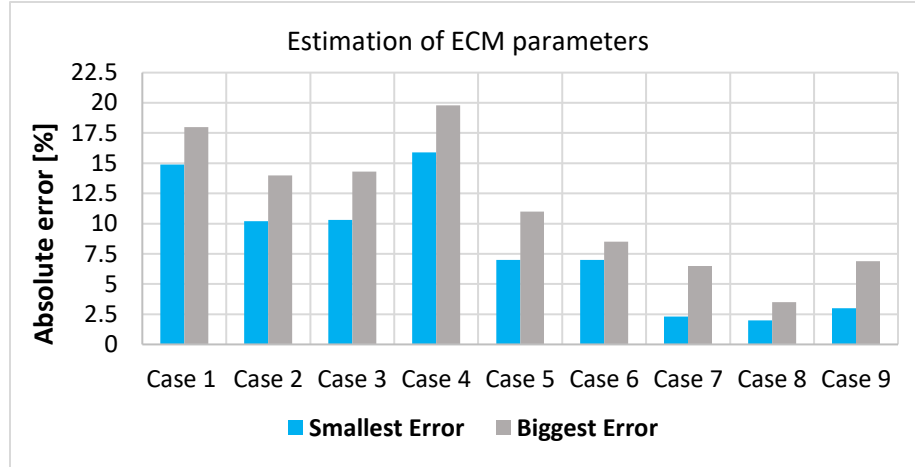
Fig. 6.18. Error plot of Li-Ion battery for each frequency regions.
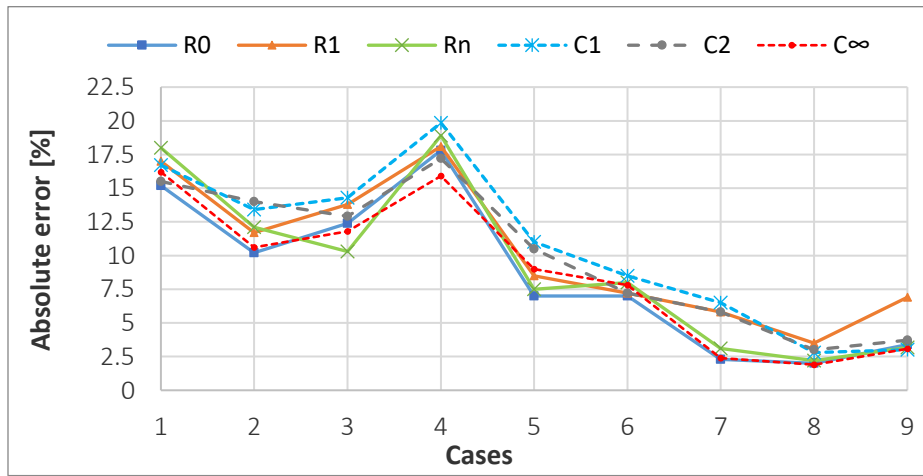
Fig. 6.19. Error plot of Li-Ion battery for each of the parameters.

The measured data were obtained during SOC 100% for all the batteries. In the case of the Pb battery 0 cycle, 100 cycle, 200 cycle, 300 cycle ,500 cycle and 600cycle information were used in this study.

Case 4- **LF** (10mHz-1Hz)/ **HF** (10Hz-100Hz), *Case 5*- **LF** (10mHz-1Hz)/ **HF** (10Hz-1kHz)

Table 6.20. Results of Case 4 for Pb.

Parameters	Measured	Estimated
R_0 (mΩ)	60.5	57.96
R_1 (Ω)	12.72	2.12
R_n (mΩ)	51	47.43
C_1 (kF)	2.5	2.605
C_n (kF)	5.2	5.47
C_∞ (MF)	4.7	4.97

Table 6.21. Results of Case 5 for Pb.

Parameters	Measured	Estimated
R_0 (mΩ)	61.3	65.1
R_1 (mΩ)	11.95	12.77
R_n (mΩ)	53.2	50.38
C_1 (kF)	2.45	2.27
C_n (kF)	5.36	5.745
C_∞ (MF)	4.85	5.15

Fig.6.20. shows the error value for each of the parameters regarding Cases 4-5.
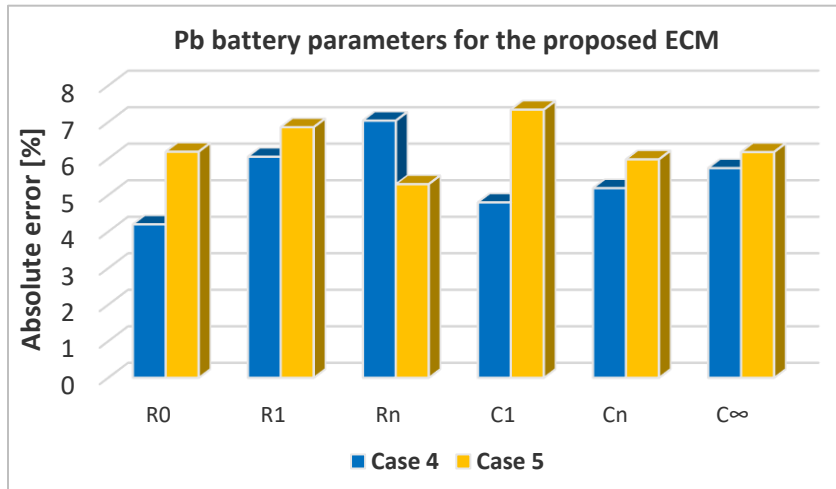
Fig. 6.20. Error plot of Pb battery plot for each of the parameters.

Fig. 6.21 show the estimation error plot of Ni-MH battery for the parameters. Case 6 in Table 6.22. and case 9 in Table 6.23. shows the best estimation and generalization ability during all the estimation process.
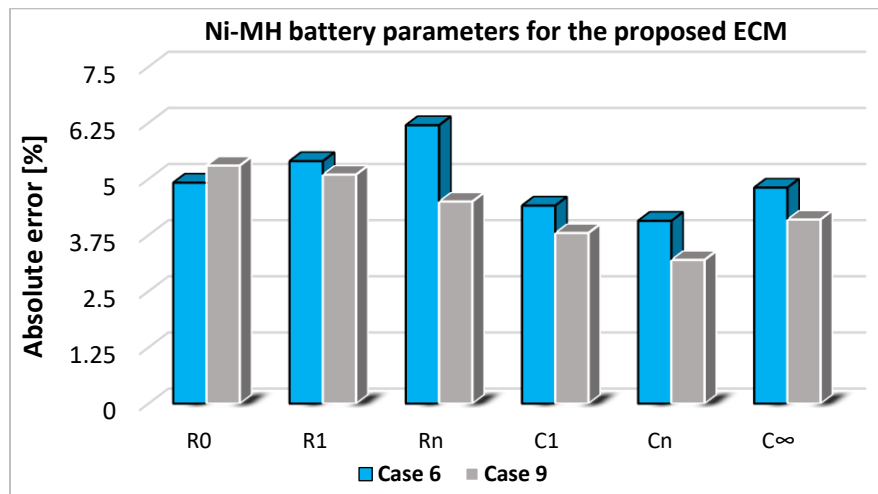
Fig. 6.21. Error plot of Ni-MH battery for each of the parameters.

Table 6.22. Results of Case 6 for Ni-MH.

Parameters	Measured	Estimated
R_0 (mΩ)	26.4	25.1
R_1 (mΩ)	5.9	6.22
R_n (mΩ)	32.4	30.39
C_1 (kF)	0.68	0.71
C_n (kF)	2.092	2.092
C_∞ (MF)	3.76	3.76

Table 6.23. Results of Case 9 for Ni-MH.

Parameters	Measured	Estimated
R_0 (mΩ)	28.2	29.69
R_1 (mΩ)	5.1	4.83
R_n (mΩ)	34.1	32.56
C_1 (kF)	0.71	0.73
C_n (kF)	2.16	2.09
C_∞ (MF)	3.89	4.05

Respectively, the frequency regions of the 2 cases for Ni-MH battery are shown as below:

Case6-**LF**(10 mHz–1 Hz)/**HF**(10 Hz–10 kHz), *Case 9*-**LF**(10 mHz–10 Hz)/**HF**(10 Hz–10 kHz).

Fig. 6.22 shows the optimal frequency region depending on the type of battery based on the matrix plot. Each battery is colored differently in order to distinguish the type. As explained above, the optimal cases are 4 and 5 for the Pb battery, which has a LF range from 10 mHz to 1 Hz and a HF range of up to 1 kHz. For Ni-MH, the best cases are 6 and 9, which shows the fact that this battery is highly dependent in the extreme regions of HF up to 10 kHz and LF up to 10 Hz. Regarding the Li-Ion, the best cases are 7 and 8. At the same time, the case 9 can be used if the user can accept errors of up to 6.7%. Furthermore, the case 9 shows good generalization. However, the author recommends the cases 7 and 8 for the optimal estimation with a LF of up to 10 Hz and a HF with a maximum frequency of 1 kHz or 10 kHz for the case 9 frequency specified in Table 5.
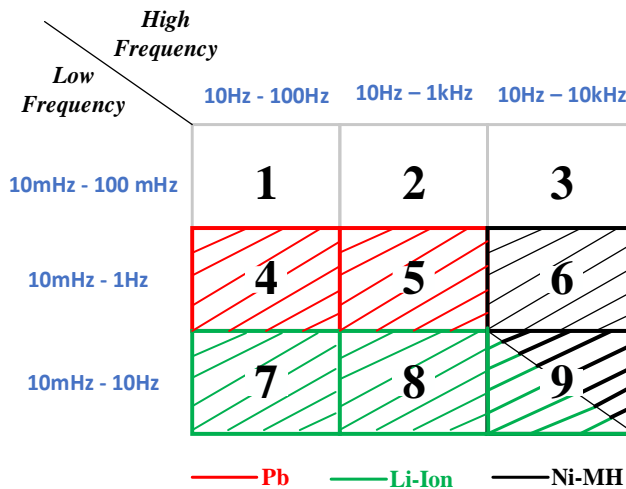
Fig. 6.22. Matrix characteristics for the optimal frequency region depending on the type of battery.

Fig.6.23 provides a simpler explanation derived from the matrix characteristics in Fig.6.22. This plot specify which frequency must be used in order to obtain a better estimation. For example, the Pb battery is recommended to be used in the LF region of up to 1 Hz but it can be used in a HF region from 10 Hz to 100 Hz or even up to 1 kHz. Thus, in the HF region, 1 decade or 2 decades can be used. If the user needs more accuracy, the data set must be studied in a frequency range with a maximum of 1 kHz but they must be aware that this higher frequency requires more data points, more calculation time and experiments. Thus, this needs more powerful hardware to handle the processing. In addition, in the case of the embedded circuit, the computational power is very important as less data will make it faster for the circuit in order to handle it. Thus, depending on

the type of the application, cost, accuracy and time, the user can choose the best regions among the recommended by the author. The cost/performance trade-off must be taken into account.
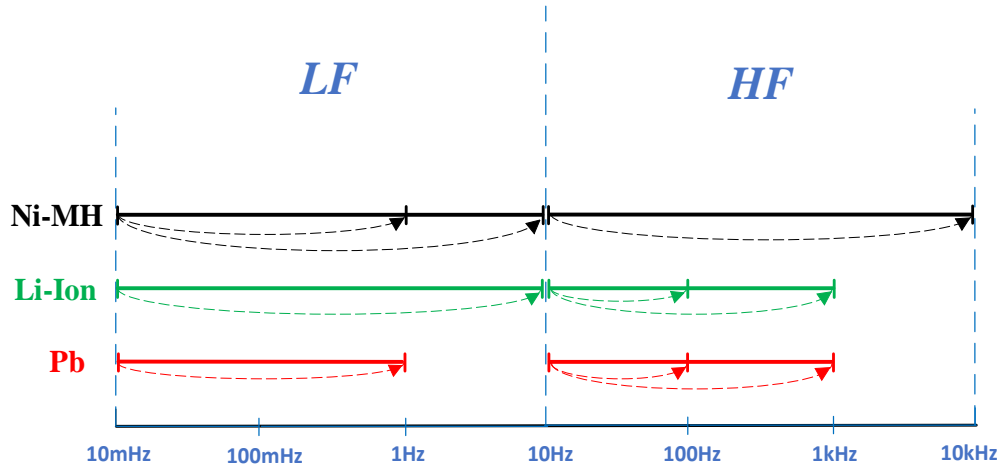
Fig. 6.23. Optimal Frequency Bandwidth for each battery type.

6.4 Conclusions

In this study, the updated and improved version of the dual ANN structure for estimating the circuit parameters of the rechargeable batteries was introduced. As already explained in the previous study [142,181,197], due to the difficulty to handle a wide range of frequency, the estimation process was divided into a high-frequency region, which is related with the maximum chargeable/dischargeable current, and a low-frequency region, which is closely related with SOH. With the help of ANNs, it was possible to estimate these variables with a small difference between the real and calculated by NN and processed in MATLAB R2018a. The updated algorithm with better estimation and calculation time, adaptive algorithm for a better generalization made possible even for different regions of frequency to estimate with high accuracy. In this study, the number of cycles was increased in order to make possible to study the batteries at the full range of deterioration from a new to totally deteriorated based on the manufacture's datasheet. In addition, this fact helps to increase the generalization of the method and it can be used for future diagnosis work, related to the SOH fade. As well the range of discharging ratio was increased, 0.1C, 0.2C, 0.5C, 0.6C, 0.8C and 1C. It was possible to obtain an accurate estimation with 2% error for the Li-Ion for frequency from 10 mHz up to 1 kHz, an estimation error of 3.3% for Ni-MH especially for high frequency regions up to 10 kHz and a minimum error of 4.1% for Pb battery which is based mostly in low frequency regions, with frequency up to 100 Hz or 1 kHz in case that a large number of data points can be obtained. The frequency points were maintained constant the same as in the previous study to confirm the model in case of a small amount of data. In the final step after optimizing and improving the algorithm and the structure of the ANN, the required inputs cells are less than 100, depending by the battery type, capacity, and the charging/discharging ratio. The number of neurons was changed a little comparing from the previous work, as in the hidden layer for the high-frequency structure 32 neurons and in the low-frequency region is 28 neurons. Through this study, it was possible to investigate further the relation of the frequency regions with parameters value of the proposed ECM. The accuracy and generalization were improved as shown in Appendix, Table A1. The estimation was calculated in just a few seconds. The future work will be the focus on obtaining a more reliable and accurate model from a practical device during dynamic loads. As well using parameters like OCV waveform and capacity fade, as online-adaptive parameter approach with the help of ANN [143,151,188,202,203,204], based on an arbitrary waveform will be investigated for the real-time diagnosis.

The main contribution of the author regarding the problems in this chapter are based on these publications:

1) **Published Journals**

   a) M. Bezha, R. Gondo, N. Nagaoka, "*An Estimation Model with Generalization Characteristics for the Internal Impedance of the Rechargeable Batteries by Means of Dual ANN Model*", MDPI Journal of Energies 2019, Vol.12, Special Issue 5, 948, pp.1-22.

2) **International Conference Papers**

   a) M. Bezha, R, Gondo, N. Nagaoka, "*A Dual ANN Model for Estimation of Internal Impedance of rechargeable cell battery*", IEEE 53rd International Universities Power Engineering Conference, UPEC2018 Glasgow, Scotland, 4th-7th September (2018).

   b) M. Bezha, N. Nagaoka, "*An ANN Model for Estimating Internal Impedance of Lithium-Ion Battery Cell for Industrial Application*", IEEE 21st International Conference on Electrical Machines and Systems ICEMS2018, KIEE, IEEE &IEEJ Committee, JEJU Korea, 7-10 October (2018).

   c) Ryo Gondo, M. Bezha, Makoto Ishii, Takahiro Shoda, Tomoyuki Suzuki, N. Nagaoka, "*Development of Scaled Simulator for Designing Power Storage System*", IEEE 54th International Universities Power Engineering Conference, UPEC 2019, Bucharest, Romania, 3rd-6th September (2019).

   d) M. Bezha, N. Nagaoka, "*A fast diagnosis for classification of re-used Li-Ion batteries for PV and EV systems by the ANN model*", IEEE 8th Global Conference on Consumer Electronics-GCCE 2019, Osaka, Japan, 15-18 October (2019).

   e) K. Yamamoto, M. Bezha, Y. Baba, N. Nagaoka, "*Investigation of voltage and current measurement of Li-Ion battery with a BMS*" 13th ISET/ISS & 6th ISLH Conference, Chonburi, Thailand, 29-30 November (2019).

7. Conclusions
7.1 New features of this study (theoretical *and practical usage for Industrial applications)*

In this thesis, important investigations and progress were made in the field of rechargeable batteries for practical applications, which finds terrain for real implementation in industrial field and at the same time in the progress of new ideas and approaches of scientific research. Although Li-Ion batteries have been used in real applications, still it can be considered an immature technology from most of the researchers. This gives the opportunity to investigate wide range of problems and difficulties. Considering this fact, the author proposed new methods by combining previous conventional methods with some new approaches and models. By observing the results of previous methods and their drawbacks, it was possible to understand where it is needed to make further investigations. The difficulty for real time SoC estimation and accurate estimation was overcame in Chapter 4. Different variables should be considered in order to express an accurate and reliable value of the actual SoC, such as the deterioration of the battery, the ratio of charging/discharging, waveform of the charging current, temperature of the total systems which includes the battery cell/module up to pack. These effects were investigated and included in the final model. One of the challenges for an accurate SoC estimation in the conventional methods is the necessity for correct initial SoC value. However, with the proposed method, based on the advance SoC estimation through the ANN model, this initial value is not required. The accuracy is very high, with average error in the range of 1.5% to 3.8% based on different ANN structures the author has investigated. Another difficulty of the SoC estimation is the initial value, where the conventional methods need this value, otherwise it will accumulate error overtime. An SoC estimation model, which can be applicable for different chemistry type for the secondary batteries known as rechargeable batteries, was proposed in this thesis. The level of reliability and security for the overall system cannot be expressed by investigations on a single cell. The characteristics of the battery module or pack have to be clarified. It was seen as an important matter from the author to investigate the BMS effect in the overall system. A single cell and 3 series-connected cells with a BMS were used in this thesis. Their applicability and advantages were shown, also the criteria of min/max voltage and over-charging/discharging was evaluated for the best performance. A new BMS circuit was proposed just for this research. As well the MTC device was improved in order to handle higher voltage which can test battery modules/pack. By improving the MTC device it was possible to develop and propose a scaled down simulator for the design of power storage system. This method shows the possibility to test a single battery cell of Li-Ion 18650 cylindrical type instead of whole battery pack. This means that it can be used as a cost-efficient method to test any power storage system before it can be built in 1:1 ratio. It was confirmed that the applicability field is limitless, application as PV system, wind turbine or even in EV battery pack. The quality and performance were elevated and fast. The computing power of the improved MTC is the same the previous model, handled by PIC MA350 microprocessor. Another important feature is the mobility of this system, which can be transported everywhere due to its small size. The application fields of the developed simulator are not restricted, because the developed simulator has a capability of arbitrary current control, i.e., waveform, amplitude, duty cycle. From the above, the developed simulator in this paper can contribute to the efficient operation and optimum design of the storage system by providing useful information to the system design. In addition, the developed simulator can contribute to the investigation of prolonging the battery life and SOC estimation, since the simulator uses a practical battery.

Through the help of ANN algorithm which was the core of the software for each of the estimation, it was possible to make a real time approach and calculation just in matter of few seconds up to 2 minutes in the worst case. And the necessity of the initial SoC was not required to make an accurate estimation. In terms of computing power, a medium PC was used which helps to accelerate the training phase, but when it come to the estimation phase even low computing power is required which helps for the cost reduction of the total system. During the training, validation and testing phase the NN structure showed robustness and stability by handling thousands of

117

vectors and samples. The most important part of the SoC estimation was the proposed advance SoC estimation. The proposed method is based on adaptive ANN model which asymptotically achieves optimal error rates for realizing stochastic rules. In addition, the number of input cells are drastically reduced up to 1/4 comparing to the previous model. The estimation can be concluded in the range from 15 to 29 seconds by 34% faster than that of the previous method on single cell or battery pack, and maintained stable during all the tests.

In chapter 5 was proposed a new model of SoH estimation based on few parameters which were used as input data for the ANN structure. Model based on voltage & current waveform and number of cycles were introduced. From single cell to pack system an investigation was made. As different battery chemistries were tested to increase the generalization of the model. These models were successful and accurate. It was possible to study new batteries up to full deteriorated one, as important process of understanding the deterioration speed and scale for battery by observing different parameters and trying to explain the physical meaning of each experiment and result. This helped to for the classification process of the re-used batteries, where the main focus was to find the most efficient time of switching the application field of the re-used batteries, in terms of cost-performance characteristics. Trying the find, the best evaluation point to switch from EV system to HEV and finally to less current drain applications as in case of Stationary storage system, where the capacity fade is the main concern. Of course, here the BMS was used in case of pack system. All these behaviors were inserted in the NN logic in order to create and correlate such nonlinear patterns and trying to explain the result obtained in case of the incorporated BMS module. At the same time a practical research was investigated in EV application. By just using two non-related information as speed and battery cell's voltage it was possible to estimate with elevated accuracy the power consumption. And as a conclusion the energy was estimated. Making possible this estimation means to give the user any possible information which in terms of practical usage and applicability for the driver shows the possible mileage of the automobile and its actual SoH. Of course, in the automobile market already exist few different services which can diagnosis the battery's health, but the innovation of this model was based by the estimation of SoH considering only two simple data which can be easily obtained through the sensors without any extra cost. And most important this diagnosis can be made in real time during operation of the car. This means that it is not necessary to stop the utilization of the car for few hours during the diagnosis made in the shop services. The further utilization of this method is not yet defined, because this model was shown as a good approach for the classification of the old batteries. It can be possible to classify an accurate level of deterioration of the battery cell/module, which means it can identify even single or specific group of cells which are most deteriorated amongst the total group of batteries. Doing this it is possible to increase the level of security for the total system without the need to swap all the battery pack, as a cost-efficient approach. As a matter of fact, an evaluation of the most relevant equivalent circuit model was necessary for this thesis.

In Chapter 6 was proposed few different ECM related with their mathematical modelling. A procedure of the parameter estimation was explained which includes the physical meaning of the variables which composes the ECM. The internal impedance can be expressed by a resistor, which expresses the voltage drop in a high frequency region, and some RC parallel circuits, which expresses the transient characteristics of the battery. The internal impedance is known as an index of the battery deterioration. C_∞. Based on different problems and the required accuracy or level of complexity a 2nd order or 3rd order model is more than acceptable for elevated quality of estimation. Specifically, this chapter was mainly focused to help the researchers for a theoretical approach based on the practical observation obtained from the experimental results. The main focus in this part was to find the optimal frequency regions (OFR) for each batter type, respectively Li-Ion, Pb and Ni-MH cells. This can explain and estimate the deterioration of the batteries based on the values of the ECM parameters.

The OFR was divided in two main regions respectively low and high frequency, and in total 9 case were introduced as possible combinations. Each of the variables which compose the ECM respectively second and

third order were used as robust and acceptable ECM order in order to explain any possible physical behavior and reaction of the batteries. As already explained in the previous study due to the difficulty to handle a wide range of frequency, the estimation process was divided into a high-frequency region, which is related with the maximum chargeable/dischargeable current, and a low-frequency region, which is closely related with SoH. The updated algorithm with better estimation and calculation time, adaptive algorithm for a better generalization made possible even for different regions of frequency to estimate with high accuracy. As well the range of discharging ratio was increased, 0.1C, 0.2C, 0.5C, 0.6C, 0.8C and 1C. It was possible to obtain an accurate estimation with 2% error for the Li-Ion for frequency from 10 mHz up to 1 kHz, an estimation error of 3.3% for Ni-MH especially for high frequency regions up to 10 kHz and a minimum error of 4.1% for Pb battery which is based mostly in low frequency regions, with frequency up to 100 Hz or 1 kHz in case that a large number of data points can be obtained. The estimation was calculated in just a few seconds.

Through this study, it was possible to investigate further the relation of the frequency regions with parameters value of the proposed ECM, without reducing the accuracy and the generalization ability of the ANN.

The proposed methods are applicable to real time diagnosis applications and to offline processing. The quality and credibility of the work was continuously confirmed by the comparison with experimental results. The author has proposed new deterioration diagnostic methods and approaches for secondary batteries, which are totally different from conventional methods. Proposal of new idea, which resolves actual problems of this field, and provision of the opportunity to investigate new problems are the main goal of the author.

The proposed methods based on this study open the door to new application fields of the secondary battery from academic perspectives to industrial applications.

8.   Appendix
8.1   Analysis of the devices and graphs

Based on the historical data Dr. Konig concluded that their main purpose was for electroplating gold and silver jewelry for the high elite society. Figs. A.1 shows the Baghdad battery, (P. Craddock. Metallurgy Expert, British Museum).
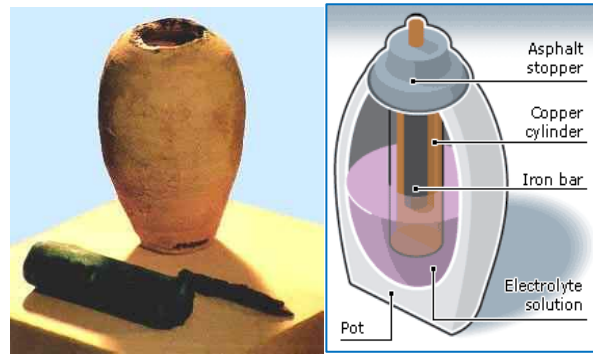
Fig. A.1. Original photo of Parthian battery and components

The proposed "near-shore aggregation" SEI formation mechanism, which explained in detail in [85]. This "solution-mediated" mechanism instead of the "surface-mediated" mechanism would allow the formation of several tens of nanometer-thick SEI film, as shown in Fig, A.2
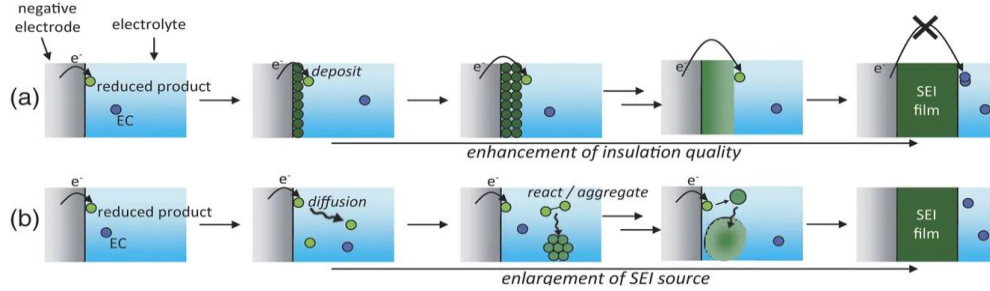
Fig. A.2. The proposed "near-shore aggregation" SEI formation mechanism – *Ushirogata at al.* [85].

Analysis and contribution of the work where Figs. A3 and A4. shows the devices used to obtain the experimental data used for the training of the ANN.

Fig. A.3. Thermo-hygrostat.
(HIFLEX KEYFLESS TL401E)

Fig. A.4**.** Evaluation system AS-510-LB4.

As already explained in the Author Contributions, most of the data were obtained by these devices, but in the same time extra data were obtained through the multi-type Secondary-Battery Charger/Discharger by Arbitrary Current Waveform. From this device extra experiments were conducted for waveforms different from CCCV mode, pulse current where used. Also, different charging/discharging ratio was conducted as: 0.1C, 0.2C, 0.3C, 0.5C, 0.8C, 1C, as shown in Fig. A5. The range of the experiments where conducted from a new battery to a full deteriorated as specified in the official specification, from 0 cycle to (500–600) cycle.

Fig. A6 shows extra information during CCCV discharging process. The author would like to investigate further the effect of ratio in the deterioration effect of the batteries related to the values of the internal resistance. Temperature as well-known variable which reduce the lifetime of the battery, should be inserted in the nonlinear characteristics. Also, other experiments based on the pulse waveform are conducted by the author, in future works these experiments will compare the effect of the pulse charging or any arbitrary waveform for a practical application in EV batteries.
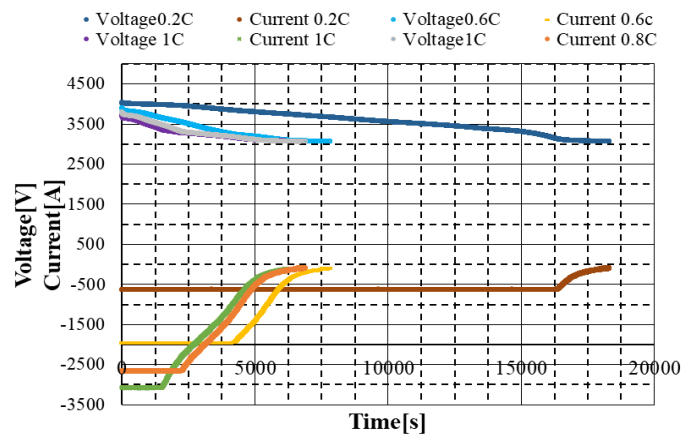
Fig. A.5. **CCCV** Discharging for different current ratio
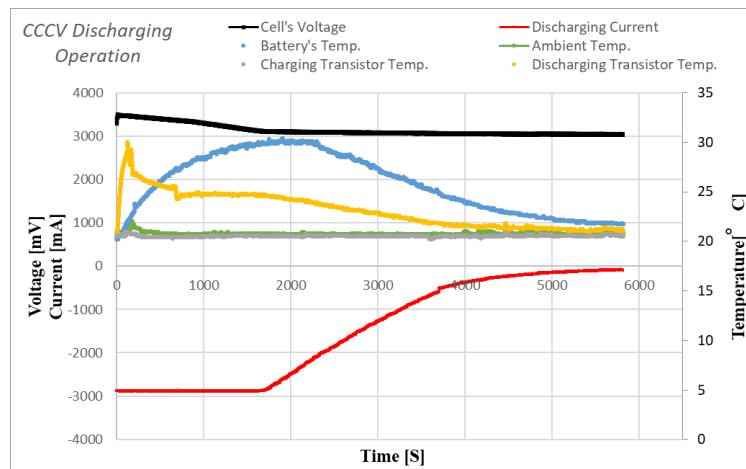
Fig. A.6. **CCCV** Discharging info at 21°C, 2.4A=0.75C ratio, 216 cycle, External Resistance=40mΩ
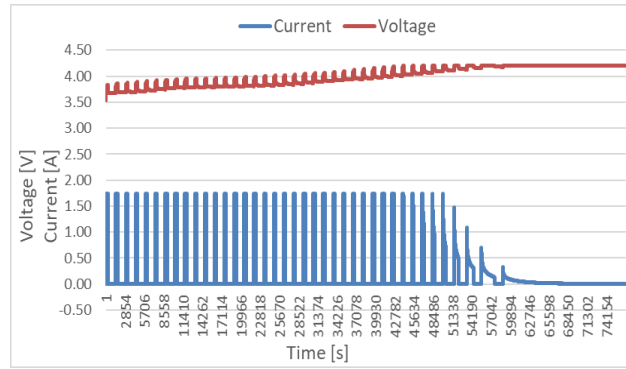
Fig. A.7. Experimental Voltage & Current waveforms.
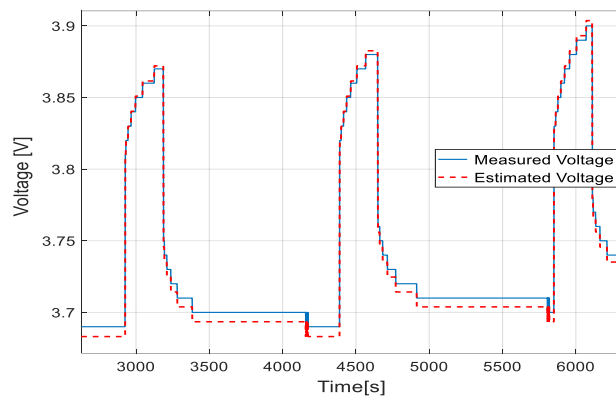
Fig. A.8. Zoomed image of the estimated test voltage

Table A.1. Comparison of accuracy between previous and actual stage of this study, related with Chapter 6.

Studies	Li-Ion Error (%)	Pb Error (%)	Ni-MH Error (%)
Previous study [142]	3	4.9	4.5
Results of actual study [#] [136]	2	4.1	3.3

\# Related with the results shown in chapter 6, [136]

Table A.2. Different Levels of automotive electrification, explanation for chapter 2[3]

	Micro Stop/ Start	Mild-HEV	Full-HEV	Plug-in Hybrid	Plug-in E-REV	H₂ Fuel Cell EV	Electric Vehicle
Functionality	Engine stop-start at idle	Engine off during deceleration, mild regenerative braking, electric power assist	Full regenerative braking, engine cycle optimization, electric launch, limited pure electric drive, allows engine downsizing	Grid recharge-able, extended electric drive during charge depletion mode, high fuel economy during short trips	Full function electric drive, initial pure electric range, significantly reduced gas, refueling, zero fuel on short trips	Full function electric drive, petroleum free, emissions free	Plug-in recharge only, 100% pure electric range, no refueling
Battery type	Power	Power	Power	Power/energy	Energy/power	Power/energy	Energy
Battery chemistry	PbA, lithium-ion	NiCd, NiMH, lithium-ion	NiCd, NiMH, lithium-ion	Lithium-ion	Lithium-ion	Lithium-ion	Lithium-ion
Battery pack size	250–1000 Wh	1–1.5 kWh	1.5–3 kWh	7–15 kWh	15 kWh+	TBD	15 kWh+
Electric range	None	None	<1 mile	10–30 miles	35+ miles	300+ miles	75+ miles

Fig. A.9 shows the industrial manufacturing process a cylindrical-cell. The schematic of the assembly cells is shown in details as below. It is important to emphasize the fact that this manufacturing process is complex due to security protocols.
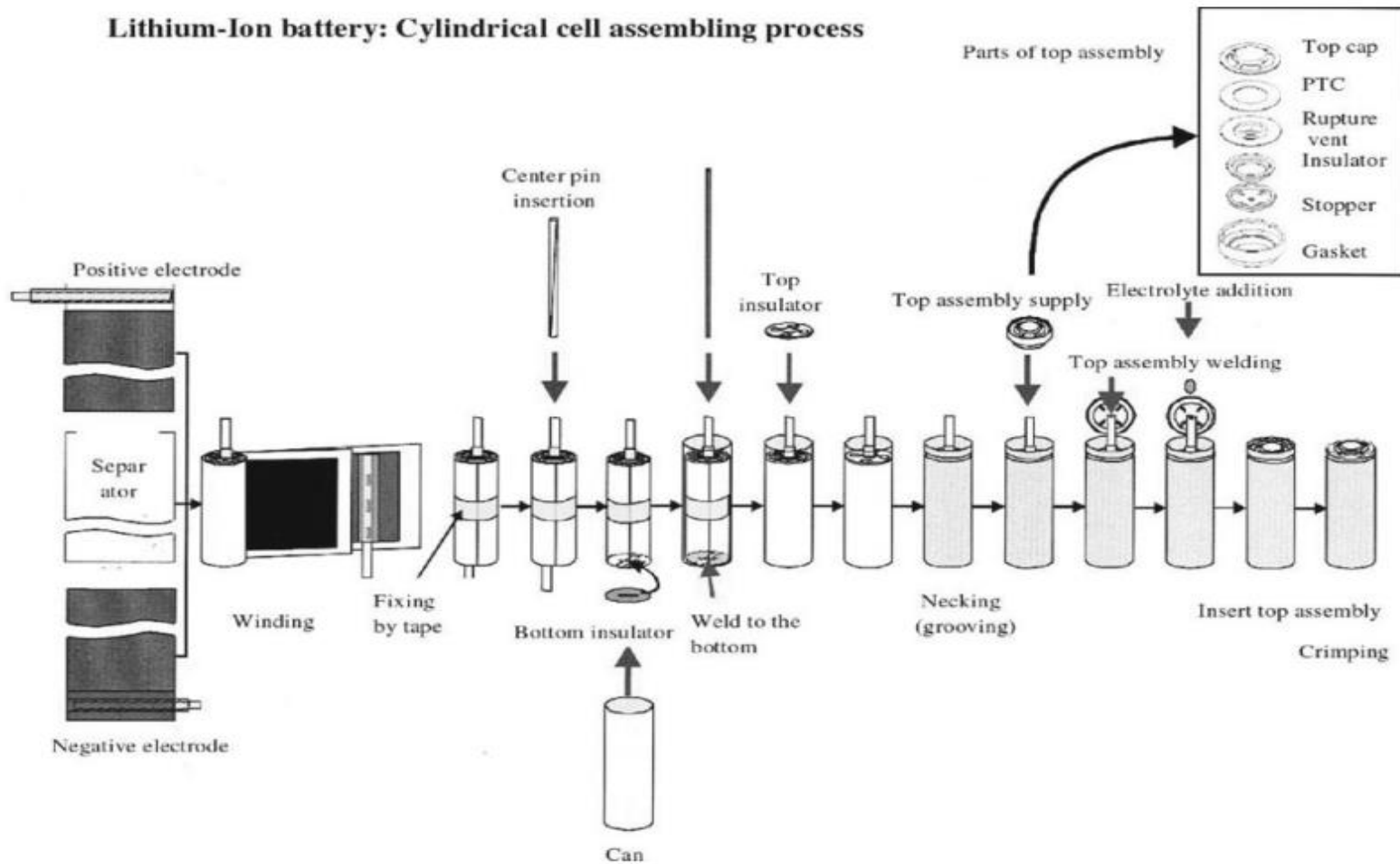
Fig. A.9. General schematic for cylindrical cell assembly, several steps such as beading a ledge near the top of the can to seal the cell cap, the cap assembly itself [4].

Rectangular lithium-ion battery assembling process
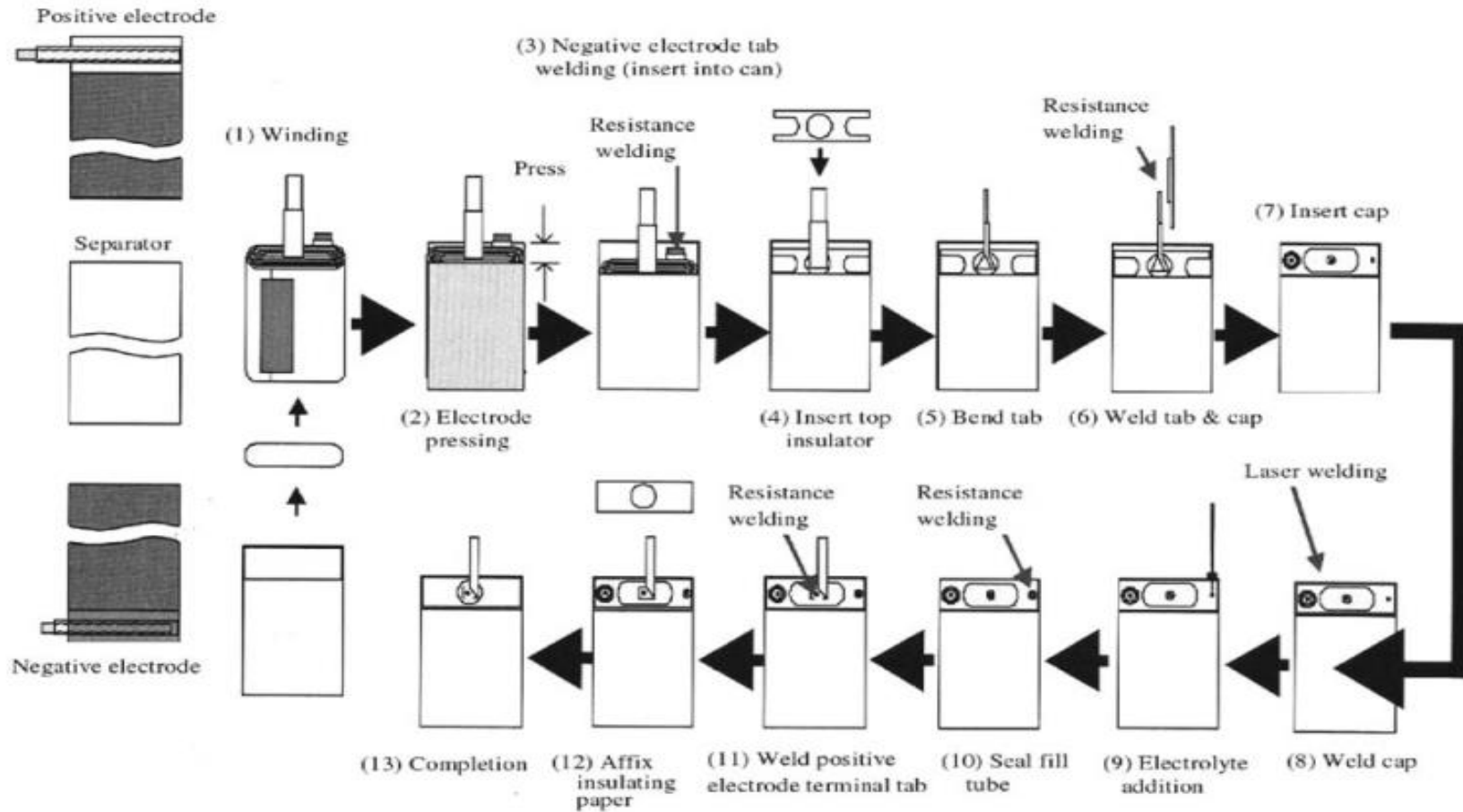
Fig. A.10. General schematic for prismatic cell assembly, several steps such as beading a ledge near the top of the can to seal the cell cap, the cap assembly itself [4].
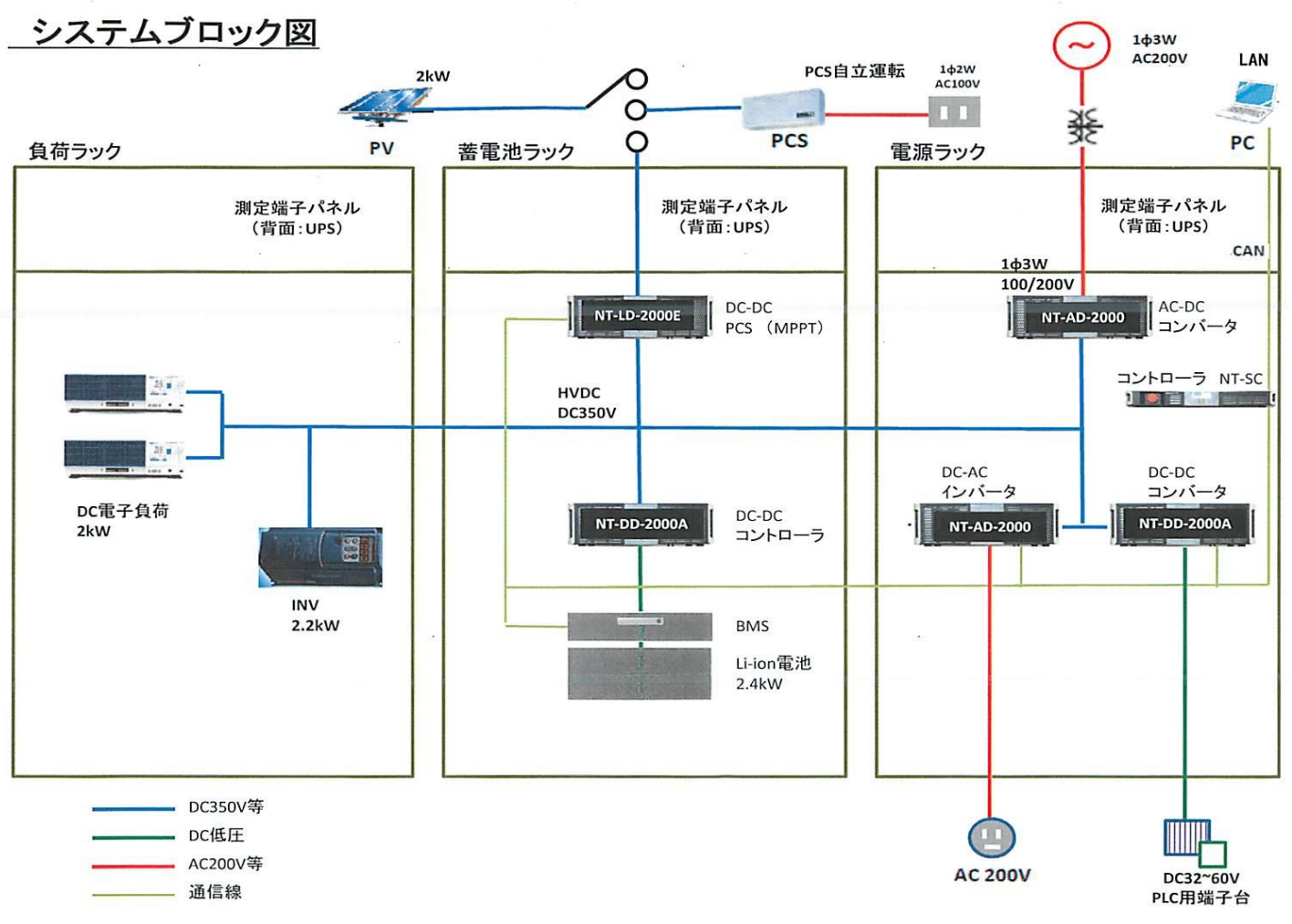
Fig. A.11. Block diagram connection for the devices used for the EV simulation, electronic loads, UPS, DC-DC converters
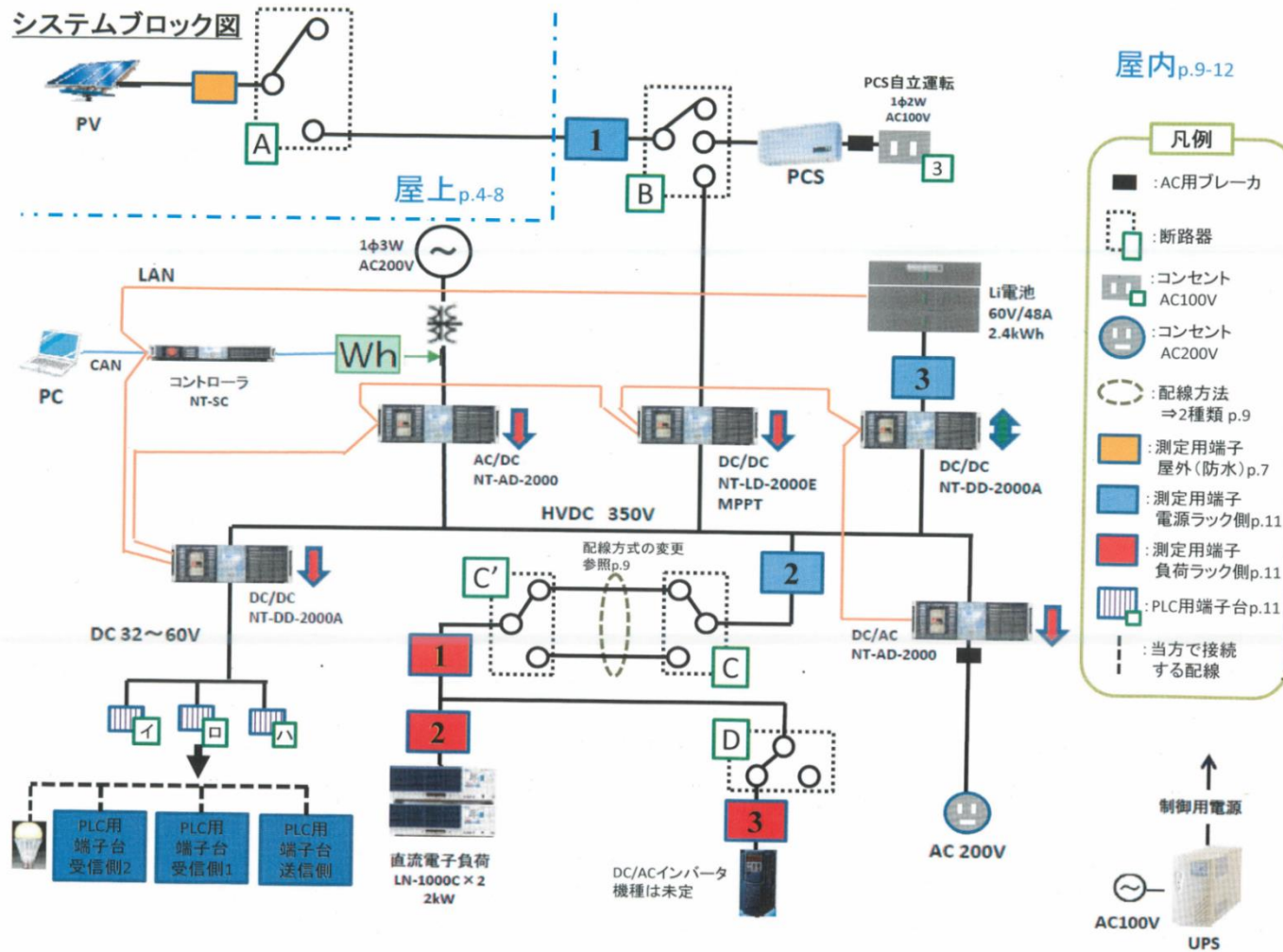
Fig. A.12. Extra details of the block diagram connection for the EV battery pack simulation, electronic loads, UPS, DC-DC converters

Fig. A.13. Devices used for the EV simulation, electronic loads, UPS, DC-DC converters

8.2 BMS circuits and components

The BM3451 works constantly to monitor each cell's voltage, the current of charge or discharge, and the temperature of the environment to provide overcharge, over-discharge, discharge overcurrent, short circuit, charge overcurrent and over-temperature protections, etc. Besides, it also can change the protection delay time of overcharge, over-discharge and discharge overcurrent by setting the external capacitors. The BM3451 provides external bleeding for cell-capacity balance function to avoid unbalanced capacity between each cell. Thus, the batteries can work for longer.

Extended function module embedded in the BM3451 ICs makes them work, for increased number of battery packs with multiple chips, and they can protect 6-cell batteries or even more than 6-cell batteries.
It introduces features like:

1) **High accuracy voltage detection for each cell.**
    - Overcharge threshold   3.6V~ 4.6 V with accuracy: ±25mV (+25℃) / ±40mV (-40℃ to +85℃)
    - Overcharge hysteresis   0.1 V with accuracy: ±50mV
    - Over-discharge threshold   3.6V~ 4.6 V with accuracy: ±80mV
    - Over-discharge hysteresis   0V/0.2V/0.4V with accuracy: ±100mV

2) **Three grades voltage detection of discharge overcurrent**
    - discharge overcurrent 1   0.025 V ~ 0.30 V   (50 mV step)
    - discharge overcurrent 2   0.2 V / 0.3V / 0.4V / 0.6 V
    - short circuit   0.8V / 1.2 V

3) **Charge overcurrent detection**
    - detection voltage   -0.03V / -0.05V / -0.1V / -0.15V / -0.2 V

4) **3/4/5 cell protection enable**

5) **Setting of output delay time**
    - overcharge, over-discharge, discharge overcurrent 1 and discharge overcurrent 2 protection delay time can be set by external capacitors

6) **Supports external bleeding for balance**

7) **Controlling the state of charge or discharge by external signals**

8) **The maximum output voltage of CO / DO: 12V**

9) **Over-temperature protection**

10) **Breaking wire protection**

11) **Low power consumption**
   - operation mode (with Temp protection）25 µA typical
   - operation mode (without Temp protection）15 µA typical
   - sleeping mode 6 µA typical

Regarding the function description for the few features are explained as below:

1) **Overcharge,**
During charging, VIN >V OVCC when IC doesn't work in the state of charge overcurrent, If any of VC1, (VC2-VC1), (VC3-VC2), (VC4-VC3) and (VC5-VC4) is higher than V DET1 and lasts longer than T OV, BM3451 chip considers that the batteries work in the state of overcharge, the output voltage of CO will become to high resistance from high level, and then it will be pulled down to low level by external resistor. The charge MOSFET will be turned off and stop charging.

2) **Over-discharge,**
  During discharging, VIN<V OVCC when IC doesn't work in the state of discharge overcurrent. If any of VC1, (VC2-VC1), (VC3-VC2), (VC4-VC3) and (VC5-VC4) is less than V DET2 and lasts longer than T_{OVD}. BM3451 chip considers that the batteries work in the state of over-discharge and the output voltage of DO will turn to GND. The discharge MOSFET will be turned off and stop discharging, then the chip will enter sleeping mode. The over-discharge protection state will be released if any of the next conditions occurs:
   a) VM =0mV, all cells' voltage is higher than V_{REL2} and stays a period of time T_{REL2}.
   b) VM <-100mV (connecting to the charger), all cells' voltage is higher than V_{DET2} and stays a period of time T_{REL2}.

3) **Discharge Overcurrent**
During discharging, the current varies with the load. The voltage of VIN becomes higher with the current increasing. When the voltage of VIN is higher than V_{OC1} and stays longer than T_{OC1}, we think the IC works in the state of discharge overcurrent 1; When the voltage of VIN is higher than V_{OC2} and stays longer than T OC2, we consider the IC works in the state of discharge overcurrent 2; When the voltage of VIN is higher than V_{SHORT} and stays longer than T_{SHORT}, we think the IC works in the state of short circuit. When any of the three states occurs, the output voltage of DO changes to low level to turn off the discharge MOSFET and stop discharging. At the same time, R VMS which is the inner pulling down resistance of VM is connected, and we know that VM is pad which we can lock the output voltage of DO by when chip works in the state of over-current discharge. Usually $V_{OC1} < V_{OC2} < V_{SHORT}$, $T_{OC1} > T_{OC2} > T_{SHORT}$. When IC works in discharge overcurrent, the output voltage of DO is locked in low level. The discharge overcurrent protection state will be released when disconnect the load.

4) **Charge Overcurrent**
During charging, if the current is biggish with VIN<V_{OVCC} and stays longer than T_{OVCC}, the BM3451 chip considers that the batteries work in the state of charge overcurrent, the output voltage of CO will be pulled down to low level and the charge MOSFET will be turned off and stop charging. Charge overcurrent protection will be released when we disconnect the charger.

5) Balance Function

Cells' balance function is used to balance the cells' capacity in a pack. When all voltages of VC1, (VC2-VC1), (VC3-VC2), (VC4-VC3) and (VC5-VC4) are lower or higher than V_{BAL}, all the external balance discharge circuits will not work. Otherwise the cell, whose voltage is higher than V_{BAL}, will turn on the external discharge circuit and make its voltage lower than V_{BAL}. During charging, If the highest voltage of five cells enters overcharge state and its cell balance circuit turns on, the charge control MOSFET turns off and the external discharge circuit works and makes the battery voltage fall down to V_{REL1} which is the overcharge release threshold, then turn on the charge control MOSFET for continuing charge. For a long enough time of charge and discharge cycles, the voltages of all cells will reach to more than V_{BAL}, and avoid the capacity differences between batteries.

6) Over-temperature

The thermostat resistor connecting to NTC pad is used to induct the pack's temperature, the resistor connecting TRH pad is used to set the reference of over-temperature protection. Assuming the resistance of NTC is R_{NTC} when the pack gets to the temperature of charge over-temperature protection, and then we set the resistance R_{TRH} of TRH be $R_{TRH} = 2* R_{NTC}$. The over-discharge protection temperature is the temperature when the resistance of NTC become to $0.54* R_{NTC}$. We can set the temperature of charge and discharge protection by changing the value of R_{TRH}.

7) Breaking wire protection

In case that one or multi wires of VC1, VC2, VC3, VC4 and VC5 are detected cut from the batteries by the BM3451 chip, the IC will consider it enters a state of breaking wire, then CO will be in high resistance and DO will turn to GND level, then the IC enters low consumption state. When the breaking wires are connected correctly again, the IC will exit breaking wire protection. Specially attention, regardless one chip application or multi-chip application, the GND pin must not be open from the battery, or the IC cannot operate normally, and it cannot protect correctly.
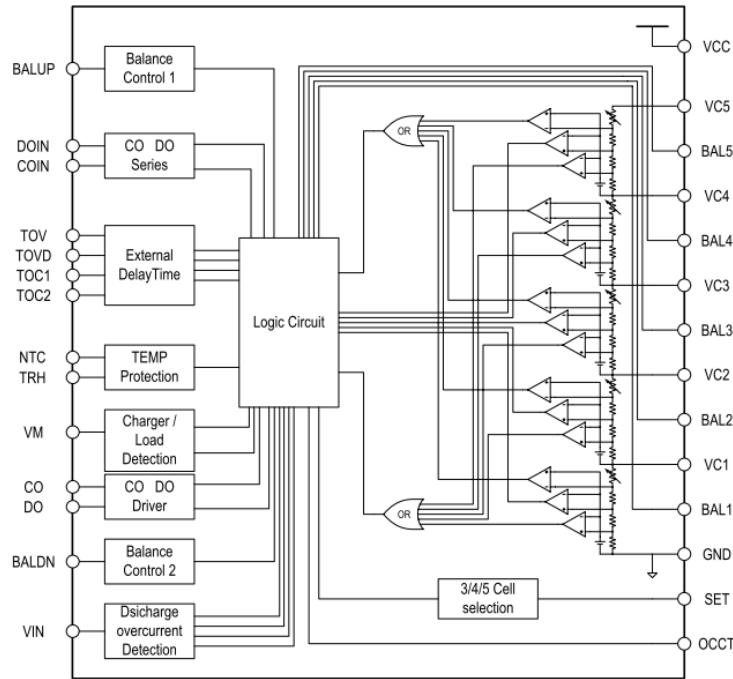
Fig. A.14. Block diagram of BM3451
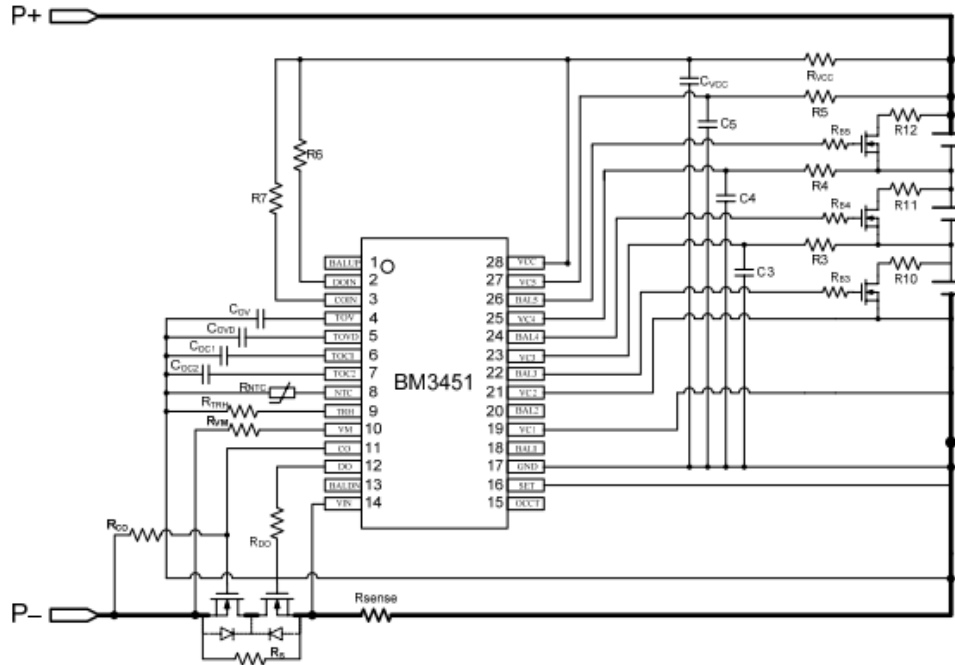
Fig. A.15. BM3451 with 3-cell application (SET connected to GND) ---with balance function
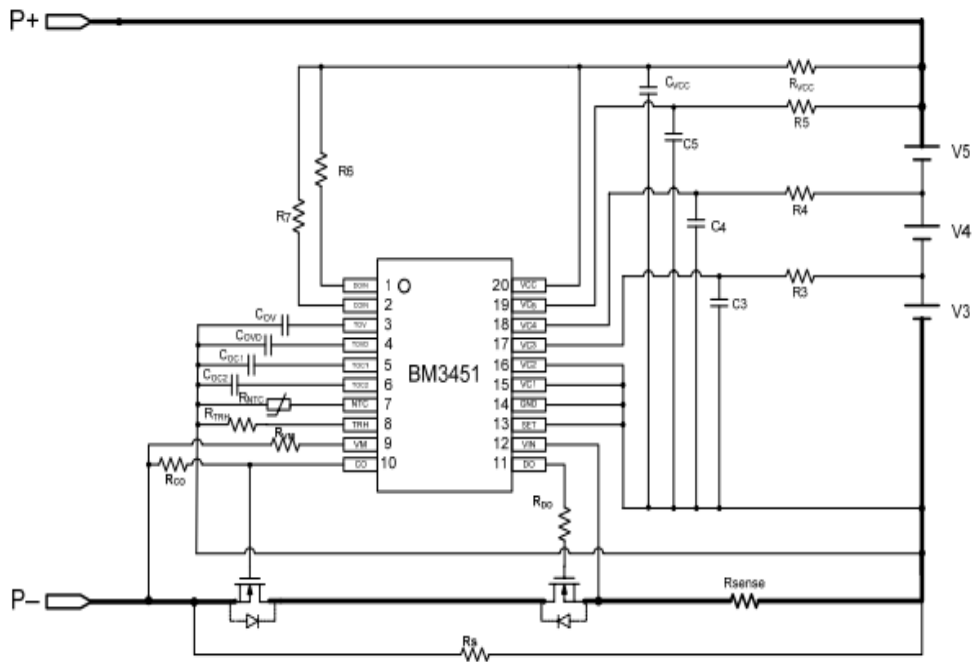
Fig. A.16. BM3451 with 3-cell application (SET connected to GND) ---without balance function

Fig. A.17. BM3451 with 4-cell application (SET connected to GND) ---with balance function

Fig. A.18. BM3451 with 4-cell application (SET connected to GND) ---without balance function
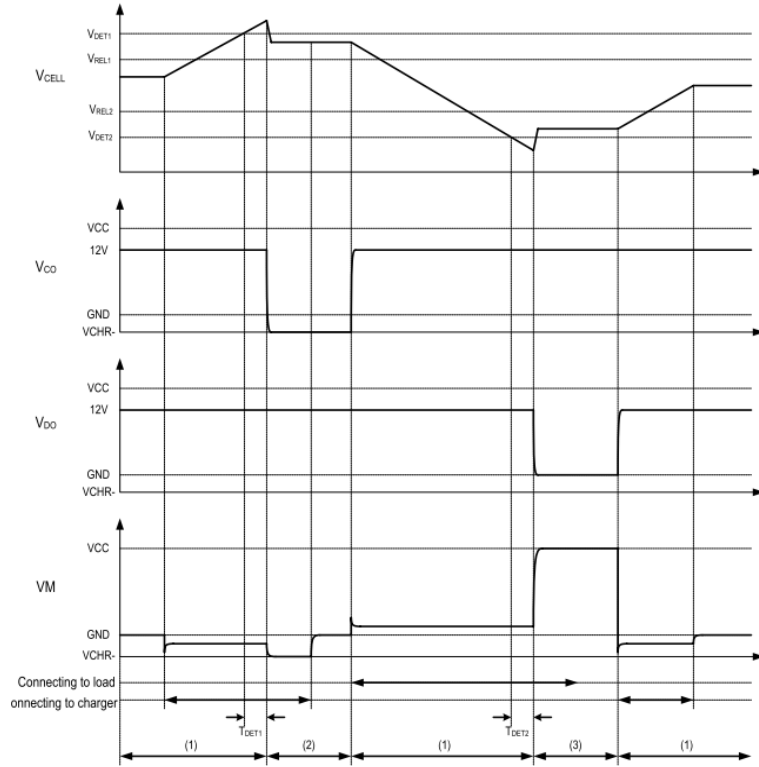
Fig. A.19. Operation Timing chart during Overcharge/Over-discharge Protection with BM3451
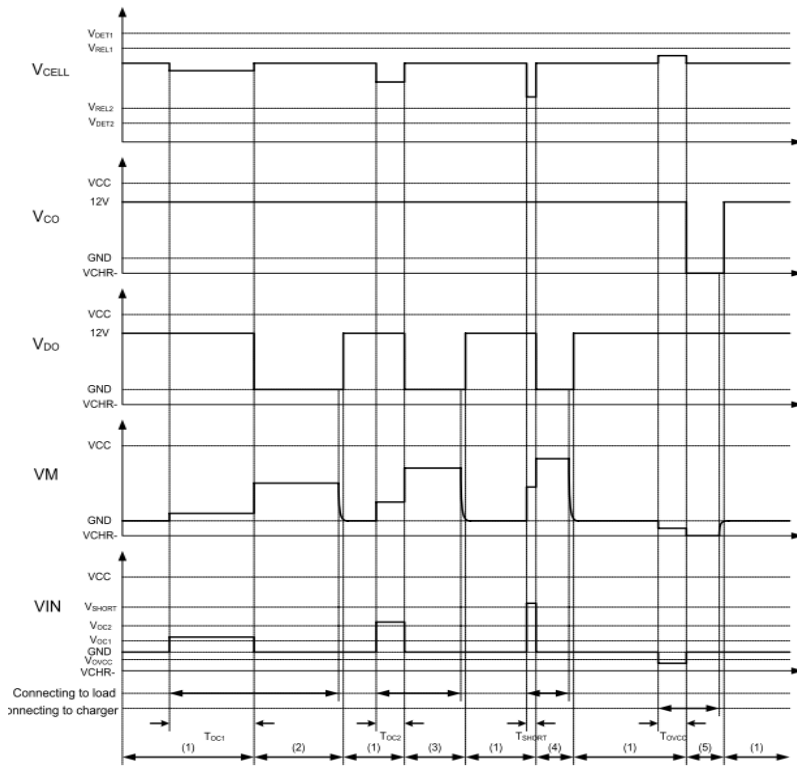
Fig. A.20. Operation Timing chart during Discharge Overcurrent/Short circuit charge/ Overcurrent Protection with BM3451

132

Another important component for the design of the 3S BMS type is switching control block, where it was based on the usage of the STD95N3L (LH6) Power MOSFET. It has the required specifications and features for the development of one of the used BMS proposed in this study, as:

➢ Extremely low on-resistance $R_{DS(on)}$
➢ Low gate drive power losses
➢ High avalanche ruggedness

Due to the new gate structure based on the 6th generation of design rule of STs, STripFET[TM] technology, the resulting power MOSFET exhibits the lowest $R_{DS(on)}$, which makes it suitable for a demanding DC-DC converter application as BMS, where high power density has to be achieved.

Table A.3. Specification of STD95N3L (LH6) Power MOSFET

Symbol	Parameter	Value	Unit
V_{DS}	Drain-source voltage ($V_{GS} = 0$)	30	V
V_{GS}	Gate-source voltage	± 20	V
I_D [(1)]	Drain current (continuous) at $T_C = 25$ °C	80	A
I_D	Drain current (continuous) at $T_C = 100$ °C	61	A
I_{DM} [(2)]	Drain current (pulsed)	320	A
P_{TOT}	Total dissipation at $T_C = 25$ °C	70	W
	Derating factor	0.47	W/°C
E_{AS} [(3)]	Single pulse avalanche energy	TBD	mJ
T_{stg}	Storage temperature	-55 to 175	°C
T_j	Max. operating junction temperature	175	°C

Table A.4. Switching on/off (inductive load) STD95N3L (LH6)

Symbol	Parameter	Test conditions	Min.	Typ.	Max.	Unit
$t_{d(on)}$	Turn-on delay time	$V_{DD} = 15$ V, $I_D = 40$ A,		TBD		ns
t_r	Rise time	$R_G = 4.7$ Ω, $V_{GS} = 5$ V		TBD		ns
$t_{d(off)}$	Turn-off delay time	$V_{DD} = 15$ V, $I_D = 40$ A,		TBD		ns
t_f	Fall time	$R_G = 4.7$ Ω, $V_{GS} = 5$ V		TBD		ns

Table A.5. Source drain diode STD95N3L (LH6)

Symbol	Parameter	Test conditions	Min.	Typ.	Max.	Unit
I_{SD}	Source-drain current				80	A
I_{SDM}[(1)]	Source-drain current (pulsed)				320	A
V_{SD}[(2)]	Forward on voltage	$I_{SD} = 40$ A, $V_{GS} = 0$			1.1	V
t_{rr}	Reverse recovery time	$I_{SD} = 80$ A,		TBD		ns
Q_{rr}	Reverse recovery charge	di/dt = 100 A/µs,		TBD		nC
I_{RRM}	Reverse recovery current	$V_{DD} = 20$ V		TBD		A

1. Pulse width limited by safe operating area
2. Pulsed: pulse duration=300µs, duty cycle 1.5%
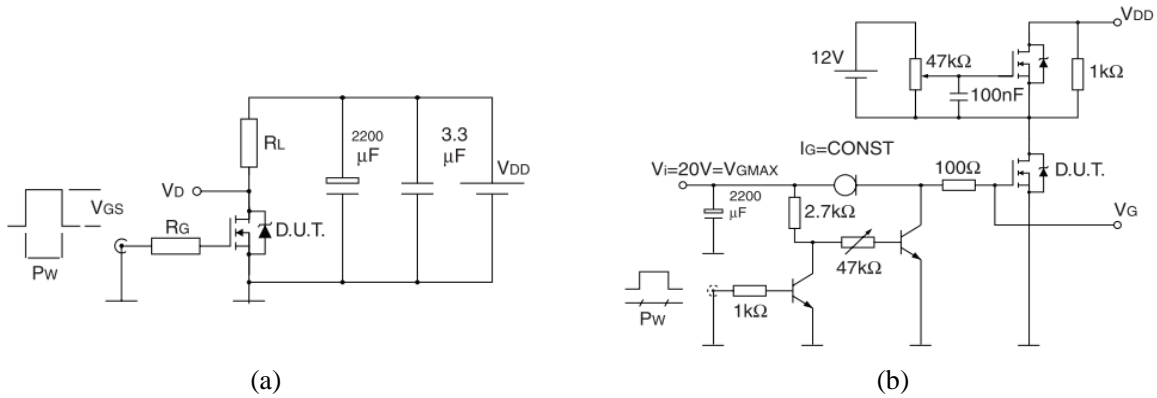
Fig. A.21. Switching times test circuit for resistive load (a), Gate charge test circuit composition (b).
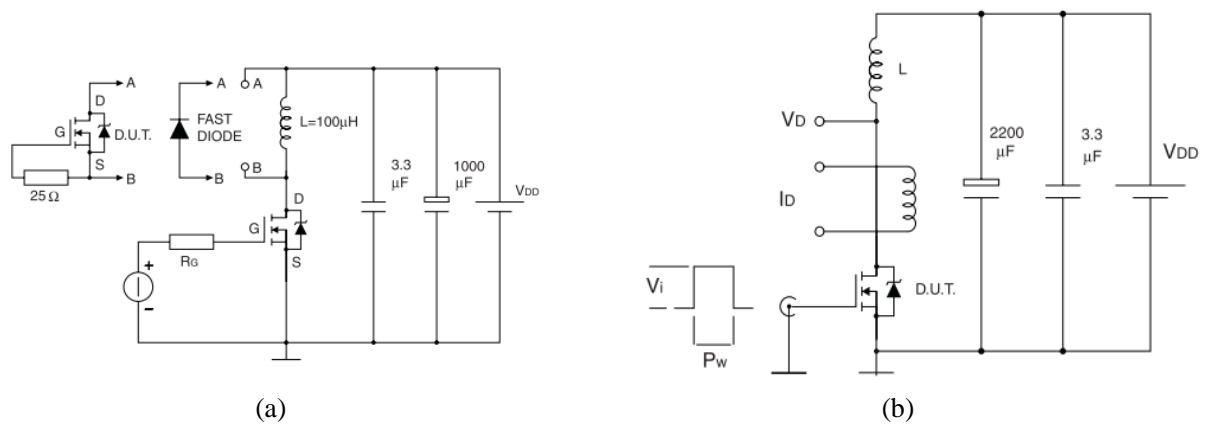
Fig. A.22. Test circuit for inductive load switching and diode recovery times (a), Unclamped Inductive load test circuit (b).

In this study a single cell BMS, standalone line Li-Ion battery charger with thermal regulation was proposed by the author. Two type of MOSFET were used for single cell BMS, LTC4054 and LTH7. These MOSFETs are a complete constant-current /constant-voltage linear charger for single cell Li-Ion batteries. Due to the low external component count makes them suitable for portable applications, small size- embedded circuits. As well no external sense resistor is needed, and no blocking diode is required due to the internal MOSFET architecture. Thermal feedback regulates the charge current to limit the die temperature during high power operation or high ambient temperature.

Features as:
➢ Programmable charge currents up to 1A
➢ Compete linear charger for single cell Li-Ion
➢ CCCV operation with thermal regulation to maximize charge rate without risk of overheating
➢ Preset 4.2V charge voltage with ±1% accuracy
➢ Automatic recharge
➢ Charge status output pin
➢ C/10 charge termination
➢ 25μA Supply current in shutdown
➢ 2.9V Trickle charge threshold
➢ Soft-start limits inrush current
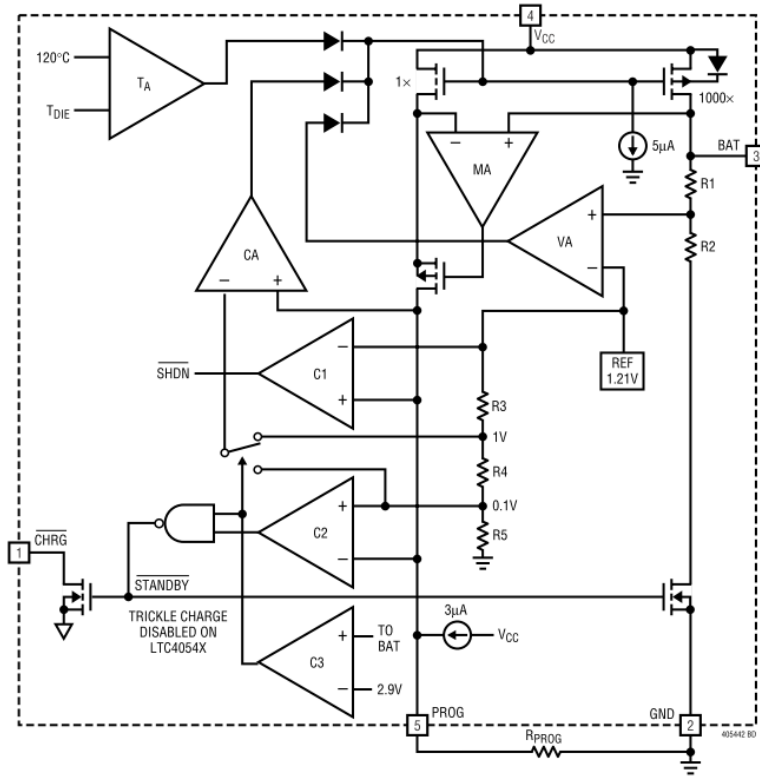
Fig. A.23. Block diagram of LTC4054-LTH7
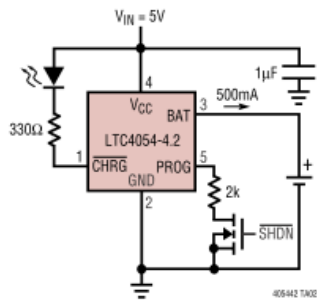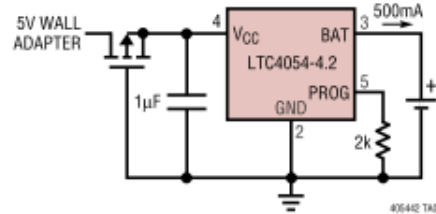
(a)   (b)

Fig. A.24. Full Featured Single Cell Li-Ion Charger (a), Basic Li-Ion Charger with Reverse Polarity Input Protection (b).
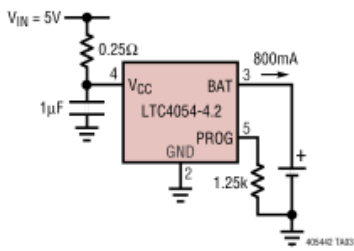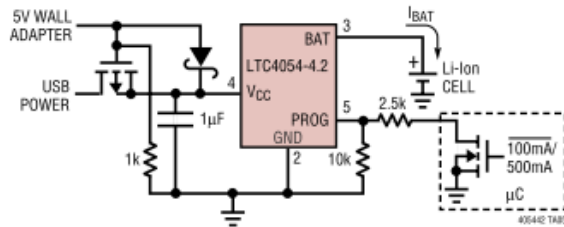
(a)   (b)

Fig. A.25. 800mA Li-Ion Charger with External Power Dissipation (a), USB/Wall Adapter Power Li-Ion Charger (b).

135
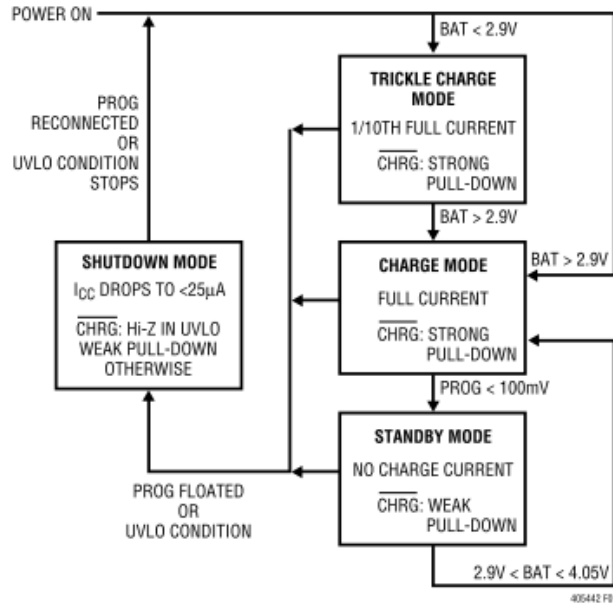
Fig. A.26. State diagram of a typical charge cycle

Regarding the normal operation protocols:

The LTC4054 is a single cell lithium-ion battery charger using a constant-current/constant-voltage algorithm. It can deliver up to 800mA of charge current (using a good thermal PCB layout) with a final float voltage accuracy of ±1%. The LTC4054 includes an internal P-channel power MOSFET and thermal regulation circuitry. No blocking diode or external current sense resistor is required; thus, the basic charger circuit requires only two external components. Furthermore, the LTC4054 is capable of operating from a USB power source.

➤ **Normal Charge Cycle**

A charge cycle begins when the voltage at the VCC pin rises above the UVLO threshold level and a 1% program resistor is connected from the PROG pin to ground or when a battery is connected to the charger output. If the BAT pin is less than 2.9V, the charger enters trickle charge mode. When the BAT pin voltage rises above 2.9V, the charger enters constant-current mode, where the programmed charge current is supplied to the battery. When the BAT pin approaches the final float voltage (4.2V), the LTC4054 enters constant-voltage mode and the charge current begins to decrease.

➤ **Controlling charge current**

The charge current is programmed using a single resistor from the PROG pin to ground. The battery charge current is 1000 times the current out of the PROG pin. The program resistor and the charge current are calculated using the following equations:

$$R_{PROG} = \frac{1000V}{I_{CHG}}, I_{CHG} = \frac{1000V}{R_{PROG}}, \tag{A1}$$

The charge current out of the BAT pin can be determined at any time by monitoring the PROG pin voltage using the following equation:

$$I_{BAT} = \frac{V_{PROG}}{R_{PROG}} \cdot 1000 \qquad (A2)$$

➢ **Charge Termination**

A charge cycle is terminated when the charge current falls to 1/10th the programmed value after the final float voltage is reached. This condition is detected by using an internal, filtered comparator to monitor the PROG pin. When charging, transient loads on the BAT pin can cause the PROG pin to fall below 100mV for short periods of time before the DC charge current has dropped to 1/10th the programmed value. The 1ms filter time (t_{TERM}) on the termination comparator ensures that transient loads of this nature do not result in premature charge cycle termination. Once the average charge current drops below 1/10th the programmed value, the LTC4054 terminates the charge cycle and ceases to provide any current through the BAT pin. In this state, all loads on the BAT pin must be supplied by the battery.

➢ **Automatic Recharge**

Once the charge cycle is terminated, the LTC4054 continuously monitors the voltage on the BAT pin using a comparator with a 2ms filter time ($t_{RECHARGE}$). A charge cycle restarts when the battery voltage falls below 4.05V (which corresponds to approximately 80% to 90% battery capacity). This ensures that the battery is kept at or near a fully charged condition and eliminates the need for periodic charge cycle initiations. CHRG output enters a strong pulldown state during recharge cycles [205-207].

➢ **Power Dissipation**

The conditions that cause the LTC4054 to reduce charge current through thermal feedback can be approximated by considering the power dissipated in the IC. Nearly all of this power dissipation is generated by the internal MOSFET—this is calculated to be approximately:

$$P_D = (VC_C - V_{BAT}) \cdot I_{BAT} \qquad (A3)$$

where PD is the power dissipated, VCC is the input supply voltage, VBAT is the battery voltage and IBAT is the charge current. The approximate ambient temperature at which the thermal feedback begins to protect the IC is:

$$T_A = 120^\circ C - P_D \theta_{JA} \qquad (A4)$$

Because of the small size of the ThinSOT package, it is very important to use a good thermal PC board layout to maximize the available charge current. The thermal path for the heat generated by the IC is from the die to the copper lead frame, through the package leads, (especially the ground lead) to the PC board copper. The PC board copper is the heat sink. The footprint copper pads should be as wide as possible and expand out to larger copper areas to spread and dissipate the heat to the surrounding ambient.

Another power management chip used in this study was the Mobile chip HT4936s, N-Channel 22-V, SOP 16 Type. The HT4936S is a monolithic, mobile power management chip that uses advanced charge-and-discharge port sharing and synchronous rectification with low external components and excellent performance. Form a good 1A-in / 1A-out 4LEDs mobile power.

Features as:

➢ Built-in maximum 1A linear charging mode, charging current adjustable externally;

- Trickle / constant current / constant voltage three-stage charging, 4.20V / 4.35V optional support 0V battery charge;

- Built-in charging can automatically reduce the charging current according to temperature rise, 130 degrees began to decline, the minimum can be reduced to 0;

- Step-up using synchronous rectification circuit, the highest efficiency over 90%, low heat, fixed 5.1V output, do not need external Resistance setting

- Boost output current 1A (BTP = 3.6V);

- With constant power output function, a complete over current, short circuit protection, built-in temperature protection automatically stop temperature rise over-temperature;
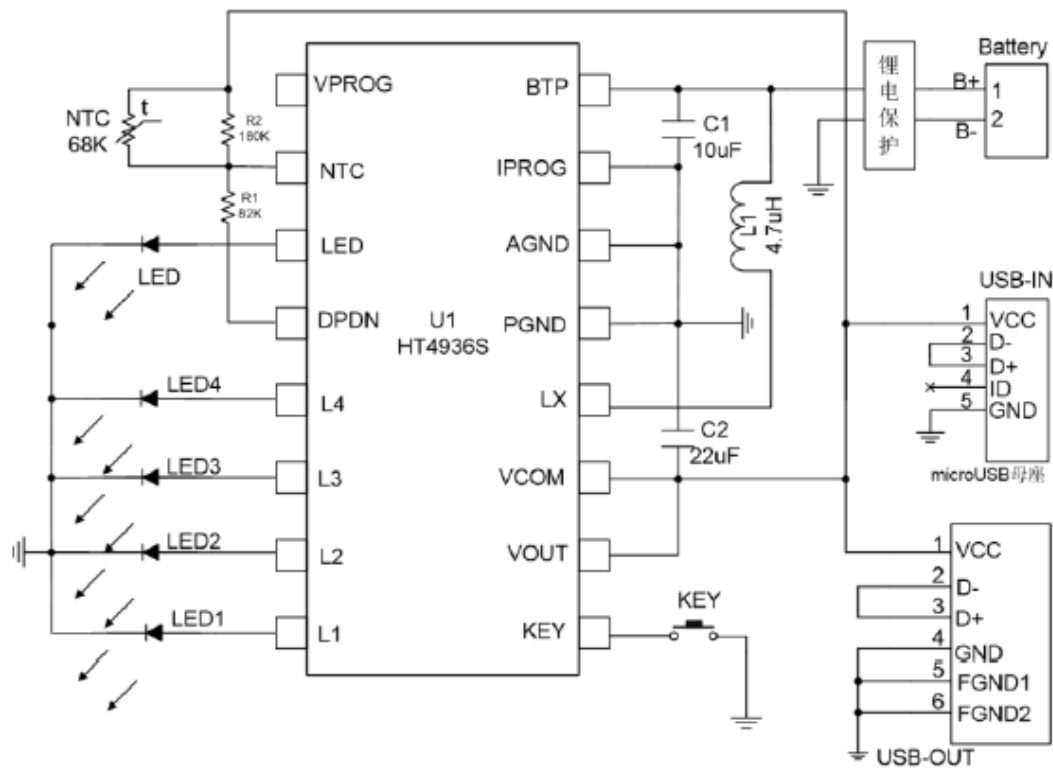
Fig. A.27. Block diagram of HT4936s IC mobile chip

The S-8254A Series is a protection IC for 3-serial- or 4-serial-cell lithium-ion / lithium polymer rechargeable batteries and includes a high-accuracy voltage detector and delay circuit. The S-8254A Series protects both 3-serial or 4-serial cells using the SEL pin for switching

Features as:

- High-accuracy voltage detection for each cell

- Three-level overcurrent protection

138

- Delay times for overcharge detection, over discharge detection and overcurrent detection 1 can be set by external capacitors (delay times for overcurrent detection 2 and 3 are fixed internally).

- Switchable between a 3-serial cell and 4-serial cell using the SEL pin

- Charge/discharge operation can be controlled via the control pins.

- Power-down function available

- High-withstand voltage Absolute maximum rating = 26 V

- Wide operating voltage range 2 V to 24 V

- Wide operating temperature range −40°C to + 85°C

- Low current consumption, During operation 30 μA max. (+25°C), During power-down 0.1 μA max. (+25°C)

- Lead-free, Sn100%, halogen-free
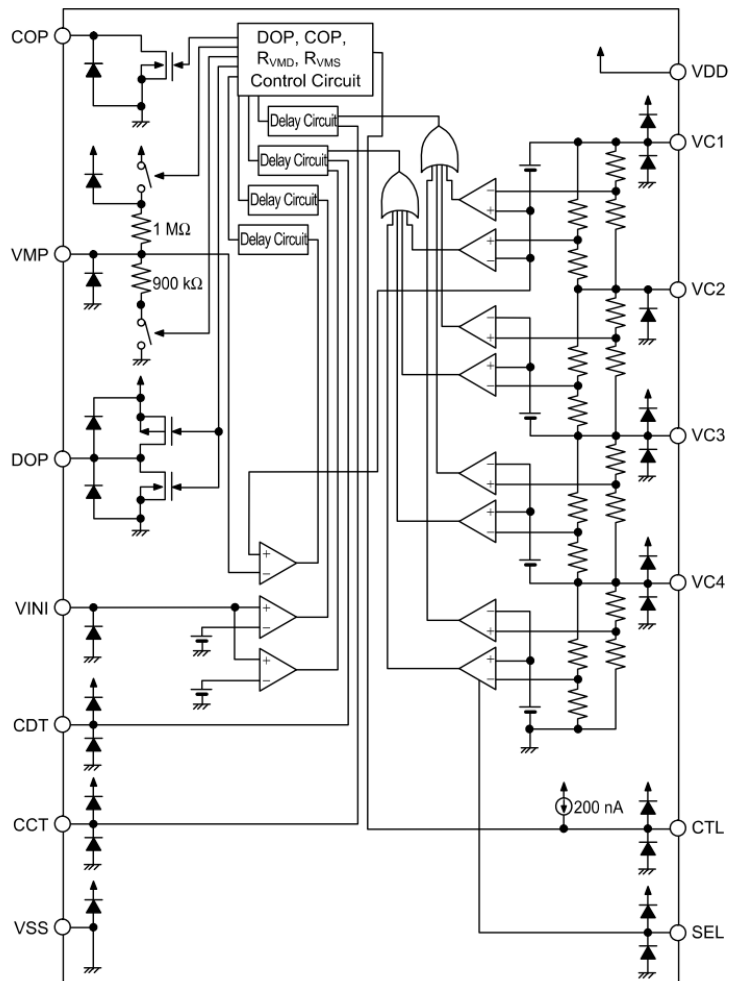
Fig. A.28. The block diagram of battery protection S8254A IC for 3 serial or 4 serial Cell pack
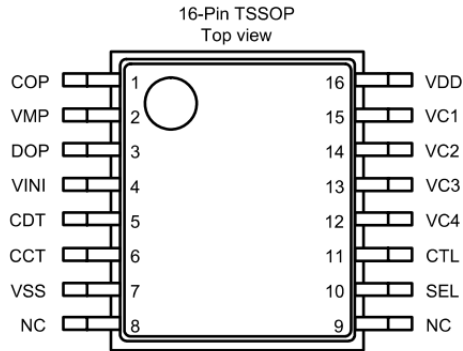
Fig. A.29. Pin configuration of S8254A IC

Table A.6. Absolute maximum ratings of S8254A IC chip

Pin No.	Symbol	Description
1	COP	FET gate connection pin for charge control (Nch open drain output)
2	VMP	Pin for voltage detection between VC1 and VMP (Pin for overcurrent 3 detection)
3	DOP	FET gate connection pin for discharge control FET (CMOS output)
4	VINI	Pin for voltage detection between VSS and VINI (Pin for overcurrent detection 1,2)
5	CDT	Capacitor connection pin for delay for overdischarge detection, delay for overcurrent detection 1
6	CCT	Capacitor connection pin for delay for overcharge current
7	VSS	Input pin for negative power supply, Connection pin for battery 4's negative voltage
8	NC [1]	No connection
9	NC [1]	No connection
10	SEL	Pin for switching 3-series or 4-series cell V$_{SS}$ level: 3-series cell, V$_{DD}$ level : 4-series cell
11	CTL	Control of charge FET and discharge FET
12	VC4	Connection pin for battery 3's negative voltage, Connection pin for battery 4's positive voltage
13	VC3	Connection pin for battery 2's negative voltage, Connection pin for battery 3's positive voltage
14	VC2	Connection pin for battery 1's negative voltage, Connection pin for battery 2's positive voltage
15	VC1	Connection pin for battery 1's positive voltage
16	VDD	Input pin for positive power supply, Connection pin for battery 1's positive voltage

[1]. The NC pin is electrically open. The NC pin can be connected to VDD or VSS.

8.3 Work under progress and future challenges

The author is working on the new circuit which will have better performance comparing to the improved MTC model, as well most of the experiments were conducted using the improved circuit. The new model v.5.1.0 has higher voltage operation comparing the old version v.4.2.1which was limited up to 9V, where the new one can operate up to 12.6V, which allows using the 3S4P BMS up to a nominal voltage of 12.6V. Also, the interface and menu are changed by giving more freedom in terms of battery selection, type of operation CCCV, pulse or arbitrary for different combinations of battery connections such as in series or parallel.

(a)   (b)
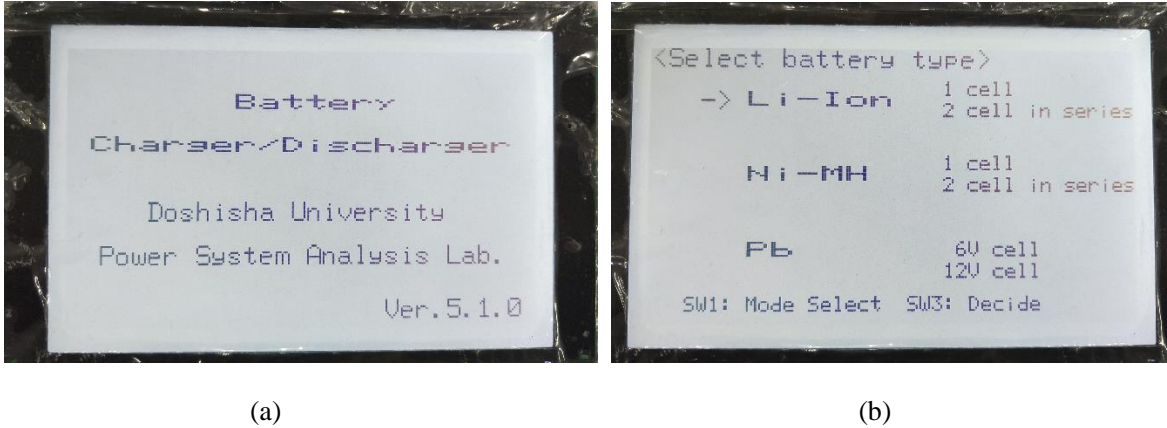
Fig. A.30. Interface of the improved MTC first page (a) and battery selection menu (b)

In fig A.31 is show the developed BMS which works for 4 cells connected in series, and up to 5 modules in parallel, it is connected with a small LED indicator that shows the actual SoC of the total pack. As well cell's information can be obtained in the small 5 pin socket selected in the red square in Fig A.31. The total current output of this BMS can reach up to 30A, which shows a great advantage for the scale-down simulator of the stationary battery storage system, and it can be used as a benchmark test.
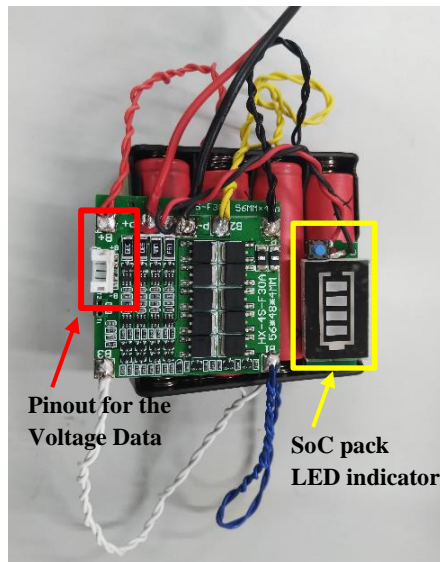
Fig. A.31. New proposed BMS 4S2P connection

In Fig. A.32 is shown the prototype for the ultimate proposed PCB circuit which can diagnosis the rechargeable batteries in real time or based on offline processing model. It shows very aggressive performance in term of computing power, IO variety and wide opportunity for updates regarding the software or even hardware upgrades as Wi-Fi remote controller, monitoring and data acquisition operation.
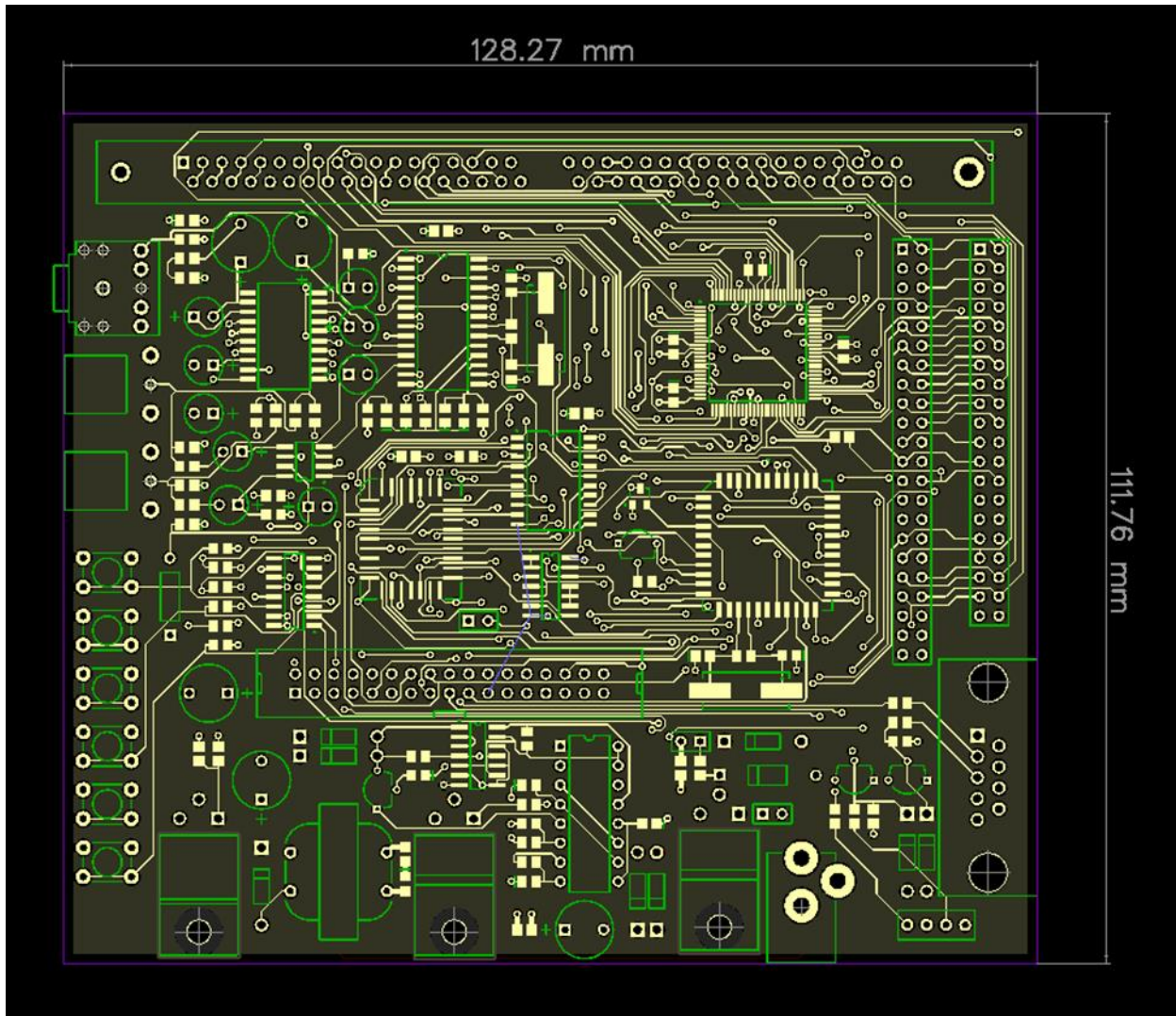
Fig. A.32. Proposed PCB for the diagnosis of rechargeable batteries, first phase of prototype.

References

1. M. Yoshio, R.J. Brodd, A. Kozawa, "Lithium-Ion Batteries, Science and Technologies", Springer Book (2009).

2. J. Newman, "Thermoelectric effects in electrochemical systems", Ind. Eng. Chem. Res.34(10), pp.3208-3216 (1995).

3. J. Warner, "The handbook of Lithium- Ion Battery Pack Design, Chemistry, Components, Types and Terminology," *Elsevier*, Vol.1, (2015).

4. B. Scrosati, J. Garche, W. Tillmetz, "Advances in Battery Technologies for Electric Vehicles," Woodhead Publishing Series in Energy: Number 80, *Elsevier*, (2015).

5. D. Pavlov, "Lead-Acid Batteries: Science and Technology: A Handbook of Lead-Acid Battery Technology and Its Influence on the Product," *Elsevier*, Vol.1, (2017).

6. Ch. Menictas, M. S. Kazacos, T. M. Lim, "Advances in Batteries for Medium-and Large-scale Energy Storage", Woodhead Publishing Series in Energy: Number 67, *Elsevier*, (2015).

7. M. Barak, "Electrochemical Power Sources, Primary and Secondary Batteries," *IEE Energy Series 1*, (1980).

8. K.S. Hariharan, P. Tagade, S. Ramachandran, "Mathematical Modelling of Lithium Batteries, from Electrochemical Models to State Estimator Algorithms" *Springer,* (2018).

9. Zh. Zhang, Sh. Sh. Zhang, "Rechargeable batteries, Materials, Technologies and New Trends," Green Energy and Technology, Springer International Publishing Switzerland (2015).

10. International Energy Agency (2014) Key world energy statistics.

11. Y-K. Sun, M-J. Lee, Cs. Yoon, "The role of AlF3 coatings in improving electrochemical cycling of Li-enriched nickel-manganese oxide electrodes for Li-ion batteries," *Adv. Matter*, Vol. 24 (9), pp.1192-1196, (2012),

12. N-S. Choi, Z. Chen, SA. Freunberger, "Challenges facing lithium batteries and electrical double-layer capacitors," *Angew Chem Int. Ed*, Vol. 51(40), pp. 9994-10024, (2012),

13. H. Yu, H. Zhou, "High-energy cathode materials (Li2MnO3-LiMO2) for lithium-ion batteries," *The Journal of Physical Chemistry Letters,* Vol. 4(8), pp.1268-1280, (2013),

14. A. Manthiram, "Materials challenges and opportunities of lithium ion batteries," *The Journal of Physical Chemistry Letters,* Vol. 2," pp.176-184, (2011)

15. Ar. Armstrong, M. Holzapfel, P. Novak, CS. Johnson, S-H. Kang, MM. Thackeray, PG. Bruce, "Demonstrating oxygen loss and associated structural reorganization in the lithium battery cathode Li[Ni$_{0.2}$Li$_{0.2}$Mn$_{0.6}$]O$_2$," *Journal of the American Chemical Society*, Vol. 128, pp.8694-8698, (2006).

16. D. Mohanty, S. Kalnaus, RA. Meisner, KJ. Rhodes, J. Li, EA. Payzant, DL. Wood Iii, C. Daniel, "Structural transformation of a lithium-rich Li1.2Co0.1Mn0.55Ni0.15O2 cathode during high

voltage cycling resolved by in situ X-ray diffraction," *Journal Power Sources*, Vol. 229, pp.239-248, (2013).

17. A. Nyten, A. Abouimrane, M. Armand, T. Gustafsson, JO. Thomas, "Electrochemical performance of Li2FeSiO4 as a new Li-battery cathode material," *Journal of Electrochemical Community*, *Elsevier,* Vol. 7, pp. 156-160, (2005).

18. MY. Saidi, J. Barker, H. Huang, JL. Swoyer, G. Adamson, "Electrochemical properties of lithium vanadium phosphate as a cathode material for lithium-ion batteries," *Journal of Electrochemical Solid-State Letters,* Vol. 5/A, pp.149-151, (2002).

19. T. Muraliganthm, A. Manthiram, "Understanding the shifts in the redox potentials of olivine LiM1-yMyPO4(M=Fe, Mn Co and Mg) solid solution cathodes," The Journal of Physical Chemistry C, Vol. 114, pp.15530-15540, (2010).

20. J. Liu, A. Manthiram, "Understanding the improved electrochemical performances of Fe-substituted 5V spinel cathode $LiMn_{1.5}Ni_{0.5}O_4$," *The Journal of Physical Chemistry C*, Vol. 113, pp. 15073-15079

21. J. Liu, A.M Manthiram, "Understanding the improvement in the electrochemical properties of surface modified 5 V $LiMn_{1.42}Co_{0.16}O_4$ spinel cathodes in lithium-ion cells," *The Chemistry of Materials,* Vol. 21, pp.1698-1707, (2009).

22. A. Wang, S. Kadam, H. Li, S. Shi, Y. Qi, "Review on modelling of the anode solid electrolyte interphase (SEI) for lithium-ion batteries," *NPJ Computational Materials*, Vol. 4, Article number 15, (2018).

23. C. X. Zu, H. Li, "Thermodynamic analysis on energy densities of batteries," *Energy & Environmental Science*, Vol. 4, pp. 2614-2624, (2011).

24. E. Buiel, JR. Dahn, "Li-insertion in hard carbon anode materials for Li-ion batteries," *Electrochimica Acta,* Vol.45, pp. 121-130, (1999).

25. Y-B. He, B. Li, M. Liu, C. Zhang, W. Lv, C. Yang, J. Li, H. Du, B. Zhang, Q-H. Yang, J-K. Kim, F. Kang, "Gassing in Li4Ti5O12-based batteries and its remedy," *Scientific Reports 2*, Article No. 913, (2012).

26. C-M. Park, J-H. Kim, H. Kim, H-J. Sohn, "Li-alloy based anode materials for Li secondary batteries," *Chemical Societies Reviews,* Vol.39, pp. 3115-3141, (2010).

27. Electric Power Research Institute, "DOE handbook of energy storage for transmission and distribution applications," (2003)

28. NS. Hochgatterer, MR. Scheweiger, S. Koller, PR. Raimann, T. Woehrle, C. Wurm, M. Winter, "Silicon/graphite composite electrodes for high-capacity anodes: influence of binder chemistry on cycling stability," *Electrochemical and Solid-State letters,* Vol.11, A pp.76-80, (2008).

29. A.N. Dey, "Film formation on lithium anode in propylene carbonate," *Journal of the Electrochemical Society*, Vol. 117, C248 (1970)

30. R. Fong, U. Von Sacken, J.R. Dahn, "Studies of lithium intercalation into carbons using nonaqueous electrochemical cells," *Journal of the Electrochemical Society,* Vol.137, pp. 2009-2013, (1990).

31. E. Peled, "The electrochemical behavior of alkali and alkaline earth metals in nonaqueous battery systems-the solid electrolyte interphase model," *Journal of the Electrochemical Society,* Vol.126, pp. 2047-2051, (1979).

32. G. Nazri, R.H Muller, "Composition of surface layers on Li electrodes in PC, $LiClO_4$ of very low water content," *Journal of the Electrochemical Society,* Vol. 132, pp. 2050-2054, (1985).

33. D. Aurbach, M.L. Daroux, P.W. Faguy, E. Yeager, "Identification of surface films formed on lithium in propylene carbonate solutions," *Journal of the Electrochemical Society,* Vol. 134, pp. 1611-1620, (1987).

34. E. Peled, D. Golodnitsky, G. Arder, "Advanced model for solid electrolyte interphase electrodes in liquid and polymer electrolytes," *Journal of the Electrochemical Society*, Vol.144, L208-L210, (1997).

35. D. Aurbach, "New insights into the interactions between electrode materials and electrolyte solutions for advanced nonaqueous batteries," *Journal of Power Sources,* Vol.81, pp. 95-111, (1999).

36. V.Cresce, a. Russel, S.M. Baker, D.R. Gaskell, K.J. & K. Xu, "In situ and quantitative characterization of solid electrolyte interphases," *Nano Letters*, Vol.14, pp. 1405-1412, (2014).

37. X.R. Zhang, J.K. Pugh & P.N. Ross, "Computation of thermodynamic oxidation potentials of organic solvents using density functional theory," *Journal of the Electrochemical Society*, Vol. 147, E183-E188, (2001).

38. T. Li, P.B. Balbuena, "Theoretical studies of the reduction of ethylene carbonate," *Chemical Physics Letters,* Vol. 317, pp. 421-429, (2000).

39. Y.X. Wang, S. Nakamura, M. Ue, P.B Balbuena, "Theoretical studies to understand surface chemistry on carbon anodes for lithium-ion batteries: reduction mechanisms of ethylene carbonate," *Journal of the American Chemical Society*, Vol. 123, pp.11708-11718, 92001).

40. J. Christensen, J. Newman, "A mathematical model for the lithium-ion negative electrode solid electrolyte interphase," *Journal of the Electrochemical Society,* Vol. 151, A1977-A1988, (2004).

41. K. Xu, A. Von Cresce, U. Lee, "Differentiating contributions to "ion transfer" barrier from interphasial resistance and Li^+ desolvation at electrolyte/graphite interface," *Langmuir,* Vol.26, pp. 11538-11543, (2010)

42. S.Q. Shi, "Direct calculation of Li-ion, transport in the solid electrolyte interphase," *Journal of the American Chemical Society*, Vol. 134, pp. 15476-15487, (2012).

43. J. Zheng, "3D visualization of inhomogeneous multi-layered structure and Young's modulus of the solid electrolyte interphase (SEI) on silicon anodes for lithium ion batteries," *Physical Chemistry Chemical Physics*, Vol. 16, pp. 13229-13238, (2014).

44. A.C. Kozen, "Next-generation lithium metal anode engineering via atomic layer deposition," *ACS Nano*, Vol. 9, pp. 3911-3915, (2011).

45. Y. Li, K. Leung, Y. Qi, "Computational exploration of the Li-electrode/electrolyte interface in the presence of a nanometer thick solid-electrolyte interphase layer," *Accounts of Chemical Research*, Vol.49, pp. 2363-2370, (2016).

46. Y.S. Meng, Arroyo-de Dompablo, E. M, "First principles computational materials design for energy storage materials in lithium-ion batteries," *Energy & Environmental Science*, Vol. 2, pp. 589-609, (2009).

47. C. Ouyang, L. Chen, "Physics towards next generation Li secondary batteries materials: a short review from computational materials design perspective," *Sci. China Phys. Mech,* Vol. 56, pp. 2278-2292, (2013).

48. A.A. Franco, "A multiscale modelling and numerical simulation of rechargeable lithium-ion batteries: concepts, methods and challenges," *RSC Advances*, Vol. 3, pp. 13027-13058, (2013).

49. V.P. Reddy, M. Blanco, R. Bugga, "Boron-based anion receptors in lithium-ion and metal -air batteries," *Journal of Power Sources,* Vol. 247, pp. 813-820, (2014).

50. S. Shi, "Multi-scale computation methods: their applications in lithium-ion battery research and development," *Chin. Phys,* Vol. B 25, (2016)

51. D. Grazioli, M. Magri, A. Salvadori, "Computational modeling of Li-ion batteries," *Comput. Mech,* Vol. 58, pp. 889–909 (2016).

52. A. Urban, D.H. Seo, G. Ceder, "Computational understanding of Li-ion batteries," *NPJ Comput. Mater*, Vol.2, (2016).

53. D. E. Galvez-Aranda, V. Ponce, J. M. Seminario, "Molecular dynamics simulations of the first charge of a Li-ion—Si-anode nanobattery," *Journal of Molecular Modelling*, Vol. 23, (2017).

54. P.B. Balbuena, "Review on Electrochemical Storage Materials and Technology," AIP Conference Proceedings, *American Institute of Physics,* Vol. 1597, pp. 82-97, (2014).

55. G. Ramos-Sanchez, "computational studies of interfacial reactions at anode materials: initial stages of the solid-electrolyte-interphase layer formation," *Journal of Electrochemical Energy Conversion and Storage,* Vol.13, (2016).

56. R. J. Blint, "Binding of ether and carbonyl oxygens to lithium ion," *Journal of the Electrochemical Society*, Vol. 142, pp. 696–702, (1995).

57. T. Li, P. B. Balbuena, "Theoretical studies of the reduction of ethylene carbonate," *Chemical Physics Letters*, Vol. 317, pp. 421–429, (2000).

58. D. Aurbach, M.D. Levi, E. Levi, A. Schechter, "Failure and stabilization mechanisms of graphite electrodes," *The Journal of Physical Chemistry B*, Vol. 101, pp. 2195–2206, (1997).

59. Y. X. Wang, S. Nakamura, M. Ue, P.B. Balbuena, "Theoretical studies to understand surface chemistry on carbon anodes for lithium-ion batteries: reduction mechanisms of ethylene carbonate," *Journal of the American Chemical Society*, Vol. 123, pp. 11708–11718, (2001).

60. X. R. Zhang, J. K. Pugh, P.N. Ross, "Computation of thermodynamic oxidation potentials of organic solvents using density functional theory," *Journal of the Electrochemical Society,* Vol. 148, E183–E188, (2001).

61. J. Yu, P.B. Balbuena, J. Budzien, K. Leung, "Hybrid DFT functional-based static and molecular dynamics studies of excess electron in liquid ethylene carbonate," *Journal of the Electrochemical Society,* Vol. 158, A400–A410, (2011).

62. M. Xu, "Investigation and application of lithium difluoro(oxalate)borate (LiDFOB) as additive to improve the thermal stability of electrolyte for lithium-ion batteries," *Journal of Power Sources*, Vol. 196, pp. 6794–6801, (2011).

63. K. Leung, J.L. Budzien, "Ab initio molecular dynamics simulations of the initial stages of solid-electrolyte interphase formation on lithium ion battery graphitic anodes," *Physical Chemistry Chemical Physics,* Vol. 12, pp. 6583–6586, (2010).

64. D. Bedrov, G.D. Smith, A.C.T. Van Duin, "Reactions of singly-reduced ethylene carbonate in lithium battery electrolytes: a molecular dynamics simulation study using the ReaxFF," *Journal of Physical Chemistry A*. Vol. 116, pp. 2978–2985, (2012).

65. J. M. Martinez de la Hoz, K. Leung, P. B. Balbuena, "Reduction mechanisms of ethylene carbonate on Si anodes of lithium-ion batteries: effects of degree of lithiation and nature of exposed surface," *ACS Applied Materials & Interfaces,* Vol. 5, pp. 13457–13465, (2013).

66. K. Leung, "Two-electron reduction of ethylene carbonate: a quantum chemistry re-examination of mechanisms," *Chemical Physics Letters*, pp. 568-569, (2013).

67. K. Leung, C.M. Tenney, "Toward first principles prediction of voltage dependences of electrolyte/electrolyte interfacial processes in lithium ion batteries," *Journal of Physical Chemistry C*. Vol. 117, pp. 24224–24235, (2013).

68. Y. Okamoto, "Ab initio calculations of thermal decomposition mechanism of LiPF6-based electrolytes for lithium-ion batteries," *Journal of the Electrochemical Society*, Vol. 160, A404–A409, (2013).

69. K. Leung, "Predicting the voltage dependence of interfacial electrochemical processes at lithium-intercalated graphite edge planes," *Physical Chemistry Chemical Physics,* Vol. 17, pp. 1637–1643, (2015).

70. M.M. Islam, A.C.T. Van Duin, "Reductive decomposition reactions of ethylene carbonate by explicit electron transfer from lithium: an eReaxFF molecular dynamics study," *The Journal of Physical Chemistry A*, Vol. 120, pp. 27128–27134, (2016).

71. Y. Jin, "Identifying the structural basis for the increased stability of the solid electrolyte interphase formed on silicon with the additive fluoroethylene carbonate," *Journal of the American Chemical Society*, Vol. 139, pp. 14992–15004, (2017).

72. M. Onuki, 'Identification of the source of evolved gas in Li-ion batteries using (13)C-labeled solvents," *Journal of the Electrochemical Society*, Vol. 155, A794–A797, (2008).

73. I. A. Shkrob, Y. Zhu, T.W. Marin, D. Abraham, "Reduction of carbonate electrolytes and the formation of solid-electrolyte interface (SEI) in lithium-ion batteries. 1. Spectroscopic observations of radical intermediates generated in one-electron reduction of carbonates," *The Journal of Physical Chemistry C.* Vol. 117, pp. 19255–19269, (2013).

74. K. Tasaki, "Solvent decompositions and physical properties of decomposition compounds in Li-ion battery electrolytes studied by DFT calculations and molecular dynamics simulations," *The Journal of Physical Chemistry B*, Vol. 109, pp. 2920–2933, (2005).

75. O. Borodin, G.D. Smith, "Quantum chemistry and molecular dynamics simulation study of dimethyl carbonate: ethylene carbonate electrolytes doped with LiPF6," *The Journal of Physical Chemistry B,* Vol. 113, pp.1763–1776, (2009).

76. A. V. W. Cresce, O. Borodin, K. Xu, "Correlating Li+ solvation sheath structure with interphasial chemistry on graphite," *The Journal of Physical Chemistry C*, Vol. 116, pp. 26111–26117, (2012).

77. P. Ganesh, P. R. C. Kent, D.-E. Jiang, "Solid-electrolyte interphase formation and electrolyte reduction at Li-ion battery graphite anodes: insights from first-principles molecular dynamics," *The Journal of Physical Chemistry C,* Vol. 116, pp. 24476–24481, (2012).

78. L. E. Camacho-Forero, T.W. Smith, P.B. Balbuena, "Effects of high and low salt concentration in electrolytes at lithium-metal anode surfaces," *The Journal of Physical Chemistry C,* Vol.121, pp. 182–194, (2017).

79. M. Ebadi, D. Brandell, C.M. Araujo, "Electrolyte decomposition on Li-metal surfaces from first-principles theory," *The Journal of Physical Chemistry,* Vol. 145, (2016).

80. F. A. Soto, J.M. Martinez de la Hoz, J.M. Seminario, P.B. Balbuena, "Modeling solid-electrolyte interfacial phenomena in silicon anodes," *Current Opinion in Chemical Engineering, Elsevier.* Vol. 13, pp. 179–185, (2016).

81. Y. Ma, P.B. Balbuena, "DFT study of reduction mechanisms of ethylene carbonate and fluoroethylene carbonate on Li+-adsorbed Si clusters," *Journal of the Electrochemical Society,* Vol. 161, pp. E3097–E3109, (2014).

82. A. Moradabadi, M. Bakhtiari, P. Kaghazchi, "Effect of anode composition on solid electrolyte interphase formation," *Electrochimica Acta*, Vol. 213, pp. 8–13, (2016).

83. L. E. Camacho-Forero, T.W. Smith, S. Bertolini, P.B. Balbuena, "Reactivity at the lithium–metal anode surface of lithium–sulfur batteries," *The Journal of Physical Chemistry C*, Vol. 119, pp. 26828–26839, (2015).

84. R.N. Methekar, P.W.C. Northrop, K. Chen, K., R.D. Braatz, V.R. Subramanian, "Kinetic Monte Carlo simulation of surface heterogeneity in graphite anodes for lithium-ion batteries: passive layer formation," *Journal of the Electrochemical Society,* Vol. 158, A363–A370, (2011).

85. K. Ushirogata, K. Sodeyama, Z. Futera, Y. Tateyama, Y. Okuno, "Near-shore aggregation mechanism of electrolyte decomposition products to explain solid electrolyte interphase formation," *Journal of the Electrochemical Society,* Vol. 162, A2670–A2678, (2015).

86. N. Takenaka, Y. Suzuki, H. Sakai, M. Nagaoka, "On electrolyte-dependent formation of solid electrolyte interphase film in lithium-ion batteries: strong sensitivity to small structural difference of electrolyte molecules," *The Journal of Physical Chemistry C*, Vol. 118, pp. 10874–10882, (2014).

87. D. Pavlov, "Lead-acid Batteries: Science and Technology," A handbook of Lead-Acid Battery Technology and its Influence on the Product, 1st Edition ELSEVIER, (2011).

88. P. Weicker, "A Systems Approach to Lithium-ion Battery Management," *Artech House*, (2014).

89. A. Kwade, J. Diekmann, "Recycling of Lithium-Ion Batteries," *Book Springer,* (2018).

90. Batteries and Fuel Cells, Chemistry Libre Texts, 20.7, MERLOT, UC Davis Library. Updated June (2019)

91. Sh-L. Lin, K-L. Huang, I-CH. Wang, I-Ch. Chou, "Characterization of Spent Nickel-Metal Hybrid Batteries and a Preliminary Economic Evaluation of the Recovery Processes,"

92. R.M. Dell, P.T. Moseley, D.A.J. Rand, "Towards Sustainable Road Transport," *Academic Press,* (2014).

93. N.P.H. Duraman, K.L. Lim, S.L.I. Chan, "Advances in Batteries for Medium and Large-Scale Energy Storage," *Woodhead Publishing Series in Energy, Science Direct,* pp.563-586, (2015).

94. K. Schmidt-Rohr, "How batteries Store and Release Energy: Explaining Basic Electrochemistry," *Journal of Chemical Education,* Vol. 95(10), pp. 1801-1810, (2018).

95. M. Wentzl, In: J. Garche (Editor-in-chief), "Encyclopedia of Electrochemical Power Sources," Elsevier, Vol. 1, pp. 401, (2009).

96. U. Ko¨hler, In: J. Garche (Editor-in-chief), "Encyclopedia of Electrochemical Power Sources," Elsevier, Vol. 1, pp. 271, (2009).

97. D.J. Lvingstone, J.M. Walker, "Artificial Neural Networks, Methods and Applications," Springer, (2008).

98. Neural Network Toolbox in MATLAB, Manual Book for advance user, (2018).

99. F. Rosenblatt, "Principles of Neurodynamics*", Spartan Press*, Washington, D.C., (1961).

100. M. Mohri, A. Rostamizadeh, A. Talwalker, "Foundations of Machine Learning," Massachusetts Institute of Technology, (2012).

101. V. Otterlo, M. Wiering, "Reinforcement Learning and Markov Decision Processes", Vol.12, pp.3-42, (2012).

102. M. Bezha, N. Nagaoka, "Online learning ANN model for SoC estimation of the Lithium-Ion battery in case of small amount of data for practical applications," *IEEE Proceedings, 10th International Conference on Power Electronics, ICPE 2019 ECCE-ASIA*, Busan Korea, pp. 688-692, (2019).

103. G. Hinton, T.J. Sejnowski, "Unsupervised Learning", MIT Press, 1999.

104. D.P. Bertsekas, J.N. Tsitsiklis, "Neuro-Dynamic Programming," Athena Scientific, (1996).

105. D.P. Bertsekas, "Dynamic Programming and Optimal Control: Approximate Dynamic Programming," Vol. II", Athena Scientific, (2012).

106. V. Otterlo, M. Wiering, "Reinforcement Learning and Markov Decision Processes," Vol.12, pp. 3-42, (2012).

107. J. Devillers, "Prediction of toxicity of organophosphorus insecticides against the midge, Chironomus riparius, via a QSAR neural network model integrating environmental variables," *Toxicology mechanisms and Methods*, Vol. 10, pp. 69–79, (2010).

108. HM. Cartwright, "Investigation of structure-biodegradability relationships in polychlorinated using self-organizing maps," *Neural Comput. & Applic.,* Vol.11, pp. 30-36, (2002)

109. V. Zitko, "Prediction of the biodegradability of organic chemicals by an artificial neural network," *Chemosphere,* Vol. 23, pp.305–312, (1991).

110. B. Fritzke, "Growing grid-a self-organizing network with constant neighborhood range and adaption strength," *Neural Processing Letters,* Vol. 2, pp. 9-13, (1995).

111. J. Blackmore, R. Miikkulainen, "Visualizing high-dimensional structure with the incremental grid growing network," In: Proc. *XIIth Internat. conf. on machine learning*. Morgan Kaufmann, San Franciso, pp.55-63, (1995).

112. M. Martinetz, KJ. Schulten (1991) A neural gas network learns topologies. In: Kohonen KMT, Simula O, Kangas, *Journal (eds) Artificial neural networks.* North Holland, Amsterdam, pp. 397-402, pp. 397–402, (1991).

113. A.J. Walker, SS. Cross, RF. Harrison, "Visualization of biomedical datasets by use of growing cell structure networks: a novel diagnostic classification technique," *The Lancet,* Vol. 354, pp. 1518-1521, (1999).

114. JWH. Wong, HM.Cartwright, "Deterministic projection by growing cell structure networks for visualization of high-dimensionality datasets," *J. Biomed Inform*, Vol. 38, pp.322–330, (2005)

115. Z. Wu, G. Yen, "A SOM projection technique with the growing structure for visualizing high-dimensional data," *Int J Neural Systems,* Vol. 13, pp. 353–365, (2003)

116. AM. Fonseca, JL. Biscaya, J. Aires-de-Sousa, "Lobo AM (2006) Geographical classification of crude oils by Kohonen self-organizing maps," *Analytica Chimica Acto,* Vol.556, pp. 374–382, (2006).

117. HM. Cartwright Neural network analysis of the degradation of oil spills, (In press). HM

118. X. Zhang, H. Li, A. Hou, J. Havel, "Artificial neural networks based on principal component analysis input selection for quantification in overlapped capillary electrophoresis peaks," *Chemometric Intell Lab Syst*, Vol. 82, pp.165–175, (2006).

119. IV. Tetko, Ai. Luik, GI. Poda, "Applications of neural networks in structure-activity relationship of a small number of molecules," *J Med Chem* Vol.36, pp.811–814, (1993).

120. Havel J, Pena-Mendez EM, Rojas-Hernandez A, Doucet J-P, Panaye A (1998) Neural networks for optimization of high-performance capillary zone electrophoresis methods: a new method using a combination of experimental design and artificial neural networks," *J. Chromatography A.* Vol.793, pp. 317-329, (1998).

121. LL. Yannis, "Artificial neural networks in liquid chromatography: efficient and improved quantitative structure-retention relationship models," *Journal of Chromatography A.* Vol. 904, pp.119–129, (2000).

122. P. Polaskova, G. Bocaz, H. Li, J. Havel, "Evaluation of calibration data in capillary electrophoresis using artificial neural networks to increase precision of analysis. *J. Chromatography A.* Vol. 979, pp. 59-67, (2002).

123. RC. Santana, Do PT, M. Santikunaporn, WE. Alvarez, JD. Taylor, EL. Sughrue, DE. Resasco, "Evaluation of different reaction strategies for the improvement of cetane number in diesel fuels," *Fuel,* Vol. 85, pp. 643-656, (2006).

124. D. Billingsley, "Octane prediction of gasoline blends using neural nets," *Proc. NPRA Comput. Conf.* (1995).

125. Basu B, Kapur GS, Sarpal AS, Meusinger R, "A neural network approach to the prediction of cetane number of diesel fuels using nuclear magnetic resonance (NMR) spectroscopy," *Energy and Fuels,* Vol.6, pp.1570–1575, (2003).

126. T. Nilsson, MR. Bassani, TO. Larsen, L. Montanarella, "Classification of species of the genus Penicillium by Curie Point pyrolysis mass spectrometry followed by multivariate analysis and artificial neural networks," *J Mass Spectrom*, Vol. 31, pp.1422–1428, (1996).

127. MS. Fernandez-Pachon, D. Villano, AM. Troncoso, MC. Garcia-Parilla, "Determination of the phenolic composition of sherry and table white wines by liquid chromatography and their relation with antioxidant activity," *Anal Chim Acta,* Vol. 563, pp.101–108, (2005).

128. G. Cao, E. Sofic, RL. Prior, "Antioxidant and prooxidant behavior of flavonoids: structure activity relationships," *Free Radic Biol Med*, Vol.22, pp. 749–760, (1997).

129. CGM. Heijnene, GRMM. Haenen, FAA. Van Acker, W. Van Der Vijgh, A. Bast, "Flavonoids as peroxynitrite scavengers: the role of the hydroxyl groups," *Toxicol in Vitro.* Vol.15, pp.3–6, (2001).

130. M.A. Hanna, M.S.H. Lipu, A. Hussain, A. Mohamed, "A review of lithium–ion battery state of charge estimation and management system in electric vehicle applications: challenges and recommendations," *Journal Renew. Sustain. Energy Rev.* Vol.78, pp. 834-854, (2017).

131. M. Yoshio, R. J. Brodd, A. Kozawa, "Lithium-Ion Batteries, Science and Technologies," *Book Springer*, (2009).

132. L. An, "Recycling of Spent Lithium-Ion Batteries," *Book Springer,* (2019).

133. J. Warner, "The handbook of Lithium-Ion Battery Pack Design, Chemistry, Components, Types and Terminology," *Elsevier*, (2015).

134. Y. Zheng, M. Ouyang, X. Han, L. Lu, J. Li, "Investigating the error sources of the online state of charge estimation methods for lithium-ion batteries in electric vehicles," *Journal of Power Sources X*, Vol. 377, pp. 161–188, (2018).

135. C. Zhang, K. Li, L. Pei, C. Zhu, "An integrated approach for real-time model-based state-of-charge estimation of lithium-ion batteries," *Journal of Power Sources*, Vol. 283, pp.24–36, (2015).

136. Wang. Q, Jiang. B, Li. B, Yan. Y, "A critical review of thermal management models and solutions of lithium- ion batteries for the development of pure electric vehicles". *Renew. Sustain. Energy Rev.*, Vol. 64, pp.106-128, (2016).

137. Thermal Dynamics in Lithium-Ion Batteries. IFAC Proc. Vol. 43, 198–203, (2010).

138. M. Bezha, R. Gondo, N. Nagaoka, "An Estimation Model with Generalization Characteristics for the Internal Impedance of the Rechargeable Batteries by Means of Dual ANN Model," *Journal of Energies MDPI*, Vol. 12, Issue 5, pp. 948-959, March 2019

139. M. Bezha and N. Nagaoka, "An ANN Model for Estimating Internal Impedance of Lithium-Ion Battery Cell for Industrial Application," IEEE *ICEMS 2018*, pp. 2105-2110, JEJU, S. Korea, (Oct. 2018).

140. N. Nagaoka and A. Ametani, "An Estimation Method of Li-Ion Battery Impedance Using Z-Transform," *2012 IEEE 13th Workshop on Control and Modeling for Power Electronics (COMPEL)*, June (2012).

141. T. Hirai, A. Ohnishi, N. Nagaoka, N. Mori, A. Ametani and S. Umeda: "Automatic Equivalent-Circuit Estimation System for Lithium-Ion Battery," *43rd International University Power Engineering Conference*, Padova, Sep. (2008).

142. T. Noro, N. Narita, T. Higo, and N. Nagaoka, "A Deterioration Diagnosis Method for Lithium-Ion Battery Based on Phase characteristics of Internal Impedance," *Proc. University Power Engineering Conference 50th International*, Staffordshire, Sep. (2015).

143. C. Fleischer, W. Waag, H.-M. Heyn, D.U. Sauer, "On-line adaptive battery impedance parameter and state estimation considering physical principles in reduced order equivalent circuit battery models: Part 1. Requirements, critical review of methods and modelling," *Journal of Power Sources,* Vol. 260, pp.276-291, (2014).

144. M. Bezha, R. Gondo, N. Nagaoka, "A Dual ANN Model for Estimation of Internal Impedance of Rechargeable Cell Batter," *53rd International Universities Power Engineering, Conferences-UPEC 2018,* Glasgow, Scotland, UK.

145. N. Nagaoka, "A numerical model of Lithium-ion battery for a life estimation", *48th International University Power Engineering Conference*, Dublin, 2013

146. J. J. G. De la Rosa, I. Lloret, C. G. Puntonet, and J. M. G´orriz, "Higher-order statistics to detect and characterize termite emissions," *Journal of Electronics Letters*, Vol. 40, No. 20, pp. 1316–1317, Ultrasonic, (September 2004).

147. M. Bezha, N. Nagaoka, "Online learning ANN model for SoC estimation of the Lithium-ion battery in case of small amount of data for practical applications", *ICPE 2019, IEEE explore proceedings*, Busan, S. Korea, May 2019.

148. M. Opper, "Online versus Offline Learning from Random Examples: General Results", University of Wurzburg, Germany.

149. R. Zhang, B. Xiz, B. Li, L. Cao, Y. Lai, W. Zheng, H. Wang, W. Wang. "State of the Art of Lithium-Ion Battery SoC Estimation for Electrical Vehicles", *Journal of Energies*, 2018.

150. M. Bezha and N. Nagaoka, "An ANN for Estimation of Power Consumption of EV/HEV for Real Time Battery Diagnosis," *IEEJ SAMCON2018*, Article No.TT2-2, Tokyo, Japan, March (2018).

151. M. Bezha and N. Nagaoka, "Predicting Voltage Characteristic of Charging Model for Li-Ion Battery with   ANN for Real Time Diagnosis," *IEEE IPEC 2018*, Niigata, Japan, May (2018).

152. C. L. Nikias and A. P. Petropulu, "Higher-Order Spectra Analysis. A Non- Linear Signal Processing" Framework. *Englewood Cliffs, NJ, Prentice- Hall*, 1993.

153. C. L. Nikias and J. M. Mendel, "Signal processing with higher-order spectra," *IEEE Signal Processing Magazine,* pp. 10–37, 1993.

154. J. M. Mendel, "Tutorial on higher-order statistics (spectra) in signal processing and system theory: Theoretical results and some applications," Proceedings of the IEEE, vol. 79, no. 3, pp. 278–305, 1991.

155. I.V. Snihir, W.J.J. Rey, E.A. Verbitsky, A. Ayeb, P.H.L. Notten, "Battery open-circuit voltage estimation by a method of statistical analysis", *Journal of Power Sources*, Vol .159, pp.1484-1487, (2006)

156. R. Gondo, Sh. Ito, K. Iifuru, N. Nagaoka, "Development of multi-type secondary-battery charger/discharger by arbitrary current waveform," UPEC2017*, 52nd International University Power Engineering Conference*, Greece, 2017.

157. S. Nagamitsu, R. Gondo, N. Nagaoka, A.A. Al- Karakchi, G. Putrus, Y.Wang, "A Novel Battery Diagnostic Method for Smart Electric Vehicle Charger," UPEC2018, *53rd International University Power Engineering Conference*, IEEE Proceedings, Glasgow, Scotland, UK, (2018).

158. Wang. Q, Jiang. B, Li. B, Yan. Y, "A critical review of thermal management models and solutions of lithium- ion batteries for the development of pure electric vehicles". *Renew. Sustain. Energy Rev*. 64, pp.106-128, (2016).

159. Thermal Dynamics in Lithium-Ion Batteries. *IFAC Proc.* Vol. 43, 198–203, (2010).

160. D. Andrea, "Battery Management Systems for Large Lithium Ion Battery Packs," *Artech House Book Boston/London,* (2010).

161. C. Lin, "Comparison of current input equivalent circuit models of electrical vehicle battery," *Chin. J. Mech. Eng.* 41, 76–81, (2005).

162. He, H.; Xiong, R.; Fan, "J. Evaluation of lithium-ion battery equivalent circuit models for state of charge estimation by an experimental approach," *Journal of Energies,* Vol.4, 582–598, (2011).

163. Schmidt, A.P.; Bitzer, M.; Imre, Á.W.; Guzzella, L. "Lumped Parameter Modeling of Electrochemical and Thermal Dynamics in Lithiun-Ion Bateries," IFAC Proceedings Volumes, Vol. 43, Issue 7, pp. 198-203, July 2010.

164. D.P. Bertsekas and J.N. Tsitsiklis, "Neuro-Dynamic Programming," *Athena Scientific*, (1996).

165. D.P. Bertsekas, "Dynamic Programming and Optimal Control: Approximate Dynamic Programming. Vol.II," *Athena Scientific.*

166. V. Otterlo, M. Wiering, "Reinforcement Learning and Markov Decision Processes," Vol.12, pp.3-42, (2012).

167. M. Mohri, A. Rostamizadeh, A. Talwalkar, "Foundations of Machine Learning," *The MIT Press*, (2012).

168. G. Hinton, T.J. Sejnowski, "Unsupervised Learning," *MIT Press*, (1999).

169. A. A. A. Al-karakchi, G. Lacey, and G. Putrus, "A method of electric vehicle charging to improve battery life," *50th International University Power Engineering Conference*, (2015).

170. A. A. A. Al-karakchi, G. Putrus, R. Das and R. Binns, "Smart EV Charging Profiles to Extend Battery life," *52nd International University Power Engineering Conference,* Heraklion, Aug. (2017).

171. N. Kawakami, Y. Iijima, "Overview of battery energy storage systems for stabilization of renewable energy in Japan," *2012 International Conference on Renewable Energy Research and Applications* (ICRERA), Nagakasi, Japan, (Mar. 2013)

172. F. Mohamad, J. The, Ch. M. Lai, L. R. Chen, "Development of Energy Storage Systems for Power Network Reliabiliy: A Review," *Journal of Energies*, MDPI, (Aug. 2018).

173. Electric Power System Standardized Model Research Expert Committee: "Standardized model of electric power system," *Technical Report of the Institute of Electrical Engineers of Japan*, No. 754, (1999).

174. M. Bezha and N. Nagaoka, "Improved ANN for Estimation of Power Consumption of EV for Real Time Battery Diagnosis", *IEEJ Journal of Industry Applications, Special Issue Section D*, Vol. 139, No.5, Japan (2019).

175. J.B. Goodenough, Y. Kim, "Challenges for rechargeable Li batteries," *Chem. Mater.* 22, pp. 587–603, (2014).

176. G. Girishkumar, B. Mccloskey, A.C. Luntz, S. Swanson, W. Wilcke, "Lithium–air battery: Promise and challenges," *Journal of Physical Chemistry Letters,* Vol. 1, pp. 2193–2203, (2010).

177. M. Dubbary, B.Y. Liaw, "Identity capacity fading mechanism in a commercial LiFePO4 cell," *Journal of Power sources*, Vol. 194, pp. 541-549, (2009).

178. J. Wang, P. Liu, J. Hicks-Garner, "Cycle-life model for graphite-LiFePo4 cells," *Journal of Power Sources*, Vol. 196, pp.3942-3948, (2011).

179. M. Swierczynski, D.-I, Stroe, A.-I, Stan, et al. "Lifetime estimation of the nanophosphate LiFePO4/C battery chemistry used in fully electric vehicles", *IEEE Transactions on Industry Applications,* Vol. 51, pp.3453-3461, (2015).

180. E.V. Thomas, H.L. Case, D.H. Doughty, et al "Accelerated power degradation of Li-Ion cells," *Journal of Power Sources*, Vol. 124, pp.254-260, (2003).

181. K. Takano, K. Nozaki, Y. Saito, A. Negishi, K. Kato, Y. Yamaguchi, "Simulation study of electrical dynamic characteristics of Lithium-Ion battery," *Journal Power Sources*, Vol. 90, pp. 214-223, (2000).

182. Arai J, Yamaki T, Yamauchi S, et al. "Development of a high-power lithium secondary battery for hybrid electric vehicles," *Journal of Power Sources*, Vol.146, pp.788-792, (2005).

183. M. Mastali, J. Vazques-Arenas, R. Fraser, M. Fowler, S. Afshar, M. Stevens, "Battery state of the charge estimation using Kalman filtering," *Journal of Power Sources,* Vol. 239, pp.294-307, (2013).

184. H. He, R. Xiong, J. Fan, "Evaluation of Lithium-Ion Battery Equivalent Circuit Models for State of Charge Estimation by an Experimental Approach," *Journal of Energies*, Vol.4, pp.582-598, (2011).

185. Taylor JR, "An introduction to error analysis," *University Science Books* (1997).

186. H. Ma, L.G. Zhang, YZ. Chen, "Recurrent neural network for vehicle dead-reckoning," *Journal of systems Engineering and Electronics*, Vol.19, no.2, pp.351-355, (2006).

187. A. Peasaran, "Battery thermal management in EVs and HEVs issues and solutions," *Advanced automotive battery conference*, Las Vegas, Nevada, pp.6-8, (2001).

188. Ala A. Hussein, "Capacity Fade Estimation in Electric Vehicle Li-Ion batteries using Artificial Neural Networks," *IEEE Transactions on Industry Applications*, Vol.51, pp.2321-2330, (2015).

189. G. Dorffner, "Neural networks for time series processing," *Neural Network World,* Vol. 4/96, (1996).

190. J. Vetter, P. Novak, M.R. Wagner, C. Veit, Moller, K.-C.; J.O. Besengard, M. Winter, M. Wohlfahrt, C. Vogler, A. Hammouche, "Ageing mechanisms in lithium-ion batteries," *J. Power Sour.* Vol. 147, pp. 269–281, (2005).

191. R. Klein, N.A. Chaturvedi, J. Christensen, J. Ahmed, R. Findeisen, A. Kojic, "Electrochemical Model Based Observer Design for a Lithium-Ion Battery," *IEEE Trans. Control Syst. Technol*. Vol. 21, pp. 289–31, (2013).

192. V. Srinivasan, C. Wang, "Analysis of Electrochemical and Thermal Behavior of Li-Ion Cells," *J. Electrochem. Soc.* Vol. 150, pp. 98–106, (2003).

193. A. Nyman, T.G. Zavalis, R. Elger, M. Behm, G. Lindbergh, "Analysis of the Polarization in a Li-Ion Battery Cell by Numerical Simulations," *J. Electrochem. Soc.* Vol. 157, pp. 1236–1246, (2010).

194. M. Doyle, J. Newman, "The use of mathematical modeling in the design of lithium/polymer battery systems," *Electrochim. Acta.* Vol. 40, pp. 2191–2196, (1995).

195. T.S. Dao, C. Schmitke, "Developing Mathematical Models of Batteries in Modelica for Energy Storage Applications," *In Proceedings of the 11th International Modelica Conference*, Versailles, France, pp. 469–477, (21–23 September 2015).

196. L. Lam, P. Bauer, E. Kelder, "A practical circuit-based model for li-ion battery cells in electric vehicle applications," *In Proceedings of the IEEE 33rd International Telecommunication Energy Conference* (INTELEC), Amsterdam, The Netherlands, pp. 1–9, (9–13 October 2011).

197. T. Ishii, N. Nagaoka, "A logarithmic segmented Laplace transform and its application to a battery diagnosis," UPEC 52nd International Universities Power Engineering Conference, Crete, Greece, IEEE Xplore, pp. 949–953, (28–31 August 2017).

198. A. Ametani, K. Imanishi, "Development of exponential Fourier transform and its application to electrical transients," *Proc. IEE*, Vol. 126, pp. 51–56, (1979).

199. A. Ametani, S. Yamaoka, "On logarithmic Fourier transform. In Proceedings of the IEE Japan Research Committee of Information Processing," *Special Technical Report IP-77-17* Archives, Tokyo, Japan, (1977).

200. S. Yang, C. Deng, Y. Zhang, Y. He, "State of Charge Estimation for Lithium-Ion Battery with a Temperature-Compensated Model," *Energies* Vol. 10, (2017).

201. C.S. Chim, Z. Gao, "State-of-Charge Estimation of Battery Pack under Varying Ambient Temperature Using an Adaptive Sequential Extreme Learning Machine," *J. Energies*, Vol. 11, (2018).

202. D. Stroe, M. Swierczynski, A. Stroe, S.K. Kaeer, R. Teodorescu, "Lithium-ion battery power degradation modelling by electrochemical impedance spectroscopy," *J. IET Renew. Power Gener.* Vol. 11, pp. 1136–1141, (2017).

203. A. Guha, A. Patra, "State of Health Estimation of Lithium-Ion Batteries Using Capacity Fade and Internal Resistance Growth Models," *IEEE Trans. Transp. Electrif. 4*, 135–146, (2018).

204. N. Somakettarin, T. Funaki, "Study on Factors for Accurate Open Circuit Voltage Characterizations in Mn-Type Li-Ion Batteries," *Artic. Batter.* (2017), 3, doi:10.3390/batteries3010008.

205. AA. Akhil, G. Huff, AB. Currier, BC. Kaun, Dm. Rastler, SB. Chen, Al. Cotter, DT. Bradshaw, WD. Gauntlett, "DOE/EPRI 2013 electricity storage handbook in collaboration with NRECA," Sandia National Laboratories, (2013).

206. Electric Power Research, "Electricity energy storage technology options," (2010).

207. International Energy Agency, "Pumped storage provides grid reliability even with net generation loss,"